Conformation-Specific Chemical Probes for Amyloid-β

by

Ashley A. Reinke

A dissertation submitted in partial fulfillment
Of the requirements for the degree of
Doctor of Philosophy
(Biological Chemistry)
In The University of Michigan
2011

Doctoral Committee:

Assistant Professor Jason E. Gestwicki, Chair
Professor Ari Gafni
Associate Professor Matthew R. Chapman
Associate Professor Andrew P. Lieberman
Associate Professor Zhaohui Xu

To my brother Matt, a fine competitor

Acknowledgements

First and foremost, I would like to thank my mentor, Jason, for his knowledge, guidance, inspiration, attitude, and patience. Because of his feedback, I will aspire to always be working smarter, not necessarily just harder. As testament to his excitement and mentorship, I always walked out of a meeting looking forward to tackling my project from a new and different angle. I would like to acknowledge and thank all of the Gestwicki lab members, both past and present. I will forever be grateful that I was able to work alongside such fun, interesting, intelligent, insightful, kind, and hard-working scientists. This lab truly presents an atmosphere of learning, collaboration, and camaraderie. I especially want to thank Andrea and Srikanth, who always took the time to go over data and manuscripts, no matter how busy they were. I want to thank Lyra for keeping spirits in the lab (very) high, and Leah for balancing out my attitude with utmost positivity since she joined the lab, and for loving coffee as much as I do. I would like to thank Matt, Sharon, Gelareh, Leah, Peter, and Jerome for all of their direct help with my experiments. To the rest of the lab, please know that you have all helped me tremendously in your own ways in getting to where I am today. I am indebted to my dissertation committee and their helpful insights into my thesis project. I am grateful that such a diverse group of experts was willing to oversee my progress. Thank you for your time and commitment. I would also like to thank the Biogerontology Training Program for financial support throughout my graduate career.

To my friends, both those whom I knew before graduate school, and those new ones that I have made in the last five years, thank you for your support. I especially would like to acknowledge Cherisse, Corissa, Diane, Heather, Katie, and Liz – I've never met a more intelligent

group of women who like beer as much as I do. Alexa – thanks for always telling me get back to work and "solve Alzheimer's." To Dad, Matt, and Braden, thank you for inspiring me to be a nerdy scientist just like you guys. Matt, thanks for making me stick with it because you're right, I'm not good at anything else. Mom, you are the world's most supportive parent, but you already know that. I thank my parents for knowing what was important, even when I did not; thank you for pushing me. Finally, to my husband Joe, I am so grateful for your unending support. Thank you for picking up and moving so that I could do this. Thanks for being so kind, for a smile at the end of *every* day, and for having the most positive attitude out of anyone I know. We can go back to Wisconsin now if you still want to.

iv

Preface

This thesis is the compilation of published and unpublished work on the development of

conformation-specific probes to target amyloid-β (Aβ). Aβ self-assembles into amyloids with

distinct quaternary structures, and these aggregates are implicated in the pathology of

Alzheimer's disease (AD). In Chapter 1, we discuss three main classes of Aβ probes and what the

binding of these ligands reveals about these amyloid structures. A portion of this discussion has

been accepted as a review for which the citation is Reinke A.A. and Gestwicki J.E., "Chemical

Probes Provide Insight into Amyloid Structures," (2011) *Chem Biol Drug Des* (in press). Chapter 2

focuses on the synthesis and structure-activity evaluation of inhibitors of Aβ self-assembly

based on curcumin. The citation for this article is Reinke A.A. and Gestwicki J.E., "Structure-

activity relationships of amyloid-β aggregation inhibitors based on curcumin: influence of linker

length and flexibility," (2007) *Chem Biol Drug Des* 70; 206-215. Aβ self-assembles into a variety

of amyloid conformations, although it is unclear how structure correlates to pathology in AD.

Toward this goal, we used small molecule screening to develop the first set of conformation-

specific chemical probes for Aβ. In Chapter 3, we present that the fluorescence of indole-based

scaffolds is particularly sensitive to pre-fibrils, but is not affected upon fibril addition, revealing

differences in amyloid structure. These data are published as Reinke A.A., Seh H.Y, and Gestwicki

J.E., "A chemical screening approach reveals that indole fluorescence is quenched by pre-fibrillar

but not fibrillar amyloid-β," (2009) *Bioorg Med Chem Lett* 19; 4952-7. From a secondary screen,

tryptophanol (TROL) was used to develop a spectroscopic assay for monitoring pre-fibril levels

that can be used side-by-side with thioflavin T, and this assay is applicable to other

amyloidogenic proteins. These findings are published in Reinke A.A. Abulwerdi G.A., and Gestwicki J.E., "Quantifying prefibrillar amyloids *in vitro* using a 'thioflavin-like' spectroscopic method," (2010) *Chembiochem* 11; 1889-95. We describe in Chapter 4 a rational design approach to developing peptide-based ligands that selectively detect low-molecular weight Aβ aggregates in mixtures. We synthesized bivalent KLVFF derivatives with varying linker lengths and flexibilities that selectively detect Aβ trimers and tetramers in human CSF. This work was in part published as Reinke A.A, Ung P.M., Quintero J.J, Carlson H.A, and Gestwicki J.E, "Chemical probes that selectively recognize the earliest Aβ oligomers in complex mixtures," (2010) *J Am Chem Soc* 132; 17655-7. Finally, Chapter 5 is a discussion of future directions for developing next-generation amyloid probes.

Table of Contents

List of Figures

List of Tables

List of Abbreviations

Aβ	amyloid-β
AD	Alzheimer's disease
ADDLs	Aβ-derived diffusible ligands
Ahx	aminohexanoic acid
APP	amyloid precursor protein
BSA	bovine serum albumin
CD	circular dichroism
CG	Chrysamine G
CR	Congo Red
CSF	cerebrospinal fluid
DCM	dichloromethane
DIC	N,N'-Diisopropylcarbodiimide
DMF	dimethylformamide
DMSO	dimethyl sulfoxide
ELISA	enzyme-linked immunosorbent assay
HCR	hydrophobic core region
HDX	hydrogen-deuterium exchange
HFIP	hexafluoroisopropanol
HMW	high molecular weight

HRP	horseradish peroxidase
HOBt	N-Hydroxybenzotriazole
(L)CP	(luminescent)-conjugated polymers
LMW	low molecular weight
LTP	long-term potentation
MD	molecular dynamics
NDGA	nordihydroguaiaretic acid
NP	neuritic plaque
PET	positron emission tomography
PICUP	photo-induced cross-linking of unmodified proteins
PIB	Pittsburgh Compound B
PSAM	peptide-self assembly mimic
RT	room temperature
RU	response units
SAR	structure-activity relationships
SPECT	single photon emission computed tomography
SPR	Surface plasmon resonance
TEA	triethylamine
TEM	transmission electron microscopy
ThS	Thioflavin S
ThT	Thioflavin T
TROL	tryptophanol
WT	wild-type

ABSTRACT

Conformation-Specific Chemical Probes for Amyloid-β

by

Ashley A. Reinke

Chair: Jason E. Gestwicki

The age-dependent accumulation of amyloid-β (Aβ) is linked to the pathology of Alzheimer's disease (AD). Both *in vitro* and *in vivo*, Aβ assembles into diverse quaternary conformations, including low-molecular weight structures (*e.g.* dimers, trimers, and tetramers), globular oligomers, protofibrils, and fibrils. Although these assemblies have been identified and partially characterized, the correlations between Aβ conformation and neurotoxicity remain unclear. Probes that differentiate between Aβ species are likely to be critical in answering this important question.

The purpose of this study is to develop small molecules that report on the presence of specific Aβ conformations. In this effort, we pursued three distinct avenues. In the first approach, we characterized the binding of well-known amyloid probes to different Aβ morphologies. In doing so, we established the profile of these widely used Aβ markers and found that most of them lack the ability to differentiate between Aβ conformers. Next, we used unbiased fluorescence

screening methods to discover the first class of chemical probes, indoles, which selectively interact with pre-fibrillar amyloids. Further, we leveraged these compounds to develop a rapid, inexpensive spectroscopic assay for monitoring pre-fibril levels *in vitro*. Finally, we used computational design to build multivalent peptide-based ligands that target the earliest Aβ aggregates, including trimers and tetramers. We found that these probes do not recognize Aβ monomers or fibrils, and that they retain specificity in human cerebrospinal fluid.

Together these studies have established the first chemical probes that target specific Aβ conformations. This work demonstrated that small molecules are indeed capable of discerning between Aβ assemblies, which contributes to our basic knowledge about the properties of Aβ aggregates. Moreover, these scaffolds are expected to become useful tools for defining how Aβ structure correlates with neurotoxicity in AD.

Chapter 1

Introduction: Interactions of chemical probes with amyloid-β: insights into amyloid structure

1.1 Abstract

Alzheimer's disease (AD) is a common neurodegenerative disorder that is characterized by the deposition of amyloids in the brain. In AD, one prominent form of amyloid is composed of repeating units of the amyloid-β (Aβ) peptide. Over the past decade, it has become clear that Aβ-derived amyloids are not structurally homogeneous; rather, they are composed of a series of structures varying in their overall size, shape, and the number of Aβ peptides they include. Recent theories suggest that these different amyloid conformations may play key roles in disease, although their relative contributions are still being discovered. Over the last two decades, small organic molecules, such as congo red, thioflavin T and their derivatives, have been powerful tools for evaluating amyloid formation *in vitro* and *in vivo*. In this Chapter, we review what these chemical probes have revealed about amyloid structure and function. Moreover, we introduce how effective design and deployment of conformationally selective probes might be used to test emerging models of AD.

1.1.1 Alzheimer's disease and amyloid-β

The self-assembly of proteins into amyloid is implicated in the pathology of many age-related neurodegenerative diseases. Alzheimer's disease (AD) is the most common and severe of these disorders, currently affecting more than 35 million people. The overall financial burden of AD and related dementias is over $604 billion in 2010 alone. These figures, along with the predicted rapid increase of individuals affected by the disorder, highlight the need for treatments and robust diagnostic methods. In AD, one of the best-studied amyloids is formed from amyloid-β (Aβ), a short (38-42 residue) fragment of the amyloid precursor protein (APP). Under physiological conditions, Aβ peptides adopt a β-sheet-type secondary structure that is prone to self-assembly into higher-order structures, including dimers, trimers, oligomers, protofibrils and the fibrils that are characteristic of late-stage AD patients. These conformations are defined by their signature appearances by electron and atomic force microscopy, their size on polyacrylamide gels, and even their method of preparation (Figure 1). Collectively, these
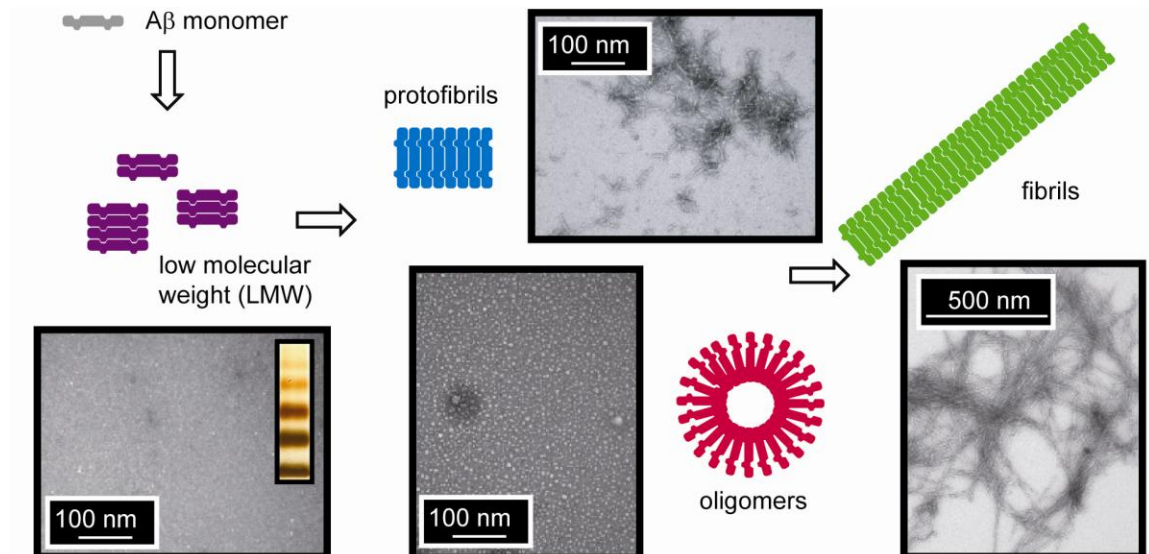
Figure 1.1 Aβ self-assembles into a variety of distinct conformations. Monomers assemble into dimers, trimers and other low molecular weight (LMW) oligomers, which proceed to form larger oligomers and protofibrils. Mature fibrils have a characteristic, elongated morphology. Electron micrographs of enriched samples are shown.

aggregates are severely neurotoxic [1, 2] and they also appear to inhibit LTP and promote synaptic loss [3-5]. The most recent, emerging variants of the Amyloid Hypothesis propose that the pre-fibrillar amyloids, such as oligomers and other soluble structures (ADDLs, protofibrils, etc.) might play a particularly central role in disease [6-9]. However, despite advances in our understanding of Aβ biochemistry and AD, the mechanisms of neurodegeneration are not yet clear.

1.1.2 Small molecules for monitoring Aβ aggregation

Small molecules have been essential tools for characterizing Aβ in many diverse ways. These probes (*e.g*. thioflavin T, congo red) are used to monitor Aβ self-assembly *in vitro,* identify Aβ deposition *in vivo*, and screen for modulators of aggregation. The original aim of chemical reporters of Aβ was to identify areas of fibril and plaque formation *in vivo* and track fibril formation *in vitro* to learn about aggregation. As mentioned, however, recent progress points toward diverse forms of non-fibrillar aggregates, such as dimers, oligomers and protofibrils. Thus, focus has shifted toward pre-fibrillar Aβ species, and the aim of chemical probe development has analogously changed. Therefore, it is pertinent to evaluate chemical probe interactions with early Aβ species along with Aβ fibrils. In this Chapter, we evaluate the interactions of thioflavin T (ThT), congo red (CR), and KLVFF with various conformations of Aβ. We focus on the binding modes of each probe as well as how each has contributed to the knowledge of amyloid structure. Finally, we discuss the status of probes currently under development to selectively recognize specific Aβ conformations.

1.2 Thioflavin T (ThT)

1.2.1 ThT fluorescence is enhanced by binding to aggregated Aβ

(a) Chemical structures of thioflavin T and BTA-1

thioflavin T (ThT)   BTA-1

benzothiazole   aniline
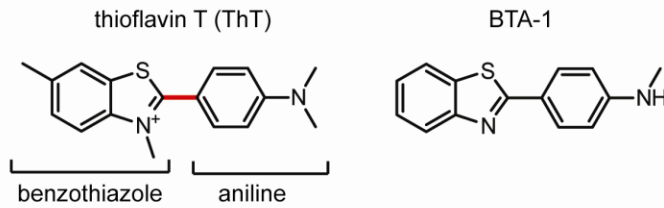
(b) Multiple ThT binding sites are present on amyloid fibrils with different densities
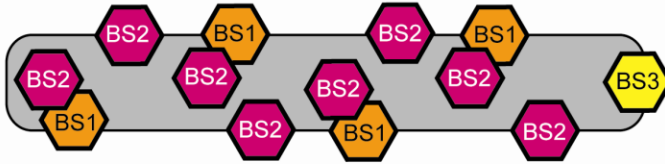
Figure 1.2 Thioflavin T (ThT) binds amyloid fibrils at multiple sites with varying densities (a) Chemical structures of ThT and a neutral analog, BTA-1. The core structure is comprised of a benzothiazole ring attached to aniline group through a carbon-carbon bond (red), whose twisting dynamics change upon amyloid binding. (b) Three distinct ThT binding sites are present on amyloid fibrils, each with a different density. BS1 and BS2 are high-density sites (one site per 4-35 Aβ monomers), whereas BS3 is less populated, with one site per 300 monomers.

Thioflavin T (ThT) is a benzothiazole-containing dye first noted to bind amyloid by Vassar and Culling in 1959 [10], and later noted to interact with patient-derived amyloids by Naiki and coworkers (Figure 1.2a) [11, 12]. This same phenomena was observed with synthetic Aβ fibrils *in vitro* [13], and further adapted by LeVine as a probe for both quantifying relative amounts of aggregated Aβ in solution and monitoring fibril formation [14]. This protocol has been largely unchanged and is perhaps the most widely employed for monitoring Aβ aggregation. These initial studies revealed the requirement of cross-β-sheet secondary structure for ThT binding; indeed, denaturation of β-sheet abolishes ThT binding. Based on its high-yielding fluorescence change in the presence of aggregated Aβ, ThT has played a role in elucidating the kinetics of Aβ self-assembly. Distinct differences in growth rate and maximum fibril formation between wild-type (WT) and mutant Aβ peptides associated with early onset AD were discovered using ThT [15, 16]. It is also used to determine the effects of seeding on Aβ monomer acquisition[17], and to evaluate the hydrogen-bond network required for Aβ self-recognition [18]. Further, the relationship between Aβ (1-40) and (1-42) kinetics *in vitro* was, in part, elucidated using ThT fluorescence [19, 20]. Finally, ThT is broadly used in screening for modulators of Aβ aggregation.

Enhanced ThT fluorescence yield serves as a universal definition of amyloid, and thus, it is used in nearly all *in vitro* investigations of amyloid aggregation. ThT fluorescence is thought to increase when bound to Aβ fibrils because the rotational freedom of the carbon-carbon bond between the benzothiazole and aniline rings is restricted (Figure 1.2a) [21, 22]. In the unbound state, the ultrafast twisting dynamics around this bond are thought to cause rapid self-quenching of the excited state, resulting in low emission. However, upon binding to fibrils, the rotational freedom is apparently reduced and the excited state is readily populated. This concept was recently confirmed using a series of synthetic ThT analogs, which varied in their flexibility [22]. The practical outcome of this mechanism is that ThT and its analogs can be used to spectroscopically quantify the amount of amyloid in a sample.

1.2.2 Using ThT to identify modulators of Aβ aggregation

Because ThT does not disrupt amyloid aggregation, it is widely used to survey the effects of other modulators (*e.g.* protein, small molecules) on self-assembly. This application has yielded many small molecule modulators [23, 24], and established the structure-activity relationships (SAR) of these scaffolds [25]. For example, the focus of Chapter 2 is establishing the SAR of curcumin, a well-known amyloid modulator. In turn, many these small molecules have helped elucidate the steps of the Aβ aggregation pathway [26]. However, ThT binds at multiple sites on Aβ (discussed below), and thus may interfere with the binding of potential modulators. Indeed, congo red (CR) has been shown to compete with ThT for binding to amyloid fibrils [27]. Although CR has been confirmed by other methods to inhibit Aβ aggregation, this artifact may lead to false-positive hits. Moreover, the fluorescence of certain exogenous compounds interferes with ThT emission. In a discussion of the potential artifacts of using ThT as a reporter in screening for inhibitors, Hudson *et al.* found that the presence of several well-known amyloid inhibitors (*e.g.*

flavonoids) interfere with the ThT fluorescence spectra [28]. Based on these findings, some groups are hesitant to rely on ThT as a screening method for small molecule inhibitors. Necula *et al.* highlighted a number of structurally diverse small molecules that interfere with ThT fluorescence in the absence of Aβ [26]. Some interfere with absorption, causing a decrease in ThT emission, while others increase cumulative fluorescence emission due to their intrinsic fluorescent properties. For these reasons, it is critical to employ several methods of monitoring Aβ aggregation in the presence of potential modulators, such as TEM, AFM, turbidity, and immunohistochemistry. Further, new high-throughput screening methods are being engineered, including ELISA approaches [29], GFP-fluorescence [30], biotin-streptavidin platforms [31], and MALDI mass spectrometry [32], for identifying new Aβ modulators.

1.2.3 Binding modes of ThT to amyloid fibrils

The dramatic response of ThT's fluorescence to solutions of amyloid suggests that an important molecular binding event takes place to restrict the motion of the compound. Thus, studying this interaction would be expected to reveal insights into the local amyloid topology and its molecular features. This strategy has been productive, with solid-state NMR [33], radiolabeling [34, 35], competition assays [27], and molecular dynamics (MD) simulations [36-38] all having been used to evaluate ThT binding to amyloids. One of the first important observations was made by LeVine, who proposed that there are multiple binding sites for ThT on amyloids [27]. Lockhart *et al.* further refined this model using fluorescence and radiolabel-based assays [34]. Together, these studies suggested the presence of three distinct binding sites (BS1, BS2, and BS3) on Aβ fibrils. Sites BS1 and BS2 are relatively abundant, with approximately one site per 4-35 Aβ monomers (Figure 1.2b). The less abundant site, BS3 is found at approximately one site for every 300 monomers. Based on FRET measurements, binding sites BS1 and BS2 are thought

to be in close proximity, however occupancy was found to be neither cooperative nor competitive.

Further insights into how ThT binds in these different sites was supplied by molecular dynamics (MD) simulations [37, 38]. Briefly, Wu *et al.* simulated ThT binding to protofibrils composed of Aβ (16-22) and characterized the formation of three unique, populated clusters [37]. Consistent with their earlier findings [38], the least populated binding cluster was located on the end of the protofibril in an orientation anti-parallel to the fibril axis. The two other clusters were more heavily populated and located parallel to the fibril axis (anti-parallel to the β-sheet). Together, these results seem to confirm Lockhart's model of two, high-density ThT sites (BS1, BS2) and a single low-density site (BS3) (Figure 1.2b). In this model, BS1 and BS2 are composed of surface grooves created by side-chains along the fibril axis, which provide much of the binding energy to the planar ThT molecule. When bound in these grooves, MD simulations suggest that the benzothiazole ring favors a flat orientation parallel to β-sheet surface, with the charged nitrogen exposed to solvent [36, 39] (Figure 1.3a). Interestingly, similar grooves have been proposed in amyloid fibrils composed of many different proteins (*e.g.* α-synuclein, prions, *etc.*), which may explain why ThT fluorescence is also sensitive to other, unrelated amyloids. However, because different amyloid-forming peptides do not share a high sequence identity, these results suggest that some degenerative feature(s), such as hydrophobicity or contacts with the peptide backbone, are responsible for ThT binding.

Consistent with this idea, a closer examination of the molecular models reveals interesting features of the two most populated ThT binding sites (Figure 1.3a) [37]. These two binding channels are lined with at least five, spatially consecutive, hydrophobic (phenylalanine and valine) side chains, which are located on opposite 'faces' of the amyloid structure. Similar findings have been observed by Koide and coworkers, who developed peptide self-assembly mimics (PSAMs) that have repetitive, β-sheet amyloid-like structure [40, 41]. These soluble model proteins are amenable to crystallization, and co-crystals with bound ThT revealed that the compound localized to channels lined with five or six aromatic and hydrophobic side-chains [40]. Interestingly, it is critical that the favorable, hydrophobic residues within the channel are spatially consecutive, as two adjacent groups of tyrosine residues separated by a lysine and glutamate showed no ThT binding [40]. Collectively, these observations converge on a model in which five, aligned aromatic and/or hydrophobic residues are critical for ThT binding, while the exact identities of the side chains are less important than their overall hydrophobicity.
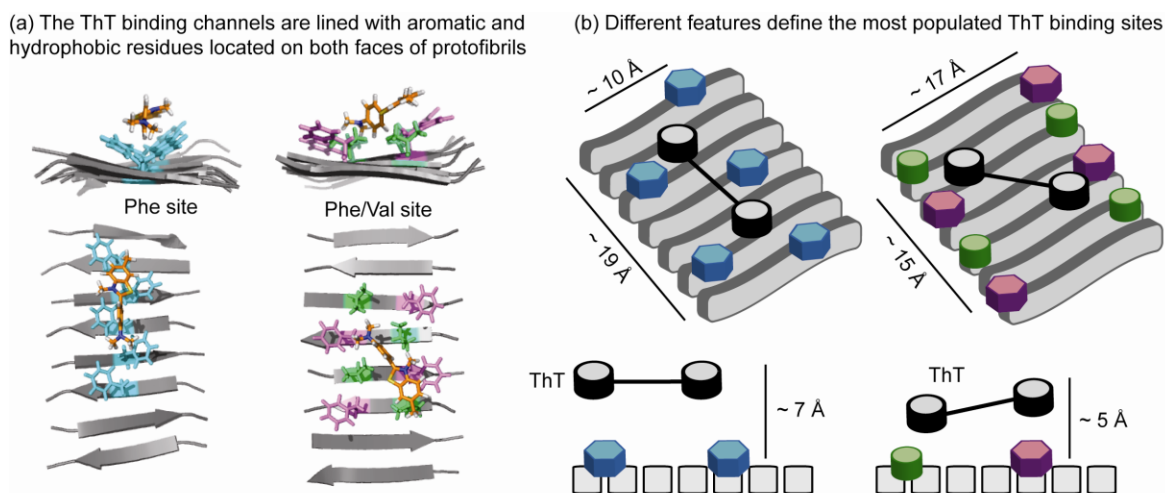
Figure 1.3 Structural definitions of distinct ThT binding sites (a) MD simulations show ThT binding to protofibrils within channels lined with hydrophobic (phenylalanine and valine) side-chains, oriented anti-parallel to the β-sheet. At least five consecutive hydrophobic and aromatic residues have been shown to be required for accommodating ThT. These structures are adapted from from previously published MD simulation data [Wu *et al.* (2008) J Mol Biol]. (b) A model of the two ThT binding sites shown in (a) reveals that unique dimensions may define these sites. The channel of one site is longer and narrower (19 X 10 Å; left) than the other (15 X 17 Å; right). Further, the depth of the channels differs as well, as the narrow site is slightly deeper (7.1 Å) compared to the wider site (5.4 Å). These partially distinct sites may represent the high-density sites BS1 and BS2 in Figure 1.2b.

An alternative binding mode was suggested by Groenning *et al.* using spectroscopy and molecular modeling to examine ThT binding to insulin fibrils. Although they confirmed that at least two distinct binding sites exist, with ThT binding predominantly parallel to the fibril axis [42, 43], they further suggest that two ThT molecules in an excited-state dimer, or 'excimer,' form, might bind to the grooves. Thus, a higher-order form of ThT, even as large as a micelle [44], might be involved in binding under some conditions and for some amyloids.

1.2.4 ThT recognizes pre-fibrillar Aβ aggregates

As mentioned previously, pre-fibrillar intermediates are now thought to correlate with neurodegeneration, which has prompted interest in evaluating ThT binding to these species. In the literature, there was initially debate over whether ThT binds oligomers and protofibrils. In fact, several groups initially defined ThT as a fibril-specific probe [45, 46]. However, methods for preparing pre-fibrillar structures have become more reliable and comprehensive studies have noted clear changes in fluorescence when ThT is added to pre-fibrils [47-49]. For example, Walsh *et al.* prepared samples of protofibrils and observed that they produce a concentration dependent increase in ThT fluorescence [49]. The binding of ThT to pre-fibrillar structures is consistent with the binding information discussed above, as pre-fibrillar structures are known to be rich in the β-sheet content proposed to be the ThT binding region [49]. For example, models of Aβ protofibrils have the requisite stretch of aligned hydrophobic residues one might expect to form the high-abundance ThT-binding site [50]. However, fibrils and pre-fibrils are not identical in their binding to ThT, as many groups have noted that the maximum fluorescence induced by pre-fibrils is less than that stimulated by fibrils. For example, ThT fluorescence is modestly increased (1.5-fold) in the presence of Aβ oligomers [48] of either 1-40 or 1-42 Aβ [47], while fibrils often yield over 100-fold improvements in fluorescence [20]. Moreover, using SPR, ThT (K_d

= 498 nM) was shown to bind Aβ oligomers, but the total number of bound molecules was significantly less than in fibrils [47]. These observations and others are likely consistent with MD simulations, because protofibrils are proposed to be more dynamic [51] and contain relatively fewer ThT-binding sites [52, 53]. Collectively, these data reveal that ThT is not specific for certain amyloid conformations.

1.2.5 Interactions of ThT analogs with Aβ

Additional insights into the nature of the ThT-binding groove can be gained from studying synthetic ThT derivatives in which the molecular features of the molecule are systematically varied. In general, ThT derivatives are composed of a benzothiazole ring system attached to a substituted aniline (Figure 2A). Derivatives of this scaffold tend to have substitutions at the amine of the aniline and at positions around the benzothiazole. Fortunately, many analogs have been explored as part of studies to develop imaging agents and, in many cases, the binding affinity of these compounds for amyloids has been reported. For example, Klunk *et al.* synthesized several neutral ThT analogs, such as BTA-1, to explore the effect of the positive charge on the benzothiazole ring (Figure 1.2a) [54]. They found that each neutral analog bound better to Aβ than ThT, with the best having 40-fold better affinities. These findings suggest that the positive charge in ThT may be detrimental for binding, which is a model supported by MD simulations indicating that the neutral BTA-1 is able to bind deeper into the hydrophobic binding grooves [37]. However, ThT does not entirely compete with BTA-1 for binding [27], and Lockhart *et al.* observed different binding patterns between the two ligands [34]. *In silico* data further reveals that the ring systems of BTA-1 are planar in the bound orientation, instead of in a twisted orientation, as observed with the charged ThT scaffold [37]. Collectively, these data

support a model in which some of the "ThT binding sites" (*i.e.* BS1, BS2 and BS3) are more favorable for ThT, while others prefer neutral ligands.

Interestingly, removal of the positive charge does not seem to affect oligomer binding, suggesting that one of the binding sites is more prevalent in these pre-fibrillar structures [55]. One possibility is that some of the sites allow deeper binding grooves, perhaps permitting neutral ligands with increased access compared to charged derivatives. This idea is supported by measurements of the dimensions of the two sites identified by modeling: one has an average depth (backbone to solvent) of 5.4 Å, while the other is 7.1 ± 0.7 Å (Figure 1.3b). This deeper site might allow better penetration of neutral derivatives and, consequently, more favorable buried surface area and better affinity. These sites are unique in other dimensions as well; the shallower site is wider (17 Å), while the deeper site is narrower (10 Å). It isn't yet clear which site is BS1 or BS2, but these differences support the model that the two sites have distinct properties. To our knowledge, structure-guided design has not yet been used to rationally exploit these differences.

Synthetic ThT derivatives have also been useful in further refining the features of the binding sites. For example, the tolerance of certain substitutions to both the benzothiazole ring system and the aniline group supports the idea that the channel is highly hydrophobic. Specifically, the benzothiazole can be replaced by a benzofuran, imidazo-pyridine, imidazole, or benzoxazole core, each of which maintains the planarity and affinity of the molecule [55-58]. Additionally, the aniline may be replaced with other flat, rigid moieties (*e.g.* stilbene, cyanobenzyl) without significant consequence to affinity [59, 60]. Insertion of a planar styrene group between the benzothiazole and aniline is also well-tolerated [59], while some substitutions, such as

bithiophenes, even improve affinity [61]. In addition, planar substitutions need not be aromatic, because methyl-piperazine groups appended to the aniline are tolerated [62]. Interestingly, some of these substitutions extend the end-to-end distance of the ThT-like molecule by over 25%, suggesting that the binding channel can accommodate relatively long molecules, as long as they are planar and hydrophobic. However, there are limitations to the size of the channel. For example, installation of a large, freely-rotatable rhenium chelate to the aniline abolished binding [63]. Appending the same group to the opposite end of the molecule actually enhanced binding by 8-fold, which suggests that the dimensions of the channel are limited in some regions.

More subtle substitutions to the benzothiazole and aniline groups also help define the nature of the ThT binding site(s). For instance, the di-methyl amine group can be moved to the benzothiazole on the opposite side of the molecule without any consequence to binding affinity [64], suggesting that ThT derivatives may be able to bind in either orientation (Figure 1.3b). However, small alkyl-type substitutions in key positions appear to impact the binding mode [65]. For example, a methyl group at the 6-position of the benzothiazole ring is favored only if no methyl substitutions are present on the amine of the aniline (K_i = 9.5 nM). Alternatively, two methyl groups on this amine were favored if the 6-position was hydrogen (K_i = 4 nM). Interestingly, a more polar, hydroxyl at the 6-position was tolerated only if the aniline was substituted with at least one methyl group, suggesting that overall hydrophobicity is a critical element for binding.

In summary, multiple experiments have converged on a model in which amyloids contain up to three different binding sites. The two major sites (BS1 and BS2) are parallel to the fibril axis and are sensitive to relatively modest increases in steric size in some positions, while they can be readily elongated in the channel if overall planarity is maintained (Figure 1.3b). The major contacts with ThT are through aromatic and/or hydrophobic side-chains in the parallel groove, and neutral derivatives bind tighter than their charged counterparts. It is important to note that BS1 and BS2 are present in roughly equivalent numbers (at least on fibrils) but that the experiments discussed here often focus on the composite affinities. Differences in the way that ThT derivatives bind the different sites might easily be masked in these studies and, moreover, little is likely learned about the requirements at BS3 in these types of experiments.

1.2.6 Development of *in vivo* amyloid tracers based on ThT

Based on its specificity for amyloid, ThT is a promising target for developing *in vivo* amyloid tracers for imaging by PET or SPECT. Optimal imaging agents for this purpose are expected to have high binding affinity and selectivity for amyloid, adequate brain uptake and clearance, chemistry commensurate with radiolabeling (*e.g.*

Figure 1.4 Derivatives of ThT used as *in vivo* markers of amyloid deposition. Structure-activity studies yielded this set of neutral ThT derivatives with improved Aβ binding and BBB permeability. [C^{11}] 6-OH-BTA-1 (PIB) is commonly utilized in clinics as an amyloid imaging agent using PET. The radiolabeled carbon is indicated with a star.

^{125}I and ^{18}F), small size, and high *in vivo* stability [66]. Although ThT is small (318 Da) and has high affinity and selectivity for Aβ, its positively charged nitrogen atom (in the benzothiazole group) limits blood-brain barrier (BBB) permeability (Figure 1.2a). Toward the goal of developing more

lipophilic derivatives, Klunk *et al.* synthesized three ThT analogs that lacked the methyl group at the nitrogen of the benzothiazole ring, thereby removing the charge [54]. As mentioned in the previous section, the neutral analogs all displayed increased affinity for Aβ, some with over a 40-fold increase in the K_i value relative to ThT (890 nM). Overall, 6-Me-BTA-1 was the tightest binder with an affinity of 20 nM (Figure 1.4). Subsequent tissue staining of AD human hippocampus showed retention of binding to Aβ plaques. Following intravascular injection of N-methyl-^{11}C-6-Me-BTA-1 into WT mice, significant brain uptake was observed after only two minutes post-injection, and 84% clearance at 60 minutes post-injection, both of which are comparable to commonly used neuroreceptor imaging agents. Similarly, TZDM [62], IBOX [55], and IMPY [67] are all neutral derivatives with improved BBB permeability relative to ThT (Figure 1.4). To facilitate radiolabeling, the methyl group at the 6-position of the benzothiazole ring was replaced by an iodine. Thus, IMPY was one of the first ThT analogs to show labeling *in vivo* in an AD mouse model by film autoradiography [56, 66]. Inclusive SAR for a large collection of these derivatives is well-established [68].

Given the improved *in vivo* properties of removing the methyl group of the benzothiazole ring, Mathis *et al.* further explored the utility of BTA derivatives as PET imaging agents. After extensive SAR of 18 analogs, 6-OH-BTA-1 showed the best profile of brain uptake and clearance (Figure 1.4). Furthermore, fluorescence staining was retained, as well as binding to synthetic Aβ (1-40) fibrils. A radiolabeled version of 6-OH-BTA-1 was later termed Pittsburgh Compound B (PIB) during its *in vivo* evaluation in AD patients by PET imaging [69]. PIB has emerged as a first-generation clinical diagnostic at dozens of institutions. These studies have highlighted the use of these *in vivo* tracers as both a diagnostic and tool for therapeutic developments [70]. Given the success of PIB with PET, studies are ongoing to develop derivatives with longer half-lives that

could be applied with SPECT imaging, which is much more accessible to many health and research centers [58, 63]. Together, these studies confirm that amyloid binders discovered *in vitro* can be used as imaging agents *in vivo*, a critical transition that may hopefully be made with conformation-specific probes.

1.3 Congo Red (CR)

1.3.1 Spectroscopic properties of CR binding to Aβ

Congo red (CR) is a sulfonic acid-based, secondary di-azo histochemical dye (Figure 1.5a). The amyloid-specific staining properties of CR were first observed by the German physician Hans Hermann Bennhold [71], and the optical properties of CR up amyloid binding have been extensively reviewed [72, 73]. Briefly, upon binding to amyloid, CR displays a characteristic birefringence when subjected to polarized light. Along with ThT, it is one of the most common tools to confirm amyloid deposition in tissue. The CR absorbance spectrum is modified in several ways in the presence of amyloid aggregates as well; the maximum CR absorbance increases and undergoes a slight redshift. This phenomenon was refined by Klunk *et al.* when evaluating CR binding to fibrils composed of insulin [74]. Importantly, this was also one of the first studies that aimed to quantify CR binding to amyloids under physiological conditions, rather than those employed for tissue staining. These findings led to a novel assay to quantify CR binding to amyloid without the need for radioactivity [75]. Almost a decade after these initial observations, Klunk *et al*. developed a spectrophotometric assay specifically for monitoring Aβ aggregation by CR, similar to that used with ThT [76, 77]. Here, we discuss the insights into amyloid structure(s) based on the binding site CR and its derivatives.

1.3.2 CR binds at least two sites on amyloids

Congo Red (CR) staining serves as a positive indicator of amyloid deposition and its optical properties have been extensively reviewed [72, 73]. Briefly, CR selectively stains amyloid *in vitro* and in brain slices, and bound material displays a characteristic birefringence under polarized light. Like ThT, binding is observed with both Aβ-derived amyloids and amyloids derived from other peptides, suggesting that shared elements, such as β-sheet structure or peptide backbone, are involved in binding. Consistent with this idea, molecular docking simulations suggest that CR binds one site anti-parallel to the β-sheets (parallel to the fibril axis) [78] on amyloid fibrils and

(a) Chemical structure of congo red
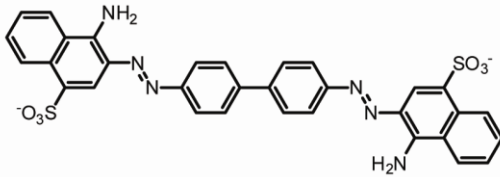
(b) CR binds at two non-equivalent sites on Aβ
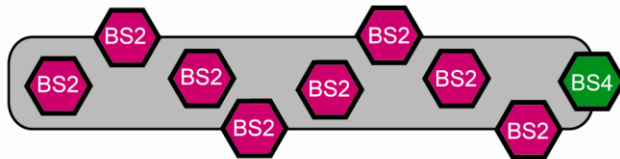
Figure 1.5 Congo red (CR) binds at two distinct sites on amyloid fibrils (a) Structure of CR. (b) Two CR binding sites exist on Aβ; BS2 is shared with ThT and is more prominent, while BS4 (likely the parallel binding mode in Figure 1.6a) is less populated. One CR binding site is thought to be present per three Aβ monomers.

protofibrils [38]. Based on the approximate length of one of the CR molecule (~19 Å) (Figure 1.5a), Klunk and colleagues proposed a model in which it requires at least five Aβ monomers for binding [78]. Lockhart *et al.* further characterized the number and types of CR-binding sites using a close analog, BSB [35]. These studies revealed two non-equivalent binding sites, one of which is shared by ThT and is present at one molecule per three Aβ monomers. Moreover, the shared binding site was found to be the highest-density ThT binding site (BS2) (Figure 1.5b). These findings clarify the seemingly contradictory, earlier observations that CR and ThT have discrete binding sites [62], while other groups have reported competition [27, 28]. To keep consistent with the existing nomenclature and as a useful tool for discussion in this review, we represent the unique CR-binding site as BS4. Insight into the nature of BS4 came from studies on

a prion-derived, amyloidogenic peptide with the sequence GNNQQNY [38]. Specifically, MD simulations revealed that CR favors binding anti-parallel to the β-sheet (in BS2), but that it also populates a second site at the 'end' of the protofibril in a parallel orientation (Figure 1.6a). This latter mode only represented approximately 11% of the total CR binding clusters, while the anti-parallel orientation was clearly preferred (78% of the total binding). This model perhaps explains the difference between CR binding affinity (K_d high nM – low μM) and its inhibition capacity (IC_{50} mid-high μM). In other words, CR may preferentially bind anti-parallel to the β-sheet, but this binding mode is not likely to inhibit fibril extension. When BS2 becomes saturated, CR may bind BS4 at the face of the growing fibril, only then disrupting monomer acquisition and elongation.

CR, like other amyloid probes, binds to amyloids independent of their amino acid sequence, and, therefore, features that are common amongst amyloids likely define the basic CR-binding site(s). Similar to ThT, the main CR binding mode appears to be defined by a channel formed from side-chains. However, in contrast to the ThT channel, the residues that line the CR binding site are polar and non-aromatic, such as Asn and Gly. In addition, despite the presence of nearby tyrosines, this aromatic residue does not appear to participate in CR binding (Figure 1.6a, left). Instead, in three of the four most populated clusters, the sulfonic acid moieties were aligned with the N-terminus, the only formal positive charge on the peptide (Figure 1.6b). These data suggest that ionic or polar interactions may be critical in CR binding. Even greater detail has been provided by molecular docking of CR to 20 NMR structures [79] composed of near full-length Aβ (9-40) [80]. These results confirmed two distinct CR binding sites, one located near Lys28 and the other at the C-terminus, making contacts with Asn27 and Val39. This is one of the first studies to implicate specific residues of the Aβ peptide in CR binding and, further, the contacts with Lys28 and Asn27 were confirmed by mutagenesis. Accordingly, these results

suggest that, in the context of full length Aβ, Lys28 may provide the requisite positive charge to interact with the sulfonic acids. Thus, the identity of the side-chains seems to play less of a role than polar contacts at the termini of the pocket. The CR-binding channel is longer (23-25 Å), and narrower (5-8 Å) than the ThT channels, although it must include a portion of ThT-binding BS2 site based on the competition results.

1.3.3 CR recognizes Aβ pre-fibrils

When CR staining of Aβ deposits was first discovered, it was thought that insoluble plaques and, later, the fibrils that compose these deposits, were responsible for the pathology of AD. However, since there is growing evidence that non-fibril species (*e.g.* pre-fibrils) correlate with pathology, there is an increased interest in determining how CR, curcumin, and other related compounds interact with these early aggregates. The first indication that CR may recognize species other than fibrils was by Walsh *et al.*, who showed that CR absorbance was altered by

(a) CR access two binding modes relative to the β-sheet direction on amyloid protofibrils

anti-parallel

parallel

(b) Charged groups of CR make polar contacts with amyloid fibrils backbone

(c) Polar contacts drive CR binding within its binding channel

5 - 8 Å
23 - 25 Å
polar contact
CR
5-6 Å
CR
~ 22 Å
~ 3 Å

Figure 1.6 CR accesses dual binding modes on amyloids (a) The predominant binding mode of CR is anti-parallel to the β-sheet (left), while the less-favored site is parallel (right). Polar and uncharged residues line the CR binding channel (blue), and aromatic residues appear to not participate in binding of the pre-dominant mode (grey). (b) The negatively charged sulfonic acids of CR interact with the positively charged N-terminus. Charged and polar groups on the terminal aromatics of CR and its analogs are favored for binding. (c) These observations present a model in where the CR binding channel is created by side-chains, which can be polar, uncharged, or hydrophobic. More importantly, contacts between the polar or charged groups of the terminal aromatics of CR make critical contacts at either end of the binding channel. Dimensions that define the channel are shown. The structures shown in (a) and (b) were adapted from previously published MD simulation data [Wu et al. (2007) J Am Chem Soc].

protofibrillar Aβ, though not to the extent that fibrils induced a spectroscopic change [49]. As mentioned with ThT, it is thought that this lower spectroscopic yield is due to the reduced number of binding sites presented on pre-fibrils relative to fibrils. Further the recognition of oligomers by CR and curcumin is supported by a recent study focusing on the disaggregation of Aβ oligomers. Using quantitative AFM, Hong *et al.* showed that both CR and curcumin, when added to a sample of preformed Aβ oligomers, reduced the levels of oligomers by half [81]. We describe in Chapter 2 that we have observed similar trends. Collectively, these disaggregation studies suggest that CR-like molecules recognize Aβ intermediates. Further study would provide insight into precisely which morphologies are targeted for rearrangement and disassembly.

Although aggregation assays can be used to determine a potential interaction between a small molecule and Aβ, these approaches do not offer insight into the binding affinity of these probes for specific conformations. In order to test direct binding to distinct Aβ species, Maezawa *et al.* used SPR to determine the affinity of CR and the structural analog BSB for soluble Aβ oligomers. They discovered that these probes recognize Aβ oligomers with low micromolar affinity (K_d = 3.2 - 19.5 μM). In Chapter 2, we further describe how curcumin, a close CR analog, also binds oligomers and LMW Aβ using an SPR platform. Finally, BSB has been shown to stain A11-reactive Aβ deposits in brain tissue from human AD hippocampi and transgenic mouse frontal cortex. Fluorescence micrographs revealed almost a complete overlap of the A11-reactive, intraneuronal Aβ oligomers with BSB binding. Finally, both BSB and CR were able to significantly reduce binding of Aβ oligomers to synapses in human AD hippocampal neurons. It remains to be found whether the same features define the CR binding site(s) on pre-fibrils and fibrils.

1.3.4 CR analogs reveal features of the amyloid-binding sites

Synthetic CR derivatives have provided further insight into the features of the binding sites on amyloids. For example, early derivatives explored the replacement of the sulfonic acids [78]. Using a radiolabeled displacement assay, Klunk *et al.* identified that other charged groups, such as carboxylic acids, could replace the sulfonic groups [78]. More recent studies found that the carboxylates were not absolutely required if phenolic hydroxyl groups were included [82]. Further SAR studies revealed that the methoxy substitutions that are located on some CR analogs are expendable [25, 62]; thus, there are likely no specific contacts made with those groups.

In addition to the polar contacts at the termini, the overall planarity of the molecules appears to be critical to their binding. Effective CR analogs, including X34 [83], BSB [84], K114 [85], IMSB [62], and methoxy-X04 [86], are all aromatic and planar and they seem to share binding sites [85] (Figure 1.7). We describe in detail in Chapter 2 that other derivatives, based on the curcumin scaffold, revealed that two terminal aromatics are necessary [25]. Interestingly, the overall size of the molecule was found to follow strict requirements, with the linker length restricted to 8-16 Å and including no more than 2-3 rotatable bonds. This general conclusion is supported by studies that indicate the more rigid enol form of curcumin is favored to bind Aβ, relative to the more flexible keto form [87, 88]. Together, these findings are consistent with a model in which the binding site for CR has limited size, with a hydrophobic channel
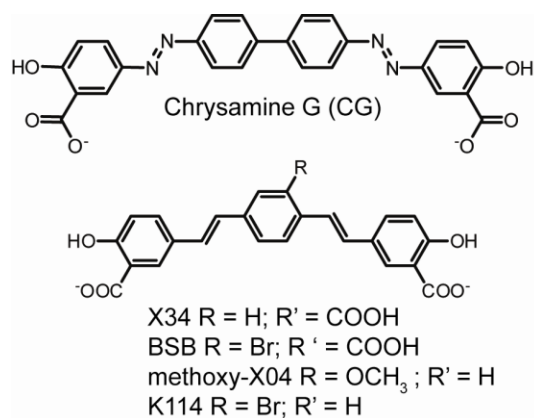
Figure 1.7 Chemical structures of CR derivatives developed for *in vivo* amyloid tracing. Chrysamine G (CG), X34, BSB, methoxy-X04, and K114 have been used to evaluate Aβ deposition in mouse models of AD. Each shows improved BBB permeability relative to CR and retains specificity for amyloid *in vivo*.

and polar (or positively charged) groups at the ends (Figure 1.6c). These same molecular contacts may be equally crucial in pre-fibrillar conformations of amyloids, as curcumin also inhibits the formation of low-molecular weight (LMW) and oligomeric Aβ [89].

1.3.5 Evolution of CR-based markers for Aβ detection *in vivo*

CR, like ThT, has been the focus of intense chemical optimization for use as an *in vivo* amyloid marker, yet, its poor BBB permeability has limited its use in patients [90]. Thus, the development of lipophilic CR analogs that retain amyloid selectivity has been an ongoing subject of research for the last two decades. The first of these derivatives were developed by Klunk and coworkers [78]. As mentioned in the previous section, CG, a CR analog, retains its affinity for Aβ (Figure 1.7). After CG was evaluated for its binding *in vitro* [78], it was tested for potential *in vivo* use by first addressing the issue of BBB permeability; CG indeed crosses the BBB in WT mice and achieves a brain:blood ratio of 10:1 [91]. Further, CG administration to WT mice caused no behavioral effects or toxicity, even at doses 10- and 100-fold greater than those used in the permeability studies. Importantly, this study also showed that CR and CG brain tissue staining patterns of Aβ are identical [91]. These initial studies suggested that the structural features of CR could be modified for *in vivo* use without sacrificing specificity.

In similar efforts to increase lipophilicity, styrylbenzene derivatives BSB, X34, methoxy-X04, K114, and IMSB were all developed (Figure 1.7) [62, 84, 86, 92]. Several of these derivatives contained potential sites for radiolabeling, which, as mentioned, is necessary for PET and SPECT imaging. In both X34 and BSB, the hydroxyl and salicylic acid substitutions on the terminal aromatics, originally from the CG scaffold, were unchanged in order to retain BBB permeability. Following optimization of their staining protocol to maximize fluorescence intensity and

contrast, Styren *et al.* performed extensive tissue staining of Aβ deposits with X34 within the frontal cortex from human AD brain tissue to confirm specificity [83]. Analogous to X34, BSB also showed specific staining of Aβ in AD brain tissue, and, in addition, BSB was also used in the first demonstration of fluorescently labeled Aβ deposits in Tg2576 mice following injection. BSB presented one of the first scaffolds that combined the capability for intense fluorescent staining with a site for potential radiolabeling.

Further, methoxy-X04, with a lower molecular weight and 10-fold higher logP compared to earlier analogs, contained a ^{11}C-radiolabeled methoxy substitution on the central aromatic ring for imaging. Following evaluation of specificity, it was used to visualize Aβ plaques in living transgenic mice by multiphoton microscopy, making methoxy-X04 one of the first compounds to be used in living animal models. This probe is still commonly used to evaluate amyloid deposition in diseased brain tissue [93]. Similarly, a fluorinated BSB analog, ^{19}F-FSB, has been administered intravenously into transgenic AD mouse models and showed no toxic effects at the concentrations necessary for amyloid labeling [94]. Thus, magnetic resonance imaging (MRI) revealed selective binding of ^{19}F-FSB to both Aβ and tau deposits in the brains of live animals. As with ThT derivatives, these scaffolds are continually being optimized for *in vivo* PET and SPECT imaging applications.

1.4 KLVFF

1.4.1 The hydrophobic core region (HCR) is critical for Aβ aggregation

Distinct regions and amino acids of the Aβ peptide have been extensively evaluated for their role in aggregation. For instance, the excess hydrophobicity added by the presence of Ile41 and Ala42 at the C-terminus greatly enhances the rate of aggregation [95]. The most characterized

area of the peptide, the hydrophobic core region (HCR), spans residues 16-20 and corresponds to the amino acids KLVFF (Figure 1.8a). Systematic substitution of the hydrophobic residues 17-20 in Aβ (10-42) for more hydrophilic amino acids reduced both fibril formation and the capacity for β-sheet secondary structure formation [96]. Interestingly, TEM analysis revealed that specific replacement of Phe19 and Phe20 resulted in the only peptides that completely ameliorated aggregation. Based on these observations, Hilbich *et al.* hypothesized that Phe19/20 are crucial for aggregation, and, in turn, that the HCR is critical for Aβ self-assembly. NOESY-NMR analysis supports this hypothesis; as few as one point mutation (F19T) in the HCR reduced folding relative to WT Aβ, and plaque formation was nearly inhibited [97]. These authors were the first to suggest that the HCR may be an attractive target for probe development.

Tjernberg *et al.* took a systematic approach in determining precisely which residues within Aβ

(a) Amyloid-β (1-42) H₂N-DAEFRHDSGYEVHHQ-KLVFF-AEDVGSNKGAIIGLMVGGVVIA-COOH

(b) Residues in the HCR align within Aβ fibrils

(c) KLVFF binds its homologous residues on the 'ends' of Aβ

Figure 1.8 KLVFF binds at the exposed 'ends' of Aβ aggregates (a) The sequence of Aβ (1-42) with the hydrophobic core region (HCR) highlighted. (b) The side-chains of the HCR align within Aβ; thus, aggregation is thought to be driven in part by self-recognition of these residues. (c) The HCR is exposed at the ends of Aβ aggregates and presents the binding site for the KLVFF; more binding sites are exposed in non-fibrils than fibrils. The structures in (b) and (c) were adapted from solid-state NMR structures (PDB:2BEG) [Luhrs *et al.* (2005) PNAS], and the structure in (c) is meant only to exemplify the general binding site of KLVFF at the ends of Aβ structures.

were necessary and sufficient for self-assembly; 10-mer truncations of the Aβ peptide were evaluated for binding to full-length Aβ, and only three of the 31 truncations (10-19, 11-20, 12-21) showed significant binding [98]. Shortened fragments of the Aβ peptide (3-10 amino acids in length) were then constructed to determine the minimal requirement for binding by an external

peptide. The 5-mer KLVFF displayed the greatest binding to Aβ (1-40), while 3- or 4-mers containing the residues KLVFF showed no binding. These effects were further confirmed by amino acid substitution analysis of the entire Aβ peptide through proline [99] and alanine [100] scanning. These studies revealed the Val18, Phe19, and Phe20 are particularly destabilized upon substitution. Interestingly, Phe19 differentially contributes toward early oligomerization, depending upon whether Aβ (1-40) or (1-42) is present [101].

Chemical modifications to the amide backbone within the HCR further highlight the importance of this region for self-assembly. Substitution of the amide bond between residues Phe19 and Phe20 with an *E*-olefin bond was performed in order to test the effects of removing the hydrogen-bond (H-bond) donating and accepting capabilities of the HCR [102]. The resulting peptide, EOAβ, was analyzed using ThT fluorescence, and displayed comparable aggregation to the wild-type (WT) peptide. However, distinct differences between WT and EOAβ were observed by circular dichroism (CD). A local minimum at 217 nm, a hallmark of cross-β-sheet structure observed in WT, was nearly absent in EOAβ, suggesting a potential difference in aggregate morphology. Indeed, evaluation by AFM and TEM revealed that EOAβ predominantly formed globular oligomers at early time points, which went on to form non-fibrillar, amorphous aggregates that were distinct from the elongated fibrils formed by WT Aβ. Removal of the H-bond donating nitrogen and leaving the H-bond acceptor unaltered by introducing an ester bond also affected aggregation [18]. Interestingly, like EOAβ, the amide-to-ester variants showed unique characteristics of Aβ aggregation that were dependent upon the location of the ester bond. Aβ peptides with ester bonds at Leu17, Val18, and Phe19 had an increased rate in self-assembly compared to WT, whereas the Phe20-ester peptide displayed a reduced rate of

24

aggregation. Thus, these variants retained the ability to self-assemble, but TEM analysis revealed that they formed amorphous aggregates that were distinct from WT Aβ fibrils.

Similarly, several groups have altered the H-bond network within the HCR by N-methylation, also resulting in Aβ peptides with distinct aggregation properties. Analogous to incorporation of an ester bond, N-methylation is a classical technique for probing the H-bond character of a peptide backbone. In order to test the contributions of two H-bond donors within the HCR, Gordon *et al.* incorporated N-methyl groups at Leu17 and Phe19 into Aβ (1-40) to generate the peptide 2NMe(Nterm) [103]. Using ThT to monitor self-assembly, 2NMe(Nterm) showed no increase in fluorescence above background, suggesting either a lack of aggregation and/or β-sheet content. Indeed, CD revealed no significant evolution of secondary structure past the initial unfolded state. TEM analysis displayed the presence of unique fibril morphology, consisting of fibrils coated with 'fuzzy' edges of amorphous aggregate. Further, the mean fibril diameter was reduced relative to WT. Collectively, these data confer the sensitivity of the HCR to even minor modifications to the H-bond network, thereby highlighting its critical contribution toward fibril formation. Because of the importance of this region toward self-assembly, these studies also suggest that the HCR could be used in rational design of chemical probes.

1.4.2 KLVFF motifs are aligned in Aβ fibrils and free sites are available at the "ends"

Mature fibrils have a largely parallel β-sheet structure, such that the residues in this region are aligned (*e.g.* Phe 19 from one strand is stacked against Phe 19 from the next monomer) (Figure 1.8b). Even in pre-fibrillar samples, which contain both parallel and anti-parallel β-sheets [104, 105], KLVFF regions are thought to be partially aligned, especially at the core Phe19 residue [106, 107]. These observations suggest that free KLVFF peptides will tend to align with their

corresponding residues in both pre-fibrillar and fibrillar amyloids. Consistent with this idea, early structure-activity studies revealed that the peptides KLVFF, QKLVFF, HQKLVFF, KLVFFA, KLVFFAE, and QKLVFFA bound with the best affinity to Aβ (1-40) fibrils [108]. This hypothesis was later confirmed using 38 fluorescently-labeled 5-mer fragments corresponding to regions of the Aβ peptide [109].

Another critical feature of the KLVFF-binding site is that it will be exposed at the 'ends' of aggregates (Figure 1.8c). Indeed, extensive hydrogen-deuterium exchange (HDX) and solution-state NMR studies have shown that these residues are poorly solvent-accessible in the core of fibrils [105, 110, 111] while they are more exposed in pre-fibrillar species. For example, only Leu17 and Val18 within the HCR are buried in LMW Aβ and only Leu17, Val18 and Phe19 In globular oligomers [110]. Thus, opposite to what was discussed for ThT- and CR-binding sites, there may be more KLVFF-binding sites in solutions of early amyloid species [112]. Moreover, in the context of this review, these observations are of interest because they suggest that KLVFF-based peptides might be used to probe the chemical and structural environment around the free "ends" of amyloids. As discussed above, ThT- and CR-like ligands populate this region (BS3 and BS4), but with low abundance and weak affinity.

1.4.3 KLVFF does not inhibit aggregation or form fibrils

KLVFF was initially characterized as an inhibitor of Aβ aggregation based on a modest reduction in fibril formation using TEM, where Aβ (1-40) was incubated with an equimolar amount of KLVFF [98]. However, since this initial observation, the collective literature regarding the effects of KLVFF on Aβ aggregation are conflicting. In contrast to initial findings, at a 1:2 stoichiometric ratio of Aβ (1-39) to ligand, light scattering revealed that KLVFF actually increased the average

molecular weight of the Aβ aggregates, suggesting that KLVFF can template Aβ aggregation [113]. Using ThT fluorescence and AFM, several groups have shown that KLVFF has no effect on Aβ (1-40) aggregation [114, 115]. In addition, we have performed ThT inhibition assays with KLVFF from two independent sources, and found that KLVFF has no effect on
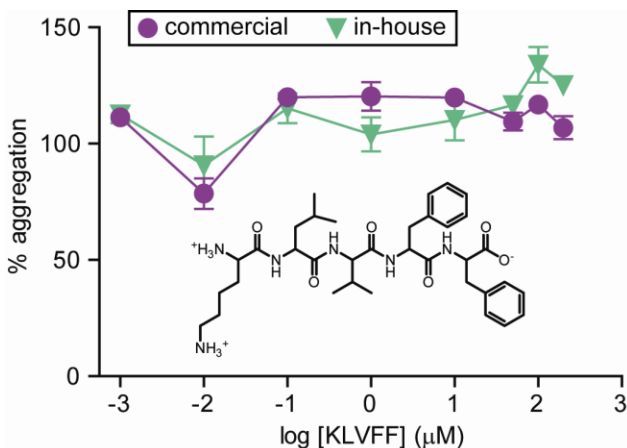
Figure 1.9 KLVFF does not inhibit Aβ aggregation. ThT fluorescence was used to quantify the amount of Aβ aggregation upon KLVFF administration. KLVFF was obtained from two sources; commercial (purple) and synthesized in-house (green). Percent aggregation does not significantly change under these conditions ($IC_{50} > 200$ μM). The chemical structure of KLVFF is shown (inset).

aggregation ($IC_{50} > 200$ μM) (Figure 1.9). Because KLVFF does not interfere with self-assembly, it may be a useful probe for Aβ structure, as we describe in detail in Chapter 4.

A second point of contention in the literature is whether KLVFF itself is capable of forming amyloid fibrils. Several studies suggest that KLVFF is not sufficient to form aggregates [116, 117]. However, as discussed in Chapter 4, slight modifications, such as including 2-3 additional residues of the Aβ sequence, results in fragments that are able to fibrillize [33, 116]. Alternatively, Meredith and coworkers suggest that KLVFF alone is sufficient to form fibrils, as shown by TEM and CR binding [118]. The authors state that although KLVFF self-assembles into fibrils, these fibrils are insufficient to cause ThT fluorescence. However, the concentration of peptide used in this experiment is not given, and perhaps high concentrations are necessary to induce aggregation. Despite these conflicting reports, KLVFF and its derivatives remain the most utilized peptide-based modulators and probes of Aβ. Below, we explore these derivatives and what they reveal about Aβ structure.

1.4.4 Using Aβ (16-22) to explore structure

Previous studies suggest that Aβ (16-22) was one of the shortest fragments capable of forming fibrils [116]. Tycko and colleagues were the first to utilize this fragment for structural studies of Aβ fibrils [33]. Balbach *et al.* employed solid-state NMR to explore β-strand orientation in
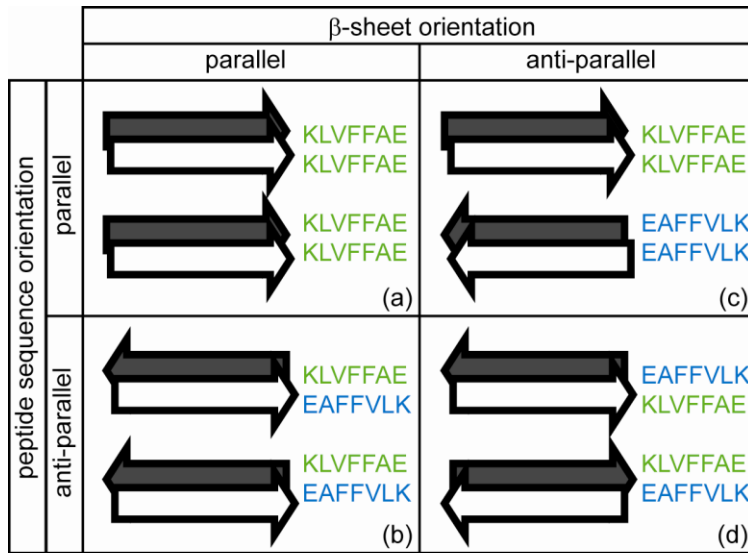
Figure 1.10 Potential β-sheet and peptide orientations of KLVFF. A fragment of the HCR within Aβ, corresponding to residues KLVFFAE, is used to model different combinations of β-sheet and peptide orientation. The β-sheet could exist in parallel (a and b) or anti-parallel (c and d) orientations, while the peptide may interact with its neighboring sequence in a parallel (a and c) or anti-parallel (b and d) fashion. See text (1.4.4) for a detailed description of the results of this molecular dynamics study. Together, these findings indicate that KLVFF may exist in more than one stable orientation.

fibrils composed of this seven-residue fragment. The NMR data suggest these fibrils were organized in an anti-parallel β-sheet orientation. Using the same approach, however, this group also indicated that full-length Aβ (1-40) fibrils adopts a parallel β-sheet structure [119]. Tycko and coworkers suggest that Aβ fibrils are capable of forming a variety of β-sheet orientations, and that the structure is dependent upon the length of the peptide used[33]. Several groups have also employed Aβ (16-22) to explore the strand orientation within and oligomers [120-122]. Ma and Nussinov used MD simulations of five different KLVFFAE octamers to explore both β-sheet orientation and the peptide directionality [120]. Three parallel and two anti-parallel β-sheet arrangements were used, with the peptides either in the same direction (parallel: KLVFFAE binds KLVFFAE) or opposing one another (anti-parallel: KLVFFAE binds EAFFVLK) (Figure 1.10). Interestingly, they found that two of the three parallel β-sheet orientations were unstable and

dissociated quickly. The third parallel arrangement was different in that its peptide orientation was anti-parallel, which lent the structure significantly more stability. Further, both anti-parallel β-sheet arrangements were quite stable, independent of peptide directionality. The stability of the anti-parallel β-sheet arrangement in oligomeric Aβ was supported by further MD simulations [121].

In addition, spectroscopic approaches have recently been used to show that the anti-parallel β-sheet orientation serves as a 'signature' of oligomeric Aβ. Cerf *et al.* developed globular, A11-reactive oligomers that were additionally assessed by electrophoresis, AFM, and ThT fluorescence [104]. The spectra of these oligomers were then compared to fibrils using attenuated total reflection (ATR) Fourier-transform infrared (FTIR) spectroscopy. Using this technique, parallel and anti-parallel β-sheets give unique spectra within the amide I region (1700-1600 cm^{-1}). Characteristically, parallel arrangements give only a major peak at 1630 cm^{-1}. In contrast, anti-parallel β-sheets display two peaks (1695 and 1630 cm^{-1}), and the ratio of these components has been shown to represent the percentage of overall anti-parallel β-sheet character. Aβ (1-42) fibrils showed only an intense peak at 1630 cm^{-1}, whereas oligomeric Aβ, independent of preparation, displayed characteristic peaks at both 1630 and 1695 cm^{-1}. The ratio of these intensities indicates that the oligomers were composed almost completely of anti-parallel β-sheet structure. In a follow-up study, the authors exploit this unique difference in FTIR spectra to monitor the progression of Aβ aggregation from oligomer to fibril [123]. In this regard, exploiting Aβ (16-22) for its aggregation abilities served as a predictive model for the behavior of the full-length peptide.

In addition to fibrils and oligomers, Aβ (16-22) has been used to investigate early Aβ oligomers. Rohrig *et al.* evaluated both the structure and stability Aβ oligomers composed of 2, 3, 4, 8, 16, and 32 peptides [122]. Interestingly, they found dimers and trimers composed of this fragment to be extremely unstable, and that only oligomers composed of at least four peptides were required for metastable intermediates. MD simulations using the full-length Aβ peptide support similar conclusions. Recent studies are in agreement that the Aβ dimer is much less stable and more dynamic than later species, independent of peptide length [112].

1.4.5 Interactions of KLVFF derivatives with Aβ

Because the natural KLVFF sequence aligns with itself in amyloids, structure-activity studies on modified KLVFF motifs can be used to probe the structural requirements in this region. For example, Cairo *et al.* used SPR to determine the affinity of 24 KLVFF-based ligands for fibrils [124]. They discovered that KLVFF has a low binding affinity (K_d = 1.4 mM), consistent with its inability to inhibit aggregation [114, 115]. The specific requirement for aromatic side-chains was demonstrated by the 10-fold loss in affinity upon removal of the terminal Phe residue and the 3-fold loss in affinity upon replacement of Phe with His residues (KLVFH, KLVHH). In contrast, systematic substitution of the Phe residues for Tyr (KLVYF, KLVFY) did not dramatically alter affinity (K_d = 1.6 – 2.4 mM). However, there appears to be limits to these substitutions because introduction of a Trp residue (KLVFW) or two Tyr residues (KLVYY) was not well tolerated. Interestingly, the all D-KLVFF stereoisomer shows no difference in binding affinity [124, 125], suggesting that the identity and order of the residues is more important than their position relative to the backbone. Consistent with this idea, substitution of the amide bond with either ester or N-methyl groups has little effect [103, 118, 126]. Collectively, these findings suggest

that the side-chains of KLVFF are critical for recognition, but that the backbone does not significantly participate in binding.

Although the core KLVFF sequence itself is somewhat sensitive to relatively minor changes, additions to either end seem well tolerated. For instance, appending polar residues, including stretches of lysines or arginines (KLVFFK$_4$, KLVFFK$_6$, and KLVFFR$_6$) significantly improves binding affinity (K_d = 37-80 μM) [124]. These residues might make favorable contacts with residues adjacent to the HCR to add additional binding energy. Further, the addition of the lysines was preferred on the C-terminal end of the molecule, as KLVFFK$_4$ displayed nearly a 5-fold better affinity than K$_4$LVFF. Similarly, addition of bulky moieties to the N-terminus of KLVFF are tolerated, and, in some cases, improve recognition. For example, replacement of the lysine of KLVFF with a sterol had no effect on Aβ binding [127]. Further, Gordon *et al.* showed that a synthetic analog of KLVFF containing an N-terminal anthranilic acid showed 5-fold higher binding to Aβ [118].
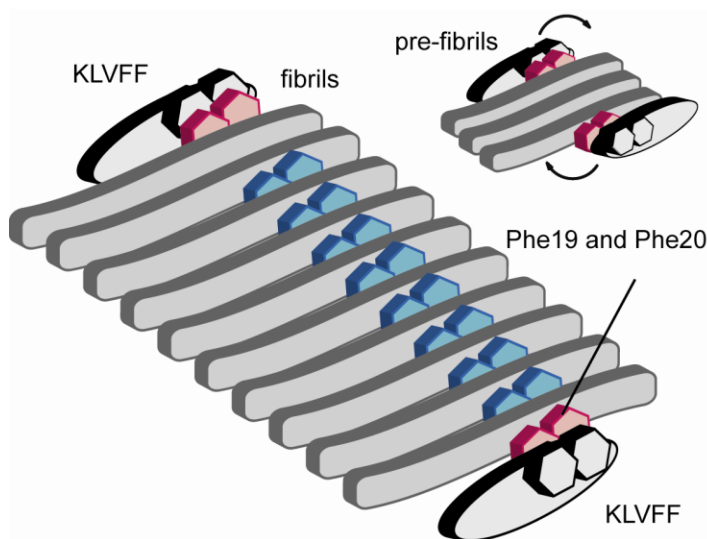
Figure 1.11 Phenylalanine contacts drives KLVFF. Binding Studies of KLVFF converge on a model in where the binding site exists on exposed ends of Aβ aggregates. These sites are present on multiple conformations of Aβ, including LMW species and fibrils. KLVFF may bind in multiple orientations and phenyl-alanine recognition drives affinity. Substitution of these residues for polar, uncharged, or even other aromatics is not well-tolerated. In pre-fibrils, two distinct orientations may be accessed.

Together, these studies produce a model in which KLVFF binds sites at the ends of amyloids in either a parallel or anti-parallel mode (Figure 1.11). The side-chains, specifically the phenylalanine residues, predominantly drive binding, with little contribution from the peptide backbone. Further, polar and non-polar groups could be appended to KLVFF to enhance its binding. In this regard, KLVFF may be a useful 'anchor' molecule for probing the surrounding regions at the ends of Aβ aggregates.

1.5 Conformation-specific Aβ probes

1.5.1 Pre-fibrillar Aβ correlates with pathology

As mentioned earlier, both *in vitro* and *in vivo*, the Aβ peptide self-assembles into a myriad of distinct conformations. These conformations are unique in their ultrastructure, and, in addition, confer a range of biological outputs. Yet, the contribution of each of these species toward disease remains unclear. The most recent evidence suggests that pre-fibrillar Aβ aggregates, including dimers, trimers, tetramers, and globular oligomers, are more neurotoxic than monomeric or fibrillar Aβ, suggesting a potential role in the pathology of AD. One of the first accounts of soluble, 'pre-amyloid' (*e.g.* pre-fibril) Aβ was by LeVine in 1995, and he later showed that synthetic Aβ forms oligomeric structures at physiological concentrations [128]. Importantly, the oligomers that are observed in the AD brain mimic both the ultrastructure and biological toxicity of those generated *in vitro* [3]. Over the past decade, studies focusing on Aβ oligomers as the key neurotoxic structure have increased dramatically. These findings show that oligomeric Aβ is sufficient to impair cognitive function [129], inhibit LTP in brain tissue [130] and rats *in vivo* [131], and promote LTD [132]. Further, oligomers have been shown to correlate with synaptic toxicity [93], which can be partially inhibited by antibodies against oligomers [4]. Pre-fibrils may impair memory by inhibiting synapse remodeling, which is required for memory

consolidation [133], or by membrane permeabilization [134-136], but the precise mechanisms of neurodegeneration remain unclear. These data have been extensively reviewed for Aβ aggregates as well as other amyloidogenic oligomers [5-8, 137-140]. As discussed in detail in Chapter 4, LMW Aβ (*e.g.* dimers, trimers, etc.) have recently been shown to also correlate with neurotoxicity.

1.5.2 LMW Aβ, oligomers, and fibrils are structurally unique

Why might chemical probes be capable of discriminating between Aβ conformations? Oligomers and fibrils, while markedly distinct in size, shape, and ultrastructure, are, at a molecular level, composed of the same peptide repeat. In fact, they both share β-sheet secondary structure, suggesting that purely by scale, small molecules may not be capable of selectively interacting with only one Aβ conformation. However, extensive NMR[105, 141, 142], microscopy [143-145], hydrogen-deuterium exchange (HDX) [51, 105, 110, 146], Fourier-transform infrared (FTIR) [104, 123], fluorescent resonance energy transfer (FRET) [147], antibody recognition [148-150], stability [151], and MD simulation [105, 112] data collectively reveal that monomeric, LMW, oligomeric, and fibrillar Aβ are indeed structurally distinct. Recently, in a series of manuscripts, Raussens and colleagues have applied FTIR spectroscopy to show that fibrils are organized into parallel β-sheets, while A11-positive oligomers were composed of anti-parallel β-sheet structure [104]. They suggest that this unique difference in secondary structure serves as a potential 'signature' for oligomeric Aβ. Interestingly, this spectroscopic signature can be exploited to monitor Aβ oligomerization over time, in where a striking inverse relationship between ThT fluorescence and oligomer-specific FTIR readout has been observed [123].

Perhaps the most relevant data regarding selective chemical probes is the evidence that Aβ conformations differ in their exposure to solvent, and thus accessibility to potential binding sites. Structural differences between LMW, oligomeric, and fibrillar Aβ have been confirmed using HDX. Wetzel and colleagues showed that the core of Aβ fibrils is extremely resistant to solvent exchange [146]. It was not until recently, however, that appreciable data emerged regarding LMW and oligomeric Aβ. Qi *et al.* showed that oligomeric and intermediate Aβ incorporated deuterium at a rate 10-fold greater than fibrils [51]. Accordingly, several studies monitored deuterium exchange for each region of the peptide over the course of aggregation [105, 110]. These data show that the accessibility of the N-terminus (1-16) and C-terminus (36-40) do not differ significantly in monomers, LMW, HMW, and fibrillar Aβ. However, the central portions of the peptide undergo significant decreases in solvent exposure upon aggregation. Specifically, residues 21-23 become almost completely inaccessible between the monomer and LMW transition, while the LMW to HMW transition is responsible for burying the majority of residues 17-19 [110]. These subtle but distinct changes could be exploited for selective binding by chemical probes. Based on these differences in accessibility, and thus binding epitopes, it follows that conformation-specific antibodies can be generated [148, 149]. Perhaps the most significant of these antibodies is the oligomer-specific A11 antibody [150]. A11 selectively recognizes the globular oligomeric form of amyloidogenic proteins, independent of sequence, providing evidence that amyloid conformations may be differentially recognized by other proteins, and lending rationale for developing analogous small molecule probes.

1.5.3 Conformation-specific small molecule inhibitors

Despite the inherent heterogeneity of Aβ aggregate samples, current protocols for generating predominately dimers [2, 152], LMW species [153], globular oligomers [1, 26, 154], and fibrils [1,

151] are established. One of the main applications of these methods has been to screen for conformation-specific small molecule inhibitors. Together with specific protocols engineered for oligomer stabilization, Necula *et al.* combined the use of their oligomer-specific antibody (A11), TEM, dot-blot analysis, and native-gel electrophoresis to screen 42 chemically diverse compounds for inhibition of oligomer or fibril formation [26]. Three separate classes of aggregation inhibitors were observed; Class I inhibited oligomerization but not fibrillization, Class II inhibited both, and Class III inhibited fibrillization but not oligomerization. These data were integral in suggesting that the pathways, at least *in vitro*, for Aβ oligomerization and fibrillization may be independent. In a follow-up study, the authors found that MB selectively inhibits oligomer formation by promoting fibril nucleation, suggesting that MB may interact preferentially with a conformation that favors fibril formation [155]. Significantly, these studies were some of the first to suggest that small molecules may interact with distinct Aβ conformations, and suggest that differences in ultrastructure may be exploited by small molecules.

1.5.4 LCPs respond uniquely to distinct amyloid conformations

Given the multitude of Aβ conformations, an ideal probe may be one that interacts with many Aβ species, with each interaction yielding a distinct readout. Toward this goal, Nilsson, Hammarstrom, and coworkers have performed pioneering studies using novel luminescent-conjugated polymers (LCPs) to selectively detect amyloids (Figure 1.12). Some of the most utilized LCPs for amyloid detection are polythiophene derivatives; these molecules display unique emission spectra based on the structure and assembly of the interacting amyloid. When these polymers engage their target, they are designed to adopt a backbone orientation that conforms to the size and shape of the bound structure. This re-arrangement aligns the polymer

scaffold and alters the apparent fluorescence properties, yielding an "optical fingerprint" specific to the bound amyloid. An advantage of LCPs over classical fluorescent dyes, such as the more rigid, planar CR and ThT, is their inherent diversity. CR and ThT have only dual spectra states (bound or unbound), while LCPs allow a spectrum of emission outcomes depending upon their interaction with different aggregation states [156]. Based on this diversity, these molecules have the potential to monitor progression from monomer to fibril with unique readouts for each intermediate. An extensive discussion on this topic has recently been reviewed by these authors [157].

Briefly, first-generation conjugated polymers (CPs) include the polythiophene-based molecule POWT, which undergoes structural transitions in the presence of peptides designed to adopt various conformations [158]. Further, the emission maxima of eight chemically diverse polythiophenes each differed in the presence of native insulin monomer versus insulin fibrils, suggesting this approach could be useful toward amyloid conformations [159, 160]. Thus, using

(a) conjugated polythiophenes

(b) indoles

(c) PG46

DAEFRHDSGYEVHHQKLVFFA***EHRWCCPGCCKTFGA***IIGLMVGGVV

signal domain

(d) bivalent KLVFF

linker region
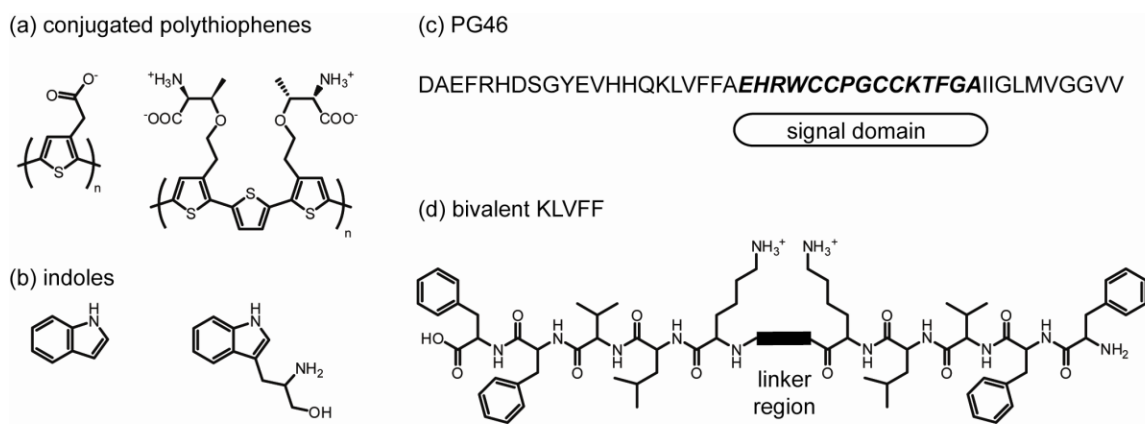
Figure 1.12 Chemical structures of conformation-selective amyloid probes (a) Luminescent conjugated poly-thiophenes (LCPs) display distinct spectroscopic properties when bound to different regions of Aβ deposits. (b) As detailed in Chapter 3, the fluorescence of indole-containing scaffolds is selectively quenched in the presence of amyloid pre-fibrils, but no change is observed upon fibril addition. This property allows for monitoring pre-fibril levels throughout the aggregation process. (c) A region of the Aβ peptide is replaced with a 'signal domain' to yield a peptide probe that induces fluorescence of a dye only in the presence of Aβ oligomers. No fluorescence is observed in the presence of LMW and fibrillar Aβ. (d) We describe in Chapter 4 that two KLVFF binding elements are joined through a flexible linker region, yielding a probe with enhanced avidity and selectivity for Aβ. These scaffolds selectively bind trimer and tetramer, with no significant recognition of monomer or high molecular weight aggregates.

multiphoton microscopy, Nilsson *et al.* applied second-generation LCPs to probe amyloid deposits in tissue [161]. Significantly, they found that their probes emitted at various wavelengths depending upon the nature of the amyloid within the tissue. For example, in the presence of senile plaques, the interaction of PTAA with $A\beta$ induced a red fluorescence, whereas a blue-green fluorescence was observed upon PTAA binding to intracellular $A\beta$. The use of LCPs has also been demonstrated *in vivo*. Berg *et al.* presented that luminescence-conjugated oligothiophenes (LCOs) could be used to image amyloid deposits composed of $A\beta$ (1-40), $A\beta$ (1-42), tau, and transthyretin in *Drosophila* [162]. Perhaps one of the most applicable findings to AD from this manuscript were that $A\beta$ (1-42) and tau, both of which deposit in brain tissue of AD patients, display distinct fluorescence staining with an LCO in a single brain tissue slice. Together, these findings do suggest that distinct amyloid morphologies co-localize in diseased brain tissue.

1.5.5 Indoles selectively detect amyloid pre-fibrils

ThT has been considered the 'gold standard' for monitoring amyloid aggregation *in vitro* and is perhaps the most used probe for quantifying fibril formation. In order to specifically monitor pre-fibril progression, we sought to identify conformation-specific $A\beta$ probes that could easily be used alongside ThT to monitor aggregation. In Chapter 3, we present a screen of a diverse small molecule collection for changes in fluorescence in the presence of pre-fibrils and fibrils [151]. Briefly, we found that the fluorescence of five indole-containing compounds was quenched in the presence of pre-fibrils, but was unchanged upon addition of fibrils (Figure 1.12). Following our initial pre-fibril selectivity screen, we tailored this fluorescence response for monitoring pre-fibril depletion over time, also described in Chapter 3, in order to optimize the change in fluorescence, we evaluated an expanded collection of 35 indole-based scaffolds [163]. The most

selective candidate, tryptophanol (TROL), was used for further assay development. We found that over time, the change in TROL fluorescence decreased, and was inversely proportion to ThT fluorescence. Further, we monitored the self-assembly of several amyloidogenic proteins over time, and found that TROL can be applied to monitor pre-fibril depletion of in other amyloid systems, making TROL the first pre-fibril selective probe for monitoring amyloid aggregation over time. We present future applications of TROL in Chapter 5.

1.5.6 Peptide-based approaches for selective Aβ probes

In addition to small molecule screening approaches, we and others have used peptide-based techniques to generate conformation-specific ligands. Recently, Hu *et al.* designed a peptide probe, PG46, containing three quarters of the amino acid sequence of Aβ (1-40) (Figure 1.12). Within the central part of the molecule, a 'signal domain' that is 15 residues in length replaced the native residues 22-30, a region that has been shown to be structurally distinct in LMW, oligomeric and fibrillar Aβ. The purpose of incorporating the signal domain, which contains a tetracysteine motif, is to interact with a conformation-sensitive dye FlAsH [164]. Upon binding to the tetracysteine motif, FlAsH becomes rapidly fluorescent. The authors hypothesize that the signal domain, and therefore FlAsH binding, may be distinct in various Aβ conformations. Indeed, FlAsH fluorescence only increased in the presence of globular, A11-positive oligomers, and no changes in fluorescence were found in the presence of LMW or fibrillar Aβ. Future application of this probe in tissue and biological samples may be useful in probing the roles of globular oligomers in disease.

As detailed in Chapter 4, we incorporate a small fragment of Aβ into probes to target LMW aggregates. As mentioned previously, KLVFF binds Aβ with a low affinity (K_d 1.4 mM). Based on

earlier evidence that multiple displays of KLVFF increase its inhibition capacity for Aβ [117, 125], as well as basic principles of multivalency [165], we hypothesized that bivalent KLVFF would bind Aβ with increased avidity. Further we envisioned that we could tailor the linker length bridging the KLVFF recognition elements for various sizes of LMW Aβ (Figure 1.12). Importantly, we found no binding of monovalent KLVFF at low micromolar concentrations. Under these same conditions, however, we observed striking recognition of dimer through pentamer with bivalent KLVFF, with favored binding to trimer and tetramer. Significantly, we did not observe any recognition of monomer or fibrils. We discuss how this approach may be broadly applicable to other amyloids in Chapter 5. Finally, we discovered that our bivalent KLVFF ligands retain specificity for trimers and tetramers in human CSF, providing a promising basis for using these probes in complex biological samples as reporters of toxic LMW Aβ.

1.6 Concluding remarks

Classic amyloid probes like ThT and CR have played a key role in our understanding of amyloid structure and the process of self-assembly. As the appreciation of the number of different amyloid structures has broadened, these scaffolds have found exciting, new roles in characterizing previously under-appreciated amyloid conformations. However, the classic probes tend to have relatively poor selectivity. Thus, the development of next-generation ligands will be an important step in further accelerating our understanding of the roles of amyloids in disease, and this thesis describes two distinct approaches of developing these probes. Further, towards that goal, one approach that might be particularly fruitful is the use of multivalent amyloid ligands. The synthesis of bivalent, 'molecular tweezers' that bind amyloids have been reported [115, 117, 125, 166-169] and we expect that these types of scaffolds may be incorporated into the next battery of tools. This is specifically demonstrated with the bivalent

KLVFF system in Chapter 4. In turn, these designed ligands might be used to ask the next generation of questions about amyloid structure and function. Where are the small molecule-binding sites positioned in relation to one another? How does the position or number of these sites change upon transition from one conformation to another? A combination of old and new chemical probes will likely be necessary to answer these questions and others.

Notes

This work has in part been published as "Insight into Amyloid Structure Using Chemical Probes"

2011 Chemical Biology and Drug Design. *In press*.

Professor Yong Duan of UC-Davis kindly provided the PDB files for small molecules (CR, ThT) docked to amyloids.

1.7 References

[1]   Dahlgren KN, Manelli AM, Stine WB, Jr., Baker LK, Krafft GA, LaDu MJ. Oligomeric and fibrillar species of amyloid-beta peptides differentially affect neuronal viability. The Journal of biological chemistry. 2002 Aug 30;277(35):32046-53.
[2]   Shankar GM, Li S, Mehta TH, Garcia-Munoz A, Shepardson NE, Smith I, et al. Amyloid-beta protein dimers isolated directly from Alzheimer's brains impair synaptic plasticity and memory. Nature medicine. 2008 Aug;14(8):837-42.
[3]   Gong Y, Chang L, Viola KL, Lacor PN, Lambert MP, Finch CE, et al. Alzheimer's disease-affected brain: presence of oligomeric A beta ligands (ADDLs) suggests a molecular basis for reversible memory loss. Proceedings of the National Academy of Sciences of the United States of America. 2003 Sep 2;100(18):10417-22.
[4]   Klyubin I, Walsh DM, Lemere CA, Cullen WK, Shankar GM, Betts V, et al. Amyloid beta protein immunotherapy neutralizes Abeta oligomers that disrupt synaptic plasticity in vivo. Nature medicine. 2005 May;11(5):556-61.
[5]   Selkoe DJ. Soluble oligomers of the amyloid beta-protein impair synaptic plasticity and behavior. Behavioural brain research. 2008 Sep 1;192(1):106-13.
[6]   Ferreira ST, Vieira MN, De Felice FG. Soluble protein oligomers as emerging toxins in Alzheimer's and other amyloid diseases. IUBMB life. 2007 Apr-May;59(4-5):332-45.
[7]   Haass C, Selkoe DJ. Soluble protein oligomers in neurodegeneration: lessons from the Alzheimer's amyloid beta-peptide. Nature reviews. 2007 Feb;8(2):101-12.

[8]   Klein WL, Stine WB, Jr., Teplow DB. Small assemblies of unmodified amyloid beta-protein are the proximate neurotoxin in Alzheimer's disease. Neurobiology of aging. 2004 May-Jun;25(5):569-80.

[9]   O'Nuallain B, Freir DB, Nicoll AJ, Risse E, Ferguson N, Herron CE, et al. Amyloid beta-protein dimers rapidly form stable synaptotoxic protofibrils. J Neurosci. 2010 Oct 27;30(43):14411-9.

[10]   Vassar PS, Culling CF. Fluorescent stains, with special reference to amyloid and connective tissues. Arch Pathol. 1959;68:487-98.

[11]   Naiki H, Higuchi K, Hosokawa M, Takeda T. Fluorometric determination of amyloid fibrils in vitro using the fluorescent dye, thioflavin T1. Analytical biochemistry. 1989 Mar;177(2):244-9.

[12]   Naiki H, Higuchi K, Matsushima K, Shimada A, Chen WH, Hosokawa M, et al. Fluorometric examination of tissue amyloid fibrils in murine senile amyloidosis: use of the fluorescent indicator, thioflavine T. Laboratory investigation; a journal of technical methods and pathology. 1990 Jun;62(6):768-73.

[13]   LeVine H, 3rd. Thioflavine T interaction with synthetic Alzheimer's disease beta-amyloid peptides: detection of amyloid aggregation in solution. Protein Sci. 1993 Mar;2(3):404-10.

[14]   LeVine H, 3rd. Quantification of beta-sheet amyloid fibril structures with thioflavin T. Methods in enzymology. 1999;309:274-84.

[15]   Brorsson AC, Bolognesi B, Tartaglia GG, Shammas SL, Favrin G, Watson I, et al. Intrinsic determinants of neurotoxic aggregate formation by the amyloid beta peptide. Biophysical journal. 2010 Apr 21;98(8):1677-84.

[16]   Walsh DM, Hartley DM, Condron MM, Selkoe DJ, Teplow DB. In vitro studies of amyloid beta-protein fibril assembly and toxicity provide clues to the aetiology of Flemish variant (Ala692-->Gly) Alzheimer's disease. The Biochemical journal. 2001 May 1;355(Pt 3):869-77.

[17]   Paravastu AK, Qahwash I, Leapman RD, Meredith SC, Tycko R. Seeded growth of beta-amyloid fibrils from Alzheimer's brain-derived fibrils produces a distinct fibril structure. Proceedings of the National Academy of Sciences of the United States of America. 2009 May 5;106(18):7443-8.

[18]   Bieschke J, Siegel SJ, Fu Y, Kelly JW. Alzheimer's Abeta peptides containing an isostructural backbone mutation afford distinct aggregate morphologies but analogous cytotoxicity. Evidence for a common low-abundance toxic structure(s)? Biochemistry. 2008 Jan 8;47(1):50-9.

[19]   Hasegawa K, Yamaguchi I, Omata S, Gejyo F, Naiki H. Interaction between A beta(1-42) and A beta(1-40) in Alzheimer's beta-amyloid fibril formation in vitro. Biochemistry. 1999 Nov 23;38(47):15514-21.

[20]   Jan A, Gokce O, Luthi-Carter R, Lashuel HA. The ratio of monomeric to aggregated forms of Abeta40 and Abeta42 is an important determinant of amyloid-beta aggregation, fibrillogenesis, and toxicity. The Journal of biological chemistry. 2008 Oct 17;283(42):28176-89.

[21]   Singh PK, Kumbhakar M, Pal H, Nath S. Ultrafast bond twisting dynamics in amyloid fibril sensor. The journal of physical chemistry. 2010 Feb 25;114(7):2541-6.

[22]   Srivastava A, Singh PK, Kumbhakar M, Mukherjee T, Chattopadyay S, Pal H, et al. Identifying the bond responsible for the fluorescence modulation in an amyloid fibril sensor. Chemistry (Weinheim an der Bergstrasse, Germany). 2010 Aug 9;16(30):9257-63.

[23]   Masuda M, Suzuki N, Taniguchi S, Oikawa T, Nonaka T, Iwatsubo T, et al. Small molecule inhibitors of alpha-synuclein filament assembly. Biochemistry. 2006 May 16;45(19):6085-94.

[24]   Ono K, Hasegawa K, Naiki H, Yamada M. Curcumin has potent anti-amyloidogenic effects for Alzheimer's beta-amyloid fibrils in vitro. Journal of neuroscience research. 2004 Mar 15;75(6):742-50.

[25]   Reinke AA, Gestwicki JE. Structure-activity relationships of amyloid beta-aggregation inhibitors based on curcumin: influence of linker length and flexibility. Chemical biology & drug design. 2007 Sep;70(3):206-15.

[26]   Necula M, Kayed R, Milton S, Glabe CG. Small molecule inhibitors of aggregation indicate that amyloid beta oligomerization and fibrillization pathways are independent and distinct. The Journal of biological chemistry. 2007 Apr 6;282(14):10311-24.

[27]   LeVine H, 3rd. Multiple ligand binding sites on A beta(1-40) fibrils. Amyloid. 2005 Mar;12(1):5-14.

[28]   Hudson SA, Ecroyd H, Kee TW, Carver JA. The thioflavin T fluorescence assay for amyloid fibril detection can be biased by the presence of exogenous compounds. The FEBS journal. 2009 Oct;276(20):5960-72.

[29]   Inbar P, Bautista MR, Takayama SA, Yang J. Assay to screen for molecules that associate with Alzheimer's related beta-amyloid fibrils. Analytical chemistry. 2008 May 1;80(9):3502-6.

[30]   Kim W, Kim Y, Min J, Kim DJ, Chang YT, Hecht MH. A high-throughput screen for compounds that inhibit aggregation of the Alzheimer's peptide. ACS chemical biology. 2006 Aug 22;1(7):461-9.

[31]   LeVine H, 3rd. Biotin-avidin interaction-based screening assay for Alzheimer's beta-peptide oligomer inhibitors. Analytical biochemistry. 2006 Sep 15;356(2):265-72.

[32]   Zovo K, Helk E, Karafin A, Tougu V, Palumaa P. Label-Free High-Throughput Screening Assay for Inhibitors of Alzheimer's Amyloid-beta Peptide Aggregation Based on MALDI MS. Analytical chemistry. 2010 Sep 21.

[33]   Balbach JJ, Ishii Y, Antzutkin ON, Leapman RD, Rizzo NW, Dyda F, et al. Amyloid fibril formation by A beta 16-22, a seven-residue fragment of the Alzheimer's beta-amyloid peptide, and structural characterization by solid state NMR. Biochemistry. 2000 Nov 14;39(45):13748-59.

[34]   Lockhart A, Ye L, Judd DB, Merritt AT, Lowe PN, Morgenstern JL, et al. Evidence for the presence of three distinct binding sites for the thioflavin T class of Alzheimer's disease PET imaging agents on beta-amyloid peptide fibrils. The Journal of biological chemistry. 2005 Mar 4;280(9):7677-84.

[35]   Ye L, Morgenstern JL, Gee AD, Hong G, Brown J, Lockhart A. Delineation of positron emission tomography imaging agent binding sites on beta-amyloid peptide fibrils. The Journal of biological chemistry. 2005 Jun 24;280(25):23599-604.

[36]   Rodriguez-Rodriguez C, Rimola A, Rodriguez-Santiago L, Ugliengo P, Alvarez-Larena A, Gutierrez-de-Teran H, et al. Crystal structure of thioflavin-T and its binding to amyloid fibrils: insights at the molecular level. Chemical communications (Cambridge, England). 2010 Feb 21;46(7):1156-8.

[37]   Wu C, Wang Z, Lei H, Duan Y, Bowers MT, Shea JE. The binding of thioflavin T and its neutral analog BTA-1 to protofibrils of the Alzheimer's disease Abeta(16-22) peptide probed by molecular dynamics simulations. Journal of molecular biology. 2008 Dec 19;384(3):718-29.

[38]   Wu C, Wang Z, Lei H, Zhang W, Duan Y. Dual binding modes of Congo red to amyloid protofibril surface observed in molecular dynamics simulations. Journal of the American Chemical Society. 2007 Feb 7;129(5):1225-32.

[39]   Dzwolak W, Pecul M. Chiral bias of amyloid fibrils revealed by the twisted conformation of Thioflavin T: an induced circular dichroism/DFT study. FEBS letters. 2005 Dec 5;579(29):6601-3.

[40]   Biancalana M, Makabe K, Koide A, Koide S. Molecular mechanism of thioflavin-T binding to the surface of beta-rich peptide self-assemblies. Journal of molecular biology. 2009 Jan 30;385(4):1052-63.

[41]   Wu C, Biancalana M, Koide S, Shea JE. Binding modes of thioflavin-T to the single-layer beta-sheet of the peptide self-assembly mimics. Journal of molecular biology. 2009 Dec 11;394(4):627-33.

[42]   Groenning M, Norrman M, Flink JM, van de Weert M, Bukrinsky JT, Schluckebier G, et al. Binding mode of Thioflavin T in insulin amyloid fibrils. Journal of structural biology. 2007 Sep;159(3):483-97.

[43]   Groenning M. Binding mode of Thioflavin T and other molecular probes in the context of amyloid fibrils-current status. Journal of chemical biology. 2009 Aug 20.

[44]   Khurana R, Coleman C, Ionescu-Zanetti C, Carter SA, Krishna V, Grover RK, et al. Mechanism of thioflavin T binding to amyloid fibrils. Journal of structural biology. 2005 Sep;151(3):229-38.

[45]   Gellermann GP, Byrnes H, Striebinger A, Ullrich K, Mueller R, Hillen H, et al. Abeta-globulomers are formed independently of the fibril pathway. Neurobiology of disease. 2008 May;30(2):212-20.

[46]   Lacor PN, Buniel MC, Chang L, Fernandez SJ, Gong Y, Viola KL, et al. Synaptic targeting by Alzheimer's-related amyloid beta oligomers. J Neurosci. 2004 Nov 10;24(45):10191-200.

[47]   Maezawa I, Hong HS, Liu R, Wu CY, Cheng RH, Kung MP, et al. Congo red and thioflavin-T analogs detect Abeta oligomers. Journal of neurochemistry. 2008 Jan;104(2):457-68.

[48]   Ryan DA, Narrow WC, Federoff HJ, Bowers WJ. An improved method for generating consistent soluble amyloid-beta oligomer preparations for in vitro neurotoxicity studies. Journal of neuroscience methods. 2010 Jul 15;190(2):171-9.

[49]   Walsh DM, Hartley DM, Kusumoto Y, Fezoui Y, Condron MM, Lomakin A, et al. Amyloid beta-protein fibrillogenesis. Structure and biological activity of protofibrillar intermediates. The Journal of biological chemistry. 1999 Sep 3;274(36):25945-52.

[50]   Lemkul JA, Bevan DR. Assessing the stability of Alzheimer's amyloid protofibrils using molecular dynamics. The journal of physical chemistry. 2010 Feb 4;114(4):1652-60.

[51]   Qi W, Zhang A, Patel D, Lee S, Harrington JL, Zhao L, et al. Simultaneous monitoring of peptide aggregate distributions, structure, and kinetics using amide hydrogen exchange: application to Abeta(1-40) fibrillogenesis. Biotechnology and bioengineering. 2008 Aug 15;100(6):1214-27.

[52]   O'Nuallain B, Shivaprasad S, Kheterpal I, Wetzel R. Thermodynamics of A beta(1-40) amyloid fibril elongation. Biochemistry. 2005 Sep 27;44(38):12709-18.

[53]   Shivaprasad S, Wetzel R. Scanning cysteine mutagenesis analysis of Abeta-(1-40) amyloid fibrils. The Journal of biological chemistry. 2006 Jan 13;281(2):993-1000.

[54]   Klunk WE, Wang Y, Huang GF, Debnath ML, Holt DP, Mathis CA. Uncharged thioflavin-T derivatives bind to amyloid-beta protein with high affinity and readily enter the brain. Life sciences. 2001 Aug 17;69(13):1471-84.

[55]   Zhuang ZP, Kung MP, Hou C, Plossl K, Skovronsky D, Gur TL, et al. IBOX(2-(4'-dimethylaminophenyl)-6-iodobenzoxazole): a ligand for imaging amyloid plaques in the brain. Nuclear medicine and biology. 2001 Nov;28(8):887-94.

[56]   Kung MP, Hou C, Zhuang ZP, Zhang B, Skovronsky D, Trojanowski JQ, et al. IMPY: an improved thioflavin-T derivative for in vivo labeling of beta-amyloid plaques. Brain research. 2002 Nov 29;956(2):202-10.

[57]   Kung MP, Zhuang ZP, Hou C, Jin LW, Kung HF. Characterization of radioiodinated ligand binding to amyloid beta plaques. J Mol Neurosci. 2003;20(3):249-54.

[58]   Ono M, Kawashima H, Nonaka A, Kawai T, Haratake M, Mori H, et al. Novel benzofuran derivatives for PET imaging of beta-amyloid plaques in Alzheimer's disease brains. Journal of medicinal chemistry. 2006 May 4;49(9):2725-30.

[59]   Lee JH, Byeon SR, Lim SJ, Oh SJ, Moon DH, Yoo KH, et al. Synthesis and evaluation of stilbenylbenzoxazole and stilbenylbenzothiazole derivatives for detecting beta-amyloid fibrils. Bioorganic & medicinal chemistry letters. 2008 Feb 15;18(4):1534-7.

[60]   Ono M, Hayashi S, Kimura H, Kawashima H, Nakayama M, Saji H. Push-pull benzothiazole derivatives as probes for detecting beta-amyloid plaques in Alzheimer's brains. Bioorganic & medicinal chemistry. 2009 Oct 1;17(19):7002-7.

[61]   Cui MC, Li ZJ, Tang RK, Liu BL. Synthesis and evaluation of novel benzothiazole derivatives based on the bithiophene structure as potential radiotracers for beta-amyloid plaques in Alzheimer's disease. Bioorganic & medicinal chemistry. 2010 Apr 1;18(7):2777-84.

[62]   Zhuang ZP, Kung MP, Hou C, Skovronsky DM, Gur TL, Plossl K, et al. Radioiodinated styrylbenzenes and thioflavins as probes for amyloid aggregates. Journal of medicinal chemistry. 2001 Jun 7;44(12):1905-14.

[63]   Lin KS, Debnath ML, Mathis CA, Klunk WE. Synthesis and beta-amyloid binding properties of rhenium 2-phenylbenzothiazoles. Bioorganic & medicinal chemistry letters. 2009 Apr 15;19(8):2258-62.

[64]   Wang Y, Mathis CA, Huang GF, Debnath ML, Holt DP, Shao L, et al. Effects of lipophilicity on the affinity and nonspecific binding of iodinated benzothiazole derivatives. J Mol Neurosci. 2003;20(3):255-60.

[65]   Mathis CA, Wang Y, Holt DP, Huang GF, Debnath ML, Klunk WE. Synthesis and evaluation of 11C-labeled 6-substituted 2-arylbenzothiazoles as amyloid imaging agents. Journal of medicinal chemistry. 2003 Jun 19;46(13):2740-54.

[66]   Kung MP, Hou C, Zhuang ZP, Cross AJ, Maier DL, Kung HF. Characterization of IMPY as a potential imaging agent for beta-amyloid plaques in double transgenic PSAPP mice. European journal of nuclear medicine and molecular imaging. 2004 Aug;31(8):1136-45.

[67]   Kung MP, Hou C, Zhuang ZP, Skovronsky DM, Zhang B, Gur TL, et al. Radioiodinated styrylbenzene derivatives as potential SPECT imaging agents for amyloid plaque detection in Alzheimer's disease. J Mol Neurosci. 2002 Aug-Oct;19(1-2):7-10.

[68]   Zhuang ZP, Kung MP, Wilson A, Lee CW, Plossl K, Hou C, et al. Structure-activity relationship of imidazo[1,2-a]pyridines as ligands for detecting beta-amyloid plaques in the brain. Journal of medicinal chemistry. 2003 Jan 16;46(2):237-43.

[69]   Klunk WE, Engler H, Nordberg A, Wang Y, Blomqvist G, Holt DP, et al. Imaging brain amyloid in Alzheimer's disease with Pittsburgh Compound-B. Annals of neurology. 2004 Mar;55(3):306-19.

[70]   Mathis CA, Lopresti BJ, Klunk WE. Impact of amyloid imaging on drug development in Alzheimer's disease. Nuclear medicine and biology. 2007 Oct;34(7):809-22.

[71]   Frid P, Anisimov SV, Popovic N. Congo red and protein aggregation in neurodegenerative diseases. Brain research reviews. 2007 Jan;53(1):135-60.

[72]   Howie AJ, Brewer DB. Optical properties of amyloid stained by Congo red: history and mechanisms. Micron. 2009 Apr;40(3):285-301.

[73]   Howie AJ, Brewer DB, Howell D, Jones AP. Physical basis of colors seen in Congo red-stained amyloid in polarized light. Laboratory investigation; a journal of technical methods and pathology. 2008 Mar;88(3):232-42.

[74]   Klunk WE, Pettegrew JW, Abraham DJ. Quantitative evaluation of congo red binding to amyloid-like proteins with a beta-pleated sheet conformation. J Histochem Cytochem. 1989 Aug;37(8):1273-81.

[75]   Klunk WE, Pettegrew JW, Abraham DJ. Two simple methods for quantifying low-affinity dye-substrate binding. J Histochem Cytochem. 1989 Aug;37(8):1293-7.

[76]   Klunk WE, Jacob RF, Mason RP. Quantifying amyloid by congo red spectral shift assay. Methods in enzymology. 1999;309:285-305.

[77]   Klunk WE, Jacob RF, Mason RP. Quantifying amyloid beta-peptide (Abeta) aggregation using the Congo red-Abeta (CR-abeta) spectrophotometric assay. Analytical biochemistry. 1999 Jan 1;266(1):66-76.

[78]   Klunk WE, Debnath ML, Pettegrew JW. Development of small molecule probes for the beta-amyloid protein of Alzheimer's disease. Neurobiology of aging. 1994 Nov-Dec;15(6):691-8.

[79]   Petkova AT, Ishii Y, Balbach JJ, Antzutkin ON, Leapman RD, Delaglio F, et al. A structural model for Alzheimer's beta -amyloid fibrils based on experimental constraints from solid state NMR. Proceedings of the National Academy of Sciences of the United States of America. 2002 Dec 24;99(26):16742-7.

[80]   Keshet B, Gray JJ, Good TA. Structurally distinct toxicity inhibitors bind at common loci on beta-amyloid fibril. Protein Sci. 2010 Sep 29.

[81]   Hong HS, Rana S, Barrigan L, Shi A, Zhang Y, Zhou F, et al. Inhibition of Alzheimer's amyloid toxicity with a tricyclic pyrone molecule in vitro and in vivo. Journal of neurochemistry. 2009 Feb;108(4):1097-108.

[82]   Mathis CA, Wang Y, Klunk WE. Imaging beta-amyloid plaques and neurofibrillary tangles in the aging human brain. Current pharmaceutical design. 2004;10(13):1469-92.

[83]   Styren SD, Hamilton RL, Styren GC, Klunk WE. X-34, a fluorescent derivative of Congo red: a novel histochemical stain for Alzheimer's disease pathology. J Histochem Cytochem. 2000 Sep;48(9):1223-32.

[84]   Skovronsky DM, Zhang B, Kung MP, Kung HF, Trojanowski JQ, Lee VM. In vivo detection of amyloid plaques in a mouse model of Alzheimer's disease. Proceedings of the National Academy of Sciences of the United States of America. 2000 Jun 20;97(13):7609-14.

[85]   Crystal AS, Giasson BI, Crowe A, Kung MP, Zhuang ZP, Trojanowski JQ, et al. A comparison of amyloid fibrillogenesis using the novel fluorescent compound K114. Journal of neurochemistry. 2003 Sep;86(6):1359-68.

[86]   Klunk WE, Bacskai BJ, Mathis CA, Kajdasz ST, McLellan ME, Frosch MP, et al. Imaging Abeta plaques in living transgenic mice with multiphoton microscopy and methoxy-X04, a systemically administered Congo red derivative. Journal of neuropathology and experimental neurology. 2002 Sep;61(9):797-805.

[87]   Ortica F, Rodgers MA. A laser flash photolysis study of curcumin in dioxane-water mixtures. Photochemistry and photobiology. 2001 Dec;74(6):745-51.

[88]   Yanagisawa D, Shirai N, Amatsubo T, Taguchi H, Hirao K, Urushitani M, et al. Relationship between the tautomeric structures of curcumin derivatives and their Abeta-binding activities in the context of therapies for Alzheimer's disease. Biomaterials. 2010 May;31(14):4179-85.

[89]   Yang F, Lim GP, Begum AN, Ubeda OJ, Simmons MR, Ambegaokar SS, et al. Curcumin inhibits formation of amyloid beta oligomers and fibrils, binds plaques, and reduces amyloid in vivo. The Journal of biological chemistry. 2005 Feb 18;280(7):5892-901.

[90]   Tubis M, Blahd WH, Nordyke RA. The preparation and use of radioiodinated Congo red in detecting amyloidosis. Journal of the American Pharmaceutical Association. 1960 Jul;49:422-5.

[91]   Klunk WE, Debnath ML, Pettegrew JW. Chrysamine-G binding to Alzheimer and control brain: autopsy study of a new amyloid probe. Neurobiology of aging. 1995 Jul-Aug;16(4):541-8.

[92]   LeVine H, 3rd. Mechanism of A beta(1-40) fibril-induced fluorescence of (trans,trans)-1-bromo-2,5-bis(4-hydroxystyryl)benzene (K114). Biochemistry. 2005 Dec 6;44(48):15937-43.

[93]   Koffie RM, Meyer-Luehmann M, Hashimoto T, Adams KW, Mielke ML, Garcia-Alloza M, et al. Oligomeric amyloid beta associates with postsynaptic densities and correlates with

excitatory synapse loss near senile plaques. Proceedings of the National Academy of Sciences of the United States of America. 2009 Mar 10;106(10):4012-7.

[94]   Higuchi M, Iwata N, Matsuba Y, Sato K, Sasamoto K, Saido TC. 19F and 1H MRI detection of amyloid beta plaques in vivo. Nature neuroscience. 2005 Apr;8(4):527-33.

[95]   Jarrett JT, Berger EP, Lansbury PT, Jr. The carboxy terminus of the beta amyloid protein is critical for the seeding of amyloid formation: implications for the pathogenesis of Alzheimer's disease. Biochemistry. 1993 May 11;32(18):4693-7.

[96]   Hilbich C, Kisters-Woike B, Reed J, Masters CL, Beyreuther K. Substitutions of hydrophobic amino acids reduce the amyloidogenicity of Alzheimer's disease beta A4 peptides. Journal of molecular biology. 1992 Nov 20;228(2):460-73.

[97]   Esler WP, Stimson ER, Ghilardi JR, Lu YA, Felix AM, Vinters HV, et al. Point substitution in the central hydrophobic cluster of a human beta-amyloid congener disrupts peptide folding and abolishes plaque competence. Biochemistry. 1996 Nov 5;35(44):13914-21.

[98]   Tjernberg LO, Naslund J, Lindqvist F, Johansson J, Karlstrom AR, Thyberg J, et al. Arrest of beta-amyloid fibril formation by a pentapeptide ligand. The Journal of biological chemistry. 1996 Apr 12;271(15):8545-8.

[99]   Williams AD, Portelius E, Kheterpal I, Guo JT, Cook KD, Xu Y, et al. Mapping abeta amyloid fibril secondary structure using scanning proline mutagenesis. Journal of molecular biology. 2004 Jan 16;335(3):833-42.

[100]   Williams AD, Shivaprasad S, Wetzel R. Alanine scanning mutagenesis of Abeta(1-40) amyloid fibril stability. Journal of molecular biology. 2006 Apr 7;357(4):1283-94.

[101]   Bitan G, Vollers SS, Teplow DB. Elucidation of primary structure elements controlling early amyloid beta-protein oligomerization. The Journal of biological chemistry. 2003 Sep 12;278(37):34882-9.

[102]   Fu Y, Bieschke J, Kelly JW. E-olefin dipeptide isostere incorporation into a polypeptide backbone enables hydrogen bond perturbation: probing the requirements for Alzheimer's amyloidogenesis. Journal of the American Chemical Society. 2005 Nov 9;127(44):15366-7.

[103]   Gordon DJ, Meredith SC. Probing the role of backbone hydrogen bonding in beta-amyloid fibrils with inhibitor peptides containing ester bonds at alternate positions. Biochemistry. 2003 Jan 21;42(2):475-85.

[104]   Cerf E, Sarroukh R, Tamamizu-Kato S, Breydo L, Derclaye S, Dufrene YF, et al. Antiparallel beta-sheet: a signature structure of the oligomeric amyloid beta-peptide. The Biochemical journal. 2009 Aug 1;421(3):415-23.

[105]   Yu L, Edalji R, Harlan JE, Holzman TF, Lopez AP, Labkovsky B, et al. Structural characterization of a soluble amyloid beta-peptide oligomer. Biochemistry. 2009 Mar 10;48(9):1870-7.

[106]   Hwang W, Zhang S, Kamm RD, Karplus M. Kinetic control of dimer structure formation in amyloid fibrillogenesis. Proceedings of the National Academy of Sciences of the United States of America. 2004 Aug 31;101(35):12916-21.

[107]   Gnanakaran S, Nussinov R, Garcia AE. Atomic-level description of amyloid beta-dimer formation. Journal of the American Chemical Society. 2006 Feb 22;128(7):2158-9.

[108]   Tjernberg LO, Lilliehook C, Callaway DJ, Naslund J, Hahne S, Thyberg J, et al. Controlling amyloid beta-peptide fibril formation with protease-stable ligands. The Journal of biological chemistry. 1997 May 9;272(19):12601-5.

[109]   Watanabe K, Segawa T, Nakamura K, Kodaka M, Konakahara T, Okuno H. Identification of the molecular interaction site of amyloid beta peptide by using a fluorescence assay. J Pept Res. 2001 Oct;58(4):342-6.

[110]   Zhang A, Qi W, Good TA, Fernandez EJ. Structural differences between Abeta(1-40) intermediate oligomers and fibrils elucidated by proteolytic fragmentation and hydrogen/deuterium exchange. Biophysical journal. 2009 Feb;96(3):1091-104.

[111]   Olofsson A, Sauer-Eriksson AE, Ohman A. The solvent protection of alzheimer amyloid-beta-(1-42) fibrils as determined by solution NMR spectroscopy. The Journal of biological chemistry. 2006 Jan 6;281(1):477-83.

[112]   Horn AH, Sticht H. Amyloid-beta42 oligomer structures from fibrils: a systematic molecular dynamics study. The journal of physical chemistry. 2010 Feb 18;114(6):2219-26.

[113]   Pallitto MM, Ghanta J, Heinzelman P, Kiessling LL, Murphy RM. Recognition sequence design for peptidyl modulators of beta-amyloid aggregation and toxicity. Biochemistry. 1999 Mar 23;38(12):3570-8.

[114]   Chalifour RJ, McLaughlin RW, Lavoie L, Morissette C, Tremblay N, Boule M, et al. Stereoselective interactions of peptide inhibitors with the beta-amyloid peptide. The Journal of biological chemistry. 2003 Sep 12;278(37):34874-81.

[115]   Ouberai M, Dumy P, Chierici S, Garcia J. Synthesis and biological evaluation of clicked curcumin and clicked KLVFFA conjugates as inhibitors of beta-amyloid fibril formation. Bioconjugate chemistry. 2009 Nov;20(11):2123-32.

[116]   Tjernberg LO, Callaway DJ, Tjernberg A, Hahne S, Lilliehook C, Terenius L, et al. A molecular model of Alzheimer amyloid beta-peptide fibril formation. The Journal of biological chemistry. 1999 Apr 30;274(18):12619-25.

[117]   Chafekar SM, Malda H, Merkx M, Meijer EW, Viertl D, Lashuel HA, et al. Branched KLVFF tetramers strongly potentiate inhibition of beta-amyloid aggregation. Chembiochem. 2007 Oct 15;8(15):1857-64.

[118]   Gordon DJ, Tappe R, Meredith SC. Design and characterization of a membrane permeable N-methyl amino acid-containing peptide that inhibits Abeta1-40 fibrillogenesis. J Pept Res. 2002 Jul;60(1):37-55.

[119]   Antzutkin ON, Balbach JJ, Leapman RD, Rizzo NW, Reed J, Tycko R. Multiple quantum solid-state NMR indicates a parallel, not antiparallel, organization of beta-sheets in Alzheimer's beta-amyloid fibrils. Proceedings of the National Academy of Sciences of the United States of America. 2000 Nov 21;97(24):13045-50.

[120]   Ma B, Nussinov R. Stabilities and conformations of Alzheimer's beta -amyloid peptide oligomers (Abeta 16-22, Abeta 16-35, and Abeta 10-35): Sequence effects. Proceedings of the National Academy of Sciences of the United States of America. 2002 Oct 29;99(22):14126-31.

[121]   Klimov DK, Thirumalai D. Dissecting the assembly of Abeta16-22 amyloid peptides into antiparallel beta sheets. Structure. 2003 Mar;11(3):295-307.

[122]   Rohrig UF, Laio A, Tantalo N, Parrinello M, Petronzio R. Stability and structure of oligomers of the Alzheimer peptide Abeta16-22: from the dimer to the 32-mer. Biophysical journal. 2006 Nov 1;91(9):3217-29.

[123]   Sarroukh R, Cerf E, Derclaye S, Dufrene YF, Goormaghtigh E, Ruysschaert JM, et al. Transformation of amyloid beta(1-40) oligomers into fibrils is characterized by a major change in secondary structure. Cell Mol Life Sci. 2010 Sep 19.

[124]   Cairo CW, Strzelec A, Murphy RM, Kiessling LL. Affinity-based inhibition of beta-amyloid toxicity. Biochemistry. 2002 Jul 9;41(27):8620-9.

[125]   Zhang G, Leibowitz MJ, Sinko PJ, Stein S. Multiple-peptide conjugates for binding beta-amyloid plaques of Alzheimer's disease. Bioconjugate chemistry. 2003 Jan-Feb;14(1):86-92.

[126]   Gordon DJ, Sciarretta KL, Meredith SC. Inhibition of beta-amyloid(40) fibrillogenesis and disassembly of beta-amyloid(40) fibrils by short beta-amyloid congeners containing N-methyl amino acids at alternate residues. Biochemistry. 2001 Jul 27;40(28):8237-45.

[127]   Findeis MA, Musso GM, Arico-Muendel CC, Benjamin HW, Hundal AM, Lee JJ, et al. Modified-peptide inhibitors of amyloid beta-peptide polymerization. Biochemistry. 1999 May 25;38(21):6791-800.

[128]   LeVine H, 3rd. Alzheimer's beta-peptide oligomer formation at physiologic concentrations. Analytical biochemistry. 2004 Dec 1;335(1):81-90.

[129]   Cleary JP, Walsh DM, Hofmeister JJ, Shankar GM, Kuskowski MA, Selkoe DJ, et al. Natural oligomers of the amyloid-beta protein specifically disrupt cognitive function. Nature neuroscience. 2005 Jan;8(1):79-84.

[130]   Wang HW, Pasternak JF, Kuo H, Ristic H, Lambert MP, Chromy B, et al. Soluble oligomers of beta amyloid (1-42) inhibit long-term potentiation but not long-term depression in rat dentate gyrus. Brain research. 2002 Jan 11;924(2):133-40.

[131]   Walsh DM, Klyubin I, Fadeeva JV, Cullen WK, Anwyl R, Wolfe MS, et al. Naturally secreted oligomers of amyloid beta protein potently inhibit hippocampal long-term potentiation in vivo. Nature. 2002 Apr 4;416(6880):535-9.

[132]   Li S, Hong S, Shepardson NE, Walsh DM, Shankar GM, Selkoe D. Soluble oligomers of amyloid Beta protein facilitate hippocampal long-term depression by disrupting neuronal glutamate uptake. Neuron. 2009 Jun 25;62(6):788-801.

[133]   Freir DB, Fedriani R, Scully D, Smith IM, Selkoe DJ, Walsh DM, et al. Abeta oligomers inhibit synapse remodelling necessary for memory consolidation. Neurobiology of aging. 2010 Jan 22.

[134]   Kagan BL, Hirakura Y, Azimov R, Azimova R, Lin MC. The channel hypothesis of Alzheimer's disease: current status. Peptides. 2002 Jul;23(7):1311-5.

[135]   Kayed R, Sokolov Y, Edmonds B, McIntire TM, Milton SC, Hall JE, et al. Permeabilization of lipid bilayers is a common conformation-dependent activity of soluble amyloid oligomers in protein misfolding diseases. The Journal of biological chemistry. 2004 Nov 5;279(45):46363-6.

[136]   Lashuel HA, Hartley D, Petre BM, Walz T, Lansbury PT, Jr. Neurodegenerative disease: amyloid pores from pathogenic mutations. Nature. 2002 Jul 18;418(6895):291.

[137]   Caughey B, Lansbury PT. Protofibrils, pores, fibrils, and neurodegeneration: separating the responsible protein aggregates from the innocent bystanders. Annual review of neuroscience. 2003;26:267-98.

[138]   Watson D, Castano E, Kokjohn TA, Kuo YM, Lyubchenko Y, Pinsky D, et al. Physicochemical characteristics of soluble oligomeric Abeta and their pathologic role in Alzheimer's disease. Neurological research. 2005 Dec;27(8):869-81.

[139]   Walsh DM, Selkoe DJ. A beta oligomers - a decade of discovery. Journal of neurochemistry. 2007 Jun;101(5):1172-84.

[140]   Glabe CG. Common mechanisms of amyloid oligomer pathogenesis in degenerative disease. Neurobiology of aging. 2006 Apr;27(4):570-5.

[141]   Ahmed M, Davis J, Aucoin D, Sato T, Ahuja S, Aimoto S, et al. Structural conversion of neurotoxic amyloid-beta(1-42) oligomers to fibrils. Nature structural & molecular biology. 2010 May;17(5):561-7.

[142]   Chimon S, Shaibat MA, Jones CR, Calero DC, Aizezi B, Ishii Y. Evidence of fibril-like beta-sheet structures in a neurotoxic amyloid intermediate of Alzheimer's beta-amyloid. Nature structural & molecular biology. 2007 Dec 2.

[143]   Yagi H, Ban T, Morigaki K, Naiki H, Goto Y. Visualization and classification of amyloid beta supramolecular assemblies. Biochemistry. 2007 Dec 25;46(51):15009-17.

[144]   Mastrangelo IA, Ahmed M, Sato T, Liu W, Wang C, Hough P, et al. High-resolution atomic force microscopy of soluble Abeta42 oligomers. Journal of molecular biology. 2006 Apr 21;358(1):106-19.

[145] Zhu M, Han S, Zhou F, Carter SA, Fink AL. Annular oligomeric amyloid intermediates observed by in situ atomic force microscopy. The Journal of biological chemistry. 2004 Jun 4;279(23):24452-9.

[146] Kheterpal I, Zhou S, Cook KD, Wetzel R. Abeta amyloid fibrils possess a core structure highly resistant to hydrogen exchange. Proceedings of the National Academy of Sciences of the United States of America. 2000 Dec 5;97(25):13597-601.

[147] Digambaranath JL, Dang L, Dembinska M, Vasyluk A, Finke JM. Conformations within soluble oligomers and insoluble aggregates revealed by resonance energy transfer. Biopolymers. 2009 Apr;93(4):299-317.

[148] Mamikonyan G, Necula M, Mkrtichyan M, Ghochikyan A, Petrushina I, Movsesyan N, et al. Anti-A beta 1-11 antibody binds to different beta-amyloid species, inhibits fibril formation, and disaggregates preformed fibrils but not the most toxic oligomers. The Journal of biological chemistry. 2007 Aug 3;282(31):22376-86.

[149] Habicht G, Haupt C, Friedrich RP, Hortschansky P, Sachse C, Meinhardt J, et al. Directed selection of a conformational antibody domain that prevents mature amyloid fibril formation by stabilizing Abeta protofibrils. Proceedings of the National Academy of Sciences of the United States of America. 2007 Dec 4;104(49):19232-7.

[150] Kayed R, Head E, Thompson JL, McIntire TM, Milton SC, Cotman CW, et al. Common structure of soluble amyloid oligomers implies common mechanism of pathogenesis. Science (New York, NY. 2003 Apr 18;300(5618):486-9.

[151] Reinke AA, Seh HY, Gestwicki JE. A chemical screening approach reveals that indole fluorescence is quenched by pre-fibrillar but not fibrillar amyloid-beta. Bioorganic & medicinal chemistry letters. 2009 Sep 1;19(17):4952-7.

[152] Yamaguchi T, Yagi H, Goto Y, Matsuzaki K, Hoshino M. A disulfide-linked amyloid-beta peptide dimer forms a protofibril-like oligomer through a distinct pathway from amyloid fibril formation. Biochemistry. 2010 Aug 24;49(33):7100-7.

[153] Bitan G, Teplow DB. Rapid photochemical cross-linking--a new tool for studies of metastable, amyloidogenic protein assemblies. Accounts of chemical research. 2004 Jun;37(6):357-64.

[154] Stine WB, Jr., Dahlgren KN, Krafft GA, LaDu MJ. In vitro characterization of conditions for amyloid-beta peptide oligomerization and fibrillogenesis. The Journal of biological chemistry. 2003 Mar 28;278(13):11612-22.

[155] Necula M, Breydo L, Milton S, Kayed R, van der Veer WE, Tone P, et al. Methylene blue inhibits amyloid Abeta oligomerization by promoting fibrillization. Biochemistry. 2007 Jul 31;46(30):8850-60.

[156] Nilsson KP, Aslund A, Berg I, Nystrom S, Konradsson P, Herland A, et al. Imaging distinct conformational states of amyloid-beta fibrils in Alzheimer's disease using novel luminescent probes. ACS chemical biology. 2007 Aug 17;2(8):553-60.

[157] Lindgren M, Hammarstrom P. Amyloid oligomers: spectroscopic characterization of amyloidogenic protein states. The FEBS journal. 2010 Mar;277(6):1380-8.

[158] Nilsson KP, Rydberg J, Baltzer L, Inganas O. Self-assembly of synthetic peptides control conformation and optical properties of a zwitterionic polythiophene derivative. Proceedings of the National Academy of Sciences of the United States of America. 2003 Sep 2;100(18):10170-4.

[159] Aslund A, Herland A, Hammarstrom P, Nilsson KP, Jonsson BH, Inganas O, et al. Studies of luminescent conjugated polythiophene derivatives: enhanced spectral discrimination of protein conformational states. Bioconjugate chemistry. 2007 Nov-Dec;18(6):1860-8.

[160]   Nilsson KP, Herland A, Hammarstrom P, Inganas O. Conjugated polyelectrolytes: conformation-sensitive optical probes for detection of amyloid fibril formation. Biochemistry. 2005 Mar 15;44(10):3718-24.

[161]   Nilsson KP, Hammarstrom P, Ahlgren F, Herland A, Schnell EA, Lindgren M, et al. Conjugated polyelectrolytes--conformation-sensitive optical probes for staining and characterization of amyloid deposits. Chembiochem. 2006 Jul;7(7):1096-104.

[162]   Berg I, Nilsson KP, Thor S, Hammarstrom P. Efficient imaging of amyloid deposits in Drosophila models of human amyloidoses. Nature protocols. 2010;5(5):935-44.

[163]   Reinke AA, Abulwerdi GA, Gestwicki JE. Quantifying prefibrillar amyloids in vitro by using a "thioflavin-like" spectroscopic method. Chembiochem. 2010 Sep 3;11(13):1889-95.

[164]   Luedtke NW, Dexter RJ, Fried DB, Schepartz A. Surveying polypeptide and protein domain conformation and association with FlAsH and ReAsH. Nature chemical biology. 2007 Dec;3(12):779-84.

[165]   Kiessling LL, Gestwicki JE, Strong LE. Synthetic multivalent ligands as probes of signal transduction. Angewandte Chemie (International ed. 2006 Apr 3;45(15):2348-68.

[166]   Shi W, Dolai S, Rizk S, Hussain A, Tariq H, Averick S, et al. Synthesis of monofunctional curcumin derivatives, clicked curcumin dimer, and a PAMAM dendrimer curcumin conjugate for therapeutic applications. Organic letters. 2007 Dec 20;9(26):5461-4.

[167]   Lenhart JA, Ling X, Gandhi R, Guo TL, Gerk PM, Brunzell DH, et al. "Clicked" bivalent ligands containing curcumin and cholesterol as multifunctional abeta oligomerization inhibitors: design, synthesis, and biological characterization. Journal of medicinal chemistry. 2010 Aug 26;53(16):6198-209.

[168]   Qin L, Vastl J, Gao J. Highly sensitive amyloid detection enabled by thioflavin T dimers. Molecular bioSystems. 2010 Oct 1;6(10):1791-5.

[169]   Reinke AA, Ung PM, Quintero JJ, Carlson HA, Gestwicki JE. Chemical Probes That Selectively Recognize the Earliest Abeta Oligomers in Complex Mixtures. Journal of the American Chemical Society. 2010 Nov 24.

Chapter 2

Interactions of curcumin-related probes with amyloid-β

2.1 Abstract

Self-assembly of the amyloid-beta (Aβ) peptide into amyloid oligomers and fibrils is one characteristic of Alzheimer's disease. Organic dyes, such as Congo Red and curcumin, bind Aβ and, at higher concentrations, block its self-assembly. These findings have generated interest in understanding the structural features that contribute to inhibitory potency. In general, Aβ ligands tend to be planar, aromatic molecules; however, a comprehensive structure-activity study has not been reported. Towards that goal, we surveyed the effects of three prominent features on inhibition of amyloid aggregation by curcumin-like compounds: the number of aromatic groups required, the substitution pattern of these rings, and the length and flexibility of the intervening linker. We found that all of these features were sensitive to alterations. For example, the optimal properties of the linker were achieved within a surprisingly narrow regime. Further, we surveyed the interactions of these molecules with two distinct forms of Aβ aggregates, oligomers and fibrils, and discovered that they bind both conformations with indistinguishable affinities. These results offer insight into the key chemical features required for inhibiting Aβ aggregation. In turn, these findings help define the nature of one docking site for small molecules on the amyloid surface.

2.1.1 Amyloid-β aggregation

The aggregation of amyloid-β (Aβ) peptide has been implicated in the pathology of patients with Alzheimer's disease [1-3]. Aβ peptides are typically 39-42 residues long and, *in vitro*, they will self-assemble into oligomeric and fibrillar structures that are reminiscent of material isolated from the diseased brain [4-9]. Recent evidence points to oligomers as the key neurotoxin [10-12] and, thus, significant efforts have been placed towards identifying small, drug-like molecules that block early stages of amyloid self-assembly [13-16]. X-ray diffraction, electron microscopy, and solid-state NMR studies suggest that Aβ multimers are stabilized by hydrophobic and hydrogen-bonding interactions within the β-sheets that form their core [17-22]. Although this general model is well supported, a detailed molecular understanding of the key toxin remains elusive. Thus, the structure-guided design of small molecules that disrupt Aβ self-assembly has been challenging.

2.1.2 Classic amyloid-β probes: curcumin and Congo Red

As discussed in Chapter 1, one approach to identifying potent inhibitors is to pattern them after naturally occurring compounds. Organic dyes, such as Congo Red (CR), Chrysamine G (CG), and curcumin, bind with high affinity to Aβ fibrils [23-27]. Additionally, CR and curcumin, an abundant component of the plant turmeric that is used in the curry spice of the same name, have been shown to inhibit Aβ (1-40) fibril formation and lower its toxicity [25, 27, 28]. Interestingly, curcumin, CR and CG all share a similar chemical scaffold; they contain two substituted aromatic groups separated by a rigid, planar backbone (Figure 2.1a). Consistent with the importance of this core, several groups have reported that other roughly curcumin-like

52

ligands are also inhibitors of Aβ aggregation [29-38]. Despite these advances, the structure-activity relationships that define potent ligands have not been systematically explored. In addition, the interactions of these scaffolds with various conformations of Aβ remain largely unexplored. We hypothesize that a better understanding of the modules necessary for activity would facilitate creation of new inhibitors, which, in turn, might reveal the key elements of the amyloid surface that are required for its aggregation and toxicity. In addition, elucidating the interactions between small molecules and unique Aβ species may help define the specific structural features that differ between morphologies.

2.1.3 Library of curcumin analogs for establishing structure-activity relationships (SAR)

In order to identify the chemical features most important for inhibition, we have constructed a library of small molecules. To simplify the study, we have focused on molecules that resemble curcumin and CR. Thus, benzothiazoles, as evaluated in Chapter 1, are believed to bind a site on the Aβ surface distinct from where CR interacts, were not included [39]. This collection consists of both known

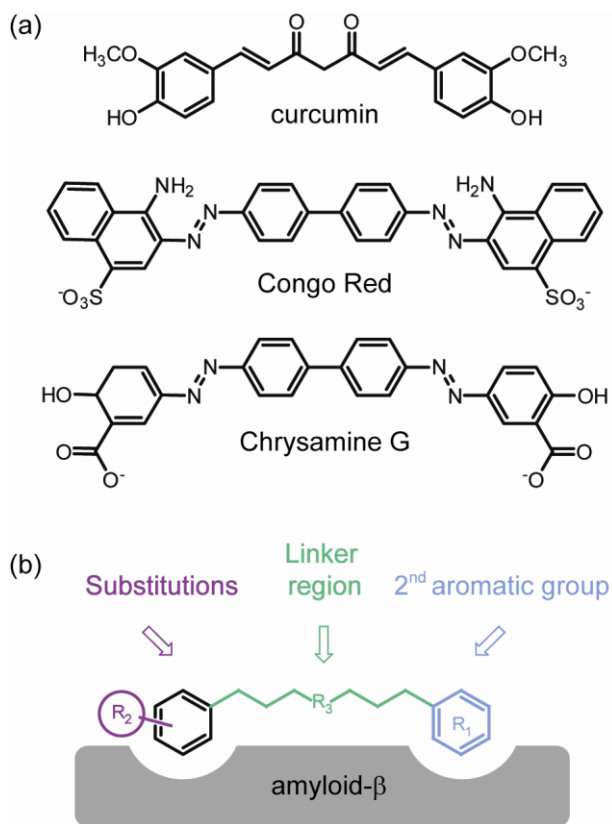
Figure 2.1 The structural components of natural Aβ ligands. (a) Chemical structures of curcumin and related compounds. (b) The structural elements common to curcumin-like amyloid ligands. These features are shown in relation to a schematic Aβ surface to illustrate how these different components may contribute to molecular recognition.

curcumin-inspired ligands and novel synthetic compounds that we generated to test the contribution of specific sub-structural elements. Collectively, this library addresses three components predicted to impact activity (Figure 2.1b). First, we hypothesized that the chemical scaffold of curcumin, containing two aromatic end groups, is optimal for inhibition and the R_1 component addresses whether compounds that lack the second aromatic group retain activity. Secondly, we predicted that substitutions on the phenyl groups are essential to activity; therefore, the R_2 study addresses the effect of altering the hydrogen-bonding properties of these substitutions. Finally, the R_3 study examines the effects of linker length and flexibility. Overall, we show that modest changes in any of the R_1, R_2, or R_3 components have profound effects on activity. This finding emphasizes the strict requirements for inhibition and these constraints lend themselves to a general model of inhibition by curcumin and related ligands.

2.1.4 Conformation-specific disaggregation and binding studies

Molecular dynamics (MD) simulations discussed in Chapter 1 reveal that curcumin-like ligands, including CR, access dual binding sites on amyloid protofibrils [40]. However, it is unclear whether curcumin displays similar binding modes on non-fibrillar aggregates. Indeed, the β-sheet orientation in oligomers and fibrils is distinct [41], and the amount of peptide surface that is solvent exposed is altered dramatically during the transition from early oligomers to fibrils [42, 43]. Collectively, these studies suggest that small molecule binding sites may differ between Aβ species. To elucidate its interactions with oligomers and fibrils, we tested the ability for curcumin to disaggregate each conformation. Interestingly, we found that curcumin disaggregates oligomers and fibrils to similar extents. In addition, surface plasmon resonance (SPR) analysis revealed that both curcumin and CR bind Aβ oligomers and fibrils with similar

affinity, suggesting that at least one small molecule binding site is common to both morphologies. Interestingly, CR and curcumin also recognized a mixture of low-molecular weight (LMW) Aβ (monomer, dimer, trimer, tetramer), indicating that the binding site required to accommodate these scaffolds is already formed in these early assemblies. Collectively, these studies reveal that, despite marked differences in ultrastructure, β-sheet organization, and solvent exposure, common molecular features likely exist within distinct Aβ aggregates. Exploring these small molecule-Aβ interactions may also be applicable for developing probes with the potential for conformation-specific recognition.

2.2 Results

2.2.1 Defining inhibitor potency using synthetic curcumin analogs

To establish the contribution of each structural module to activity, we assembled a collection of compounds that resemble portions of the curcumin scaffold. Some of these molecules were gathered from the literature and others were built from simple components (Figure 2.2). We envisioned that this library could be used to address the three prominent structural features, R_1, R_2, and R_3,that are observed in naturally occurring ligands. To resolve the contribution of these features, comparisons were made between compounds that, as best as possible, isolate a single chemical signature while retaining the character of the remaining two. To test the activity of compounds in this collection, we employed the well known thioflavin T (ThT) assay; this dye is fluorescent in the presence of Aβ aggregates and it is commonly used to characterize inhibitors [44, 45]. In these experiments, we examined the half-maximal concentration (IC_{50}) required and expressed these values as relative potency ($1/IC_{50}$). By comparing the potency of various library

members, we hoped to provide insight into the relative importance of the different structural features.

2.2.2 R_1 Component: Contributions of terminal aromatics

Curcumin is composed of two relatively polar aromatic groups connected by a rigid linker. Thus, in our first experiments, we asked whether both aromatic groups were required for activity. Using the ThT assay, we found that simple compounds with a single aromatic group (**1**-**5**) did not decrease aggregation of 25 µM Aβ (1-42), even at high (500 µM) concentrations (Table 2.1). Conversely, curcumin inhibits Aβ aggregation (IC_{50} ~10 µM), consistent with previous findings [27, 28]. These data demonstrate that compounds lacking a second phenyl are less potent inhibitors of aggregation.
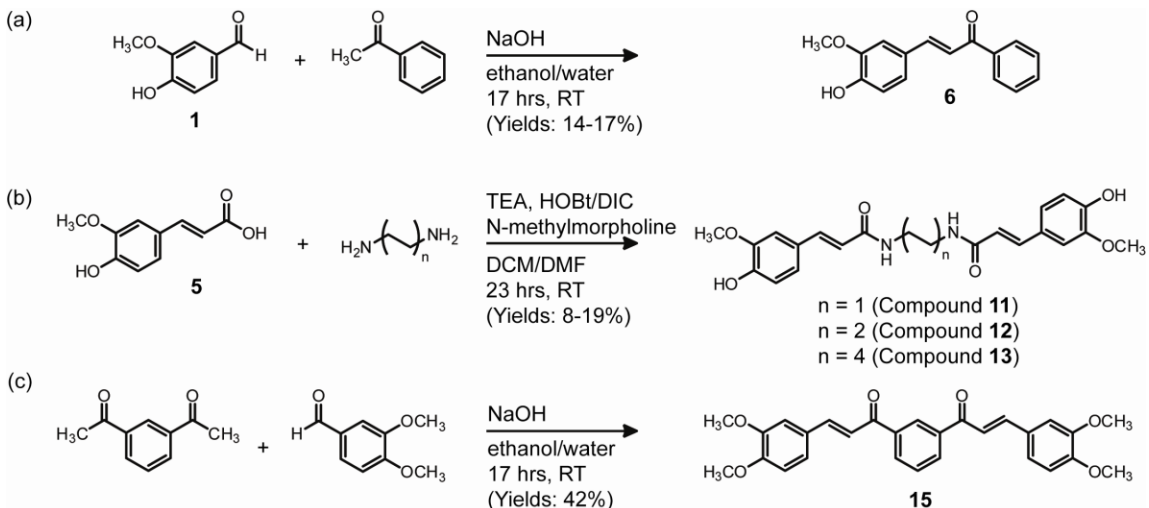
Figure 2.2 Synthesis of curcumin mimetics. (a) Addition of acetophenone to vanillin (**1**) in basic conditions afforded the aldol condensation product (**6**). (b) Amide coupling of ferulic acid (**5**) to alkyl diamines provided the desired compounds (**11**-**13**). (c) Similarly, (**15**) was synthesized via aldol condensation by addition of excess 3,4-dimethoxybenzaldehyde to diacetylbenzene.

2.2.3 R_2 Component: Terminal aromatic substitution patterns

Curcumin contains a 3-methoxy-4-hydroxy substitution pattern on its aromatic end groups. Similarly, CR displays sulfonic acids in an equivalent position and CG has pendant carboxylates. Thus, we were interested in learning if polar, hydrogen-bonding groups are required. To test this hypothesis, the activities of compounds **15-17** were assayed. Compound **16** has the same substitution pattern as curcumin, and, similarly, inhibits aggregation with an IC_{50} value of 0.5 μM [30]. Compound **17** is identical to **16** except that it displays a 3,4-dimethoxy pattern and, interestingly, it has no activity when tested at concentrations up to 100 μM (Figure 2.3). To further explore this requirement, we assembled compound **15** by a dual aldol condensation (Figure 2.3). This molecule has a chemical scaffold that resembles curcumin, except that it lacks the hydroxyl substitutions and, like compound **17**, it is also inactive (Figure 2.3). Thus, these results suggest that aromatic substitutions capable of taking part in hydrogen bonding are important for activity. This finding might have been predicted by the invariance of these groups in the natural
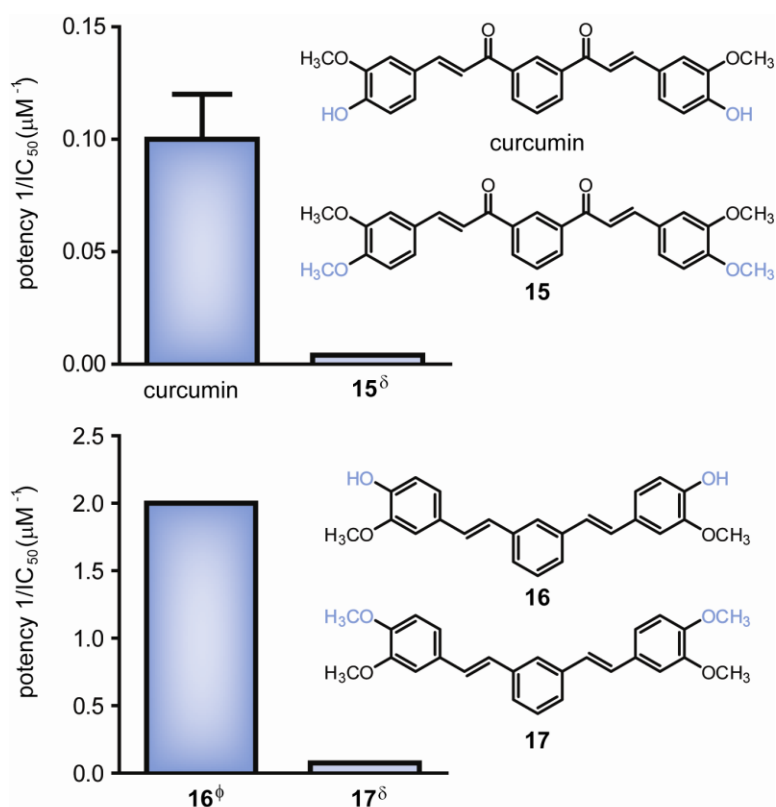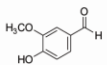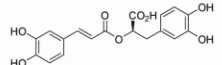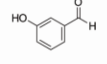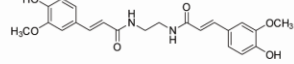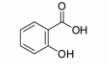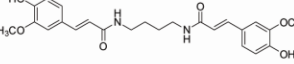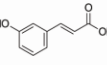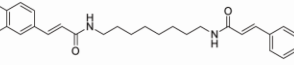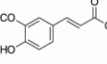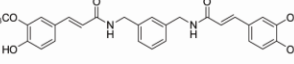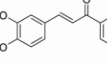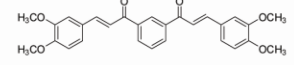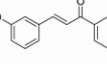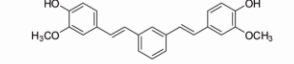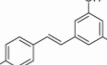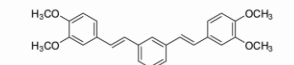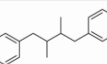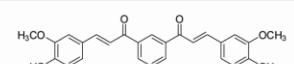
Figure 2.3 Hydroxy substitution on the aromatic end groups are required for inhibition. Dimethoxy-substituted compounds (**15**, **17**) did not inhibit aggregates as well as those with hydroxy substitutions. Potency values (1/IC50) were calculated from either concentrations of compound (up to 100 μM) against 25 μM Aβ (1-42). Each concentration was plated in triplicate and error is expressed as standard deviation. [δ]Indicates IC50 is greater than 100 μM. [φ]IC50 values reported by Lee *et al.*

amyloid ligands, however, these studies demonstrate that these groups serve a functional role and are neither coincidental nor present solely for improved aqueous solubility.

Several other known inhibitors support these observations; compound **9**, with two hydroxyl substitutions, blocks Aβ aggregation (IC_{50} = 10 μM) [32, 33] and compound **10** has also been shown to significantly reduce fibril formation [31]. Together, the results of the R_2 study suggest that the aromatic end groups require one or more polar, hydrogen-bonding substitutions for optimal inhibition of Aβ aggregation.

Table 1 Structure-activity relationships library: compounds tested for inhibtion of Aβ aggregation

Structure	Compound #	IC50 (μM)	Purity	Yield*	Structure	Compound #	IC50 (μM)	Purity	Yield*
(structure)	1 vanillin	> 100	99%	NA	(structure)	10 rosmarinic acid	12 μM[1]	NA	NA
(structure)	2 3-hydroxy-benzaldehyde	> 100	99%	NA	(structure)	11	91	90%	16%
(structure)	3 salicylic acid	> 100	99%	NA	(structure)	12	> 100	85%	15%
(structure)	4 3-hydroxy-cinnamic acid	> 100	99%	NA	(structure)	13	> 100	90%	8%
(structure)	5 ferulic acid	> 100	99%	NA	(structure)	14	> 100	90%	19%
(structure)	6	> 100	> 95%	13%	(structure)	15	> 100	80%	42%
(structure)	7	> 100	> 95%	17%	(structure)	16	0.5 μM[2]	NA	NA
(structure)	8 resveratrol	11	99%	NA	(structure)	17	> 100	> 95%	25%
(structure)	9 nordihydro-guaiaretic acid	10	> 97%	NA	(structure)	curcumin	10	> 95%	NA

[1] IC50 value reported by Masuda *et al.*
[2] IC50 value reported by Lee *et al.*
*Compounds labeled NA were purchased from Sigma and used without further purification.

2.2.4 R_3 Component: Linker length

The distance between the terminal aromatic regions of curcumin, CR, and CG are all strikingly similar. Based on this observation, we hypothesized that the length of the linker would be important for activity. To test this idea, we compared the potency of a series of ligands that vary in linker length. In order to systematically assess the effect of this feature, we constructed a series of ferulic acid dimers. Ferulic acid (**5**) was used because it contains the same 3,4-substitution pattern as curcumin and, to sample a range of lengths, compounds **11**-**14** were synthesized via amide coupling of **5** to alkyl diamines containing two, four, or eight carbons (Figure 2.2). Purified yields ranged from 8-19% and these coupling efficiencies were primarily limited by the poor solubility of ferulic acid and the resulting dimers. Despite these modest yields, this synthetic method provided sufficient material to explore the effects of linker length on potency.

Interestingly, of the four compounds in this series, only the ethyl-diamide dimer (**11**), with a linker length of approximately 16 Å, had appreciable activity (IC_{50} = 91 µM). Compounds **12-14**, with linkers ranging from 19 to 26 Å displayed no activity when tested up to 100 µM (Figure 2.4). These results suggest that the activity of curcumin-like compounds is restricted to those with a length of roughly 16-19 Å or shorter. To examine the lower limit, we synthesized compounds **6** and **7** using an aldol condensation (Figure 2.2). Both these compounds have linkers of approximately 6 Å and they each failed to inhibit fibril formation when tested up to 100 µM. Interestingly, both compounds meet the requirements proposed by the R_1 and R_2 studies, but their activity appears to be limited by their short lengths. Inhibition returned in compounds with lengths of ~8 to 10 Å, as shown by compounds **9** and **10** [31]. Based on these results, we propose a lower constraint of approximately 6-8 Å. Thus, by creating and testing curcumin-like

59

compounds of varying lengths, we identified upper and lower bounds (Figure 2.4, shaded region).

2.2.5 R$_3$ Component: Linker flexibility

The notably rigid quality of natural Aβ ligands led us to predict that flexibility might also influence activity. To facilitate this analysis, relative flexibility was approximated by comparing the total number of freely rotating sp^3-hybridized carbons within the backbone. Interestingly, the flexibility of curcumin might vary between its β-diketone and enol forms, but the
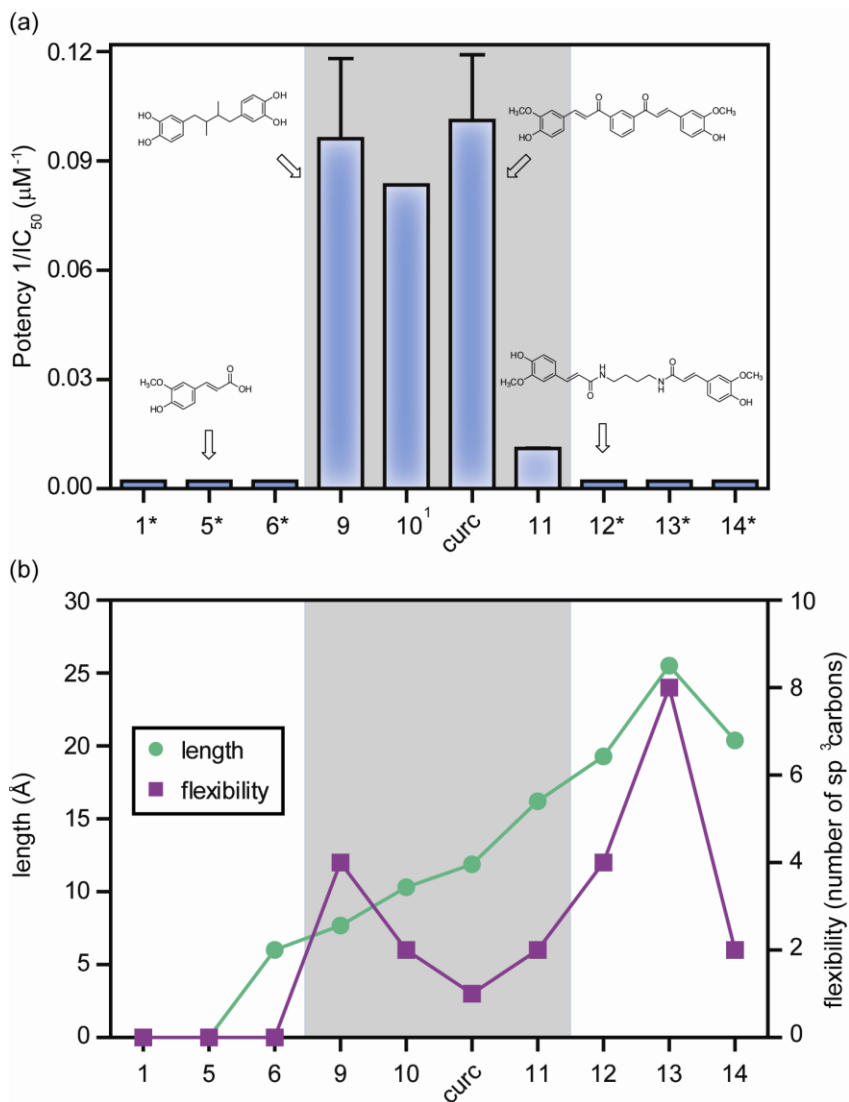
Figure 2.4 Linker length and flexibility define a narrow region of optimal potency. (a) Linker length and flexibility strongly influence potency. A narrow range of linker length and flexibility defines the optimal window for Aβ inhibition (shaded region). Representative chemical structures are shown, and all compounds were tested up to 100 μM against 25 μM Aβ (1-42) in triplicate. Error is expressed as standard deviation. Asterisk (*) indicates IC50 > 100 μM. [1]IC50 value reported by Masuda *et al*. (b) Quantitative comparison of linker length and flexibility. Linker length (green) and flexibility (purple) are compared. Compounds with optimal activity are in the shaded region. Activity decreases when the linker is too short, too long, or too flexible. See Experimental Methods for quantitation methods.

60

β-diketone predominates in aqueous environments, like the buffer used in our ThT assays [46]. Compound **11** contains two such carbons and is therefore less rigid than curcumin. As mentioned above, this compound inhibits Aβ aggregation (IC$_{50}$ = 91 µM), although the potency is weak. Increasingly flexible compounds, such as the butyl-diamide dimer (**12**) with four sp^3-hybridized carbons, had no activity. Conversely, rigid molecules, including **9** and **10**, are good inhibitors [31]. These findings suggest that the linker has a low tolerance for more than one or two sp^3-hybridized carbons.During the course of these experiments, we noticed that length and flexibility are not independent variables. For example, the meta-xylene based dimer (**14**) has a rigid backbone with only two sp^3-hybridized carbons, yet, its long linker length appears to prevent this molecule from inhibiting aggregation. Moreover, compounds **6** and **7** are rigid, but the backbone of these molecules is only about 6 Å; thus, they do not meet the length requirement. Together, we conclude that both the length and flexibility of the linker region strictly define the activity of curcumin-like amyloid inhibitors (Figure 2.4).

2.2.6 Curcumin disaggregates oligomers and fibrils

Based on its property to inhibit general Aβ self-assembly, we wanted to use curcumin as a tool to probe differences in small molecule binding sites between Aβ conformations. As highlighted in Chapter 1, early and intermediate Aβ conformations, such as oligomers, seem to correlate with toxicity in AD, rather than large, elongated fibrils. This generates interest in classifying how small molecules interact with distinct conformers, with the goal of yielding probes that may be sensitive to certain morphologies. Many amyloid ligands have been tested for their ability to disassemble pre-formed aggregates [47-49]. These studies reveal that small molecule can disrupt protein-protein interactions following aggregation. However, these studies are limited in

that they characterize only the ability for small molecules to modulate fibrillar Aβ. Many are performed *in vivo* in transgenic AD mouse models, and therefore only quantify reduction in plaque deposition [50]. Toward the goal of identifying conformation-specific ligands, we wanted to encompass Aβ structures with more biological relevance; thus, we examined the ability for curcumin to disaggregate both pre-formed oligomers and fibrils.
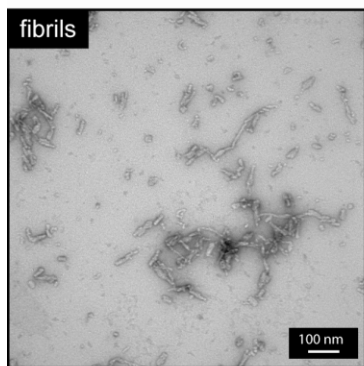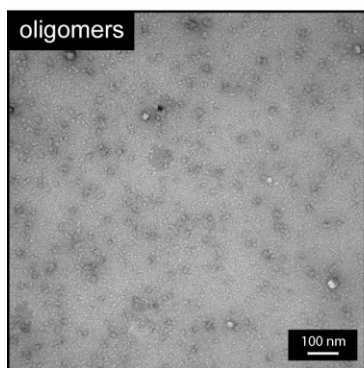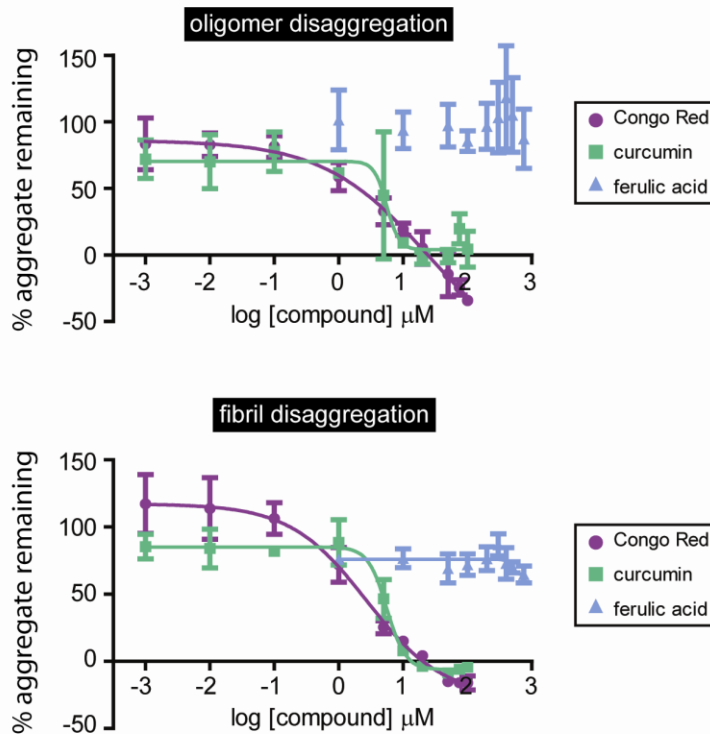
Figure 2.5 Disaggregation of preformed fibrils and oligomers by Congo Red and curcumin. (a) Transmission electron microscopy (TEM) was used to verify the presence of oligomers and fibrils prepared using distinct conditions developed by Stine *et al*. (b) Congo Red (purple) or curcumin (green) (1 nM - 75 μM) were incubated with oligomers and fibrils and the remaining amount of aggregate was quantified using ThT fluorescence. DMSO treated oligomers and fibrils were treated as 100% aggregation, and the percentage of ThT reactive remaining aggregate after compound was calculated. Congo Red and curcumin both show a concentration-dependent reduction in aggregate after a 24-hour incubation with oligomers or fibrils. In contrast, ferulic acid (blue; 1 - 750 μM), which does not inhibit aggregation, also does not disassemble pre-formed aggregates. Samples were performed in triplicate and the error bars represent the standard deviation.

In our experiments, we allowed Aβ to aggregate for 24 hours prior to adding inhibitor. Oligomers and fibrils were prepared using previously established methods [51], and transmission electron microscopy (TEM) was used to confirm the presence of each morphology (Figure 2.5a). After 24 hours, oligomer preparations remain free of linear protofibrils and elongated fibrils. The fibril samples predominantly contained short, linear protofibrils with some larger fibrillar deposits. Following curcumin or CR addition (1 nM – 100 μM), these samples were incubated for an additional 24 hours to allow for disassembly to take place. The relative amount of resulting aggregate was measured relative to a DMSO-treated control by ThT fluorescence, and this comparison is expressed as 'percent aggregation' (Figure 2.5b, c). Interestingly, we found that treatment of both preformed oligomers and fibrils with curcumin results in a dramatic, concentration-dependent reduction in ThT-reactive material, and similar results were found with CR treatment (Figure 2.5b). Our SAR studies revealed that ferulic acid (FA) does not inhibit aggregation. Thus, we employed FA (100 μM – 750 μM) as a negative control in the disaggregation experiments, and revealed that it indeed has no effect on pre-formed aggregates (Figure 2.5b). These data indicate that curcumin-like ligands disrupt Aβ protein-protein interactions, even after aggregation has occurred, in both fibrils and oligomers.

2.2.7 CR and curcumin bind Aβ oligomers and fibrils with similar affinity

Based on the disaggregation properties, we hypothesized that CR may bind both oligomers and fibrils. However, it wasn't clear if they bind these structures with the same affinity. To test this, we developed a binding assay using surface plasmon resonance (SPR). We reviewed in Chapter 1 the advantages of applying SPR for characterizing binding interactions with self-assembling proteins such as Aβ. Preformed oligomers and fibrils were immobilized on a carboxy-methyl

dextran coated CM5 chip following activation by a 1:1 mixture of 0.4 M EDC and 0.1 M NHS. Immobilization response units (RUs) for oligomers and fibrils ranged from 500 - 1000 RUs. The surface was exposed to CR (10 nM – 75 µM), and, as expected, we observed a clear dose-dependent increase in CR binding to Aβ (1-42) fibrils (Figure 2.6a). Harsh regeneration conditions were avoided in order to prevent disruption between the non-covalently associated Aβ molecules. Thus, the surface was regenerated with HEPES-buffer saline (HBS) for at least 60 minutes following CR injection. The association endpoint values were fit as a function of concentration in order to determine an apparent binding affinity (Figure 2.6b, d). Surprisingly, we found that CR binds oligomers (K_d = 28.5 ± 3.6 µM) and fibrils (K_d = 42.4 ± 1.5 µM) with indistinguishable affinity. Interestingly, we also observed that the maximum response was lower upon binding to oligomers relative to fibrils, indicating that there may be a different number of binding sites between the two species. The fact that CR binds distinct species with similar affinity suggests that these structures share a binding site.

Recent evidence suggests that low-molecular weight (LMW) Aβ (*e.g.* dimers, trimers, tetramers, pentamers) are highly neurotoxic, inhibit long-term potentiation, and disrupt synaptic plasticity [52-55]. Thus, we asked whether CR was capable of binding LMW aggregates of Aβ (1-42). LMW aggregates were prepared in basic buffer and passing through 10,000 MWCO filters, as previously described [56], and immobilized immediately following filtration. Our LMW Aβ preparations consisted primarily of monomer, trimer, and tetramer, along with small amounts of dimer, as visualized by native-gel electrophoresis. This pattern is similar to those previously reported [41]. To confirm the homogeneity of these samples, we also performed TEM analysis and confirmed the absence of large oligomers or fibrils. Using these structures in the SPR assay,

we found that, surprisingly, CR binds this mixture of early assemblies with comparable affinity

(K_d = 35.2 ± 1.6 μM) to larger aggregates (Figure 2.6b, d). This finding might be consistent with
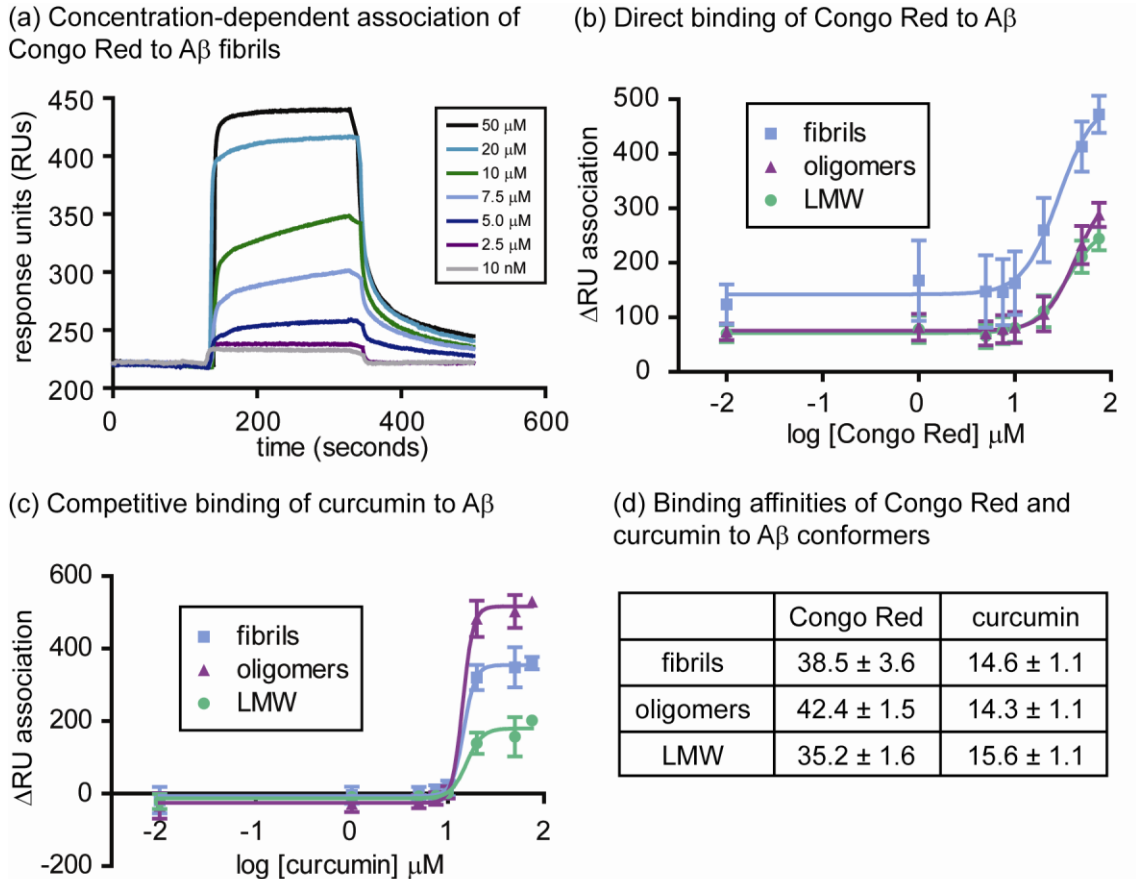
Figure 2.6 Binding profiles of Congo Red and curcumin to distinct Aβ conformations using SPR.
(a) Increasing Congo Red concentrations were exposed to immobilized fibrils, oligomers, or
LMW Aβ. A representative set of curves is shown for CR binding to fibrils. Congo Red (b) and
curcumin (c) bind all three conformations. Each ligand was tested from 10 nM-75 μM. Binding
affinities were determined in triplicate and error bars represent the standard deviation.
(d) Binding affinities for fibrils, oligomers and LMW Aβ are similar. Congo Red affinities were
determined directly, yielding a K_d, while curcumin competed with Congo Red for binding,
resulting in K_i values.

recent studies indicating that CR-like molecules minimally require four Aβ peptides (e.g.

tetramer) for binding [23]. Like we found with globular oligomers, overall RU values were lower

than that observed with fibrils, perhaps indicating a reduced number of sites.

Similarly, we sought to characterize the binding of curcumin to LMW, oligomer, and fibrils using SPR. However, we found that the molecular weight of curcumin (368 Da) is insufficient to give a reproducible signal in this platform. To circumvent this issue, we used curcumin to displace CR (20 μM) and determined the K_i values. Importantly, these studies assume that curcumin and CR share bindings sites on amyloids. Using this approach, we found that curcumin showed strikingly similar K_i values for oligomers, fibrils, and LMW Aβ (K_d range = 14.3 – 15.6 μM) (Figure 2.6c, d). In contrast to CR, however, curcumin displayed the highest association to oligomers, followed by fibrils and then LMW Aβ, indicating that perhaps CR and curcumin have both common and divergent binding sites (Figure 2.6c).

2.3 Discussion

A casual glance at naturally occurring amyloid ligands, such as curcumin, CR and CG suggest that common structural features might dictate their binding to amyloids; however, a systematic analysis of these perceived commonalities had not been performed. Thus, the main goal of this study was to understand which features of these inhibitors are critical for activity. As part of these experiments, we hoped to provide context in which to explain the activity of previously described, synthetic inhibitors [29-38]. In addition, we hoped that these studies might guide the rational design of new compounds.

Our approach was to assay a library of compounds that collectively address three distinct structural features that were predicted to be critical for inhibition of Aβ aggregation. Our findings indicate that alteration or elimination of any one of the three major components results in a significant loss of activity (Figure 2.7a). First, in the R_1 study, we found that simple

aromatics do not have activity. It is worth noting that, although the majority of known amyloid ligands have at least two phenyl groups, a handful of compounds with a single phenyl ring have been shown to inhibit Aβ by other experimental approaches [35, 57]. These observations are not necessarily in conflict, because it is likely that distinct experimental platforms (*e.g.* ThT, direct binding, etc.) and subtle changes in handling (*e.g.* different buffers, temperatures, time, etc.) may give rise to different outcomes. In the second portion of our analyses, we found that loss of the hydroxyl group on the aromatic rings abolishes activity. This result is consistent with the architecture of natural amyloid ligands, such as curcumin and CR. In addition, polar functional groups (and often, hydroxyls) are commonly seen in other reported ligands [27, 31, 35, 36]. Our results suggest that these features are indispensable for activity.

Finally, results from the R_3 study establish that the optimal linker region is restricted to a defined length and rigidity. Specifically, we found that ligands containing linkers between 8 and 16 Å that are rigid (less than 1-2 freely rotating carbons) are the best inhibitors. Interestingly, many of the best amyloid ligands fall within the observed optimal range. For example, CG, CG, RS-0406, and rosmarinic acid all meet the requirements [23-25, 31, 34]. In addition, the linker component seems to be one of the most significant features, because compounds that fulfill the other sub-structural requirements, such as aromatic substitution, still fail to inhibit if they have a short linker. An interesting exception to this observation is compound **8** (resveratrol) (IC$_{50}$ = 11 μM). Despite its short linker length, this compound is active, suggesting a possible alternative mechanism for inhibition or binding to a different site on the amyloid, such as the benzothiazole site where Thioflavin T binds. Despite this finding, our studies show that the length and flexibility of the linker is, in general, a critical component of potent inhibitors.

Global analysis of the three features allows us to construct a preliminary model for how ligands related to curcumin might interact with the Aβ surface. From the R_1 study, we predict that there should be at least two binding sites to accommodate the aromatic end groups (Figure 2.7b). The Aβ peptide contains four aromatic (*e.g.* Phe[4], Tyr[10], Phe[19], Phe[20]) and other hydrophobic residues that are critical for aggregation [58, 59]; thus, it is reasonable to predict that there are adequate opportunities for functionally important hydrophobic interactions. In turn, the R_2 study predicts that there might be good options for hydrogen bonding within these pockets, but

(a) Features important for activity of curcumin-inspired Aβ ligands

R_3 substructure; linker length and flexibility are limited to a narrow regime; approximate optimal length lies between 8Å and 16Å; inclusion of 2-3 freely rotable carbon centers is not well tolerated

R_2 substructure; a hydroxyl substitution on the aromatic end group is necessary for inhibition

R_1 substructure; a second terminal phenyl group is required for activity

8-16Å

amyloid-β

(b) "Goldie-Locks" model showing how linker characteristics contribute to potency

Curcumin

Too long

Too short

Too flexible
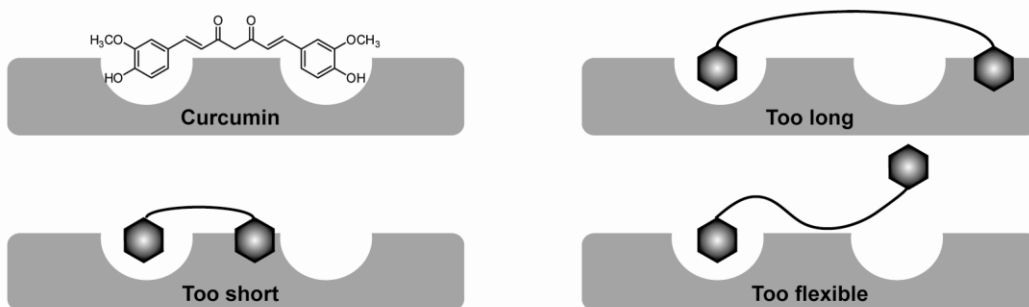
Figure 2.7 Three structural features of curcumin-like compounds that are important for activity. (a) Schematic depiction of the three regions (R_1, R_2, and R_3) that were identified and the approximate features that describe potent ligands. (b) Goldie-Locks model. Based on our results, we propose that the substitution pattern and linker properties of curcumin are just right. Importantly, the length and flexibility of the linker both contribute to defining the optimal range.

the nature of these contacts is not clear. One of the interesting aspects of this study is that it provides an approximate distance between the docking sites. Specifically, we found that lengths below 6-8 Å and beyond 16-19 Å are not well tolerated, so the sites likely lie between 8 and 16 Å from each other. There are probably at least two pockets involved in defining this distance, but it is unclear if multiple primary and/or secondary interactions are involved. Regardless, to emphasize the strict requirements for optimal binding and the diminished activity outside this zone, we refer to this illustration as the "Goldie Locks" model (Figure 2.7b). In the model, too much flexibility (*e.g.* > 2 freely rotating centers) allows for greater sampling of chemical space by the second aromatic group and, as a result, the high entropic penalty paid for docking this group disfavors binding. Importantly, none of these requirements describe the features of thiazolidine- or benzothiazole-class inhibitors [60-62], which are typically short, uncharged, and relatively non-polar, and it seems likely that a different model applies to these compounds. This conclusion is consistent with recent evidence that there are at least two distinct sites for small molecules on amyloids [39, 63-65]. Moreover, as implied above, it is possible that resveratrol, which is an outlier in our study, may access this alternative site. Together, these studies provide a model for how organic compounds bind the surface of amyloids and prevent self-assembly.

The fact that CR and curcumin recognize non-fibrillar Aβ aggregates is now supported by several additional studies [27, 66, 67]. Our disaggregation results are in agreement with Hong *et al.*, who employed quantitative AFM analysis to show that CR and curcumin indeed disassemble pre-formed globular oligomers [66]. Yang *et al.* showed that curcumin inhibits the formation of tetramers and pentamers as well [27]. As a result, native-gel electrophoresis revealed that monomer was the only species remaining in the presence of curcumin. In addition, Maezawa *et al*. employed SPR to characterize the binding of several amyloid ligands to globular Aβ oligomers

[67]. They discovered that CR, and a structural analog BSB, bind oligomers with low-micromolar affinity. Moreover, they compared labeling of oligomers with BSB to an oligomer-specific antibody (A11 [68]) in brain tissue derived from both human patients and transgenic mouse models. BSB fluorescence co-localized almost completely with A11 binding, indicating that in complex biological environments, CR-like ligands retain recognition of non-fibrillar aggregates. CR and BSB were also shown to dramatically reduce binding of oligomers to synapses in human AD hippocampal neurons. These data have important implications for tracing deposition of various conformations *in vivo*. Finally, curcumin has been shown to not only decrease $A\beta$ plaque deposition [50, 69], but also significantly reduce (85%) the levels of soluble $A\beta$ when injected peripherally into Tg2576 AD mice models [27]. Collectively, these data indicate that curcumin-like ligands recognize a variety of $A\beta$ structures both *in vitro* and *in vivo*. Because of its diverse recognition and successful profile in lowering aggregated $A\beta$ levels *in vivo*, current analogs are being developed to improve the pharmacokinetic profile of curcumin and its related ligands [26, 70].

Using an SPR platform, we discovered that CR and curcumin bind $A\beta$ oligomers and fibrils with roughly the same affinity, suggesting at least one common binding site. Indeed, the earliest studies characterizing the interactions of CR with $A\beta$ proposed that approximately four $A\beta$ molecules were necessary to accommodate CR [71], which would be a repeating unit that would be expected in both oligomers and fibrils. Further supporting this idea, our LMW $A\beta$ preparation contained tetrameric species, which may be responsible for the majority of binding. Due to challenges in isolating only one size of $A\beta$ aggregate, it has been difficult to discern precisely

how each of these LMW species contributes to CR binding. Future work may help determine whether these amyloid structures share a subset of common binding sites.

In the absence of additional structural findings, some clues into the interaction between CR and amyloids can be gained from simulations. Although its exact binding site remains elusive, molecular dynamics (MD) [40], fluorescence [39], and NMR [72] studies suggest that CR accesses multiple binding sites on amyloid aggregates. MD simulations also suggest that CR displays dual binding modes on protofibrils; the predominant site is located parallel to the fibril axis, while the less-populated site lies anti-parallel to the fibril axis at the 'end' of the aggregate [40]. Whether these same contacts are made in non-fibrillar aggregates has yet to be explored. However, structural advancements in characterizing both globular [73] and LMW Aβ [74, 75] may soon allow for full characterization of the interactions of small molecules with these important toxic species.

We have used a collection of curcumin-inspired ligands to chemically "map" the Aβ surface. We predict that further studies into the interaction between small molecules and Aβ will provide information that will supplement the work emerging from structural studies. These findings may contribute to our understanding of the features that propagate aggregation and, perhaps, encode for neurotoxicity and, together, these studies might inform those seeking better inhibitors and chemical probes.

2.4 Experimental Procedures

2.4.1 Materials

Solvents were purchased from Fisher and used without further purification. Vanillin, 3-hydroxybenzaldehyde, salicylic acid, 3-hydroxy-cinnamic acid, ferulic acid, resveratrol, and nordihydroguaiaretic acid (NDGA) were purchased from Sigma (Milwaukee, WI). Rosmarinic acid was purchased from Caymen Chemical (Ann Arbor, MI), and curcumin and Congo Red were purchased from Fluka (Milwaukee, WI). All compounds were used without further purification.

2.4.2 Synthesis and characterization

Compounds **6** and **7** were prepared via an aldol reaction based on previous findings [76]. Briefly, acetophenone (5 mmol) was added to 10 mL 9:1 ethanol:water and stirred at 0 °C for 10 minutes. 25 mmol NaOH was added and the reaction was allowed to stir for another 10 minutes at 0°C. 5 mmol of the appropriate aldehyde was added and the reaction proceeded for 17 hours at room temperature. Each reaction was extracted twice with dichloromethane (DCM) and brine addition. Products were characterized by mass spectrometry and ^{1}H NMR. The 4-hydroxy-3-methoxy benzaldehyde (vanillin)-based chalcone (**6**) afforded a brown oil (yield 14%) at a > 95% purity (exact mass calculated for $C_{16}H_{14}O_3$: 254.3, observed (M+H): 255.1, 100%). The 3-hydroxybenzaldehyde-based chalcone (**7**) formed a light brown solid (yield 17%) at a >95% purity (exact mass calculated for $C_{15}H_{12}O_2$: 224.3, observed (M+H): 225.1, 100%). NMR was in agreement with previously published findings [76].

Compounds **11-14** were prepared via amide coupling of ferulic acid (**5**) and various diamines. Synthesis was patterned after the approach of Spasova *et al.* [77]. Ferulic acid ((E)-3-(4-hydroxy-3-methoxyphenyl)prop-2-enoic acid) (3 mmol) was dissolved in 6-10 mL 1:1 dimethylformamide (DMF):DCM, followed by the addition of triethylamine (TEA) (0.75 mmol). The reaction was

allowed to stir for 10 minutes at 0°C. N-hydroxybenzotriazole (HOBt, 3 mmol) and N,N'-diisopropylcarbodiimide (DIC, 8 mmol) were added directly to the mixture. 1.5 mmol of N-methylmorpholine dissolved in DCM (2 mL) was added and stirred at 0°C for another 7 minutes. 0.75 mmol of either ethylenediamine, diaminobutane, diaminooctane, or m-xylylenediamine was dissolved in 2-3 mL DCM and slowly added to the reaction mixture. The reactions proceeded at room temperature for 23 hours (ethylenediamine, diaminobutane, diaminooctane reactions) or 46 hours (m-xylylenediamine reaction), after which 1 equivalent of 5% $NaHCO_3$ was added. Upon agitation, an orange to brown solid precipitated. In each case, the solid was obtained by filtration and washed with cold water. Each solid was then dissolved in a 1:1 methanol/DCM mixture, and precipitated a second time with brine. Filtration of this solid yielded the final products. **11**-**14** were characterized by mass spectrometry and ^{1}H NMR (Appendix 2.5).

Compound   **11**   (2*E*,2'*E*)-*N*,*N*'-(ethane-1,2-diyl)bis(3-(4-hydroxy-3-methoxyphenyl)prop-2-enamide) (yield 16%): Exact mass calculated for $C_{22}H_{24}N_2O_6$: 412.4, observed (M+Na^{+}): 435.1 (20%). ^{1}H NMR (500 MHz; DMSO) δ 3.28 (s, 4H), δ 3.80 (s, 6H), δ 6.43 (d, 2H), δ 6.78 (d, 2H), δ 6.98 (d, 2H), δ 7.10 (s, 2H), δ 7.33 (d, 2H), δ 8.1 (s, 2H).

Compound   **12**   (2*E*,2'*E*)-*N*,*N*'-(butane-1,4-diyl)bis(3-(4-hydroxy-3-methoxyphenyl)prop-2-enamide) (yield 15%): Exact mass calculated for $C_{24}H_{28}N_2O_6$: 440.2, observed (M+Na^{+}): 463.2 (100%). ^{1}H NMR (500 MHz; DMSO) δ 1.47 (s, 4H), δ 3.17 (s, 4H), δ 3.78 (s, 6H), δ 6.39 (d, 2H), δ 6.73 (d, 2H), δ 6.93 (d, 2H), δ 7.06 (s, 2H), δ 7.29 (d, 2H), δ 7.98 (s, 2H).

Compound **13** (2*E*,2'*E*)-*N*,*N*'-(octane-1,8-diyl)bis(3-(4-hydroxy-3-methoxyphenyl)prop-2-enamide) (yield 8%): Exact mass calculated for $C_{28}H_{36}N_2O_6$: 496.3, observed (M+Na$^+$): 519.2 (100%). ^{1}H NMR (500 MHz; DMSO) δ 1.29 (s, 8H), δ 1.44 (s, 4H), δ 3.14 (s, 4H), δ 3.78 (s, 6H), δ 6.38 (d, 2H), δ 6.74 (d, 2H), δ 6.94 (d, 2H), δ 7.06 (s, 2H), δ 7.28 (d, 2H), δ 7.91 (s, 2H).

Compound **14** (2*E*,2'*E*)-*N*,*N*'-(1,3-phenylenebis(methylene))bis(3-(4-hydroxy-3-methoxyphenyl)prop-2-enamide) (yield 19%): Exact mass calculated for $C_{28}H_{28}N_2O_6$: 488.5, observed (M+Na$^+$): 511.1 (100%). ^{1}H NMR (500 MHz; DMSO) δ 3.78 (s, 6H), δ 4.37 (s, 4H), δ 6.47 (d, 2H), δ 6.75 (d, 2H), δ 6.95 (d, 2H), δ 7.08 (s, 2H), δ 7.17 (d, 2H), δ 7.22 (s, 1H), δ 7.29 (t, 1H), δ 7.35 (d, 2H), δ 8.47 (t, 2H).

Compound **15** (2*E*,2'*E*)-1,1'-(1,3-phenylene)bis(3-(3,4-dimethoxyphenyl)prop-2-en-1-one) was formed via an aldol reaction. 1,3-diacetylbenzene (1.4 mmol) was added to 25 mL ethanol and stirred for 10 minutes at 0 °C. 14.4 mmol NaOH was added and the reaction stirred for another 10 minutes at 0 °C. 8.3 mmol of 3,4-dimethoxybenzaldehyde (veratraldehyde) was added and the reaction proceeded at room temperature for 13 hours. 5 mL water was added to promote precipitation of a yellow solid. The mixture was vacuum-filtered and washed with cold water to afford a bright yellow solid (yield 42%) of 80% purity. The product was characterized by mass spectrometry and ^{1}H NMR. Exact mass calculated for $C_{28}H_{26}O_6$: 458.2, observed (M+H): 459.2 (100%). ^{1}H NMR (500 MHz; DMSO) δ 3.82 (s, 6H), δ 3.87 (s, 6H), δ 7.03 (d, 2H), δ 7.16 (d, 2H), δ 7.44 (d, 2H), δ 7.56 (d, 2H) δ 7.76 (s, 1H), δ 7.79 (d, 1H), δ 7.91 (d, 1H), δ 8.41 (d, 2H).

Compound **17** (1,3-bis(3,4-dimethoxystyryl)benzene) was prepared according to Lee *et al.* [30]. Briefly, 1,3-bis(diethoxyphosphinylmethyl) benzene was synthesized according to Plater and Jackson [78]. 0.7 mmol of 1,3-bis(diethoxyphosphinylmethyl) benzene was resuspended in 50 mL of anhydrous tetraydrofuran (THF). 2.0 mmol of sodium tert-butoxide was added and the reaction stirred at 0 °C for 20 minutes. Veratraldehyde (3.6 mmol) was then added and the mixture was allowed to stir for another 45 minutes at room temperature. 50 mL of chilled water was then slowly added over 10 minutes, and the reaction stirred for a final 30 minutes at room temperature. The final mixture was extracted twice with ethyl acetate, and washed once each with 5% $NaHCO_3$, then brine. A crude column purification was performed in 50:50 ethyl acetate:hexanes to yield three separate fractions. A white solid precipitated from the first fraction and was filtered and washed with ethyl acetate (yield 25%). The final white powder was characterized by mass spectrometry and NMR. Exact mass calculated for $C_{26}H_{26}O_4$: 402.2, observed ($M+Na^+$): 425.2 (100%). NMR spectra were in agreement with previously published results [30].

2.4.3 Defining linker length and flexibility

Linker length was quantified by summing the bond lengths according to the following values: C-C 1.54 Å, C=C 1.34 Å, C-O 1.43 Å, and C-N 1.47 Å [79]. Linker flexibility is not based on dynamic simulations but simple quantification of sp^3 carbons. Curcumin can be depicted as either a β-diketone or enol form. The β-diketone predominates in aqueous environments [46]. Based on this finding, we have roughly approximated curcumin as having a single sp^3-hybridized carbon center.

2.4.4 Amyloid-β preperation

Amyloid β (1-42) peptide was purchased from AnaSpec. A 1 mg sample of peptide was dissolved in 200 μL hexafluoroisopropanol (HFIP) and aliquoted to obtain 0.1 mg stocks. HFIP was removed under nitrogen to provide a thin film. Stocks were stored at -30°C until ready for use. Immediately prior to the start of the experiment, an aliquot was first fully resuspended in DMSO followed by PBS (pH 7.4) to a final concentration of 25 μM (10% final DMSO concentration). Aliqouts were then sonicated for one minute at room temperature and immediately dispensed into 96-well plates (see below).

2.4.5 Thioflavin T (ThT) assay

Inhibition of Aβ (1-42) aggregation was measured using a Thioflavin T (ThT) binding assay. Stocks of each compound (10 mM) were prepared in DMSO and 1 μL of each was added to the wells of black, opaque Corning 96-well plates such that the final solvent concentration was 10%. Compounds were tested over a broad concentration range (1 nM to 100 μM) using 8-11 concentrations points. Controls: Compounds alone and positive/negative controls. Each concentration was prepared in independent triplicates and a solvent control was included. 9 μL of 25 μM Aβ (1-42) sample (see Aβ preparation above) was added to each well and the samples mixed by gentle tapping. Plates were covered to minimize evaporation and incubated in the dark at room temperature for 46-48 hours with no agitation. After the incubation period, 200 μL of 5 μM ThT in 50 mM glycine (pH 8.0) was added to each well. Fluorescence was measured on a SpectraMax M5 (Molecular Devices) multi-mode plate reader with excitation and emission wavelengths at 446 nm and 490 nm, respectively. Data was fit by non-linear regression analysis using GraphPad Prism software.

2.4.6 Disaggregation assay

Established protocols were used to prepare oligomer and fibril samples [51]. Briefly, 0.1 mg aliquots of Aβ (1-42) were first fully resuspended in DMSO followed by DMEM-F12 for oligomers, or PBS (pH 7.4) for fibrils, to a final concentration of 25 μM (10% final DMSO concentration). Aliqouts were then sonicated for one minute at room temperature and either placed in a 37 °C shaker (fibrils) or at 4 °C without agitation (oligomers). Following incubation for 24 hours, samples were dispensed into 96-well plates (9 μL/well) in triplicate. Compounds (1 nM – 100 μM) were prepared and administered as described in the previous section. The plates were then incubated at their respective temperatures for an additional 24 hours. Aggregation was measured by ThT fluorescence as described. DMSO-treated wells served as 100% aggregation controls, and the percent disaggregation was calculated using this value as a standard.

2.4.7 Surface Plasmon Resonance (SPR)

Aβ (1-42) oligomers and fibrils were prepared as described. A CM5 chip (GE Healthcare) was docked and equilibrated with HBS buffer (10 mM HEPES, 150 mM NaCl, pH 7.4 containing 0.005% Tween-20) overnight at 5 uL/min. All experiments were performed at 25 °C. Each lane was activated with 50 μL of NHS (400 μM) and EDC (200 μM) in water at 10 uL/min, after which Aβ samples were immediately immobilized at 5 μL/min. Average contact times were at least 20 minutes for oligomers and 10 minutes for fibrils. Average immobilization responses for oligomers and fibrils were approximately 1000 RUs and 750 RUs, respectively. LMW Aβ was prepared using published methods [56]. Briefly, 1 mg of Aβ (1-42) was suspended in 650 μL of 2 mM NaOH and 10 μL 100 mM NaOH was added to reach complete solubilization. Following

sonication on ice for 15 minutes, the sample was passed through a 10,000 MWCO filter that had been washed with water prior to filtration. Filtration was performed at 11,000 rpm at 4 °C for 15 minutes. Filtrate was immediately loaded onto an activated lane of a CM5 chip. After immobilization of all Aβ species, the chip was equilibrated for at least 4 hours at 5 μL/min. Varying concentrations of Congo Red (10 nM – 75 μM) were prepared in PBS (final DMSO < 5%), and 20 μL were injected at 5 μL/min. For competition experiments, Congo Red (20 μM) and curcumin (10 nM – 75 μM) were combined in PBS immediately prior to injection. Higher concentrations (> 10 μM) of small molecules were prepared immediately before injection to avoid extensive self-association. For both direct and competition binding, the binding surface was regenerated with HBS buffer for at least 60 minutes or until the baseline response was reached. Data was fit thermodynamically by using the change in RU value 5 seconds prior to the end of the association phase. The concentration dependent change in immobilization was then fit by non-linear regression analysis using GraphPad Prism software, from which K_d or K_i values were determined.

Notes

Ashley 12 1 /opt/topspin aareinke

DAB-FA dimer

Compound12

[rel]

[ppm]

2.1722
2.2703
1.4735
2.5075
2.5109
3.1689
3.1764
3.6201
3.6332
3.6463
3.6614
3.7807
5.5574
5.5572
5.5722
6.3784
6.4097
6.7312
6.7473
6.9287
6.9450
7.0601
7.2761
7.3073
7.9783

1.0010
1.0140
1.3083
2.3934
0.5434
2.9884
0.3360
0.2689
1.0087
1.0177
1.0585
1.0903
1.0650
1.0000

Compound13

1.0026
1.0150
1.2843
1.4373
1.9969
2.5079
3.1381
3.1487
3.7820
4.0290
4.0431
5.7674
6.3686
6.3997
6.7307
6.7460
6.9306
6.9463
7.0633
7.2694
7.3005
7.9067

[ppm]
0.2421
4.4605
2.2133
0.1113
1.7560
2.2233
3.5357
0.1417
0.0794
1.0228
0.9880
0.9889
1.0845
1.0788
1.0000

2   4   6   8

[rel]   20   15   10   5   0

Ashley 14 1 /opt/topspin aareinke
m-xd-FA dimer

Compound14

1.1670
1.1812
1.1945
1.1954

1.9966

2.5099

3.7778

4.0283
4.0427

4.3682
4.3796

5.7678
5.7687

6.4561
6.4874
6.7430
6.7591
6.9469
6.9615
7.0782
7.1670
7.1814
7.2167
7.2766
7.2915
7.3068
7.3355
7.3667

8.4671
8.4787
8.4899

0.5326
0.3186
0.1967 [ppm]

0.1722

1.1447

3.2518

0.1415

2.2508

0.1712

1.1238

1.1194

1.1322
1.1855
0.5058
0.6164
1.1467

1.0000

[rel]   20   15   10   5   0

Ashley 19 1 /opt/topspin aareinke
1,3-dab(ver)2

Compound15

2.9737

3.3529

3.8257
3.8316
3.8689
3.8752

7.2819

18.1489
18.7051

7.0303
7.0470
7.1621
7.1785
7.3891
7.3924
7.4412
7.4547
7.5477
7.5679
7.5832
7.7663
7.7973
7.8983
7.9293
8.4099
8.4253
8.7050
9.8431

4.5226
1.2830
1.8087
4.0111
6.9380
5.3771
3.8919
3.2169
1.4005
1.0000

[rel]
20
15
10
5
0

[ppm]
10
8
6
4

83
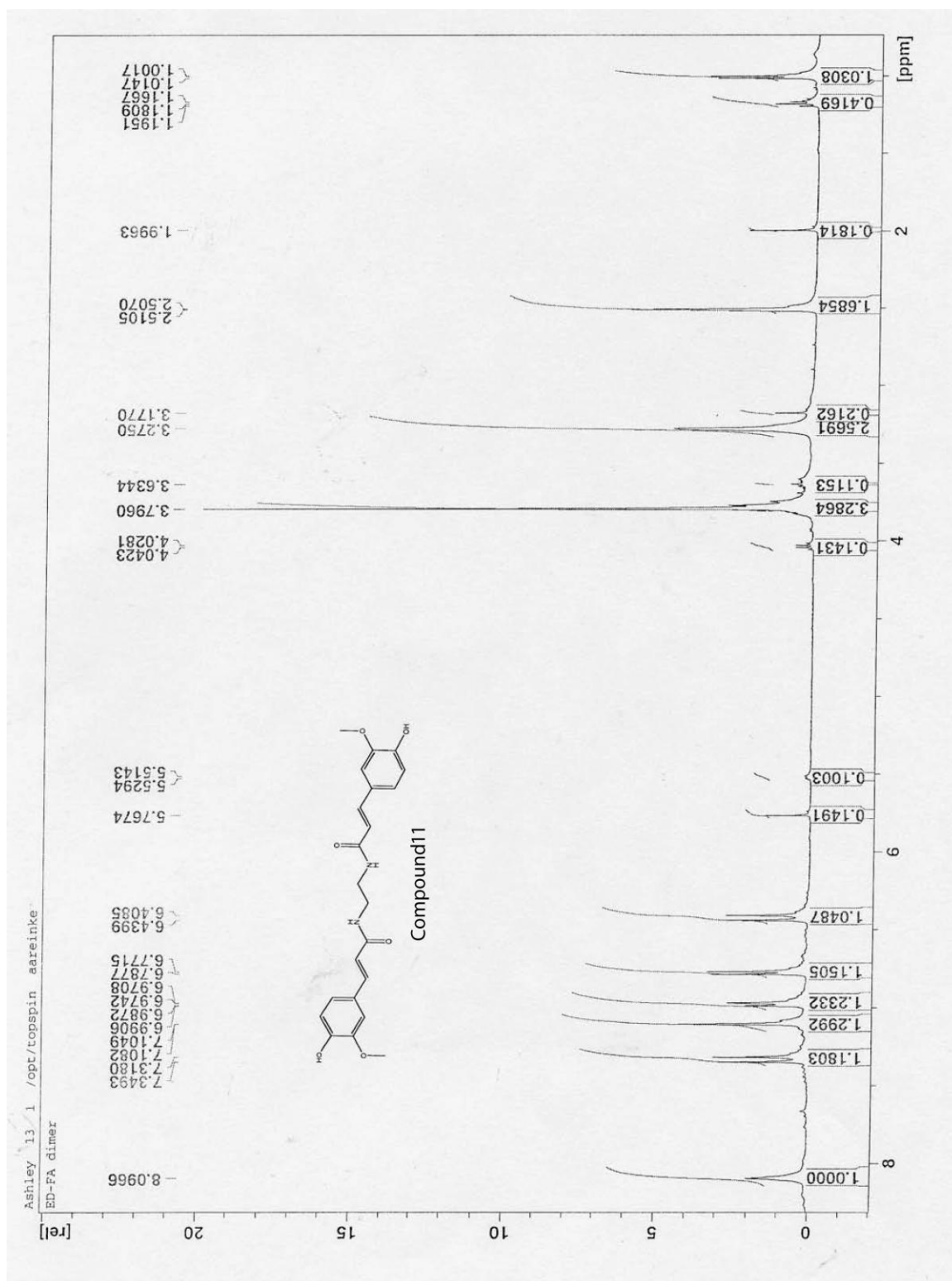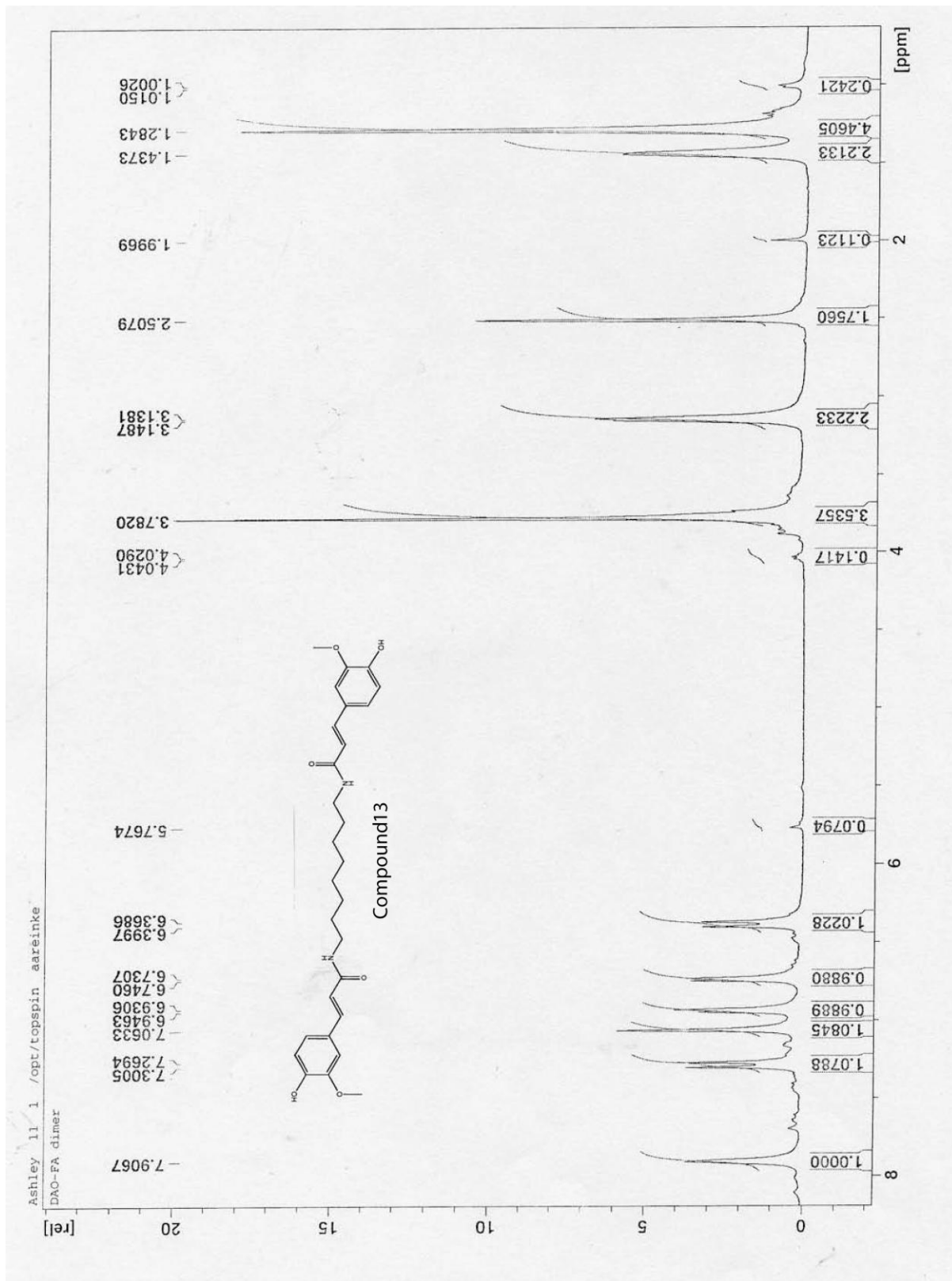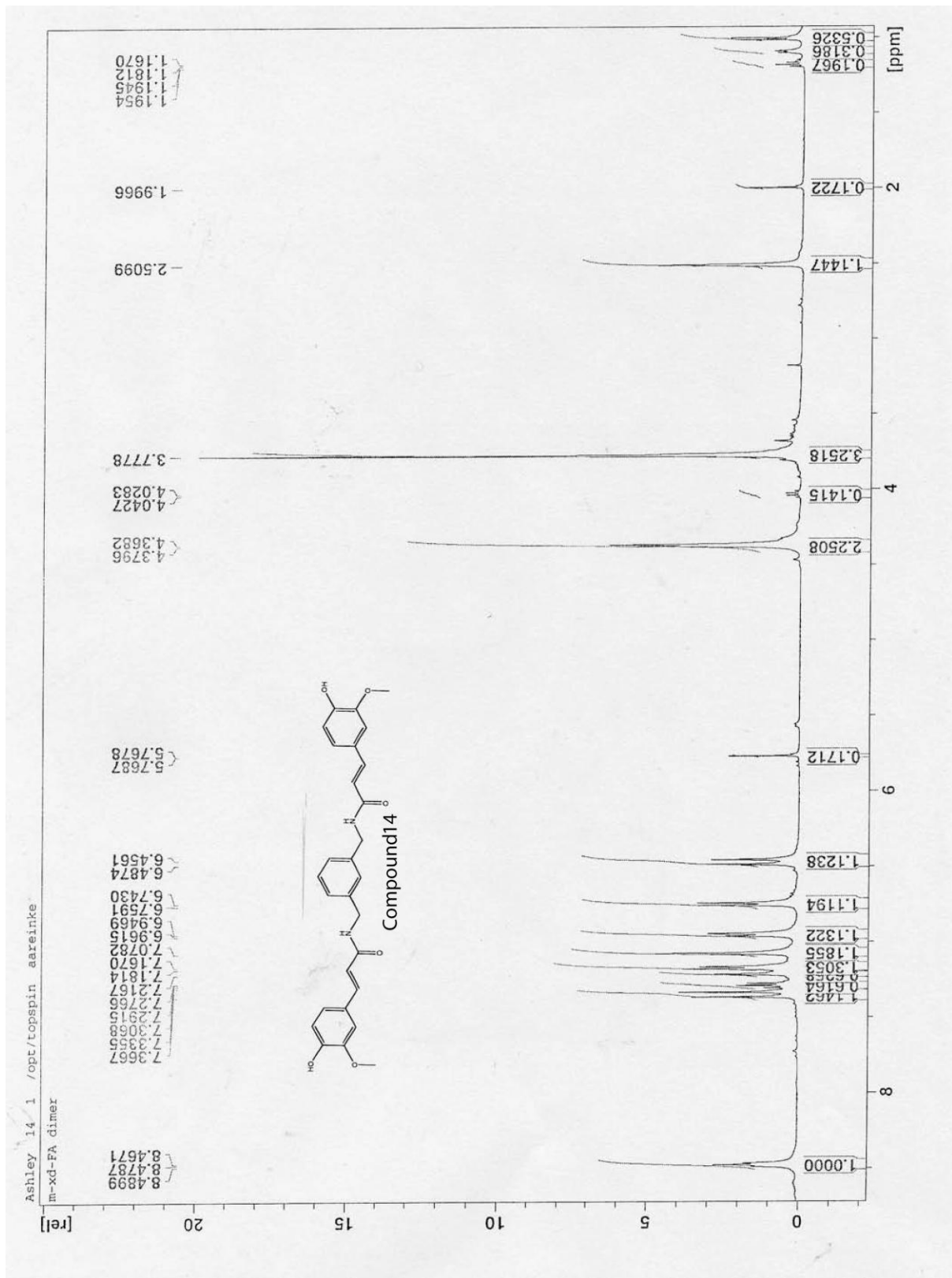
2.6 References

[1]   Caughey B, Lansbury PT. Protofibrils, pores, fibrils, and neurodegeneration: separating the responsible protein aggregates from the innocent bystanders. Annual review of neuroscience. 2003;26:267-98.

[2]   Glabe CC. Amyloid accumulation and pathogensis of Alzheimer's disease: significance of monomeric, oligomeric and fibrillar Abeta. Sub-cellular biochemistry. 2005;38:167-77.

[3]   Selkoe DJ. The molecular pathology of Alzheimer's disease. Neuron. 1991 Apr;6(4):487-98.

[4]   Ghosh AK, Kumaragurubaran N, Tang J. Recent developments of structure based beta-secretase inhibitors for Alzheimer's disease. Current topics in medicinal chemistry. 2005;5(16):1609-22.

[5]   Haass C, Schlossmacher MG, Hung AY, Vigo-Pelfrey C, Mellon A, Ostaszewski BL, et al. Amyloid beta-peptide is produced by cultured cells during normal metabolism. Nature. 1992 Sep 24;359(6393):322-5.

[6]   Jarrett JT, Lansbury PT, Jr. Seeding "one-dimensional crystallization" of amyloid: a pathogenic mechanism in Alzheimer's disease and scrapie? Cell. 1993 Jun 18;73(6):1055-8.

[7]   Morgan C, Colombres M, Nunez MT, Inestrosa NC. Structure and function of amyloid in Alzheimer's disease. Progress in neurobiology. 2004 Dec;74(6):323-49.

[8]   Smith TJ, Stains CI, Meyer SC, Ghosh I. Inhibition of beta-amyloid fibrillization by directed evolution of a beta-sheet presenting miniature protein. Journal of the American Chemical Society. 2006 Nov 15;128(45):14456-7.

[9]   Urbanc B, Cruz L, Teplow DB, Stanley HE. Computer simulations of Alzheimer's amyloid beta-protein folding and assembly. Current Alzheimer research. 2006 Dec;3(5):493-504.

[10]   Barghorn S, Nimmrich V, Striebinger A, Krantz C, Keller P, Janson B, et al. Globular amyloid beta-peptide oligomer - a homogenous and stable neuropathological protein in Alzheimer's disease. Journal of neurochemistry. 2005 Nov;95(3):834-47.

[11]   Glabe CG, Kayed R. Common structure and toxic function of amyloid oligomers implies a common mechanism of pathogenesis. Neurology. 2006 Jan 24;66(2 Suppl 1):S74-8.

[12]   Walsh DM, Klyubin I, Fadeeva JV, Rowan MJ, Selkoe DJ. Amyloid-beta oligomers: their production, toxicity and therapeutic inhibition. Biochemical Society transactions. 2002 Aug;30(4):552-7.

[13]   Cohen FE, Kelly JW. Therapeutic approaches to protein-misfolding diseases. Nature. 2003 Dec 18;426(6968):905-9.

[14]   Evans CG, Wisen S, Gestwicki JE. Heat shock proteins 70 and 90 inhibit early stages of amyloid beta-(1-42) aggregation in vitro. The Journal of biological chemistry. 2006 Nov 3;281(44):33182-91.

[15]   Findeis MA. Approaches to discovery and characterization of inhibitors of amyloid beta-peptide polymerization. Biochimica et biophysica acta. 2000 Jul 26;1502(1):76-84.

[16]   Lee VM. Amyloid binding ligands as Alzheimer's disease therapies. Neurobiology of aging. 2002 Nov-Dec;23(6):1039-42.

[17]   Buchete NV, Hummer G. Structure and dynamics of parallel beta-sheets, hydrophobic core, and loops in Alzheimer's A beta fibrils. Biophysical journal. 2007 May 1;92(9):3032-9.

[18]   Eisenberg D, Nelson R, Sawaya MR, Balbirnie M, Sambashivan S, Ivanova MI, et al. The structural biology of protein aggregation diseases: Fundamental questions and some answers. Accounts of chemical research. 2006 Sep;39(9):568-75.

[19]   Luhrs T, Ritter C, Adrian M, Riek-Loher D, Bohrmann B, Dobeli H, et al. 3D structure of Alzheimer's amyloid-beta(1-42) fibrils. Proceedings of the National Academy of Sciences of the United States of America. 2005 Nov 29;102(48):17342-7.

[20]   Makabe K, McElheny D, Tereshko V, Hilyard A, Gawlak G, Yan S, et al. Atomic structures of peptide self-assembly mimics. Proceedings of the National Academy of Sciences of the United States of America. 2006 Nov 21;103(47):17753-8.

[21]   Makin OS, Serpell LC. Structures for amyloid fibrils. The FEBS journal. 2005 Dec;272(23):5950-61.

[22]   Oyler NA, Tycko R. Absolute structural constraints on amyloid fibrils from solid-state NMR spectroscopy of partially oriented samples. Journal of the American Chemical Society. 2004 Apr 14;126(14):4478-9.

[23]   Klunk WE, Debnath ML, Pettegrew JW. Chrysamine-G binding to Alzheimer and control brain: autopsy study of a new amyloid probe. Neurobiology of aging. 1995 Jul-Aug;16(4):541-8.

[24]   Klunk WE, Pettegrew JW, Abraham DJ. Quantitative evaluation of congo red binding to amyloid-like proteins with a beta-pleated sheet conformation. J Histochem Cytochem. 1989 Aug;37(8):1273-81.

[25]   Lorenzo A, Yankner BA. Beta-amyloid neurotoxicity requires fibril formation and is inhibited by congo red. Proceedings of the National Academy of Sciences of the United States of America. 1994 Dec 6;91(25):12243-7.

[26]   Ryu EK, Choe YS, Lee KH, Choi Y, Kim BT. Curcumin and dehydrozingerone derivatives: synthesis, radiolabeling, and evaluation for beta-amyloid plaque imaging. Journal of medicinal chemistry. 2006 Oct 5;49(20):6111-9.

[27]   Yang F, Lim GP, Begum AN, Ubeda OJ, Simmons MR, Ambegaokar SS, et al. Curcumin inhibits formation of amyloid beta oligomers and fibrils, binds plaques, and reduces amyloid in vivo. The Journal of biological chemistry. 2005 Feb 18;280(7):5892-901.

[28]   Ono K, Hasegawa K, Naiki H, Yamada M. Curcumin has potent anti-amyloidogenic effects for Alzheimer's beta-amyloid fibrils in vitro. Journal of neuroscience research. 2004 Mar 15;75(6):742-50.

[29]   Kung HF, Lee CW, Zhuang ZP, Kung MP, Hou C, Plossl K. Novel stilbenes as probes for amyloid plaques. Journal of the American Chemical Society. 2001 Dec 19;123(50):12740-1.

[30]   Lee KH, Shin BH, Shin KJ, Kim DJ, Yu J. A hybrid molecule that prohibits amyloid fibrils and alleviates neuronal toxicity induced by beta-amyloid (1-42). Biochemical and biophysical research communications. 2005 Mar 25;328(4):816-23.

[31]   Masuda M, Suzuki N, Taniguchi S, Oikawa T, Nonaka T, Iwatsubo T, et al. Small molecule inhibitors of alpha-synuclein filament assembly. Biochemistry. 2006 May 16;45(19):6085-94.

[32]   Moss MA, Varvel NH, Nichols MR, Reed DK, Rosenberry TL. Nordihydroguaiaretic acid does not disaggregate beta-amyloid(1-40) protofibrils but does inhibit growth arising from direct protofibril association. Molecular pharmacology. 2004 Sep;66(3):592-600.

[33]   Naiki H, Hasegawa K, Yamaguchi I, Nakamura H, Gejyo F, Nakakuki K. Apolipoprotein E and antioxidants have different mechanisms of inhibiting Alzheimer's beta-amyloid fibril formation in vitro. Biochemistry. 1998 Dec 22;37(51):17882-9.

[34]   Nakagami Y, Nishimura S, Murasugi T, Kaneko I, Meguro M, Marumoto S, et al. A novel beta-sheet breaker, RS-0406, reverses amyloid beta-induced cytotoxicity and impairment of long-term potentiation in vitro. British journal of pharmacology. 2002 Nov;137(5):676-82.

[35]   Necula M, Kayed R, Milton S, Glabe CG. Small molecule inhibitors of aggregation indicate that amyloid beta oligomerization and fibrillization pathways are independent and distinct. The Journal of biological chemistry. 2007 Apr 6;282(14):10311-24.

[36]   Porat Y, Abramowitz A, Gazit E. Inhibition of amyloid fibril formation by polyphenols: structural similarity and aromatic interactions as a common inhibition mechanism. Chemical biology & drug design. 2006 Jan;67(1):27-37.

[37]   Riviere C, Richard T, Quentin L, Krisa S, Merillon JM, Monti JP. Inhibitory activity of stilbenes on Alzheimer's beta-amyloid fibrils in vitro. Bioorganic & medicinal chemistry. 2007 Jan 15;15(2):1160-7.

[38]   Taniguchi S, Suzuki N, Masuda M, Hisanaga S, Iwatsubo T, Goedert M, et al. Inhibition of heparin-induced tau filament formation by phenothiazines, polyphenols, and porphyrins. The Journal of biological chemistry. 2005 Mar 4;280(9):7614-23.

[39]   Ye L, Morgenstern JL, Gee AD, Hong G, Brown J, Lockhart A. Delineation of positron emission tomography imaging agent binding sites on beta-amyloid peptide fibrils. The Journal of biological chemistry. 2005 Jun 24;280(25):23599-604.

[40]   Wu C, Wang Z, Lei H, Zhang W, Duan Y. Dual binding modes of Congo red to amyloid protofibril surface observed in molecular dynamics simulations. Journal of the American Chemical Society. 2007 Feb 7;129(5):1225-32.

[41]   Cerf E, Sarroukh R, Tamamizu-Kato S, Breydo L, Derclaye S, Dufrene YF, et al. Antiparallel beta-sheet: a signature structure of the oligomeric amyloid beta-peptide. The Biochemical journal. 2009 Aug 1;421(3):415-23.

[42]   Qi W, Zhang A, Patel D, Lee S, Harrington JL, Zhao L, et al. Simultaneous monitoring of peptide aggregate distributions, structure, and kinetics using amide hydrogen exchange: application to Abeta(1-40) fibrillogenesis. Biotechnology and bioengineering. 2008 Aug 15;100(6):1214-27.

[43]   Zhang A, Qi W, Good TA, Fernandez EJ. Structural differences between Abeta(1-40) intermediate oligomers and fibrils elucidated by proteolytic fragmentation and hydrogen/deuterium exchange. Biophysical journal. 2009 Feb;96(3):1091-104.

[44]   LeVine H, 3rd. Thioflavine T interaction with synthetic Alzheimer's disease beta-amyloid peptides: detection of amyloid aggregation in solution. Protein Sci. 1993 Mar;2(3):404-10.

[45]   LeVine H, 3rd. Quantification of beta-sheet amyloid fibril structures with thioflavin T. Methods in enzymology. 1999;309:274-84.

[46]   Ortica F, Rodgers MA. A laser flash photolysis study of curcumin in dioxane-water mixtures. Photochemistry and photobiology. 2001 Dec;74(6):745-51.

[47]   Dinamarca MC, Cerpa W, Garrido J, Hancke JL, Inestrosa NC. Hyperforin prevents beta-amyloid neurotoxicity and spatial memory impairments by disaggregation of Alzheimer's amyloid-beta-deposits. Molecular psychiatry. 2006 Nov;11(11):1032-48.

[48]   Li J, Zhu M, Manning-Bog AB, Di Monte DA, Fink AL. Dopamine and L-dopa disaggregate amyloid fibrils: implications for Parkinson's and Alzheimer's disease. Faseb J. 2004 Jun;18(9):962-4.

[49]   Meng F, Abedini A, Plesner A, Verchere CB, Raleigh DP. The flavanol (-)-epigallocatechin 3-gallate inhibits amyloid formation by islet amyloid polypeptide, disaggregates amyloid fibrils, and protects cultured cells against IAPP-induced toxicity. Biochemistry. 2010 Sep 21;49(37):8127-33.

[50]   Garcia-Alloza M, Borrelli LA, Rozkalne A, Hyman BT, Bacskai BJ. Curcumin labels amyloid pathology in vivo, disrupts existing plaques, and partially restores distorted neurites in an Alzheimer mouse model. Journal of neurochemistry. 2007 Aug;102(4):1095-104.

[51]   Stine WB, Jr., Dahlgren KN, Krafft GA, LaDu MJ. In vitro characterization of conditions for amyloid-beta peptide oligomerization and fibrillogenesis. The Journal of biological chemistry. 2003 Mar 28;278(13):11612-22.

[52]   Hung LW, Ciccotosto GD, Giannakis E, Tew DJ, Perez K, Masters CL, et al. Amyloid-beta peptide (Abeta) neurotoxicity is modulated by the rate of peptide aggregation: Abeta dimers and trimers correlate with neurotoxicity. J Neurosci. 2008 Nov 12;28(46):11950-8.

[53]   Klyubin I, Betts V, Welzel AT, Blennow K, Zetterberg H, Wallin A, et al. Amyloid beta protein dimer-containing human CSF disrupts synaptic plasticity: prevention by systemic passive immunization. J Neurosci. 2008 Apr 16;28(16):4231-7.

[54]   Selkoe DJ. Soluble oligomers of the amyloid beta-protein impair synaptic plasticity and behavior. Behavioural brain research. 2008 Sep 1;192(1):106-13.

[55]   Shankar GM, Li S, Mehta TH, Garcia-Munoz A, Shepardson NE, Smith I, et al. Amyloid-beta protein dimers isolated directly from Alzheimer's brains impair synaptic plasticity and memory. Nature medicine. 2008 Aug;14(8):837-42.

[56]   Zhang Q, Powers ET, Nieva J, Huff ME, Dendle MA, Bieschke J, et al. Metabolite-initiated protein misfolding may trigger Alzheimer's disease. Proceedings of the National Academy of Sciences of the United States of America. 2004 Apr 6;101(14):4752-7.

[57]   De Felice FG, Vieira MN, Saraiva LM, Figueroa-Villar JD, Garcia-Abreu J, Liu R, et al. Targeting the neurotoxic species in Alzheimer's disease: inhibitors of Abeta oligomerization. Faseb J. 2004 Sep;18(12):1366-72.

[58]   Shivaprasad S, Wetzel R. Scanning cysteine mutagenesis analysis of Abeta-(1-40) amyloid fibrils. The Journal of biological chemistry. 2006 Jan 13;281(2):993-1000.

[59]   Williams AD, Shivaprasad S, Wetzel R. Alanine scanning mutagenesis of Abeta(1-40) amyloid fibril stability. Journal of molecular biology. 2006 Apr 7;357(4):1283-94.

[60]   Campiglia P, Esposito C, Scrima M, Gomez-Monterrey I, Bertamino A, Grieco P, et al. Conformational stability of Abeta-(25-35) in the presence of thiazolidine derivatives. Chemical biology & drug design. 2007 Feb;69(2):111-8.

[61]   Zhuang ZP, Kung MP, Wilson A, Lee CW, Plossl K, Hou C, et al. Structure-activity relationship of imidazo[1,2-a]pyridines as ligands for detecting beta-amyloid plaques in the brain. Journal of medicinal chemistry. 2003 Jan 16;46(2):237-43.

[62]   Chandra R, Kung MP, Kung HF. Design, synthesis, and structure-activity relationship of novel thiophene derivatives for beta-amyloid plaque imaging. Bioorganic & medicinal chemistry letters. 2006 Mar 1;16(5):1350-2.

[63]   Lockhart A, Ye L, Judd DB, Merritt AT, Lowe PN, Morgenstern JL, et al. Evidence for the presence of three distinct binding sites for the thioflavin T class of Alzheimer's disease PET imaging agents on beta-amyloid peptide fibrils. The Journal of biological chemistry. 2005 Mar 4;280(9):7677-84.

[64]   LeVine H, 3rd. Mechanism of A beta(1-40) fibril-induced fluorescence of (trans,trans)-1-bromo-2,5-bis(4-hydroxystyryl)benzene (K114). Biochemistry. 2005 Dec 6;44(48):15937-43.

[65]   Nesterov EE, Skoch J, Hyman BT, Klunk WE, Bacskai BJ, Swager TM. In vivo optical imaging of amyloid aggregates in brain: design of fluorescent markers. Angewandte Chemie (International ed. 2005 Aug 26;44(34):5452-6.

[66]   Hong HS, Rana S, Barrigan L, Shi A, Zhang Y, Zhou F, et al. Inhibition of Alzheimer's amyloid toxicity with a tricyclic pyrone molecule in vitro and in vivo. Journal of neurochemistry. 2009 Feb;108(4):1097-108.

[67]   Maezawa I, Hong HS, Liu R, Wu CY, Cheng RH, Kung MP, et al. Congo red and thioflavin-T analogs detect Abeta oligomers. Journal of neurochemistry. 2008 Jan;104(2):457-68.

[68]   Kayed R, Head E, Thompson JL, McIntire TM, Milton SC, Cotman CW, et al. Common structure of soluble amyloid oligomers implies common mechanism of pathogenesis. Science (New York, NY. 2003 Apr 18;300(5618):486-9.

[69]   Begum AN, Jones MR, Lim GP, Morihara T, Kim P, Heath DD, et al. Curcumin structure-function, bioavailability, and efficacy in models of neuroinflammation and Alzheimer's disease. The Journal of pharmacology and experimental therapeutics. 2008 Jul;326(1):196-208.

[70]   Ran C, Xu X, Raymond SB, Ferrara BJ, Neal K, Bacskai BJ, et al. Design, synthesis, and testing of difluoroboron-derivatized curcumins as near-infrared probes for in vivo detection of amyloid-beta deposits. Journal of the American Chemical Society. 2009 Oct 28;131(42):15257-61.

[71]   Klunk WE, Debnath ML, Pettegrew JW. Development of small molecule probes for the beta-amyloid protein of Alzheimer's disease. Neurobiology of aging. 1994 Nov-Dec;15(6):691-8.

[72]   Keshet B, Gray JJ, Good TA. Structurally distinct toxicity inhibitors bind at common loci on beta-amyloid fibril. Protein Sci. 2010 Sep 29.

[73]   Chimon S, Shaibat MA, Jones CR, Calero DC, Aizezi B, Ishii Y. Evidence of fibril-like beta-sheet structures in a neurotoxic amyloid intermediate of Alzheimer's beta-amyloid. Nature structural & molecular biology. 2007 Dec 2.

[74]   Pedersen MO, Mikkelsen K, Behrens MA, Pedersen JS, Enghild JJ, Skrydstrup T, et al. NMR Reveals Two-Step Association of Congo Red to Amyloid beta in Low-Molecular-Weight Aggregates. The journal of physical chemistry. 2010 Dec 9;114(48):16003-10.

[75]   Yu L, Edalji R, Harlan JE, Holzman TF, Lopez AP, Labkovsky B, et al. Structural characterization of a soluble amyloid beta-peptide oligomer. Biochemistry. 2009 Mar 10;48(9):1870-7.

[76]   Ansari FL, Nazir S, Noureen H, Mirza B. Combinatorial synthesis and antibacterial evaluation of an indexed chalcone library. Chemistry & biodiversity. 2005 Dec;2(12):1656-64.

[77]   Spasova M, Kortenska-Kancheva V, Totseva I, Ivanova G, Georgiev L, Milkova T. Synthesis of cinnamoyl and hydroxycinnamoyl amino acid conjugates and evaluation of their antioxidant activity. J Pept Sci. 2006 May;12(5):369-75.

[78]   Plater MJ, Jackson T. Polyaromatic amines. Part 3: Synthesis of poly(diarylamino)styrenes and related compounds. Tetrahedron. 2003;59:4673-85.

[79]   Hodgman CD, Veazey WR, Weast RC. Handbook of chemistry and physics; a ready-reference book of chemical and physical data. Cleveland: Cleveland Rubber Co. 1998.

Chapter 3

Chemical screening reveals a conformation-specific amyloid probe:

monitoring pre-fibril depletion with indoles

3.1 Abstract

As discussed in Chapter 1, there is interest in finding simple, spectroscopic methods for specifically quantifying oligomeric and pre-fibrillar amyloid structures. Such probes would be expected to supplement reagents, such as conformationally-selective antibodies, in many important applications. However, known fluorescent probes such as the dyes thioflavin T and Congo Red, lack selectivity and, rather, seem to bind both fibrils and pre-fibrils. To identify molecules that might differentiate between these architectures, we employed an unbiased, fluorescence-based interaction assay to screen a collection of 84 known Aβ ligands against pre-formed oligomers and fibrils. In these studies, we found that the fluorescence of indole-based compounds was selectively quenched (~15%) in the presence of oligomers, but remained unchanged after addition of fibrils. Based on this pilot screen, we characterized an additional 37 indoles and selected the most promising example, tryptophanol (TROL), to use in a quantitative "thioflavin-like" assay. Using this probe, we found that pre-fibrils are largely depleted during Aβ aggregation *in vitro* but that they remain present after apparent saturation of the ThT signal. These results suggest that a combination of TROL and ThT provides greater insight into the process of amyloid formation by Aβ. In addition, we found that TROL also recognizes other amyloid-prone proteins, including ataxin-3, amylin and CsgA. Thus, this assay may be an inexpensive spectroscopic method for quantifying amyloid pre-fibrils *in vitro*.

3.1.1 Amyloid-β assembles into structurally and functionally distinct, oligomeric conformers

As discussed in Chapters 1 and 2, many neurodegenerative disorders, including Alzheimer's and Parkinson's diseases, are characterized by the age-dependent accumulation of aggregated protein, known as amyloid, in the brain [1, 2]. In each disease, a different protein is implicated; for example, in AD, the amyloid-β (Aβ) peptide self-associates to form insoluble fibrils that deposit in the classic neuritic plaque (NP) pathology. These visually striking fibrils
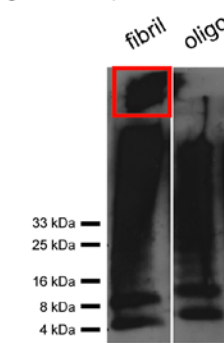
(a) Aβ self-assembles into a variety of toxic-prefibrillar conformations

monomer | pre-fibril | oligomer | fibril
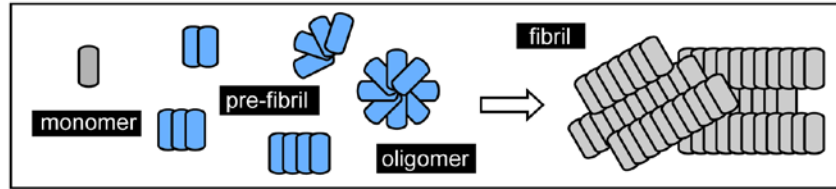
(b) Fibrils and oligomers have distinct ultrastructures by TEM

Aβ (1-42) oligomers | Aβ (1-42) fibrils
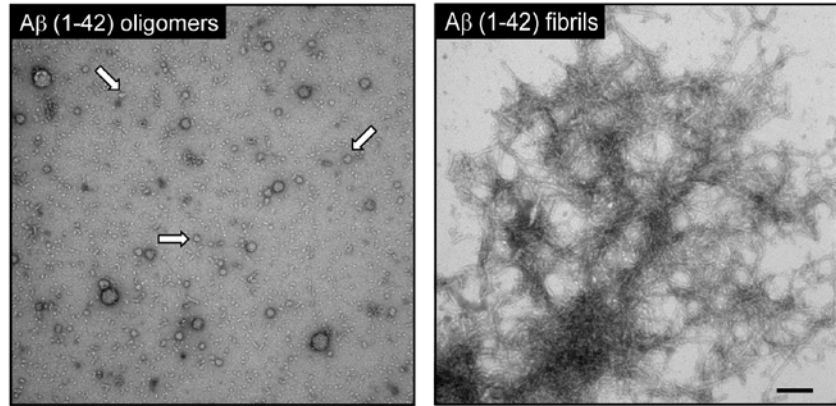
(c) Fibril preparations contain high MW structures by native gel electrophoresis

fibril | oligomers

33 kDa
25 kDa
16 kDa
8 kDa
4 kDa

(d) Oligomers are more senstive to chemical denaturation than fibrils
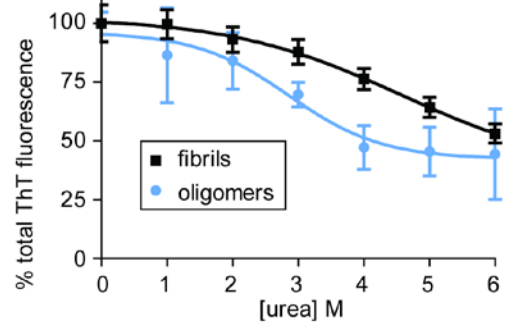
% total ThT fluorescence vs [urea] M

■ fibrils
● oligomers

Figure 3.1 Characterization of the differences in shape, size, and stability of Aβ (1-42) fibrils and oligomers. (a) The Aβ aggregation scheme shows the representative species of pre-fibrils, such as dimers, trimers, tetramers, and globular oligomers, which eventually self-associate to form fibrils. Our aim was to develop an assay that could selectively detect pre-fibrillar Aβ in a mixture of these conformations.(b) Analysis of 25 μM Aβ (1-42) oligomers (left) and fibrils (right) by transmission electron microscopy (TEM). Fibrils were prepared in PBS at 37°C; oligomers were prepared in DMEM-F12 at 4°C (see Experimental Methods). Samples were incubated for 48 hours. Bar = 100 nm. (c) Native gel electrophoresis and Western blot of fibrils and oligomers using anti-Aβ antibody (6E10). Oligomer preparations lack the high molecular weight material present in fibrils (red box). (d) Oligomers are less stable than fibrils. Chemical denaturation of preformed aggregates with urea shows that Aβ oligomers are more sensitive to destabilizing conditions than fibrils.

were initially thought to be linked to neurotoxicity but, more recently, it has been found that Aβ

forms a variety of other conformations, including dimers, trimers, and globular oligomers (Figure 3.1a). Collectively, these pre-fibrillar structures appear to be of special importance in disease. For instance, as highlighted in Chapter 1, AD pathology is specifically correlated with the presence of pre-fibrils and oligomers, but not fibrils [3-5]. Also, recent studies show that Aβ dimers and trimers are more neurotoxic than fibrils to cultured neurons [6-10]. Together, these observations and others have generated interest in finding reagents that specifically detect pre-fibrillar amyloids [3, 11, 12].

3.1.2 *In vitro* conditions for oligomer and fibril preparations are established

Conditions such as temperature, time, salinity, and pH, have been established that promote the progression of Aβ monomers into predominantly oligomers or fibrils *in vitro* [13, 14]. The oligomers formed in this way share the properties of soluble Aβ preparations from AD patients, namely high levels of toxicity and spherical appearance by transmission electron microscopy (TEM) and atomic force microscopy (AFM) [15-17]. We employed these conditions to generate oligomers for our disaggregation and binding studies in Chapter 2. Moreover, a powerful use of fabricated oligomers is in studies of their structure. For example, recent NMR and hydrogen-deuterium exchange (HDX) reports show that Aβ oligomers are predominantly composed of β-sheets, but that the exposure of side chains as well as the packing of this β-sheet character in these species is distinct from fibrils [18-20]. These studies also show that oligomers are less stable than fibrils, which are known to be more densely packed and resistant to denaturation. Collectively, these reports suggest that different Aβ conformations possess unique structural and biological properties. Yet, the molecular features that distinguish Aβ oligomers from fibrils have not been clearly established, and, surprisingly, reagents that discriminate between these structures are few [3, 21, 22]. However, it is clear that cellular components (*e.g.* proteins, lipids)

are somehow able to distinguish between oligomers and fibrils and, thus, it is important to identify how differences in their molecular surfaces might be recognized.

3.1.3 Rationale: Use enriched samples to identify conformation-specific Aβ probes

Small organic dyes are commonly used to quantify the total amount of aggregated Aβ *in vitro* and ThT is considered the "gold-standard" of these probes [23-25, 28-34]. Briefly, ThT becomes fluorescent in the presence of aggregated, but not monomeric, amyloid [24]. Thus, its fluorescence can be used to robustly and inexpensively monitor the aggregation process. However, although ThT can report on aggregation, it does not distinguish between Aβ conformations. This lack of selectivity appears to be common among known amyloid ligands. For example, in Chapter 2, we demonstrated that CR binds different Aβ conformations with similar affinity. This finding might be expected, based on the similarities in the secondary structure of Aβ oligomers and fibrils; however, Necula *et al.* recently reported that certain chemical inhibitors selectively block formation of Aβ oligomers [21, 22]. In addition, we discussed in Chapter 1 other recent studies suggesting the potential of small molecules to exploit subtle differences in architecture to differentially engage pre-fibrillar and fibrillar Aβ. However, none of these methods has been successfully converted into an inexpensive, "ThT-like" assay. In this Chapter, we report the results of screening 84 structurally diverse small molecules against pre-formed oligomers and fibrils in a fluorescence assay with the goal of developing a robust, spectroscopic, "ThT-like" assay to selectively detect pre-fibrils in complex Aβ mixtures.

3.2 Results

3.2.1 Preparation and characterization of Aβ (1-42) fibrils and oligomers

We were interested in testing whether small molecules could differentiate between oligomers and fibrils. Toward this goal, we employed the well-established conditions introduced above (and in Chapter 2) to generate relatively homogeneous populations of Aβ oligomers and fibrils [13-15]. Briefly, Aβ (1-42) oligomers were prepared by incubation in DMEM-F12 at 4 °C, and fibrils were prepared by incubating in PBS at 37 °C. After 48 hours, these samples were analyzed by transmission electron microscopy (TEM), which confirmed that pre-fibril samples were free of the elongated, linear structures commonly observed in the fibril preparations (Figure 3.1a). To independently confirm these findings, the samples were cross-linked using glutaraldehyde and analyzed by non-denaturing gel electrophoresis followed by Western blotting using an anti-Aβ antibody (6E10) (Figure 3.1b). Consistent with previous reports [15], oligomers solutions lack the high molecular weight species that are present in the fibril preparation. Finally, the relative stabilities of the structures were probed by denaturation. Because the Aβ (1-42) peptide lacks a convenient tryptophan for monitoring integrity, we employed ThT reactivity to follow the response of the amyloid structure to denaturant. These studies confirmed that Aβ oligomers are less stable than fibrils (EC_{50} = 3.1 ± 1.0 M for oligomers and 8.0 ± 2.0 M for fibrils; Figure 3.1c), generally consistent with previous findings [18, 20].

3.2.2 Bis-ANS fluorescence is increased by both Aβ oligomers and fibrils

Although the common dyes ThT, curcumin and Congo Red are unable to differentiate between Aβ oligomers and fibrils [23, 24], we first considered whether another common fluorescent probe, Bis-ANS (4,4'-Bis (1-anilinonaphthalene 8-sulfonate)) might possess this activity (Figure 3.2a). Bis-ANS fluorescence increases upon binding hydrophobic regions of proteins, and is therefore widely employed to probe this property [35, 36]. Based on this literature, we reasoned that Bis-ANS may reveal differences between in Aβ oligomers and fibrils. To test this model, we

measured changes in Bis-ANS fluorescence in the presence of pre-formed Aβ (1-42) structures. In these experiments, fluorescence increased 4-fold upon addition to Aβ fibrils, consistent with previous studies [37-39]. However, we found that the fluorescence increase in the presence of Aβ oligomers was indistinguishable from the fibril-induced response (Figure 3.2b). Thus, Bis-ANS does not discriminate between oligomers and fibrils, suggesting that it interacts with either a shared structural element or that it is otherwise insensitive to differences between Aβ structures.

(a) Chemical structure of Bis-ANS

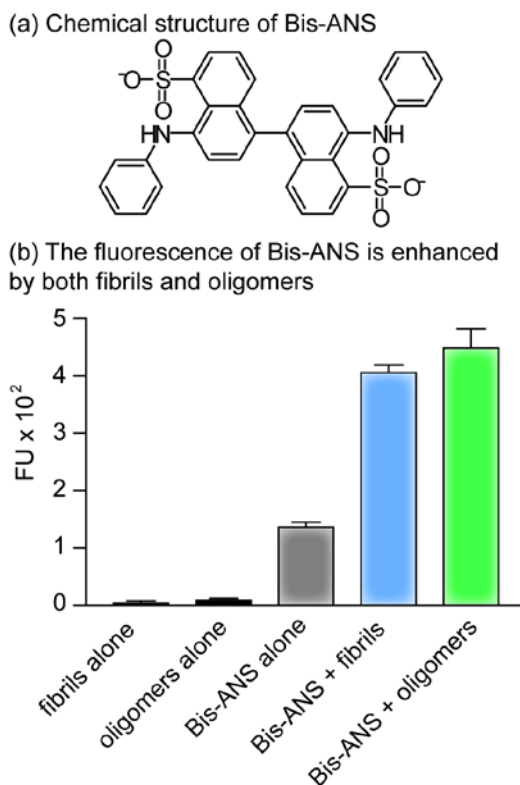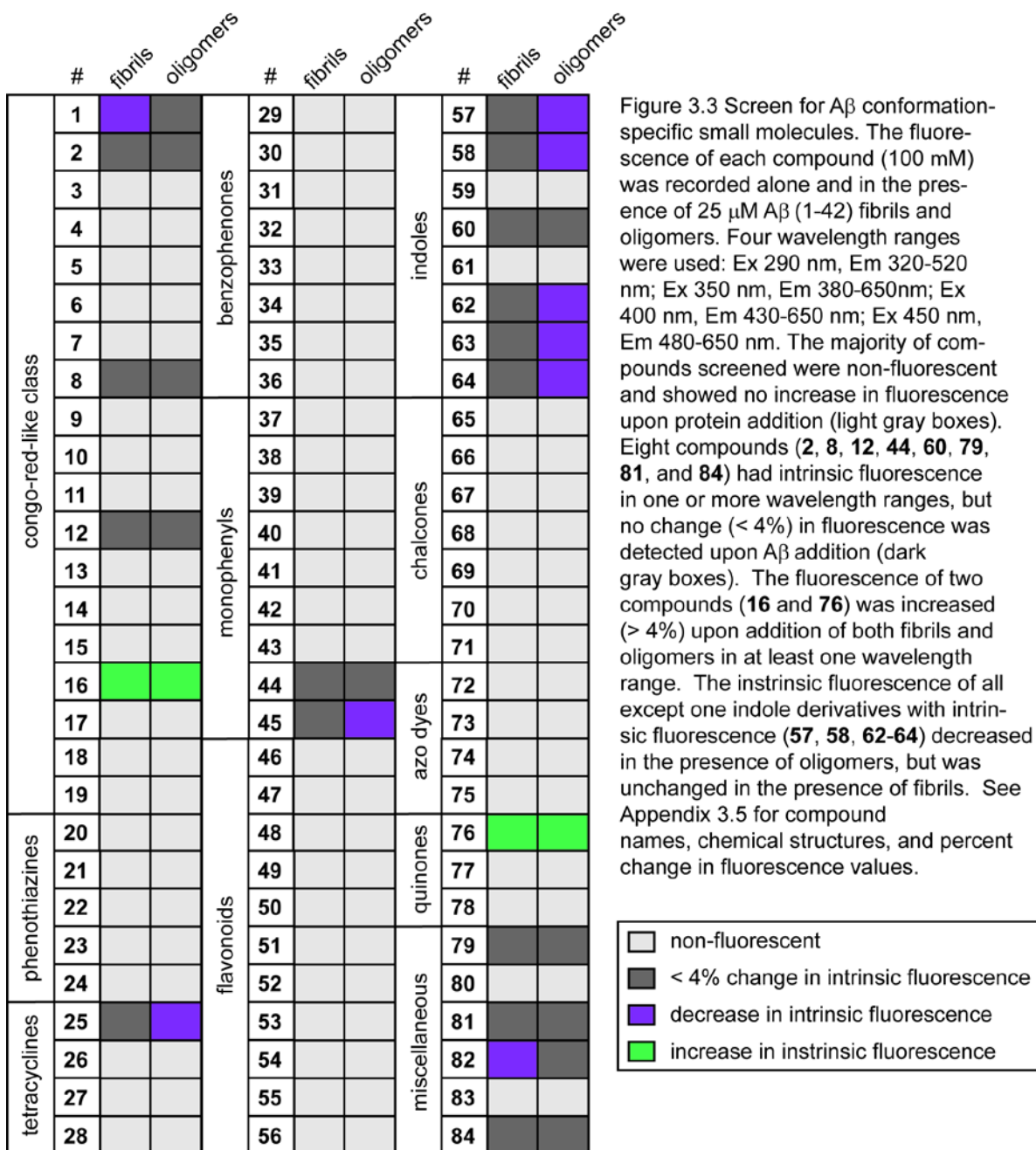(b) The fluorescence of Bis-ANS is enhanced by both fibrils and oligomers

Figure 3.2 Bis-ANS fluorescence increases upon addition of both Aβ (1-42) oligomers and fibrils. (a) Chemical structure of Bis-ANS. (b) Fluorescence of 25 μM Bis-ANS (in 30 mM citrate pH 2.4) alone and in the presence of 25 μM Aβ fibrils or oligomers (Ex 385 nm, Em 520 nm). Fluorescence of fibrils and oligomers alone is shown for comparison. Error is expressed as the standard deviation of six replicates. Fluorescence was read two minutes after Aβ addition.

3.2.3 Pilot fluorescence screen for Aβ conformation-specific small molecules

Because Bis-ANS failed to distinguish between Aβ conformations, we turned to a screening approach. Specifically, we collected a library of 84 structurally diverse small molecules, which included more than 11 distinct chemical scaffolds, including sulfonated dyes, curcumins, phenothiazines, tetracyclines, benzophenones, monophenyls, flavonoids, indoles, chalcones, azo dyes and quinones (Appendix 3.5). These compounds were largely selected based on their reported ability to inhibit Aβ aggregation or bind Aβ fibrils [21, 22, 40-42], in the hopes that these probes might be enriched for those with the potential to recognize features unique to Aβ structures. Importantly, in the

selection of these compounds, we also favored low molecular mass (< 500 Da) compounds because we were interested in understanding the response of amyloids to small, organic probes. Finally, many of the chosen compounds contained conjugated ring systems that, like Bis-ANS and ThT, might provide convenient fluorescence signatures.

Figure 3.3 Screen for Aβ conformation-specific small molecules. The fluorescence of each compound (100 mM) was recorded alone and in the presence of 25 μM Aβ (1-42) fibrils and oligomers. Four wavelength ranges were used: Ex 290 nm, Em 320-520 nm; Ex 350 nm, Em 380-650nm; Ex 400 nm, Em 430-650 nm; Ex 450 nm, Em 480-650 nm. The majority of compounds screened were non-fluorescent and showed no increase in fluorescence upon protein addition (light gray boxes). Eight compounds (**2**, **8**, **12**, **44**, **60**, **79**, **81**, and **84**) had intrinsic fluorescence in one or more wavelength ranges, but no change (< 4%) in fluorescence was detected upon Aβ addition (dark gray boxes). The fluorescence of two compounds (**16** and **76**) was increased (> 4%) upon addition of both fibrils and oligomers in at least one wavelength range. The instrinsic fluorescence of all except one indole derivatives with intrinsic fluorescence (**57**, **58**, **62-64**) decreased in the presence of oligomers, but was unchanged in the presence of fibrils. See Appendix 3.5 for compound names, chemical structures, and percent change in fluorescence values.

Legend:
- non-fluorescent
- < 4% change in intrinsic fluorescence
- decrease in intrinsic fluorescence
- increase in instrinsic fluorescence

Guided by these principles, we screened the chemical collection for fluorescence changes in the presence of preformed Aβ oligomers or fibrils (Figure 3.3). For most of the compounds, we found that their fluorescence was insensitive to amyloids. This result is not interpreted as a failure to bind, only a failure of Aβ to impact the compound's fluorescence. Other members of the collection, such as **16** and **76**, displayed behaviors reminiscent of Bis-ANS; their fluorescence was indiscriminately altered in the presence of both oligomers and fibrils. However, we found that the fluorescence of nine compounds (**1**, **25**, **45**, **57**, **58**, **62**-**64** and **82**) was sensitive to either fibrils or oligomers. Interestingly, five of these compounds (**57**, **58**, **62**-**64**) contained an indole and their fluorescence was partially quenched in the presence of Aβ oligomers but not fibrils. To our knowledge, these are the first molecules shown to discriminate between pre-formed amyloid forms *in vitro*. Based on the structural similarity between five of the nine active compounds, we further explored the activity of indole (**58**).

3.2.4 Indole fluorescence is quenched by Aβ oligomers but not fibrils

To confirm the screening result, we performed a spectral scan on indole (**58**). Consistent with the finding at a single wavelength, no significant change in the indole spectra was observed upon addition of 25 μM Aβ (1-42) fibrils (Figure 3.4a). However, the excitation and emission intensities decreased in the presence of 25 μM oligomers (Figure 3.4b); excitation was quenched by approximately 8% at 280 nm and emission at 350 nm was reduced by 17%. After exposure to aggregated Aβ, the fluorescence of other amyloid probes, such as ThT, requires a short incubation to achieve maximal signal [24, 25]. To explore the kinetics of indole quenching, we monitored the fluorescence immediately after addition of Aβ (Figure 3.5a). Specifically, indole was added to oligomers, fibrils, or low molecular weight (LMW) Aβ peptide and fluorescence was recorded every 30 seconds for one hour. LMW Aβ contained no visible aggregates by TEM

(a) The fluorescence of indole (**58**) does not change in the presence of Aβ fibrils

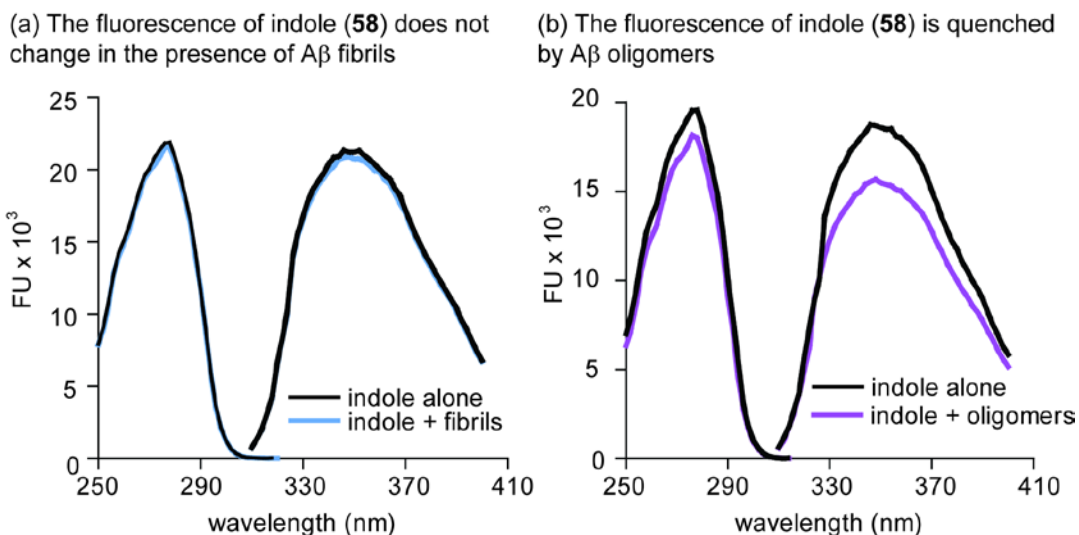(b) The fluorescence of indole (**58**) is quenched by Aβ oligomers

Figure 3.4 Fluorescence spectra of indole indicates quenching in the presence of oligomers but not fibrils. Excitation and emission spectra of indole in the absence and presence of 25 μM Aβ (1-42) (a) fibrils and (b) oligomers (Ex 250-320 nm, Em 350; Ex 280 nm, Em 310-410 nm). Fluorescence was read 30 minutes after Aβ addition. Results are representative of three independent replicates.

analysis and we used this preparation to exemplify pre-oligomeric species. To compare the samples, we expressed the results as the percent change in total indole fluorescence. Using this approach, we found that both oligomer and LMW Aβ quenched fluorescence, and that this effect reached a maximum of 12% after 15 minutes. Consistent with our previous experiment, only a minor (0.5%) change was observed in the fibril sample. Using a one-phase exponential fit, we calculated the observed rate constants (k_{obs}) and showed that LMW Aβ (0.130 ± 0.002 min^{-1}) and oligomers (0.272 ± 0.011 min^{-1}) share similar kinetics (Figure 3.5a). Together, these findings suggest the presence of a binding site that is exposed in both oligomeric and LMW Aβ architectures but inaccessible or otherwise unavailable in fibrils.

Because TEM analysis shows that fibril preparations contain a fractional amount of oligomers after two days, we hypothesized that the minor quenching observed in the fibril sample might be due to contaminating oligomers or LMW Aβ structures. Given that the prevalence of these species decreases with incubation time, we permitted fibril preparations to aggregate for 17

(a) Fluorescence quenching by LMW and oligomeric Aβ is time-dependent

(b) Indole fluorescence at 30 minutes

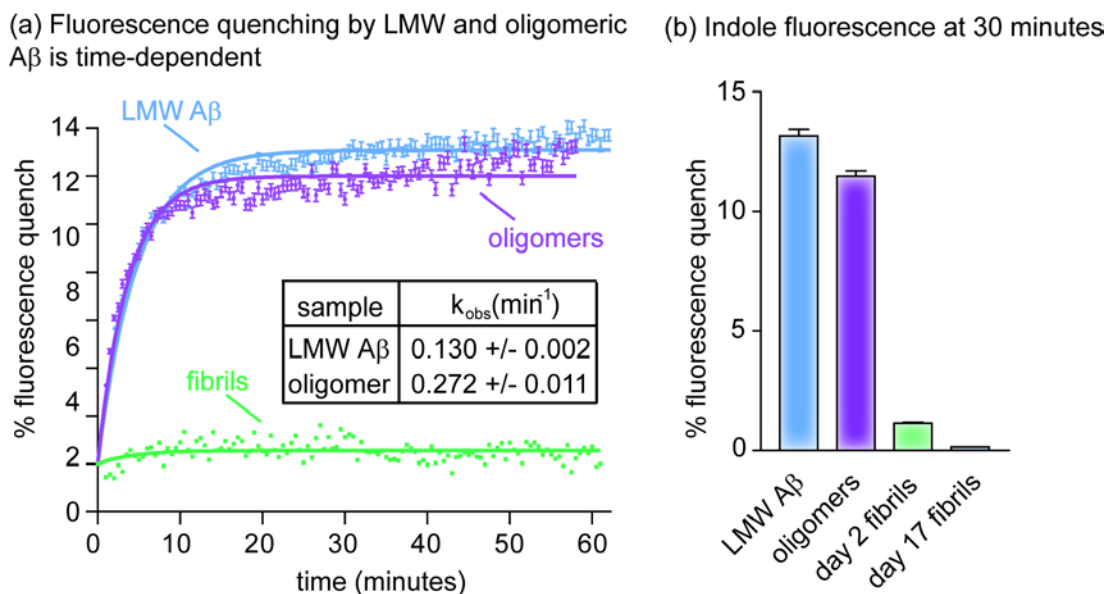| sample	$k_{obs}(min^{-1})$
LMW Aβ	0.130 +/- 0.002
oligomer	0.272 +/- 0.011

Figure 3.5 Indole fluorescence is quenched by low-molecular weight and oligomeric Aβ (1-42), but not fibrils. (a) Indole fluorescence was monitored kinetically in the presence of low molecular weight (LMW) Aβ, oligomers, and fibrils (Ex 280 nm, Em 350). Results are plotted as percent quench in fluorescence. (b) Percent decrease in indole fluorescence following a 30 minute incubation with LMW Aβ, oligomers, day 2 fibrils, or day 17 fibrils. In both panels error is expressed as the standard deviation of six replicates.

days prior to recording the change in indole fluorescence (Figures 3.5b and 3.6c). Using this approach, we found that the quench is insignificant in the aged samples, consistent with minor LMW or oligomer contribution at earlier incubation times.

3.2.5 Characterization of indole quenching by Aβ oligomers versus fibrils

To further characterize the interaction between the parent compound indole (**58**) and Aβ conformations, we varied parameters of the fluorescence assay, including pH, indole concentration and structure, Aβ incubation time, and Aβ concentration (Figure 3.6 and 3.7). In these experiments, we observed no significant trends over the pH range tested (pH 2.2-8.2), which is expected based upon the pKa of indole (~ 21 in DMSO) (Figure 3.6a) [43]. When indole concentration was increased, an overall decrease in activity was observed, an effect that is likely
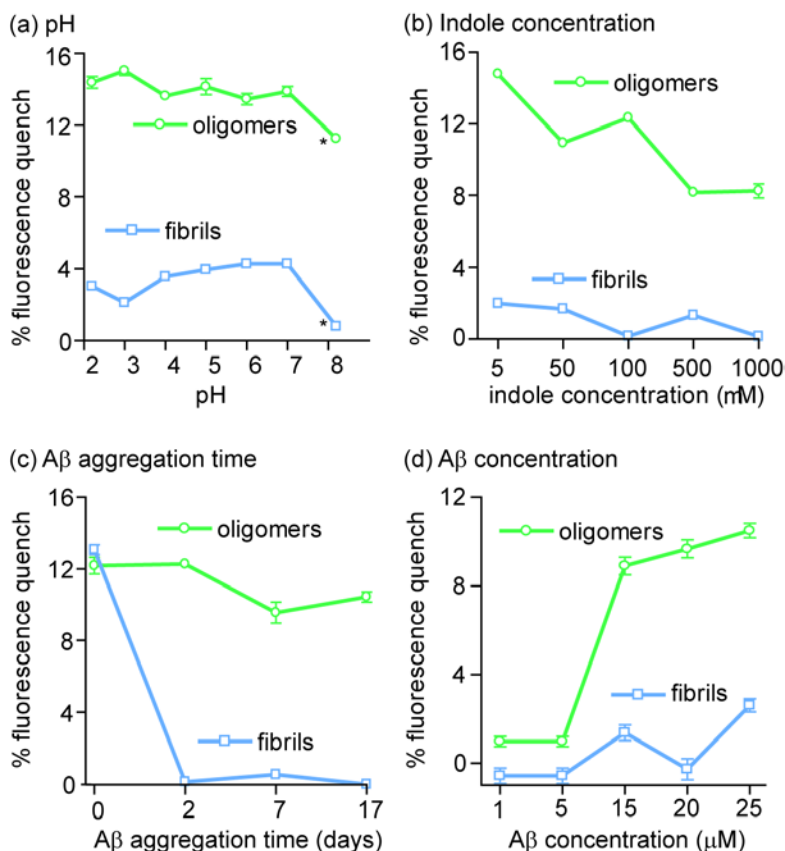
Figure 3.6 Characterization of indole quenching by Aβ oligomers versus fibrils. (a-d) Indole fluorescence was recorded following a 30 minute incubation with Aβ (1-42) oligomers or fibrils (Ex 280 nm, Em 350 nm), and all results are expressed as percent decrease in indole fluorescence. Unless noted, indole and Aβ concentrations remained constant at 100 μM and 25 μM, respectively, in 50 mM glycine (pH 8.2). In panel a, indole was prepared in PBS or *50 mM glycine. For all experiments, error bars are expressed as the standard deviation of three replicates.

caused by self-quenching interactions at high concentrations (Figure 3.6b). Interestingly, the substituted indoles (**57**, **58**, **62**-**64**) behaved similarly in the presence of oligomers, suggesting that oligomers are able to accommodate indoles decorated with various functional groups (Figure 3.7a). To explore the sensitivity of the interaction, we determined the lowest concentration of oligomers at which we could detect quenching of indole (**58**) and found that this value was between 5-15 μM (Figure 3.6d). Finally, amyloid experiments are often subject to heterogeneity in sample preparations, so we wanted to explore whether the observed indole activity was reproducible across independent samples. To test this idea, four separate aliquots of oligomers and fibrils were prepared and we found good reproducibility (less than 5% variance) between these trials (Figure 3.7b). Finally, using TEM and ThT approaches, we found that indole has no affect on aggregation of fresh Aβ (Figure 3.8). Together, these experiments help define the experimental parameters for indole interactions with Aβ oligomers.

3.2.6 Small amounts of Aβ oligomer in fibril preparations can be detected by indole
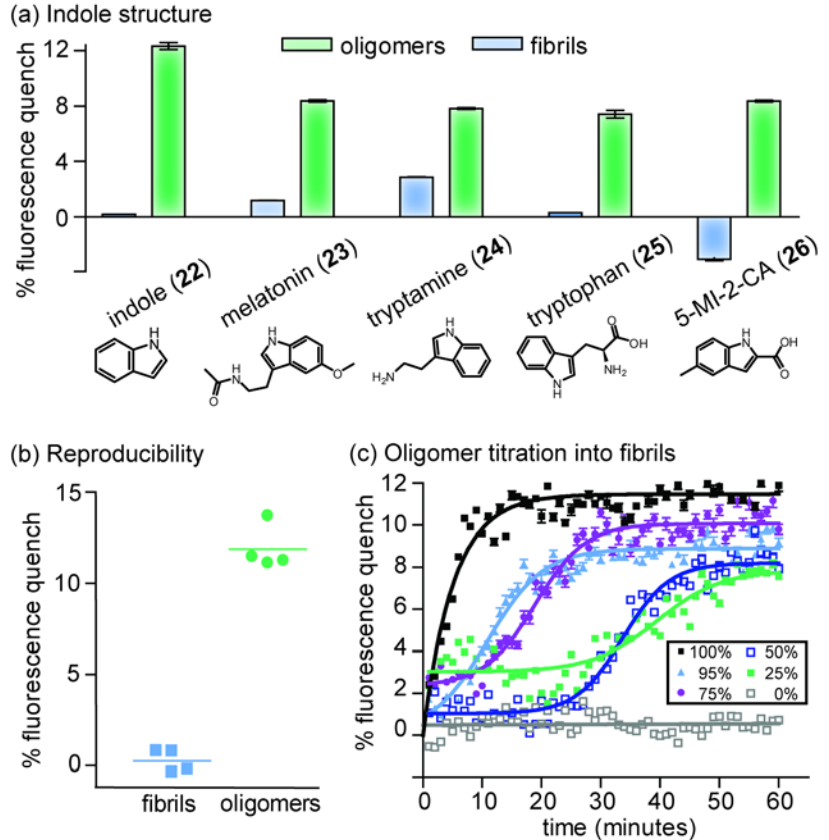

Figure 3.7 Comparing indole structures, reproducibility, and the effects of fibril titration into oligomer samples (a) The change in fluorescence of five indoles in the presence of oligomers (green) and fibrils (blue). (5-MI-2-CA = 5-methylindole-2-carboxylic acid). (b) Four aliquots of Aβ fibrils and oligomers were prepared independently to test the reproducibility of the indole fluorescence quenching. (c) Oligomers were titrated into fibril preparations, and the percentages indicate the amount of oligomer added to fibrils (0% = fibril only; 100% = oligomer only). For all experiments, error bars are expressed as the standard deviation of three replicates.

Common amyloid probes, such as ThT, cannot distinguish between amyloid forms and, therefore, they can't be used to quantify the percentage of oligomer content in a heterogeneous amyloid preparation. Towards that goal, we were interested in testing whether quenching of indole fluorescence by oligomers could be detected in a background of fibrils. Specifically, oligomers and fibrils were prepared separately and then mixed at known ratios, while maintaining the total protein concentration (Figure 3.7c). Using this approach, we observed that even a minor percentage of oligomer (~25%) could be measured in a mixed population. One interesting aspect of these results was that there was a delay in the quenching of samples that contained fibrils. Specifically, we found that the length of the lag phase was proportional to the percentage of fibrils present, suggesting that, despite failure to trigger a quench, indole might

(a) ThT Inhibition Assay

(b) ThT and indole do not compete for binding to Aβ (1-42) aggregates

(c) Indole addition does not disrupt Aβ aggregation
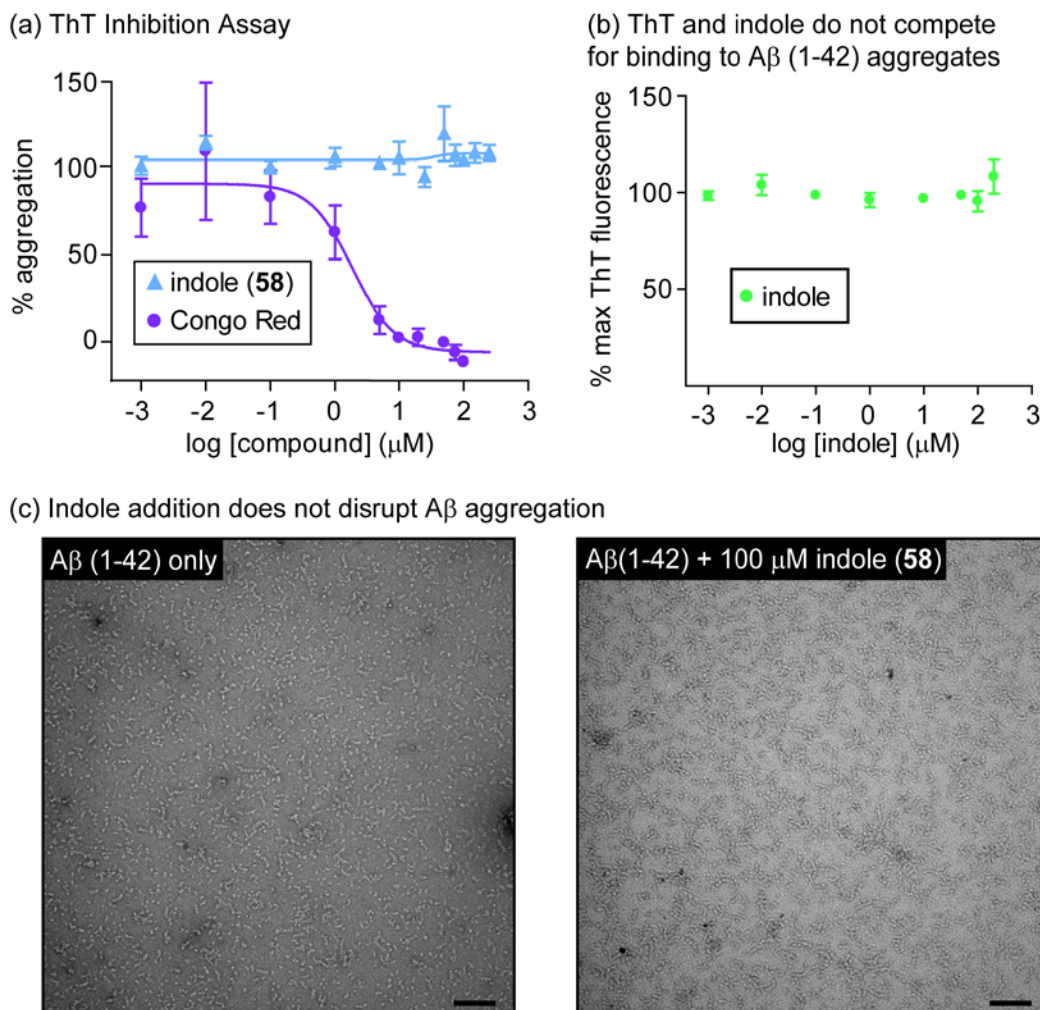
Aβ (1-42) only

Aβ(1-42) + 100 μM indole (58)

Figure 3.8 Indole does not block Aβ (1-42) aggregation by thioflavin T (ThT) and TEM. (a) Varying concentrations (1 nM - 250 μM) of indole were added to Aβ (1-42) prior to aggregation, and samples were incubated for 48 hours, followed by addition of ThT to measure the relative amount of aggregated Aβ. Indole did not disrupt Aβ aggregation compared to the positive control Congo Red. Error is expressed as the standard deviation of three (Congo Red) or six (indole) replicates. (b) Aβ (1-42) (25 mM in PBS, pH 7.4) was incubated at 37°C for 48 hours. Varying concentrations (1 nM - 200 μM) of indole (in 50 mM glycine pH 8.3) were added to the pre-formed aggregates. Immediately, ThT was added and the fluorescence was recorded. ThT and indole do not compete for binding to Aβ. Data is expressed as percent maximum ThT fluorescence of aggregates treated with DMSO only. Error bars represent the standard deviation of three replicates. (c) Indole (100 μM) was added to Aβ (1-42) prior to aggregation and incubated at room temperature for 48 hours followed by imaging with TEM (Bar = 100 nm). Aβ aggregation is not disrupted by the addition of indole.

transiently interact with fibrils. Because ThT and indole do not compete for the same site (Figure

3.8), these probes might be used in concert to study amyloid formation. It is important to note

that experiments in this area would likely be restricted to *in vitro* studies because indole is known to bind non-amyloid targets that would be present in biological settings.

3.2.7 The first ten residues of Aβ are dispensable for indole quenching

Indole (**58**) is known to undergo cation-π and π-π interactions with specific aromatic and cationic groups, including Phe, Tyr, His, Arg and Lys side chains [37]. Because of this property, it has been widely used as a probe of protein structure and dynamics [37, 44-47]. Moreover, the Ghiron group pioneered the use of indole fluorescence to probe the relative packing and permeability of proteins, revealing that a wide range of densities are observed within protein interiors [48, 49]. Thus, we reasoned that we might also exploit this property to explore molecular differences between oligomers and fibrils. Fortunately, the Aβ (1-42) sequence contains only four aromatic and six cationic residues most suitable for this type of interaction: Phe[4], Arg[5], His[6], Tyr[10], His[13], His[14], Lys[16], Phe[19], Phe[20] and Lys[28] (Figure 3.9a). Lys[16], Phe[19] and Phe[20] are located in the hydrophobic core region (HCR) and cannot be mutated or removed without losing the propensity for aggregation [50-52]. However, four of the other candidate residues (Phe[4], Arg[5], His[6] and Tyr[10]) are contained within the first ten residues, a region that is believed to be dispensable for aggregation [53, 54]. Therefore, as a first step to isolating residues that might be responsible for indole quenching by amyloid oligomers, we employed a commercially available truncation mutant Aβ (11-40). Using TEM, we first confirmed that Aβ (1-42), Aβ (1-40) and the truncated Aβ (11-40) peptide all form globular oligomers with approximately equal dimensions (Figure 3.9b). We then recorded changes in indole fluorescence upon addition of these structures (Figure 3.9c). As expected, indole quenching in response to Aβ (1-40) oligomers (K_{obs} = 0.28 ± 0.012 min^{-1}) is comparable to Aβ (1-42) oligomers (K_{obs} = 0.27 ± 0.011 min^{-1}), suggesting that removal of the last two residues (Ile[41], Ala[42]) has no influence on

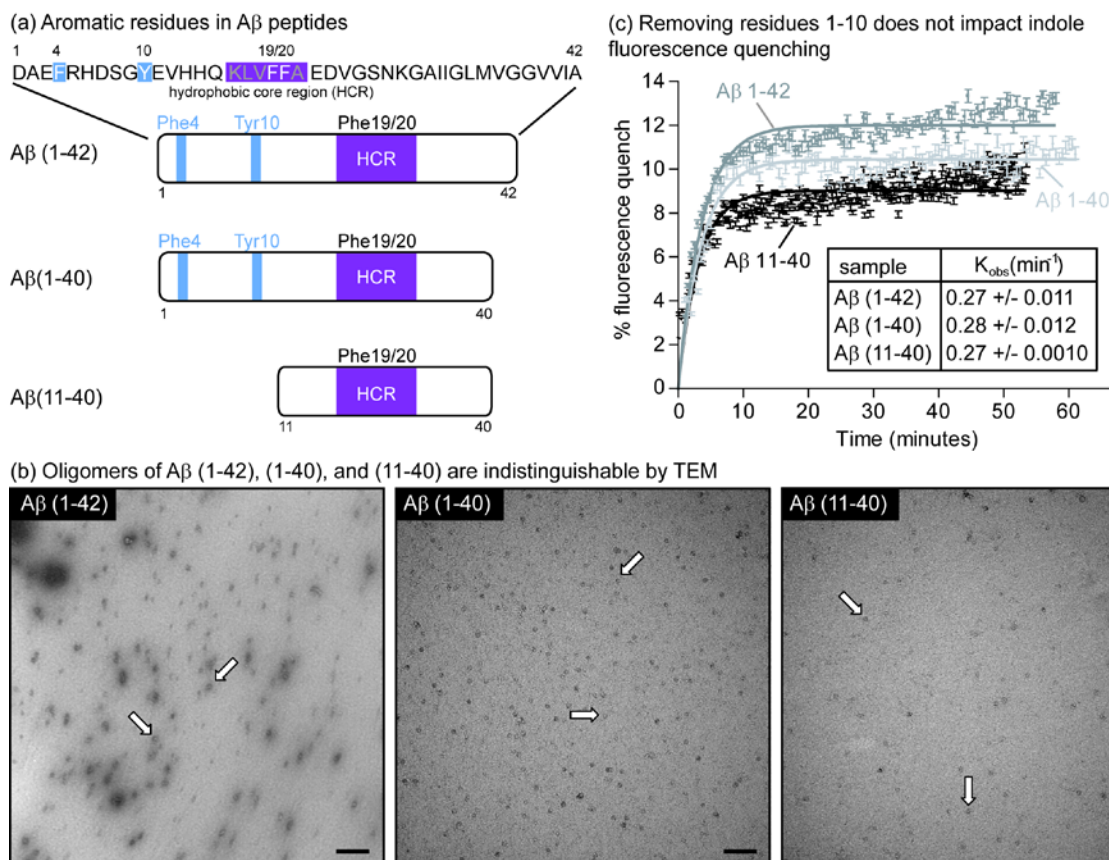(a) Aromatic residues in Aβ peptides

```
1      4        10           19/20                    42
DAEFRHDSGYEVHHQKLVFFA EDVGSNKGAIIGLMVGGVVIA
                     hydrophobic core region (HCR)
```

(c) Removing residues 1-10 does not impact indole fluorescence quenching

sample	K_{obs}(min^{-1})
Aβ (1-42)	0.27 +/- 0.011
Aβ (1-40)	0.28 +/- 0.012
Aβ (11-40)	0.27 +/- 0.0010

(b) Oligomers of Aβ (1-42), (1-40), and (11-40) are indistinguishable by TEM

Figure 3.9 Phe^4 and Tyr^{10} are not required for indole fluorescence quenching. (a) Schematic of aromatic residues in Aβ (1-42), Aβ (1-40), and Aβ (11-40) with likely indole docking sites (Phe^4, Tyr^{10}, Phe$^{19/20}$) shown. (b) Analysis by TEM shows similar morphologies amongst Aβ (1-42), Aβ (1-40), and Aβ (11-40) oligomer preparations. Bar = 100 nm. (c) The percent quench in indole fluorescence was recorded over time (Ex 280 nm, Em 350 nm) in the presence of Aβ peptides. Removal of the first 10 residues did not disrupt fluorescence quenching. Error is expressed as the standard deviation of six replicates.

indole binding. Interestingly, Aβ (11-40) oligomers also retained a full capacity to quench indole fluorescence (K_{obs} = 0.27 ± 0.001 min^{-1}). These results indicate that the first ten residues of Aβ are dispensable for indole quenching.

3.2.8 A secondary screen identifies TROL as a reagent with 18-fold selectivity for pre-fibrillar Aβ

Based on the results of our chemically diverse pilot screen, our objective was to empirically identify indole derivatives with improved signal intensity and selectivity. Toward that aim, we collected 37 substituted indoles (Appendix 3.5) and incubated each of them (100 μM) with solutions enriched for either Aβ pre-fibrils or Aβ fibrils. As previously reported, the pre-fibrillar

solution contains a mixture of spherical oligomers and smaller aggregates [14, 55]. Because we observed indole quenching by both LMW Aβ and oligomers (Figure 3.5a, b), we broadened our screening criteria to include both of these groups of architectures, termed 'pre-fibrils.' Following a 60-minute incubation, the fluorescence of each sample was then recorded and compared to that of the indole alone. Because we were interested in the compound's selectivity, we calculated the ratio of the fluorescence change between the pre-fibril and fibril samples and termed this value "pre-fibrillar selectivity". This analysis confirmed that ThT and another common probe, Bis-ANS, had poor pre-fibrillar selectivity (values of 0.2 and 1.1, respectively; Figure 3.10) [39, 55]. However, we identified ten compounds (**3**, **6**, **12**, **13**, **18**, **19**, **20**, **22**, **24**, and **34**) with better selectivity than the initial indole (Figure 3.10 and Appendix 3.5). From these studies, we focused on compound **22** (tryptophanol; TROL) because of its combination of high fluorescence intensity, selectivity (approximately 18-fold), and relatively large quench (approximately 25%).

Focused indole fluorescence screen reveals compounds with enhanced pre-fibrillar selectivity
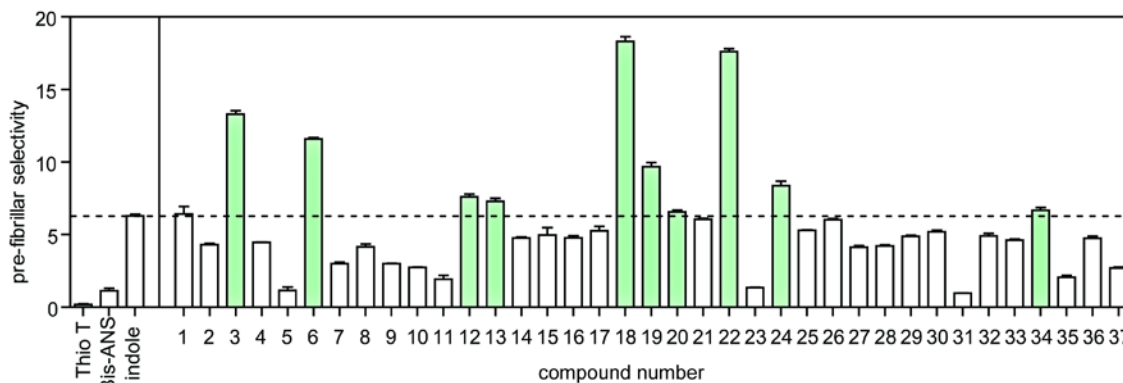
Figure 3.10 Assessment of pre-fibrillar selectivity of a focused indole collection. A library of 37 indole-containing compounds was screened for changes in fluorescence in the absence and presence of Aβ pre-fibrils and fibrils. The percent quench in fluorescence was determined for each compound, and the ratio (pre-fibril:fibril) of the percent change is shown (pre-fibrillar selectivity) relative to ThT (0.2) and Bis-ANS (1.1). Ten compounds (green bars) showed higher pre-fibrillar selectivity relative to indole (6.3), our previously best characterized hit (dashed line). We chose tryptophanol (**22**) for further investigation and assay development.

3.2.9 Tryptophanol (TROL) assay optimization and reproducibility

To scrutinize TROL as a potential fluorescent probe, we performed characterization studies similar to those performed with indole. In contrast, we shifted our focus to evaluate parameters that have previously been shown to be important in the ThT protocol. These included pH and buffer analyte, probe preparation, concentration and volume, and incubation time and temperature (Figure 3.11). Accordingly, we varied these factors and selected the conditions in which the greatest signal was achieved. Briefly, TROL signal was not significantly affected by pH or buffer salts, except for in PBS at basic pH (pH = 12.7) (Figure 3.11a). However, in other buffer systems at pH 12.6-13.7, fluorescence quenching was relatively unaffected. Thus, like indole, TROL signal showed only modest dependence upon pH. We chose to use the most commonly employed buffer for ThT assays, 50 mM glycine pH 8.2, as these conditions yielded nearly the highest TROL signal. Like indole, we also found that lower TROL volumes and concentrations yielded higher signal and faster equilibration time (Figure 3.11b, c). These findings are likely explained by self-association of the indoles at high concentrations. Finally, we investigated whether aged TROL samples remained efficacious in the assay. This is an important parameter, as ThT is known to self-assemble and change its fluorescence parameters over time. We found that, indeed, TROL showed over a 2-fold higher signal when prepared and used immediately (Figure 3.11d).

These experiments resulted in the optimized protocol shown in Table 3.1. Briefly, we found that the fluorescence equilibrates within 15 minutes following a brief, five minute incubation at 37 °C, as long as the TROL concentration was 10 μM, the volume was 100 μL and the TROL stock solution was used soon after preparation (Figure 3.11). We also noticed that gently mixing the solutions with a pipette accelerated the equilibration of the signal. After incorporating these optimized procedures, we were pleased to find that the general procedures for the TROL and
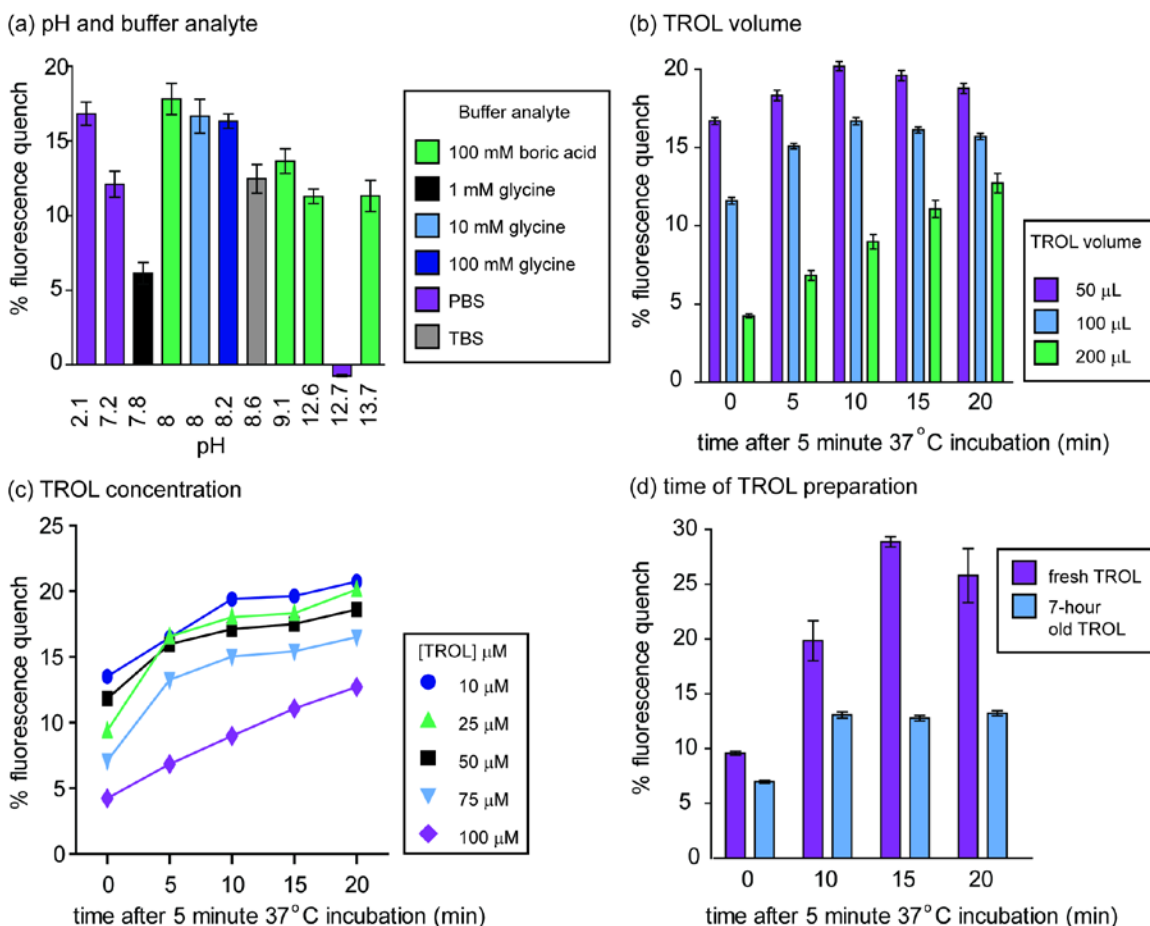
Figure 3.11 Optimizing pH, volume, concentration, and time of preparation of the TROL reagent (a) 100 μM TROL was prepared in a variety of buffers at pH values ranging from 7.2-9.1, and 150 μL added to pre-fibrils. Samples were incubated for 12 minutes at 37 $^{\circ}$C followed by 30 minutes at room temperature, after which the fluorescence was recorded relative to TROL alone. The optimized pH range lies between 8-8.2. Although 100 mM boric acid (pH 8) displayed a high signal, we chose a glycine-based buffer at pH 8.2 because it is the most commonly accepted buffer for the ThT assay. (b) 50, 100, or 200 μL (80 μM) of TROL was added to pre-fibrils. The fluorescence was recorded at 0, 5, 10, 15, and 20 minutes following incubation at 37 $^{\circ}$C (five minutes). The amount of TROL impacted both the signal and equilibrium time. Lower amounts of TROL (100 μL or less) displayed faster signal equilibration as well as optimal reactivity. (c) TROL concentration was varied from 10 - 100 μM and the assay was developed as described in (b). Similar to TROL volume, high concentrations (> 100 μM) displayed lower signal and slower equilibration. Alternatively, at 10 μM, the signal was highest and remained unchanged after approximately 10 minutes. (d) To test the impact of the time of TROL preparation on signal, we compared freshly prepared and aged (7 hours) TROL samples. The preparations equilibrated similarly, but aged TROL displayed a > 50% lower signal, suggesting TROL should be prepared immediately prior to the start of an experiment for optimal reactivity. For each experiment, 10 μL of 25 μM Aβ (1-42) pre-fibrils were used unless otherwise noted, all samples were plated in triplicate, and error bars represent the standard deviation. With the exception of (a), 50 mM glycine pH 8.2 was used for all experiments. Unless otherwise stated, the assay was developed using the protocol in Table 3.1.

ThT assays were roughly parallel (Table 3.1), suggesting that they could be conveniently employed side-by-side.

As mentioned, Aβ aggregation reactions can be heterogeneous, which often results in variability when comparing samples from different stock solutions or vendors. Therefore, as with indole, we wanted

Table 1: Comparison of the pre-fibrillar TROL assay to the ThT assay

Tryptophanol (TROL) assay	Thioflavin T (ThT) assay
(1) add 10 μL of amyloid solution to 96-well plate*	(1) add 10 μL of amyloid solution to 96-well plate*
(2) add 100 μL TROL (10 μM) per well (50 mM glycine, pH 8.2, 0.01% DMSO)	(2) filter (0.22 μm) 5 μM ThT (50 mM glycine, pH 8.2)
(3) mix by pipetting and incubate 5 minutes (37°C)	(3) add 200 μL ThT per well
(4) incubate 15 minutes (room temperature)	(4) mix by pipetting and incubate 15 minutes (room temperature)
(5) read fluorescence (Ex 280/Em 355)	(5) read fluorescence (Ex 280/Em 355)

*96-well black, opaque, flat-bottom plate

to explicitly study the repeatability of the TROL signal. Using several batches of both Aβ (1-40) and (1-42) obtained from two vendors, we performed reproducibility profiling experiments. These studies revealed that pre-fibrils consistently quenched TROL fluorescence by over 20%, while fibrils routinely had little signal (Figure 3.12a, b). Further, the TROL signal was similar regardless of whether Aβ (1-40) or (1-42) were used.

3.2.10 TROL detects pre-fibrillar Aβ in the presence of pre-formed fibrils

Based upon the fact that indole fluorescence is quenched even in the presence of fibrils (Figure 3.5g), we hypothesized that we might find similar patterns with TROL. Furthermore, for the TROL assay to be applicable in monitoring aggregation, the probe must be able to reliably detect pre-fibrils in mixtures of different amyloid conformations. To address this possibility, we added increasing amounts of pre-fibrillar Aβ (1-40) to solutions of fibrils. These well-defined mixtures were then immediately incubated with TROL. Using this approach, we found that the TROL signal could reliably detect pre-fibrils even in mixtures (Figure 3.12c). We also estimated that the lower limit for detection of pre-fibrillar Aβ is approximately 7.5 μM (or 30% of the mixture).

Based upon these findings, we predicted that TROL might be used to quantify pre-fibrillar Aβ during amyloid formation, analogous to how ThT is used to track total aggregation.
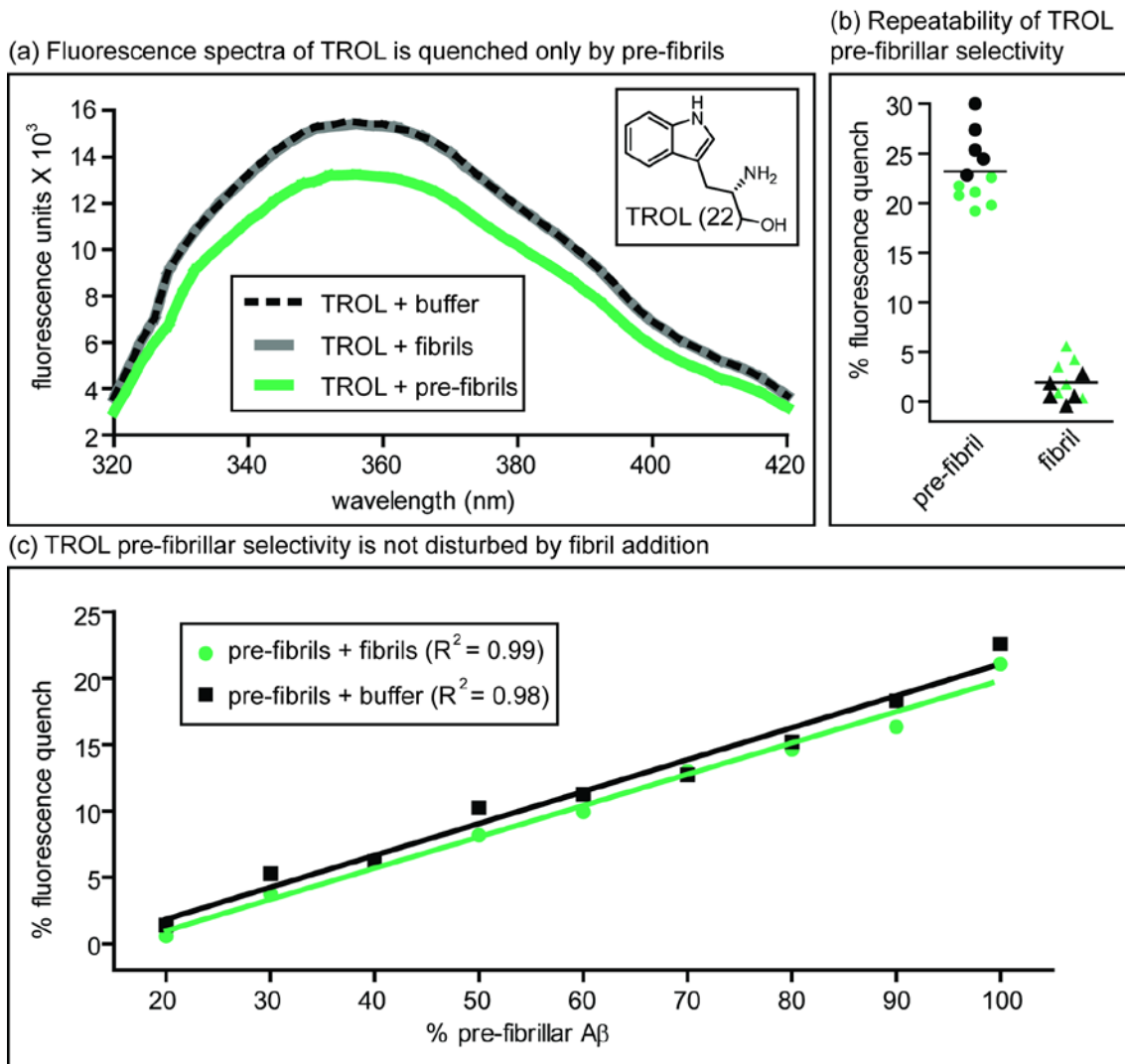
Figure 3.12 TROL selectively detects pre-fibrils upon pre-formed fibril addition (a) The fluorescence spectra of TROL (Ex 280 nm) in the presence of 25 μM Aβ pre-fibrils (green), fibrils (grey), or PBS (black dashed) shows the selective quenching effect in the presence of pre-fibrils. Inset: chemical structure of tryptophanol (TROL). (b) The TROL quenching effect is robust and repeatable. Aliquots of either Aβ (1-40) (black) or (1-42) (green) were tested for pre-fibrillar selectivity. These data include samples from different vendors and shipments. (c) Increasing amounts of Aβ fibrils or PBS were titrated into a solution of pre-fibrils. The change in TROL fluorescence is identical in each experiment, showing that the presence of fibrils does not disrupt the ability to detect pre-fibrillar Aβ. The change in TROL fluorescence increases linearly with the concentration of pre-fibrils in solution.

3.2.11 Monitoring the depletion of pre-fibrillar Aβ during aggregation using TROL

One use of ThT is to monitor the kinetics of aggregate formation [52, 56-59]. Similarly, we hypothesized that the TROL signal might dissipate during depletion of its target, revealing when pre-fibrils progress to fibrils during the aggregation pathway. To test this idea, Aβ (1-40) was incubated at 37 °C and, at the indicated times, 10 μL aliquots were removed and plated in two sets of triplicates. The TROL and ThT assays were then performed concurrently. From these experiments, we observed a roughly inverse relationship between the signals (Figure 3.13a). As expected, at early time points (0, 0.5, and 1 hour), both signals were relatively stable, with the TROL assay showing maximum pre-fibrillar content and ThT indicating low amounts of total aggregated Aβ. Between 1 and 1.5 hours, the TROL signal decreased dramatically, while the ThT signal increased by 30%, suggesting that more advanced Aβ aggregates begin to accumulate during this time. Interestingly, the TROL signal remained clearly present after the ThT signal reached equilibrium (*e.g.* 1.5 hrs). These findings suggest that the fibrillization process (and, specifically, depletion of pre-fibrillar content) remains active after the ThT signal has equilibrated. Similar trends were observed for Aβ (1-42) (Figure 3.13a).

Neither the TROL nor the ThT signal is sufficient to make any definitive conclusions about pre-fibrillar or fibrillar content. Rather, complementary techniques, such as gel electrophoresis and transmission electron microscopy (TEM), are commonly employed to supplement studies of Aβ aggregation [14, 60, 61]. For example, one feature of large fibrils is that they are retained at the stacking gel during electrophoresis. We used this method to probe when these structures form in relation to the TROL and ThT signals. Using the general anti-Aβ antibody (6E10), we observed a marked increase in a high molecular weight band during aggregation (Figure 3.13b). Specifically, this band emerged at 2.5 hours and its relative intensity increased until

(a) TROL reveals a depletion of pre-fibrillar Aβ (1-40) and (1-42) during aggregation

(b) Appearance of high-molecular weight Aβ (1-40) fibrils

(c) TEM supports the depletion of Aβ (1-40) pre-fibrils
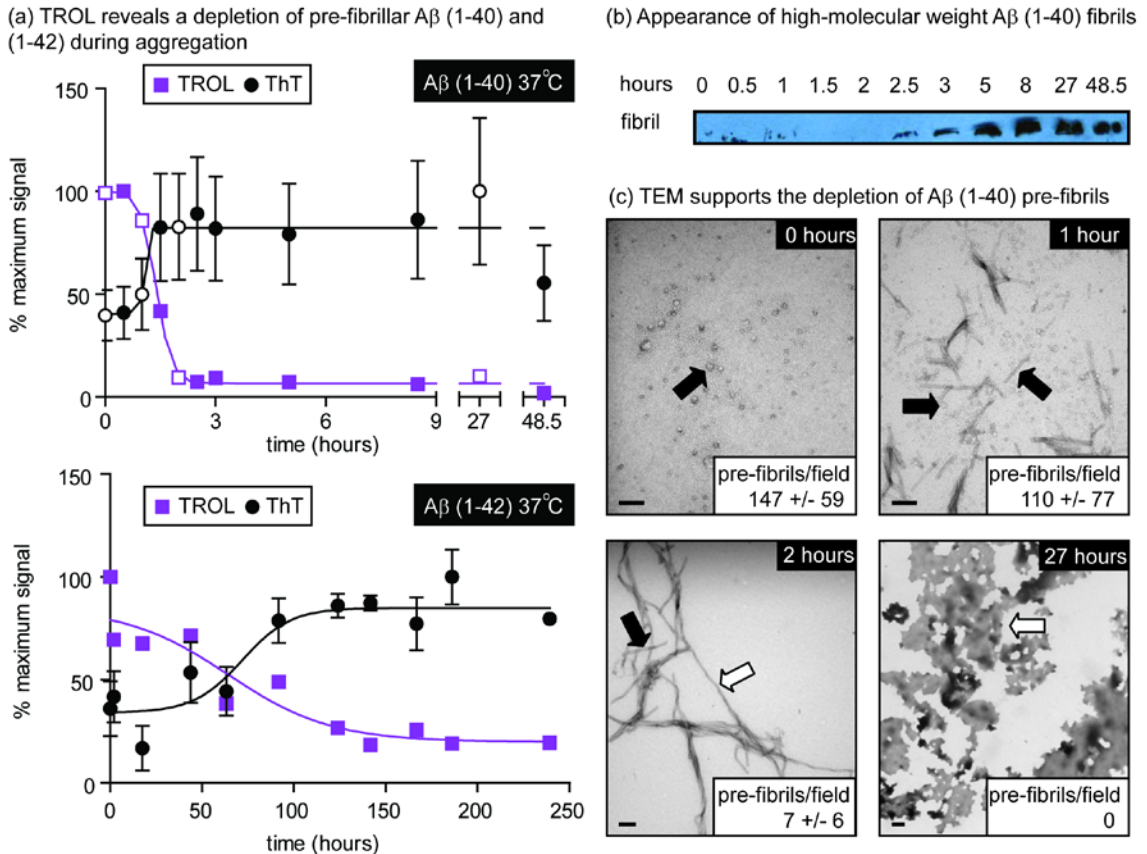
Figure 3.13 Monitoring the decrease of pre-fibrillar Aβ over time using TROL (a) 25 μM Aβ (1-40) or (1-42) was suspended in PBS and incubated at 37°C with shaking. At the indicated time points, 10 μL was removed and tested for either TROL or ThT reactivity in triplicate. Open squares (TROL) and circles (ThT) for Aβ (1-40) correspond to the samples used in the electron microscopy experiments. Error bars represent standard deviation. In some cases the error is smaller than the data symbol. (b) A general anti-Aβ antibody (6E10) was used to monitor high-molecular weight fibrils. At the indicated time points, samples were separated by electrophoresis and the interface between the stacking and resolving gels was blotted. (c) TEM was used to evaluate the content of Aβ mixtures. The levels of pre-fibrils were roughly quantified at each time point, (average pre-fibrils per 13.2 μm² field). Pre-fibrils were defined as globular oligomers and linear protofibrils less than 500 nm in length. Bar = 100 nm. Arrows indicate pre-fibrils (black arrow) and fibrils (open arrow).

approximately 8 hours. It then remained throughout the rest of the time-course. In comparison, the TROL response equilibrated at around 2.0 hours, suggesting that this probe's signal is exclusive of the formation of high molecular mass Aβ fibrils. Interestingly, the ThT fluorescence was saturated approximately 1.0 hours prior to the appearance of the large fibrils; it had reached ~90% of its maximum signal at 1.5 hours. Thus, these results suggest that disappearance of the TROL signal better correlated with the appearance of the fibrils, likely because ThT was unable to distinguish between pre-fibrillar and fibrillar conformations.

Next, we used TEM to analyze the pre-fibrillar and fibrillar content at various times during Aβ (1-40) aggregation (Figure 3.13c). We specifically focused on the 1 and 2 hour times because changes in the sensitivity to TROL and ThT seemed to occur in this period. To allow quantitative comparisons, the average number of pre-fibrillar, spherical oligomers per field (13.2 μm^2) was determined. As expected, many pre-fibrillar structures were observed a few minutes after the initiation of aggregation (147 ± 59 pre-fibrils per field). By 1 hour, this number had decreased to 110 ± 77 pre-fibrils per field, corresponding with the appearance of some short fibrils. At 2 hours, the total level of pre-fibrils was depleted dramatically (~ 7 per field), and the sample consisted largely of mature fibrils (average length greater than 500 nm) (Figure 3.13c). By 27 hours, large amorphous deposits predominated and the smaller structures had been entirely depleted. Together, these results support a model in which TROL recognizes pre-fibrillar Aβ.

3.2.12 TROL signal diminishes during aggregation of ataxin-3, amylin, and CsgA, but not α-synuclein

Many proteins involved in aggregation disorders, such as human islet amyloid polypeptide (hIAPP or amylin) and α-synuclein, assemble into amyloids whose morphologies are nearly indistinguishable from those formed by Aβ [3, 62-64]. In addition, a growing number of functional amyloids are being described, including those assembled from the bacterial protein CsgA [65]. Despite the fact that none of these amyloid-forming proteins share obvious sequence homology, they all form β-sheet rich fibrils and they interact with ThT [66]. To test whether TROL can also recognize multiple amyloid-forming proteins, we performed assays on α-synuclein, amylin (hIAPP), ataxin-3, and CsgA, using known procedures (see Experimental Procedures). Interestingly, we found that the TROL signal diminished during the aggregation of CsgA, amylin, and ataxin-3 (Figure 3.14a-c), but not during α-synuclein self-assembly (Figure

3.14d). For the sensitive amyloids, TROL fluorescence decreased concurrently with the increase in ThT fluorescence, qualitatively similar to what we observed with Aβ (1-40). For α-synuclein, we did not observe any change in fluorescence, suggesting that either these fibrils quench TROL fluorescence or that pre-fibrils remain during the entire time course. Regardless, these results demonstrate that the TROL response is not restricted to Aβ, but that it likely responds to a common pre-fibrillar characteristic of multiple amyloid systems.
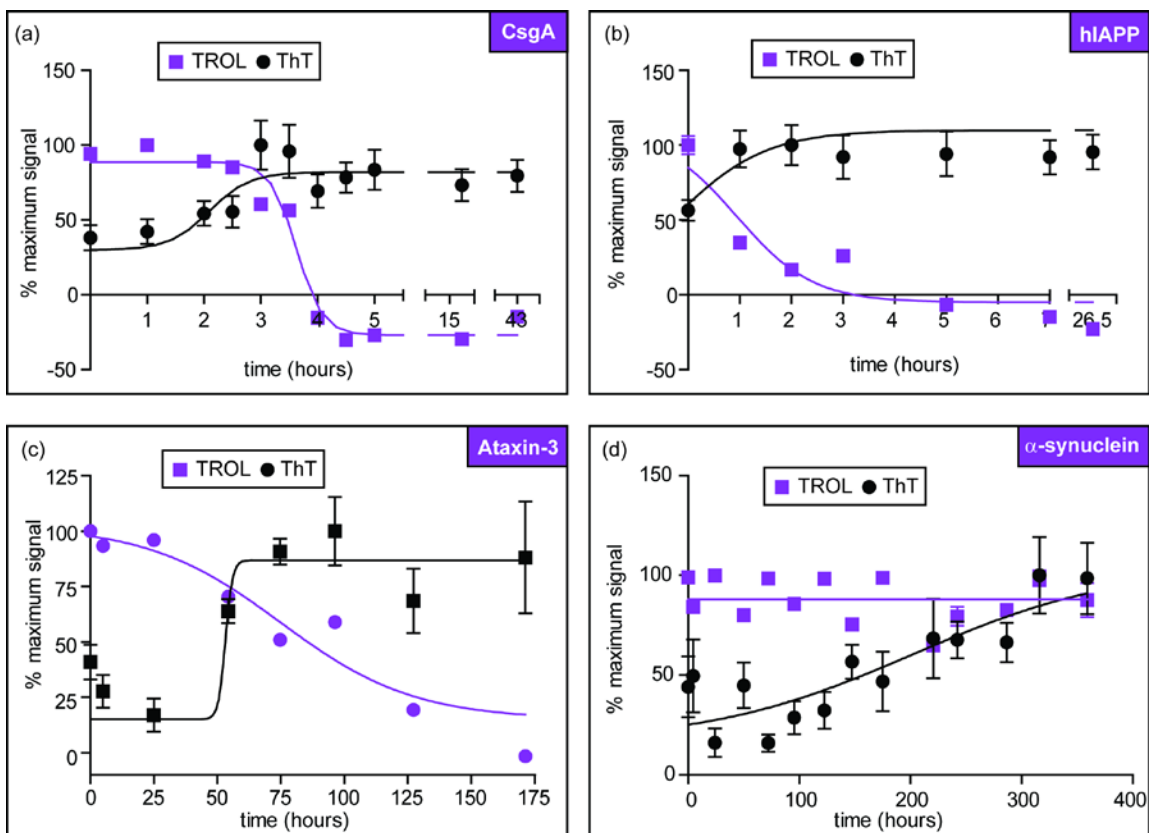
Figure 3.14 TROL is sensitive to pre-fibrillar forms of several amyloidogenic proteins The TROL assay was conducted with four amyloid-forming proteins to establish its applicability for other pre-fibrillar proteins. ThT fluorescence was recorded simultaneously to monitor fibril formation. TROL detects pre-fibrillar forms of (a) CsgA (25 μM), (b) hIAPP/amylin (20 μM), and (c) ataxin-3 (10 μM) andcan therefore be used to quantify the disappearance of pre-fibrils over time in these systems, similar to Aβ. (d) TROL fluorescence is quenched in the presence of α-synuclein pre-fibrils. However, this signal does not decrease over time, despite a 10-fold increase in ThT signal, suggesting that the TROL binding epitope may be present in both α-synuclein pre-fibrils and fibrils.

3.3. Discussion

Different Aβ conformations have been largely defined by their solubility, appearance in TEM, reactivity with select antibodies, and neurotoxicity. While it is known that these structures are all composed of β-sheet rich Aβ peptide, it is unclear how this monomer is assembled in a structurally unique way in each conformation. The structural properties of elongated, mature fibrils have been partially revealed, but other conformations, including oligomers, have been resistant to these inquiries. We hypothesize that these molecular differences are likely paramount for defining biological activity. Therefore, to probe the landscape of Aβ in its various configurations, we employed samples enriched for oligomers or fibrils and screened 84 structurally diverse small molecules. We chose small molecules for this study because their low mass (< 500 Da) might allow us to explore specific aspects of amyloid structure, such as relative permeability to small, chemical probes. In these pilot studies, we discovered that five indole-containing compounds are sensitive to pre-fibrillar structures but not fibrils.

The identification of indoles in the diverse chemical screen was fortuitous because previous reports support its use as a probe of protein structure [37, 45, 47]. Specifically, its fluorescence signature is exquisitely sensitive to cation-π and π-π interactions with amide bonds, aromatic groups and cationic side chains [67-69]. Moreover, to engage in fluorescence quenching interactions, the indole must be relatively close and appropriately aligned with the corresponding residue [67]. In order for quenching to occur, the probe must permeate into the protein and, therefore, differences in quenching have been used to model side chain packing and relative density [48, 49]. This property benefits from the fact that indole (**58**) is a small (117 Da), compact molecule that is expected to be relatively permeable. The full length Aβ (1-42) peptide contains no tryptophans and only ten residues that are most suitable for interaction

with indole: Phe[4], Arg[5], His[6], Tyr[10], His[13], His[14], Lys[16], Phe[19], Phe[20] and Lys[28]. Moreover, Aβ (11-40), a truncated form of the peptide, removes four of these potential partners. Using this truncation mutant, we found that the first ten residues are dispensable for quenching (see Figure 3.7). Thus, from these observations, we conclude that other residues, such as His[13], His[14], Lys[16], Phe[19], Phe[20] and Lys[28], are more buried and/or less accessible in fibrils than in LMW-Aβ or oligomers. Thus, we interpret these results as suggestive of a dramatic change in packing during assembly of fibrils from pre-fibrillar structures.

Together with previous studies, these results might help refine models of amyloid structure and function. For example, Chimon *et al*. showed that both Aβ oligomers and fibrils are composed predominantly of well-ordered β-sheets but oligomers lack the stable tertiary packing characteristic of fibrils [18]. Hydrogen-deuterium exchange (HDE) studies provide qualitatively similar results, as this method indicates that LMW-Aβ and oligomers are more solvent exposed than linear protofibrils or fibrils [19, 70]. Further, high-resolution AFM studies suggest that oligomers are composed of monomers assembled in a disc-like pattern, different than the dense packing between β-sheet rich peptides in fibrils [16]. These studies all suggest that LMW-Aβ and oligomers have a more loosely packed core and that fibrils are relatively dense. The present report adds to these studies by suggesting a minimal collection of amino acids that appear to become relatively buried in fibrils. This is an important finding, because most previous studies have not classified the accessibility of specific residues; however, a recent manuscript from Olofsson *et al.* described the HDE rates for each residue in fibrils of Aβ (1-40). In that study, the HCR residues, including Lys[16], Phe[19] and Phe[20], were found to be have slow exchange rates [71]. Conversely, His[13], His[14] and the first ten residues of Aβ (1-40), all underwent fast exchange. Our results are consistent with these findings and, together, they support a model in which core Aβ

residues are relatively buried in fibrils. However, even with these advancements, it is clear that important questions about amyloid structure remain. Terms such as "relatively exposed", "buried" or "loosely packed" imply differences in the arrangement of Aβ monomers, but these classifications are awaiting verification at atomic resolution, while the apparent heterogeneity of oligomers continues to obscure these details. However, a continued pursuit of molecular differences is important because these likely govern molecular recognition in biological settings and, thus, the relative toxicities of the amyloid structures.

Existing chemical dyes for the rapid *in vitro* quantification of amyloids, such as ThT and Bis-ANS, have been invaluable for studying the aggregation process, but they do not distinguish between pre-fibrillar and fibrillar Aβ. Here, based on our secondary screen, we report the development of the TROL assay: an analogous, fluorescence-based method for the specific detection of pre-fibrillar Aβ *in vitro*. We found that pre-fibrils quenched TROL fluorescence and that this effect was not disrupted by the presence of fibrils. When used together with ThT, we found evidence that Aβ pre-fibrils continue to be present after equilibration of the ThT signal, at least under the conditions we employed (Figure 3.13a). Thus, the aggregation process is likely ongoing, producing mature fibrils from pools of pre-fibrillar structures, a conclusion that is supported by the electrophoresis (Figure 3.13b), electron microscopy studies (Figure 3.13c) and previous literature reports [17, 72-74]. When envisioning other applications of this reagent, it is important to note that TROL is likely not suitable for use *in vivo*. Several groups have noted that indole fluorescence is altered by non-amyloidogenic proteins, such as BSA, limiting its use to in vitro applications [75, 76]. Despite this limitation, there are likely multiple, potential applications of the TROL protocol, such as studying the contributions of individual residues on pre-fibril formation or rapidly quantifying pre-fibrillar content prior to measuring relative toxicity.

Pre-fibrillar Aβ levels are thought to correlate with AD pathology better than the amount of fibrils [5, 8]. Despite this emerging consensus, there is still considerable debate as to what exactly constitutes the key, neurotoxic structure(s). Because there is good evidence for a number of these structures, including dimers, spherical oligomers of various sizes and other intermediate assemblies [1, 8, 77], it seems plausible that multiple Aβ conformations contribute to disease. These challenges highlight the need to develop multiple classes of informative amyloid reporters, including those that selectively recognize individual conformations (*e.g.* oligomers) and those that more broadly encompass the known neurotoxic structures (*e.g.* dimers, oligomers, etc.). In response to the first of these needs, a series of useful antibodies have been developed against specific antigens [3, 11]. Towards the second aim, assays such as TROL might provide a survey of total pre-fibrillar content.

What feature of an amyloid pre-fibril is recognized by indoles? This probe appears to react with multiple structures, likely encompassing oligomeric and monomeric Aβ, but its main feature is that it fails to recognize fibrillar Aβ. We hypothesize that indoles might either recognize a unique structural feature of pre-fibrillar amyloids or, more likely, that its normal binding site is precluded or otherwise altered in fibrils. Further work is needed to differentiate between these possibilities. Additional details of the structure and binding site(s) of this reagent might lead to rational design of probes that discriminate even better between amyloid morphologies. Proposed methods for determining the binding site, as well as future applications of TROL, are presented in Chapter 5.

3.4 Experimental Procedures

3.4.1 Materials

Amyloid-β (1-40), (5-40), and (11-40) peptides were purchased from Anaspec (San Jose, CA). Aβ (1-42) peptide was purchased from EZBiolab (Westfield, IN) or Anaspec (San Jose, CA). DMSO and HFIP were purchased from Sigma-Aldrich. Compounds used in the fluorescence and indole screens were synthesized internally or purchased from Anaspec, Sigma-Alrich, Fluka, Fisher Scientific, TCI America (Portland, OR), and Caymen Chemicals (Ann Arbor, MI). Tryptophanol (TROL) from Sigma and TCI America yielded identical results. Anti-amyloid β antibody (6E10) was purchased from Calbiochem (San Diego, CA) or Covance (Dedham, MA). Secondary antibodies were purchased from Bio-Rad (Hercules, CA) or Abcam (Cambridge, MA). Fluorescence readings were taken on a SpectraMax M5 multi-mode plate reader (Molecular Devices, Sunnyvale, CA). All fluorescence assays were performed in black, opaque, flat-bottom 96-well plates (Corning Inc., Corning, NY). Sealing films were purchased from Nalge Nunc International (Rochester, NY).

3.4.2 Amyloid-β preparation

One milligram samples of Aβ (1-42) peptide were dissolved in 200 μL hexafluoroisopropanol (HFIP) and aliquoted to obtain 0.1 mg stocks. HFIP was removed under nitrogen to provide a thin film and these stocks were stored at -30°C until ready for use. Immediately prior to the start of each experiment, an aliquot was dissolved in DMSO (see below). Fibrils were obtained by adding phosphate buffered saline (PBS; pH 7.4) to a final concentration of 25 μM (1% final DMSO concentration). These solutions were vortexed, sonicated for 75 seconds, and agitated for 48 hours at 37 °C. Oligomers and pre-fibrils were obtained by adding DMEM-F12 media (Gibco) to a final concentration of 25 μM (1% final DMSO concentration), followed by vortexing, sonicating for 75 seconds, and incubating for 48 hours at 4 °C without agitation. LMW Aβ was

obtained by adding PBS (pH 7.4) to a final concentration of 25 μM (1% final DMSO concentration), vortexing, sonicating for 75 seconds and using these samples immediately.

3.4.3 Transmission electron microscopy (TEM)

Freshly suspended Aβ or aggregated sample (25 μM; 5 μL) was added to glow-discharged, Formvar/carbon 300-mesh copper grids (Electron Microscopy Sciences, Hatfield, PA) and incubated for 1.5 minutes at room temperature. Excess sample was blotted off with filter paper and each grid was washed twice with ddH2O. 3 μL of 1% uranylacetate in methanol was then added to the grid for one minute. Excess solution was wicked away using filter paper and the grids were dried for 15 minutes. Grids were visualized on a Phillips CM-100 transmission electron microscope at 80 kV and magnification settings ranging from 10,500 – 92,000X. The levels of pre-fibrils per field were quantified by tallying the number of spherical oligomers and short protofibrils in each micrograph. The average number of pre-fibrils was then calculated from between 5 and 16 micrographs.

3.4.4 Native-gel electrophoresis and Western blotting

For denaturing studies, Aβ (1-42) fibrils and oligomers were prepared at 25 μM as described and cross-linked using gluteraldehyde (0.04% final concentration) for 40 minutes at room temperature. The reaction was quenched with glycine pH 8.2 (final concentration of 10 mM) and SDS-loading dye (non-reducing) was added (25% final volume). Each sample (8 μg) was separated on a 10-20% gradient tris-tricine gel (Bio-Rad). For aggregation studies, Aβ (1-40) samples from the indicated times were flash frozen and stored at -80 °C. Once thawed, 15 μL of each sample was separated on a 10-20% tris-tricine gradient gel (Invitrogen) using non-denaturing, non-reducing loading buffer (300 mM tris-HCl, 8% glycerol, 0.01% bromophenol

blue). Following separation by electrophoresis, gels were transferred to nitrocellulose (1 hour, 4 °C, 175 milliamps). The nitrocellulose was blocked in either 10% non-fat dried milk or 3% BSA in TBS-T (140 mM sodium chloride, 25 mM tris, 0.1% Tween-20) for 60-90 minutes at room temperature, incubated in anti- The membrane was washed (3 X 5 minutes) with TBS-T and either incubated overnight at 4 °C in 1:2000 6E10 containing 1.5% BSA in TBS-T, or for one hour at room temperature in 1:1000 6E10 containing 1.5% BSA in TBS-T. The membrane was then washed again (3 X 5 minutes) and probed with HRP-conjugated goat anti-mouse antibody (1:10,000) in 3% BSA in TBS-T for one hour at room temperature. Protein bands were visualized using the Bio-Rad or PerkinElmer ECL kit according to the manufacturer's instructions.

3.4.5 Urea denaturation of preformed Aβ aggregates

Aβ fibrils and oligomers were prepared at (25 μM) as described and an aliquot (10 μL) dispensed into 96-well plate format (black Corning). Urea (30 μL) at varying concentrations (0 M – 6 M) was added to these samples, mixed thoroughly, and the solutions were incubated for 40 minutes at room temperature. Following this treatment, 200 μL ThT (5 μM in 50 mM glycine, pH 8.2) was added and these samples were then incubated for 15 minutes and the fluorescence recorded (Ex 446 nm; Em 490 nm). Control experiments confirmed that urea did not impact the intrinsic fluorescence of the ThT reagent and TEM experiments confirmed a disruption in ultrastructure (not shown).

3.4.6 Bis-ANS Fluorescence

4,4'-dianilino-1,1'-binaphthyl-5,5'-disulfonate (Bis-ANS) (100 μL; 25 μM in 30 mM citrate pH 2.4, 1% DMSO) was added to 9 μL Aβ fibrils or oligomers (25 μM) or 9 μL PBS or DMEM-F12 (1% DMSO) in a black 96-well plate (Corning Costar). Fluorescence was measured after 2 minutes (Ex

385 nm, Em 520 nm, cutoff 515 nm). Experiments were performed using six replicates. Background fluorescence of fibrils, oligomers, PBS, and DMEM-F12 in the presence of 100 μL buffer alone (30 mM citrate pH 2.4, 1% DMSO) was subtracted.

3.4.7 Fluorescence screens: (1) Pilot: amyloid ligand library and (2) Secondary: indole collection

Each compound was dissolved in DMSO to a final concentration of 100 mM and then diluted to 50 μM with ddH2O (1% final DMSO concentration). 100 μL of each compound was added to 9 μL Aβ fibrils or oligomers (25 μM) or 9 μL PBS or DMEM-F12 (1% DMSO) in triplicate to a black 96-well plate and incubated for 10 minutes. Fluorescence spectra were then recorded at four excitation and emission values: a) Ex 290 nm, Em 320-520 nm; b) Ex 350 nm, Em 380-650 nm; c) Ex 400 nm, Em 430-620 nm; d) Ex 450, Em 480-650. Background fluorescence of fibrils, oligomers, PBS, and DMEM-F12 in the presence of 100 μL ddH2O only (1% DMSO) was subtracted. For indole time-course experiments, the fluorescence of six replicates was measured every 30 seconds for 1 hour (Ex 280 nm, Em 350 nm, cutoff 325 nm) and this data was fit using a one-phase exponential association in GraphPad Prism software. For the detailed studies of the indoles (**57**, **58**, **62-64**) (5-methylindole-2-carboxylic acid, indole, melatonin, tryptamine, and tryptophan), each compound was dissolved in DMSO to a final concentration of 100 mM and diluted to 100 μM in 50 mM glycine pH 8.2 (1% final DMSO concentration). To determine pH effects, pH was varied in either PBS (pH 2.2-7.0) or 50 mM glycine (pH 8.2). For the oligomer titration experiment, fibrils and oligomers were prepared as described and mixed in varying percentages (0, 5, 10, 25, 50, 75, 95, and 100% oligomer), while maintaining a constant protein concentration.

Prior to screening the indole collection, the excitation and emission maxima of each indole derivative were determined at 100 μM in 0.01% DMSO and 50 mM glycine, pH 8.2 (Supplemental Table 1). Then, 150 μL of 100 μM compound was added to black 96 well plates with either 10 μL of 25 μM pre-fibrils or fibrils. As a control, the fluorescence of each compound was also determined by adding 10 μL of either DMEM-F12 or PBS in place of pre-fibrils or fibrils, respectively. Plates were sealed and incubated in the dark for 60 minutes at room temperature, after which fluorescence was recorded at the appropriate excitation and emission maximum.

3.4.8 TROL assay protocol

To a sample of 10 μL of amyloid (e.g. Aβ (1-40) 25 μM in PBS) or corresponding buffer was added 100 μL of 10 μM TROL (0.01% DMSO) in 50 mM glycine (pH 8.2) in black 96-well plates. These samples were mixed three times by gentle pipetting. The plate was then sealed and incubated at 37 °C for 5 minutes. The plate was cooled for 15 minutes at room temperature in the dark. Following gentle tapping of the plate, the fluorescence was recorded (Ex 280 nm, Em 355 nm).

3.4.9 Thioflavin T (ThT) assay

For testing whether indole inhibits Aβ self-assembly, ThT fluorescence was applied. The inhibition assay was performed as described [41]. Briefly, 12 concentrations of indole were prepared in PBS containing 10% DMSO. 9 μL of 25 μM Aβ (1-42) in PBS (1% DMSO) was added to 1 μL of each compound in a 96-well plate and were incubated at room temperature for 48 hours. The relative amount of aggregate was measured by addition of 200 μL ThT (5 μM in 50 mM glycine, pH 8.2) and compared to a DMSO-treated control. Fluorescence of ThT alone was subtracted from each sample and data was fit by non-linear regression analysis using GraphPad

Prism software. To confirm that indole and ThT do not compete for the same binding site on Aβ, the two ligands were added simultaneously to pre-formed Aβ aggregates. Briefly, 1 μL of indole (1 nM – 200 μM) in PBS (10% DMSO) was added to 9 μL of pre-formed Aβ fibrils in a 96-well plate. Immediately, 200 μL ThT (5 μM in 50 mM glycine, pH 8.2) was added to each sample, incubated for 15 minutes at room temperature, and the fluorescence was recorded (E_x 446 nm; E_m 490 nm). All experiments were performed in triplicate.

To monitor aggregation over time, the ThT assay was performed using previously established methods [25, 41, 55, 78]. Briefly, 10 μL of protein or the corresponding buffer was plated in triplicate in a 96-well black plate. 5 μM ThT was prepared in 50 mM glycine (pH 8.2) and filtered (0.22 μm). ThT (200 μL) was then added, the solution mixed by pipetting and then the plates were incubated at room temperature for 15 minutes. Following gentle tapping, the fluorescence was recorded (Ex 446 nm, Em 490 nm).

3.4.10 Monitoring amyloid aggregation over time

Aβ (1-40) or Aβ (1-42) was suspended in PBS (1% DMSO) to a final concentration of 25 μM. Aβ (1-40) was incubated at 37 °C with shaking, and Aβ (1-42) was incubated at room temperature (without shaking). The ThT signal and kinetics of its appearance correlate well with previous reports under identical conditions [19]. Recombinant ataxin-3 (Q80) was expressed and purified as previous reported [79]. A 75 μM stock solution was diluted to 10 μM in PBS and incubated at 37 °C with shaking for aggregation [80]. hIAPP/amylin peptide (Anaspec, San Jose, CA) was suspended in HFIP, aliquoted and lyophilized. The lyophilized powder was then brought up in PBS (1% DMSO) to a final concentration of 20 μM and incubated at 37 °C with shaking [81]. Recombinant CsgA was expressed and purified as reported [82]. A 68 μM stock solution was

diluted to 25 μM in PBS and incubated at room temperature (without shaking) for aggregation [83]. Recombinant α-synuclein was expressed and purified as reported [84]. This protein was suspended in PBS to yield a 20 μM solution and agitated at 37 °C [85]. For each of these amyloid-forming proteins, 10 μL was plated in triplicate at each time point. Prior to plating, each sample was inverted twice, except for CsgA, which was also vortexed. The TROL and ThT assays were then performed according to the optimized protocols described (Table 3.1).

Notes
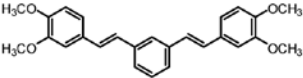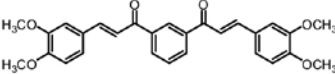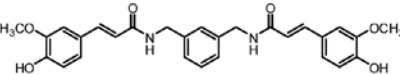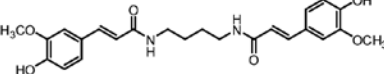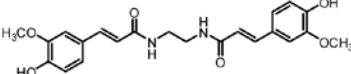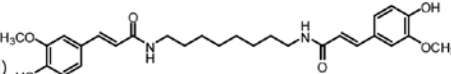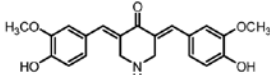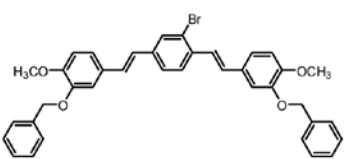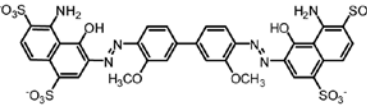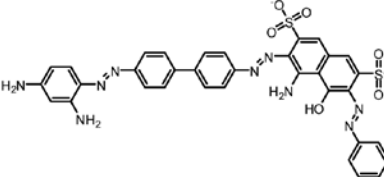
This work has been partially published as "A chemical screening approach reveals that indole fluorescence is quenched by pre-fibrillar but not fibrillar amyloid-β." **2009** Bioorganic and Medicinal Chemistry Letters. *19*; 4952-7; and "Quantifying prefibrillar amyloids in vitro by using a "thioflavin-like" spectroscopic method." **2010** Chembiochem. *11*; 1889-95.

Ashley A. Reinke and Jason E. Gestwicki designed the experiments. Ashley A. Reinke conducted the experiments. Gelareh Abulwerdi assisted with the secondary indole screening. Recombinant CsgA, α-synuclein, and ataxin-3 were kindly prepared by Yizhou Zhou, Elizabeth Rhoades, and Matthew Scaglione, respectively.

3.5 Appendix of pilot and secondary fluorescence screening results
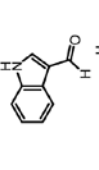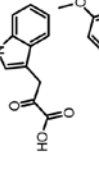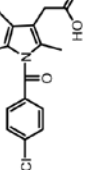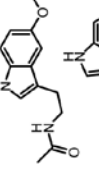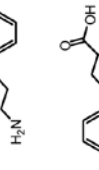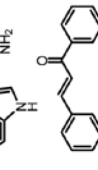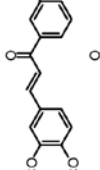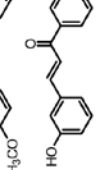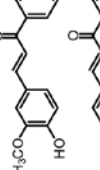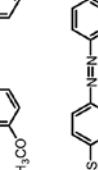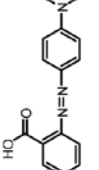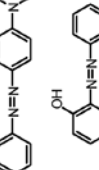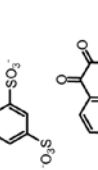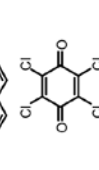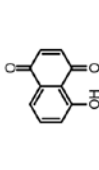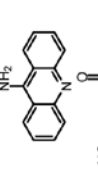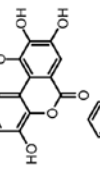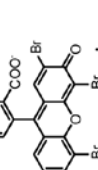
3.5.1 Pilot screen

Appendix 3.5.1 Chemical structures of the library members and the fluorescence screening results. Compound numbers correspond to Figure 3.3 in the text. The fluorescence of each compound was recorded alone or in the presence of Aβ fibrils or oligomers at four wavelength ranges; [(A) Ex 290, Em 320-520; (B) Ex 350, Em 380-650; (C) Ex 350, Em 430-620; (D) Ex 450, Em 480-650], and the percent change in small molecule fluorescence upon Aβ addition was calculated. Less than 4% change in fluorescence was used as a cutoff for reporting total changes in fluorescence, and percent changes that were three or greater standard deviations of the mean were considered significant. An increase (+) or decrease (-) in fluorescence is denoted before each reported value and the excitation and emission values used to determine the percent change are listed.

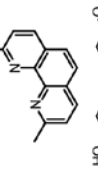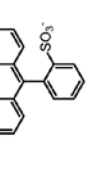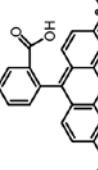| #	name	chemical structure	% change (fibrils)	% change (oligomers)
1	1,3-bis(3,4-dimethoxystyryl)benzene		-6.0 +/- 0.9% Ex 350; Em 420	< 4% Ex 350; Em 420
2	(2E,2'E)-1,1'-(1,3-phenylene) bis(3-(3,4-dimethoxyphenyl) prop-2-en-1one)		< 4% Ex 350; Em 470	< 4% Ex 350; Em 470
3	(2E,2'E)-N,N'-(1,3-phenylenebis (methylene))bis(3-(4-hydroxy-3-methoxyphenyl)acrylamide)		NA	NA
4	(2E,2'E)-N,N'-(butane-1,4-diyl) bis(3-(4-hydroxy-3-methoxyphenyl) acrylamide		NA	NA
5	(2E,2'E)-N,N'-(ethane-1,2-diyl) bis(3-(4-hydroxy-3-methoxyphenyl) acrylamide		NA	NA
6	(2E,2'E)-N,N'-(octane-1,8-diyl) bis(3-(4-hydroxy-3-methoxyphenyl) acrylamide		NA	NA
7	(3E,5E)-3,5-bis(4-hydroxy-3-methoxybenzylidene) piperidin-4-one*		NA	NA
8	4,4'-(1E,1'E)-2,2'-(2-bromo-1,4-phenylene)bis(ethane-2,1-diyl)bis(2-(benzyloxy)-1-methoxybenzene**		< 4% Ex 350; Em 500	< 4% Ex 350; Em 500
9	Chicago Sky Blue		NA	NA
10	Chlorazol Black		NA	NA
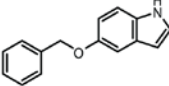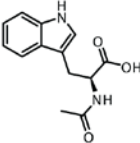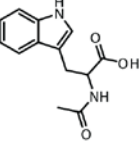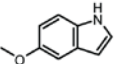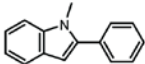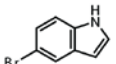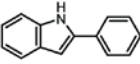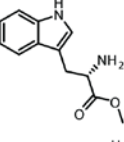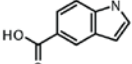
#	name	chemical structure	% change (fibrils)	% change (oligomers)
11	Chrysamine G		NA	NA
12	Congo Red		< 4% (B) 350/420	< 4% (B) 350/420
13	curcumin		NA	NA
14	lacmoid		NA	NA
15	Nordihydroguaiaretic acid		NA	NA
16	resveratrol		+ 11.1 +/- 1% (A) 290/390	+ 47.7 +/- 5.2% (A) 290/390
17	Rosmarinic acid		NA	NA
18	tetramethoxycurcumin		NA	NA
19	trismethoxyresveratrol		NA	NA
20	Azure A		NA	NA
21	Azure C		NA	NA
22	Methylene Blue		NA	NA
23	perphenazine		NA	NA
24	thionin acetate		NA	NA
25	meclocycline sulfosalicylate		< 4% (A) 290/410	- 9.3 +/- 2% (A) 290/410
26	minocycline		NA	NA
27	rolitetracycline		NA	NA
28	tetracycline		NA	NA
29	2,2-dihydroxybenzophenone		NA	NA
30	2,3,4-trihydroxybenzophenone		NA	NA
31	3,4,5-trismethoxybenzophenone		NA	NA
32	4,4-dihydroxybenzophenone		NA	NA
33	4,4-methylenediphenol		NA	NA
34	anthrone		NA	NA
35	benzophenone		NA	NA
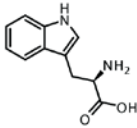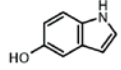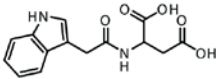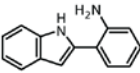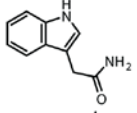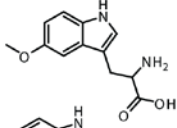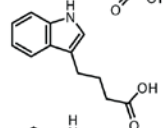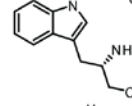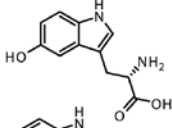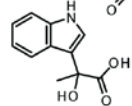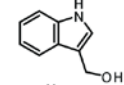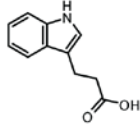
#	name	chemical structure	% change (fibrils)	% change (oligomers)
36	fenofibrate		NA	NA
37	2-hydroxy-3-methoxy benzaldehyde		NA	NA
38	3-hydroxybenzaldehyde		NA	NA
39	3-hydroxycinnamate		NA	NA
40	3,4-dimethoxybenzaldehyde		NA	NA
41	4-methoxybenzaldehyde		NA	NA
42	acetophenone		NA	NA
43	dopamine		NA	NA
44	ferulic acid		< 4% (A) 290/410	< 4% (A) 290/410
45	salicylic acid		< 4% 280/413	- 9.5 +/- 0.9% 280/413
46	apigenin		NA	NA
47	(+)-catechin		NA	NA
48	(-)-epicatechin		NA	NA
49	epigallocatechin gallate (EGCG)		NA	NA
50	flavone		NA	NA
51	genistein		NA	NA
52	kaempferol		NA	NA
53	myricetin		NA	NA
54	naringenin		NA	NA
55	quercetin		NA	NA
56	taxifolin		NA	NA
57	5-methylindole-2-carboxylic acid		< 4% 280/350	-8.4 +/- 0.1% 280/350
58	indole		< 4% 280/350	-12.3 +/- 0.3% 280/350

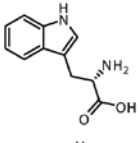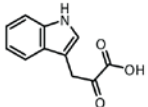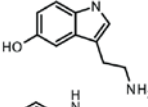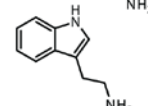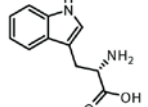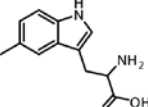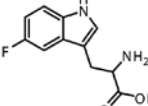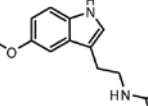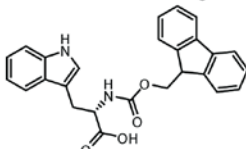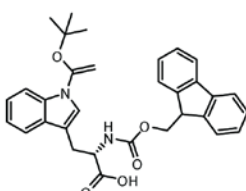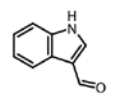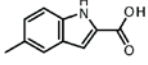| #	name	chemical structure	% change (fibrils)	% change (oligomers)
59	indole-3-carboxaldehyde		NA	NA
60	indole-3-pyruvic acid		< 4% (A) 290/350	< 4% (A) 290/350
61	indomethacin		NA	NA
62	melatonin		< 4% 280/350	- 8.4 +/- 0.1% 280/350
63	tryptamine		< 4% 280/350	- 7.8 +/- 0.1% 280/350
64	tryptophan		< 4% 280/350	- 7.4 +/- 0.3% 280/350
65	(E)-chalcone		NA	NA
66	(E)-1-(3-aminophenyl)-3-(3,4-dimethoxyphenyl)prop-2-en-1-one		NA	NA
67	(E)-1-(3-aminophenyl)-3-(4-hydroxy-3-methoxyphenyl)prop-2-en-1-one		NA	NA
68	(E)-3-(3,4-dimethoxyphenyl)-1-phenylprop-2-en-1-one		NA	NA
69	(E)-3-(3-hydroxyphenyl)-1-phenylprop-2-en-1-one		NA	NA
70	(E)-3-(4-hydroxy-3-methoxyphenyl)-1-phenylprop-2-en-1-one		NA	NA
71	(E)-3-(4-methoxyphenyl)-1-phenylprop-2-en-1-one		NA	NA
72	methyl orange		NA	NA

#	name	chemical structure	% change (fibrils)	% change (oligomers)
73	methyl red		NA	NA
74	methyl yellow		NA	NA
75	Orange G		NA	NA
76	1,2-naphthoquinone		+ 85.8 +/- 2.1% (A) 290/460	+ 25.1 +/- 4.7% (A) 290/460
77	2,3,5,6-tetrachloro-p-benzoquinone (chloranil)		NA	NA
78	5-hydroxy-1,4-naphthoquinone (juglone)		NA	NA
79	9-aminoacridine		< 4% (C) 400/460	< 4% (C) 400/460
80	ellagic acid		NA	NA
81	Eosin Y		< 4% (C) 400/540	< 4% (C) 400/540
82	neocuproine		- 6.5 +/- 0.7% (A) 290/370	< 4% (A) 290/370
83	phenol red		NA	NA
84	Rhodamine B		< 4% (D) 450/520	< 4% (D) 450/520

127

3.5.2 Indole screen

Appendix 3.5.2 Compound names, chemical structures, maximum excitation and emission wavelengths, and the percent change in fluorescence values (%FQ) of the indole library collection.

#	compound name	Ex	Em	chemical structure	% FQ pre-fibrils	% FQ fibrils	pre-fibrillar selectivity
	indole	280	350		9.7	1.5	6.3
1	5-benzyloxyindole	270	330		16.0	2.5	6.4
2	N-acetyl-L-tryptophan	280	360		11.6	2.7	4.3
3	N-acetyl-DL-tryptophan	280	360		11.5	0.9	13.3
4	5-methoxyindole	280	335		11.7	2.6	4.5
5	1-methyl-2-phenylindole	280	375		18.1	15.7	1.2
6	7-azaindole	280	390		11.5	1.0	11.6
7	5-bromoindole	265	340		17.0	5.7	3.0
8	2-phenylindole	310	375		13.3	3.2	4.2
9	tryptophol (2-(1H-indol-3-yl)ethanol)	280	365		11.1	3.7	3.0
10	3-methylindole	280	370		13.7	5.0	2.7
11	L-tryptophan methyl ester	280	355		3.0	1.6	1.9
12	indole-5-carboxylic acid	280	390		24.5	3.2	7.6

#	compound name	Ex	Em	chemical structure	% FQ pre-fibrils	% FQ fibrils	pre-fibrillar selectivity
13	D-tryptophan ((R)-2-amino-3-(1H-indol-3-yl)propanoic acid)	280	360		9.9	1.4	7.3
14	5-hydroxyindole	280	335		8.1	1.7	4.8
15	indene	280	370		13.5	2.7	5.0
16	N-(3-indolylacetyl)-DL-aspartic acid	280	360		11.4	2.4	4.8
17	2-(2-aminophenyl)indole	290	415		14.2	2.7	5.3
18	indole-3-acetamide	280	355		9.2	0.5	18.3
19	1-methylindole	280	350		11.7	1.2	9.7
20	5-methoxy-DL-tryptophan	280	340		9.0	1.4	6.6
21	indole-3-butyric acid	280	370		13.4	2.2	6.1
22	L-tryptophanol ((S)-2-amino-3-(1H-indol-3-yl)propan-1-ol)	280	355		23.8	1.4	17.6
23	5-hydroxy-L-tryptophan	280	340		2.4	1.8	1.3
24	DL-3-indolelactic acid	280	365		18.7	2.2	8.4
25	indole-3-carbinol	280	360		17.4	3.3	5.3
26	3-indole-propionic acid	280	365		16.6	2.8	6.0

#	compound name	Ex	Em	chemical structure	% FQ pre-fibrils	% FQ fibrils	pre-fibrillar selectivity
27	indole-3-pyruvic acid	275	355		13.3	3.2	4.1
28	serotonin (3-(2-aminoethyl)-1H-indol-5-ol)	280	335		14.5	3.4	4.2
29	tryptamine (2-(1H-indol-3-yl)ethan-amine)	280	360		13.4	2.8	4.9
30	L-tryptophan ((S)-2-amino-3-(1H-indol-3-yl)propanoic acid)	280	360		14.9	2.9	5.2
31	5-methyl-DL-tryptophan	280	350		3.1	3.3	1.0
32	5-fluoro-DL-tryptophan	270	330		14.7	3.0	4.9
33	melatonin (N-(2-(5-methoxy-1H-indol-3-yl)ethyl)acet-amide	280	355		2.6	0.6	4.6
34	N-⍺-Fmoc-L-tryptophan	280	355		10.0	1.5	6.7
35	N-⍺-Fmoc-N-in-Boc-L-tryptophan	270	315		3.6	1.7	2.1
36	indole-3-carboxaldehyde	270	325		14.4	3.0	4.7
37	5-methylindole-2-carboxylic acid	280	350		8.4	3.1	2.7

3.6 References

[1]   Caughey B, Lansbury PT. Protofibrils, pores, fibrils, and neurodegeneration: separating the responsible protein aggregates from the innocent bystanders. Annual review of neuroscience. 2003;26:267-98.

[2]   Haass C, Selkoe DJ. Soluble protein oligomers in neurodegeneration: lessons from the Alzheimer's amyloid beta-peptide. Nature reviews. 2007 Feb;8(2):101-12.

[3]   Kayed R, Head E, Thompson JL, McIntire TM, Milton SC, Cotman CW, et al. Common structure of soluble amyloid oligomers implies common mechanism of pathogenesis. Science (New York, NY. 2003 Apr 18;300(5618):486-9.

[4]   Walsh DM, Klyubin I, Fadeeva JV, Cullen WK, Anwyl R, Wolfe MS, et al. Naturally secreted oligomers of amyloid beta protein potently inhibit hippocampal long-term potentiation in vivo. Nature. 2002 Apr 4;416(6880):535-9.

[5]   Walsh DM, Klyubin I, Fadeeva JV, Rowan MJ, Selkoe DJ. Amyloid-beta oligomers: their production, toxicity and therapeutic inhibition. Biochemical Society transactions. 2002 Aug;30(4):552-7.

[6]   Hung LW, Ciccotosto GD, Giannakis E, Tew DJ, Perez K, Masters CL, et al. Amyloid-beta peptide (Abeta) neurotoxicity is modulated by the rate of peptide aggregation: Abeta dimers and trimers correlate with neurotoxicity. J Neurosci. 2008 Nov 12;28(46):11950-8.

[7]   Klyubin I, Betts V, Welzel AT, Blennow K, Zetterberg H, Wallin A, et al. Amyloid beta protein dimer-containing human CSF disrupts synaptic plasticity: prevention by systemic passive immunization. J Neurosci. 2008 Apr 16;28(16):4231-7.

[8]   Ono K, Condron MM, Teplow DB. Structure-neurotoxicity relationships of amyloid beta-protein oligomers. Proceedings of the National Academy of Sciences of the United States of America. 2009 Sep 1;106(35):14745-50.

[9]   Shankar GM, Li S, Mehta TH, Garcia-Munoz A, Shepardson NE, Smith I, et al. Amyloid-beta protein dimers isolated directly from Alzheimer's brains impair synaptic plasticity and memory. Nature medicine. 2008 Aug;14(8):837-42.

[10]   Townsend M, Shankar GM, Mehta T, Walsh DM, Selkoe DJ. Effects of secreted oligomers of amyloid beta-protein on hippocampal synaptic plasticity: a potent role for trimers. The Journal of physiology. 2006 Apr 15;572(Pt 2):477-92.

[11]   Glabe CG. Conformation-dependent antibodies target diseases of protein misfolding. Trends in biochemical sciences. 2004 Oct;29(10):542-7.

[12]   Mamikonyan G, Necula M, Mkrtichyan M, Ghochikyan A, Petrushina I, Movsesyan N, et al. Anti-A beta 1-11 antibody binds to different beta-amyloid species, inhibits fibril formation, and disaggregates preformed fibrils but not the most toxic oligomers. The Journal of biological chemistry. 2007 Aug 3;282(31):22376-86.

[13]   Dahlgren KN, Manelli AM, Stine WB, Jr., Baker LK, Krafft GA, LaDu MJ. Oligomeric and fibrillar species of amyloid-beta peptides differentially affect neuronal viability. The Journal of biological chemistry. 2002 Aug 30;277(35):32046-53.

[14]   Stine WB, Jr., Dahlgren KN, Krafft GA, LaDu MJ. In vitro characterization of conditions for amyloid-beta peptide oligomerization and fibrillogenesis. The Journal of biological chemistry. 2003 Mar 28;278(13):11612-22.

[15]   Chromy BA, Nowak RJ, Lambert MP, Viola KL, Chang L, Velasco PT, et al. Self-assembly of Abeta(1-42) into globular neurotoxins. Biochemistry. 2003 Nov 11;42(44):12749-60.

[16]   Mastrangelo IA, Ahmed M, Sato T, Liu W, Wang C, Hough P, et al. High-resolution atomic force microscopy of soluble Abeta42 oligomers. Journal of molecular biology. 2006 Apr 21;358(1):106-19.

[17]   Yagi H, Ban T, Morigaki K, Naiki H, Goto Y. Visualization and classification of amyloid beta supramolecular assemblies. Biochemistry. 2007 Dec 25;46(51):15009-17.

[18]   Chimon S, Shaibat MA, Jones CR, Calero DC, Aizezi B, Ishii Y. Evidence of fibril-like beta-sheet structures in a neurotoxic amyloid intermediate of Alzheimer's beta-amyloid. Nature structural & molecular biology. 2007 Dec 2.

[19]   Qi W, Zhang A, Patel D, Lee S, Harrington JL, Zhao L, et al. Simultaneous monitoring of peptide aggregate distributions, structure, and kinetics using amide hydrogen exchange: application to Abeta(1-40) fibrillogenesis. Biotechnology and bioengineering. 2008 Aug 15;100(6):1214-27.

[20]   Yu L, Edalji R, Harlan JE, Holzman TF, Lopez AP, Labkovsky B, et al. Structural characterization of a soluble amyloid beta-peptide oligomer. Biochemistry. 2009 Mar 10;48(9):1870-7.

[21]   Necula M, Breydo L, Milton S, Kayed R, van der Veer WE, Tone P, et al. Methylene blue inhibits amyloid Abeta oligomerization by promoting fibrillization. Biochemistry. 2007 Jul 31;46(30):8850-60.

[22]   Necula M, Kayed R, Milton S, Glabe CG. Small molecule inhibitors of aggregation indicate that amyloid beta oligomerization and fibrillization pathways are independent and distinct. The Journal of biological chemistry. 2007 Apr 6;282(14):10311-24.

[23]   Klunk WE, Pettegrew JW, Abraham DJ. Quantitative evaluation of congo red binding to amyloid-like proteins with a beta-pleated sheet conformation. J Histochem Cytochem. 1989 Aug;37(8):1273-81.

[24]   LeVine H, 3rd. Thioflavine T interaction with synthetic Alzheimer's disease beta-amyloid peptides: detection of amyloid aggregation in solution. Protein Sci. 1993 Mar;2(3):404-10.

[25]   LeVine H, 3rd. Quantification of beta-sheet amyloid fibril structures with thioflavin T. Methods in enzymology. 1999;309:274-84.

[26]   Wu C, Wang Z, Lei H, Zhang W, Duan Y. Dual binding modes of Congo red to amyloid protofibril surface observed in molecular dynamics simulations. Journal of the American Chemical Society. 2007 Feb 7;129(5):1225-32.

[27]   Maezawa I, Hong HS, Liu R, Wu CY, Cheng RH, Kung MP, et al. Congo red and thioflavin-T analogs detect Abeta oligomers. Journal of neurochemistry. 2008 Jan;104(2):457-68.

[28]   Yang F, Lim GP, Begum AN, Ubeda OJ, Simmons MR, Ambegaokar SS, et al. Curcumin inhibits formation of amyloid beta oligomers and fibrils, binds plaques, and reduces amyloid in vivo. The Journal of biological chemistry. 2005 Feb 18;280(7):5892-901.

[29]   Frid P, Anisimov SV, Popovic N. Congo red and protein aggregation in neurodegenerative diseases. Brain research reviews. 2007 Jan;53(1):135-60.

[30]   Naiki H, Higuchi K, Hosokawa M, Takeda T. Fluorometric determination of amyloid fibrils in vitro using the fluorescent dye, thioflavin T1. Analytical biochemistry. 1989 Mar;177(2):244-9.

[31]   Biancalana M, Koide S. Molecular mechanism of Thioflavin-T binding to amyloid fibrils. Biochimica et biophysica acta. 2010 Jul;1804(7):1405-12.

[32]   Findeis MA. Approaches to discovery and characterization of inhibitors of amyloid beta-peptide polymerization. Biochimica et biophysica acta. 2000 Jul 26;1502(1):76-84.

[33]   Ono K, Hasegawa K, Naiki H, Yamada M. Curcumin has potent anti-amyloidogenic effects for Alzheimer's beta-amyloid fibrils in vitro. Journal of neuroscience research. 2004 Mar 15;75(6):742-50.

[34]   Walsh DM, Hartley DM, Kusumoto Y, Fezoui Y, Condron MM, Lomakin A, et al. Amyloid beta-protein fibrillogenesis. Structure and biological activity of protofibrillar intermediates. J Biol Chem. 1999 Sep 3;274(36):25945-52.

[35]   Das KP, Surewicz WK. Temperature-induced exposure of hydrophobic surfaces and its effect on the chaperone activity of alpha-crystallin. FEBS letters. 1995 Aug 7;369(2-3):321-5.

[36]   Shi Y, Fan DJ, Li SX, Zhang HJ, Perrett S, Zhou JM. Identification of a potential hydrophobic peptide binding site in the C-terminal arm of trigger factor. Protein Sci. 2007 Jun;16(6):1165-75.

[37]   Chen YR, Glabe CG. Distinct early folding and aggregation properties of Alzheimer amyloid-beta peptides Abeta40 and Abeta42: stable trimer or tetramer formation by Abeta42. The Journal of biological chemistry. 2006 Aug 25;281(34):24414-22.

[38]   LeVine H, 3rd. 4,4(')-Dianilino-1,1(')-binaphthyl-5,5(')-disulfonate: report on non-beta-sheet conformers of Alzheimer's peptide beta(1-40). Archives of biochemistry and biophysics. 2002 Aug 1;404(1):106-15.

[39]   Lindgren M, Sorgjerd K, Hammarstrom P. Detection and characterization of aggregates, prefibrillar amyloidogenic oligomers, and protofibrils using fluorescence spectroscopy. Biophysical journal. 2005 Jun;88(6):4200-12.

[40]   Masuda M, Suzuki N, Taniguchi S, Oikawa T, Nonaka T, Iwatsubo T, et al. Small molecule inhibitors of alpha-synuclein filament assembly. Biochemistry. 2006 May 16;45(19):6085-94.

[41]   Reinke AA, Gestwicki JE. Structure-activity relationships of amyloid beta-aggregation inhibitors based on curcumin: influence of linker length and flexibility. Chemical biology & drug design. 2007 Sep;70(3):206-15.

[42]   Taniguchi S, Suzuki N, Masuda M, Hisanaga S, Iwatsubo T, Goedert M, et al. Inhibition of heparin-induced tau filament formation by phenothiazines, polyphenols, and porphyrins. The Journal of biological chemistry. 2005 Mar 4;280(9):7614-23.

[43]   Bordwell F, Drucker G, Fried H. Acidities of carbon and nitrogen acids: the aromaticity of the cyclopentadienyl anion. J Org Chem. 1981;46(632-635).

[44]   Kurzban GP, Gitlin G, Bayer EA, Wilchek M, Horowitz PM. Biotin binding changes the conformation and decreases tryptophan accessibility of streptavidin. Journal of protein chemistry. 1990 Dec;9(6):673-82.

[45]   Lakshmikanth GS, Krishnamoorthy G. Solvent-exposed tryptophans probe the dynamics at protein surfaces. Biophysical journal. 1999 Aug;77(2):1100-6.

[46]   Nanda V, Brand L. Aromatic interactions in homeodomains contribute to the low quantum yield of a conserved, buried tryptophan. Proteins. 2000 Jul 1;40(1):112-25.

[47]   Royer CA. Probing protein folding and conformational transitions with fluorescence. Chemical reviews. 2006 May;106(5):1769-84.

[48]   Eftink MR, Ghiron CA. Exposure of tryptophanyl residues in proteins. Quantitative determination by fluorescence quenching studies. Biochemistry. 1976 Feb 10;15(3):672-80.

[49]   Eftink MR, Ghiron CA. Exposure of tryptophanyl residues and protein dynamics. Biochemistry. 1977 Dec 13;16(25):5546-51.

[50]   Hilbich C, Kisters-Woike B, Reed J, Masters CL, Beyreuther K. Substitutions of hydrophobic amino acids reduce the amyloidogenicity of Alzheimer's disease beta A4 peptides. Journal of molecular biology. 1992 Nov 20;228(2):460-73.

[51]   Tjernberg LO, Naslund J, Lindqvist F, Johansson J, Karlstrom AR, Thyberg J, et al. Arrest of beta-amyloid fibril formation by a pentapeptide ligand. The Journal of biological chemistry. 1996 Apr 12;271(15):8545-8.

[52]   Williams AD, Shivaprasad S, Wetzel R. Alanine scanning mutagenesis of Abeta(1-40) amyloid fibril stability. Journal of molecular biology. 2006 Apr 7;357(4):1283-94.

[53]   Gowing E, Roher AE, Woods AS, Cotter RJ, Chaney M, Little SP, et al. Chemical characterization of A beta 17-42 peptide, a component of diffuse amyloid deposits of Alzheimer disease. The Journal of biological chemistry. 1994 Apr 15;269(15):10987-90.

[54]   Pike CJ, Overman MJ, Cotman CW. Amino-terminal deletions enhance aggregation of beta-amyloid peptides in vitro. The Journal of biological chemistry. 1995 Oct 13;270(41):23895-8.

[55]   Reinke AA, Seh HY, Gestwicki JE. A chemical screening approach reveals that indole fluorescence is quenched by pre-fibrillar but not fibrillar amyloid-beta. Bioorganic & medicinal chemistry letters. 2009 Sep 1;19(17):4952-7.

[56]   Colby DW, Zhang Q, Wang S, Groth D, Legname G, Riesner D, et al. Prion detection by an amyloid seeding assay. Proceedings of the National Academy of Sciences of the United States of America. 2007 Dec 26;104(52):20914-9.

[57]   Hasegawa K, Yamaguchi I, Omata S, Gejyo F, Naiki H. Interaction between A beta(1-42) and A beta(1-40) in Alzheimer's beta-amyloid fibril formation in vitro. Biochemistry. 1999 Nov 23;38(47):15514-21.

[58]   Jan A, Gokce O, Luthi-Carter R, Lashuel HA. The ratio of monomeric to aggregated forms of Abeta40 and Abeta42 is an important determinant of amyloid-beta aggregation, fibrillogenesis, and toxicity. The Journal of biological chemistry. 2008 Oct 17;283(42):28176-89.

[59]   Maji SK, Ogorzalek Loo RR, Inayathullah M, Spring SM, Vollers SS, Condron MM, et al. Amino acid position-specific contributions to amyloid beta-protein oligomerization. The Journal of biological chemistry. 2009 Aug 28;284(35):23580-91.

[60]   Bowerman CJ, Ryan DM, Nissan DA, Nilsson BL. The effect of increasing hydrophobicity on the self-assembly of amphipathic beta-sheet peptides. Molecular bioSystems. 2009 Sep;5(9):1058-69.

[61]   Nilsson MR. Techniques to study amyloid fibril formation in vitro. Methods (San Diego, Calif. 2004 Sep;34(1):151-60.

[62]   Conway KA, Lee SJ, Rochet JC, Ding TT, Williamson RE, Lansbury PT, Jr. Acceleration of oligomerization, not fibrillization, is a shared property of both alpha-synuclein mutations linked to early-onset Parkinson's disease: implications for pathogenesis and therapy. Proceedings of the National Academy of Sciences of the United States of America. 2000 Jan 18;97(2):571-6.

[63]   Rahimi F, Shanmugam A, Bitan G. Structure-function relationships of pre-fibrillar protein assemblies in Alzheimer's disease and related disorders. Current Alzheimer research. 2008 Jun;5(3):319-41.

[64]   Takahashi Y, Okamoto Y, Popiel HA, Fujikake N, Toda T, Kinjo M, et al. Detection of polyglutamine protein oligomers in cells by fluorescence correlation spectroscopy. The Journal of biological chemistry. 2007 Aug 17;282(33):24039-48.

[65]   Wang X, Chapman MR. Curli provide the template for understanding controlled amyloid propagation. Prion. 2008 Apr;2(2):57-60.

[66]   Jahn TR, Makin OS, Morris KL, Marshall KE, Tian P, Sikorski P, et al. The common architecture of cross-beta amyloid. J Mol Biol. 2009 Jan 29;395(4):717-27.

[67]   Gallivan JP, Dougherty DA. Cation-pi interactions in structural biology. Proceedings of the National Academy of Sciences of the United States of America. 1999 Aug 17;96(17):9459-64.

[68]   Ma JC, Dougherty DA. The Cationminus signpi Interaction. Chemical reviews. 1997 Aug 5;97(5):1303-24.

[69]   Mecozzi S, West AP, Jr., Dougherty DA. Cation-pi interactions in aromatics of biological and medicinal interest: electrostatic potential surfaces as a useful qualitative guide. Proceedings of the National Academy of Sciences of the United States of America. 1996 Oct 1;93(20):10566-71.

[70]   Kheterpal I, Lashuel HA, Hartley DM, Walz T, Lansbury PT, Jr., Wetzel R. Abeta protofibrils possess a stable core structure resistant to hydrogen exchange. Biochemistry. 2003 Dec 9;42(48):14092-8.

[71]   Olofsson A, Sauer-Eriksson AE, Ohman A. The solvent protection of alzheimer amyloid-beta-(1-42) fibrils as determined by solution NMR spectroscopy. The Journal of biological chemistry. 2006 Jan 6;281(1):477-83.

[72]   Ban T, Yamaguchi K, Goto Y. Direct observation of amyloid fibril growth, propagation, and adaptation. Accounts of chemical research. 2006 Sep;39(9):663-70.

[73]   Shahi P, Sharma R, Sanger S, Kumar I, Jolly RS. Formation of amyloid fibrils via longitudinal growth of oligomers. Biochemistry. 2007 Jun 26;46(25):7365-73.

[74]   Zhu M, Han S, Zhou F, Carter SA, Fink AL. Annular oligomeric amyloid intermediates observed by in situ atomic force microscopy. The Journal of biological chemistry. 2004 Jun 4;279(23):24452-9.

[75]   Bogdan M, Pirnau A, Floare C, Bugeac C. Binding interaction of indomethacin with human serum albumin. Journal of pharmaceutical and biomedical analysis. 2008 Aug 5;47(4-5):981-4.

[76]   Singh AK, Asefa A. A fluorescence study of differently substituted 3-styrylindoles and their interaction with bovine serum albumin. Luminescence. 2009 Mar-Apr;24(2):123-30.

[77]   Cerf E, Sarroukh R, Tamamizu-Kato S, Breydo L, Derclaye S, Dufrene YF, et al. Antiparallel beta-sheet: a signature structure of the oligomeric amyloid beta-peptide. The Biochemical journal. 2009 Aug 1;421(3):415-23.

[78]   Evans CG, Wisen S, Gestwicki JE. Heat shock proteins 70 and 90 inhibit early stages of amyloid beta-(1-42) aggregation in vitro. The Journal of biological chemistry. 2006 Nov 3;281(44):33182-91.

[79]   Todi SV, Laco MN, Winborn BJ, Travis SM, Wen HM, Paulson HL. Cellular turnover of the polyglutamine disease protein ataxin-3 is regulated by its catalytic activity. J Biol Chem. 2007 Oct 5;282(40):29348-58.

[80]   Ellisdon AM, Thomas B, Bottomley SP. The two-stage pathway of ataxin-3 fibrillogenesis involves a polyglutamine-independent step. J Biol Chem. 2006 Jun 23;281(25):16888-96.

[81]   Koo BW, Miranker AD. Contribution of the intrinsic disulfide to the assembly mechanism of islet amyloid. Protein Sci. 2005 Jan;14(1):231-9.

[82]   Wang X, Zhou Y, Ren JJ, Hammer ND, Chapman MR. Gatekeeper residues in the major curlin subunit modulate bacterial amyloid fiber biogenesis. Proc Natl Acad Sci U S A. 2009 Jan 5;107(1):163-8.

[83]   Wang X, Smith DR, Jones JW, Chapman MR. In vitro polymerization of a functional Escherichia coli amyloid protein. J Biol Chem. 2007 Feb 9;282(6):3713-9.

[84]   Trexler AJ, Rhoades E. Alpha-synuclein binds large unilamellar vesicles as an extended helix. Biochemistry. 2009 Mar 24;48(11):2304-6.

[85]   Waxman EA, Giasson BI. A novel, high-efficiency cellular model of fibrillar alpha-synuclein inclusions and the examination of mutations that inhibit amyloid formation. J Neurochem. 2010 Feb 2.

Chapter 4

Peptide-based chemical probes that selectively recognize the earliest

amyloid-β oligomers in complex mixtures

4.1 Abstract

Alzheimer's disease (AD) is characterized by the self-assembly of amyloid beta (Aβ) peptides. Recent models implicate the earliest Aβ oligomers, such as trimers and tetramers, in disease. However, the roles of these structures remain uncertain, in part, because selective probes of their formation are not available. Towards that goal, we generated 12 bivalent versions of the known Aβ ligand, the pentapeptide KLVFF. We found that compounds containing sufficiently long linkers (~19 to 24 Å,) recognized primarily Aβ trimers and tetramers, with little binding to either monomers or higher order structures. Interestingly, we observed that the relative orientation of the KLVFF motifs partially controlled the reliance on linker length. Further, by reducing the flexibility of the linker, selectivity for trimers and tetramers was enhanced. Selectivity was maintained in a background of cerebrospinal fluid (CSF), suggesting that, with further optimization, these compounds might be useful probes for early Aβ oligomers in complex biological mixtures. Towards that goal, preliminary tissue staining studies reveal that these probes visualize Aβ deposits *ex vivo* in brain sections derived from transgenic AD mouse models.

4.1.1 Low-molecular weight (LMW) Aβ is neurotoxic

As discussed in Chapter 1, methods for isolating early, small oligomers of Aβ have recently led to a model in which low-molecular weight (LMW) species, including dimers, trimers, and tetramers, may be linked to pathology [1-7]. For example, Selkoe and colleagues showed that both synthetic Aβ dimers and LMW Aβ derived from human AD brain tissue potently inhibited long-term potentiation (LTP) in neurons [6]. Similarly, cerebrospinal fluid (CSF) obtained from AD patients strongly disrupted synaptic plasticity, while immunodepletion of dimeric Aβ reduced this activity [2]. Consistent with these findings, recent *in vivo* evidence reveals a correlation between trimer levels in the cerebral cortex and cognitive impairment in a transgenic AD model [3]. *In vitro*, this effect was also

(a) Low-molecular weight (LMW) Aβ is cytotoxic
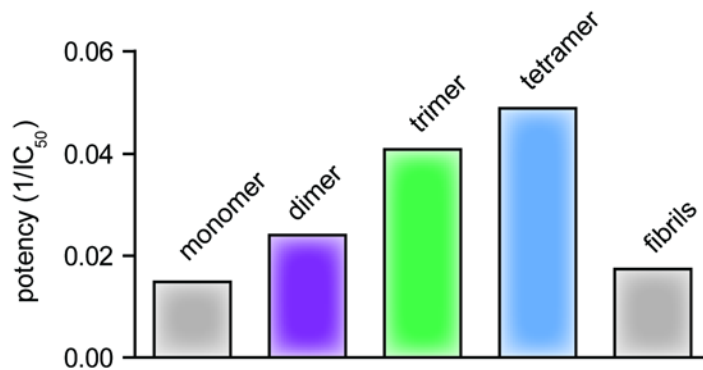
(b) Sequence of amyloid-β (1-40)

H$_2$N-DAEFRHDSGYEVHHQ-KLVFF-AEDVGSNKGAIIGLMVGGVV-COOH

(c) Schematic of the amyloid aggregation pathway
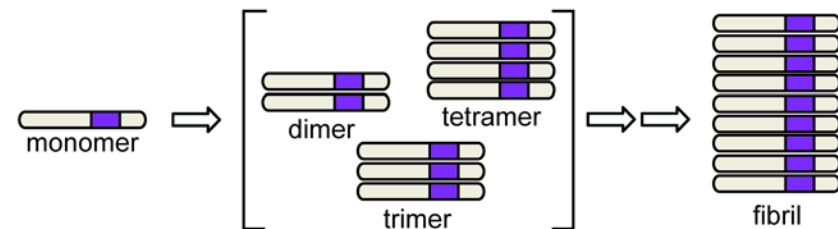
Figure 4.1 LMW Aβ and the KLVFF region. (a) Teplow and coworkers (Ono *et al.* PNAS **2009**) determined the IC$_{50}$ for low-molecular weight (LMW) Aβ in cell culture. The potency (1/IC$_{50}$ is shown). (b) The sequence of Aβ. (c) Schematic of the Aβ aggregation pathway, highlighting the early, soluble structures and the resulting insoluble fibrils. The purple segment models residues 16-20 corresponding to residues KLVFF. Association of this region drives self-assembly as is buried upon aggregation, but KLVFF remains exposed at the 'ends' of Aβ aggregates.

observed by Hung *et al.*, who found that reductions in the level of dimer and trimer by favoring rapid fibrilization attenuated toxicity in primary neuronal cultures [1]. Finally, Teplow and coworkers established that purified trimer and tetramer (IC_{50} = 20-25 μM) are over three-fold more neurotoxic than monomer, dimer, and fibrils *in vitro* [4] (Figure 4.1a). Collectively, these findings suggest that the earliest Aβ aggregates might be particularly important in disease. However, a recent study suggests that Aβ dimers proceed particularly rapidly to protofibrils and that it is the protofibrillar material that strongly reduces LTP [8]. Clearly, there is a strong need for molecules that selectively recognize these early aggregates. Ideally, such molecules could be used to follow the formation and fate of these structures in dynamic mixtures. Toward this important goal, we utilized molecular modeling and the self-recognition properties of the Aβ peptide to construct such probes.

4.1.2 Amyloid-β (16-20): KLVFF

The Aβ peptide is a 40 or 42 amino acid fragment of the amyloid precursor protein (APP) (Figure 4.1b). Portions of this peptide are thought to form β-sheets upon release from APP and subsequent stacking of these region appears to nucleate Aβ self-association [9, 10]. Within these sites, residues 16 through 20, KLVFF, are especially important [11]. Specifically, this motif is thought to interact with itself in adjacent β-strands, with the phenylalanine residues forming key, repetitive inter-molecular contacts [12-18]. The interactions of KLVFF with itself have been studied extensively. As discussed in Chapter 1, Tjernberg *et al*. first proposed that KLVFF binds its homologous residues on Aβ, a hypothesis which was later confirmed using fluorescence binding platforms [16, 19]. Hydrogen-deuterium exchange (HDX) studies revealed that KLVFF is solvent exposed in early species, but becomes predominantly buried upon fibril formation [20, 21]. Together, these studies have suggested that many Aβ structures have an exposed KLVFF

motif at each "end" [22-28] (Figure 4.1c). Consistent with this model, KLVFF-based peptides will inhibit Aβ aggregation at high concentrations, presumably by blocking these sites.

4.1.3 Multivalent ligands and amyloids

Although KLVFF has been shown to modulate aggregation, it binds only weakly to Aβ (K_d > 1 mM)[29] and multivalent displays of this peptide have been found to be required for potent inhibition [30-33]. This finding is consistent with a large amount of literature on multivalent binding, which is known to significantly enhance avidity and selectivity in many systems by elevating local ligand concentration, favoring multi-site binding and other mechanisms [34]. For example, multivalent ligands access binding modes that are not available to their monovalent counterparts, including chelation, subsite binding, clustering, and statistical rebinding [34]. These mechanisms have been utilized in probing signal transduction pathways, and, in addition, these principles have been demonstrated in the context of amyloid [35-38]. For instance, a monovalent quinacrine derivative was shown to be inactive against Aβ self-assembly, while a tetravalent version of quinacrine linked through a rigid, cyclic peptide backbone resulted in a potent inhibitor of aggregation (IC_{50} = 20 μM) [36]. Similarly, two ThT units conjugated through a PEG linker also showed over a 70-fold increase in binding affinity to Aβ fibrils relative to monovalent ThT [39]. We have also observed that linking multiple conjugates enhances the potency of a small molecule toward inhibition of Aβ aggregation. As demonstrated in Chapter 2, we found that ferulic acid alone had no effect on Aβ self-assembly (IC_{50} > 500 μM). However, by linking two ferulic acid molecules through a diamine linker, the potency was greatly enhanced (IC_{50} = 91 μM) [40].

Based on these observations, we envisioned that bridging two KLVFF peptides with a linker of the appropriate length might provide a probe for the earliest Aβ oligomers (Figure 4.2a). This strategy was designed to address a central challenge in building probes that are specific for a subset of Aβ structures. Namely, these oligomers are assembled from identical monomer units and; therefore, they contain many degenerate molecular features, such as high β-sheet content. By exploiting one of their few distinguishing properties (*e.g.* end-to-end distance between KLVFF motifs), we hoped to circumvent these issues.

4.2 Results

4.2.1 Molecular dynamics (MD) simulations

To estimate the minimal distance needed to span the ends of an early Aβ aggregate, we assembled a representative KLVFF-based probe *in silico* and then employed molecular dynamics (MD) simulations to examine its binding to a model Aβ repeating unit. First, we determined the approximate distances for an Aβ dimer and trimer (Figure 4.2b). MD simulations revealed two distinct populations for the length across a dimer; a major population at 14-14.5 Å, and a minor population at 18 Å. This finding is consistent with the dynamic nature of Aβ dimers, confirming that these structures may sample more than one structural state [18]. Further, we observed only one population for the trimer length at approximately 19.5 Å. Based upon these measurements, we extrapolated the approximate length of a tetramer using ~ 5 Å / Aβ monomer as an estimate, resulting in a length of roughly 25 Å. Subsequently, using molecular docking, we constructed a molecular model of how we propose a bivalent KLVFF ligand may bind to an Aβ trimer (Figure 4.2c). It should be emphasized that these distances are considered approximate and only serve as a rough guide for designing the synthesis of divalent KLVFF-based probes. We still considered it important to empirically test these predictions because of

uncertainty in the available structural information and the inherent dynamics of small amyloid structures.
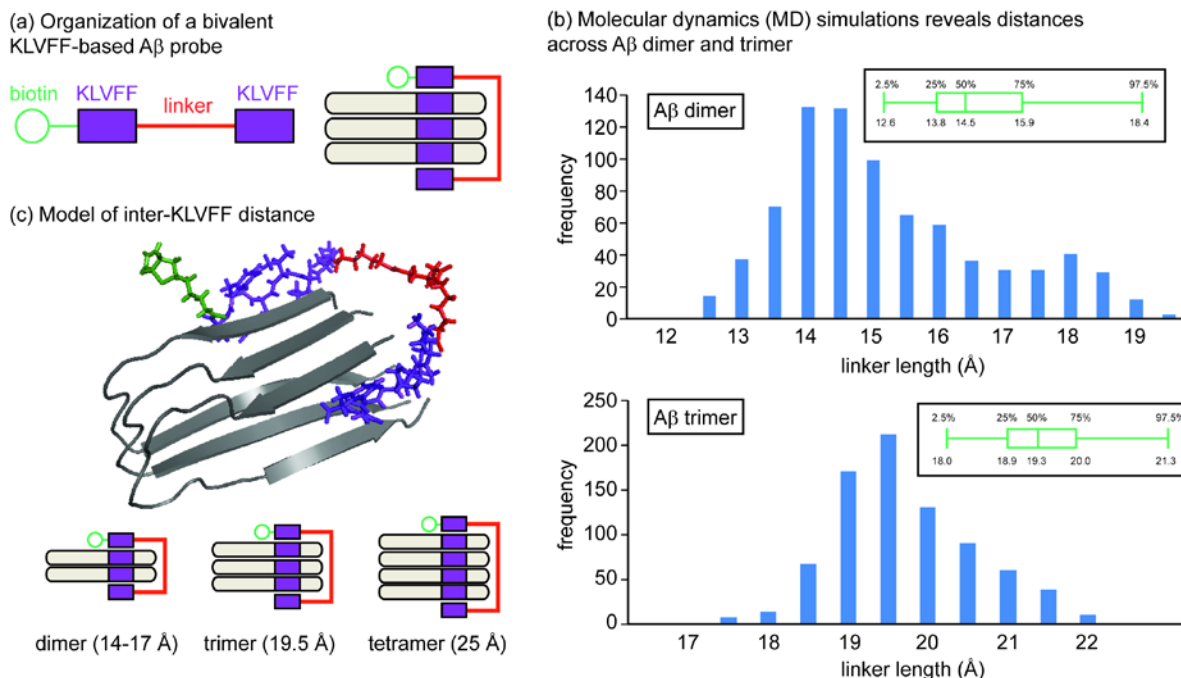
Figure 4.2 Design of bivalent KLVFF-based ligands. (a) Schematic representation of a bivalent, KLVFF probe. The Aβ is shown in grey, the KLVFF in purple, the linker in red and the biotin tag in green. (b) Molecular dynamics simulations reveal approximate distances across Aβ dimer (top) and trimer (bottom). Distances were measured between residue 16 (Lys) on two or three Aβ molecules and frequency with which each distance was observed is plotted. As expected, the dimer populates a broader range of distances, suggesting it is more dynamic than its trimer counterpart. We observed the major median for a dimer at 14-14.5 Å, and a second minor population around 17.5-18 Å. For a trimer, a narrower range of distances was seen, with only one main population, corresponding to a distance about 19.5 Å. (c) Representative snapshot of a molecular dynamics simulation. A bivalent KLVFF construct was docked onto an Aβ trimer. Based on similar simulations, an extended linker distance between KLVFF sites was estimated.

4.2.2 Synthesis of biotinylated peptides and characterization

The measurements obtained through MD simulations were used to guide our synthesis of bivalent KLVFF-based ligands. Using microwave-assisted, solid-phase peptide coupling, we first constructed a control compound in which the KLVFF peptide was linked to biotin (Figure 4.3b). Similarly, we generated eight bivalent KLVFF derivatives (**a7**, **a13**, **a19**, **a24**, **p7**, **p13**, **p19**, **p24**), each containing two KLVFF recognition elements separated by a linker region and a biotin added at the N-terminus. Because the KLVFF region is thought to interact in two orientations relative to its neighboring strand (*e.g.* KLVFF binds either KLVFF or FFVLK), we developed two sets of

derivatives. Thus, the second KLVFF motif was added such that the linker was predicted to be 'anti-parallel' or 'parallel' to the Aβ molecule (Figure 4.3a). The anti-parallel or 'a' series contained the sequence FFVLK – linker – *KLVFF*A – biotin (Figure 4.3c), while the parallel or 'p' series consisted of FFVLK – linker – *FFVLK*A – biotin (Figure 4.3d). The linker region of these eight
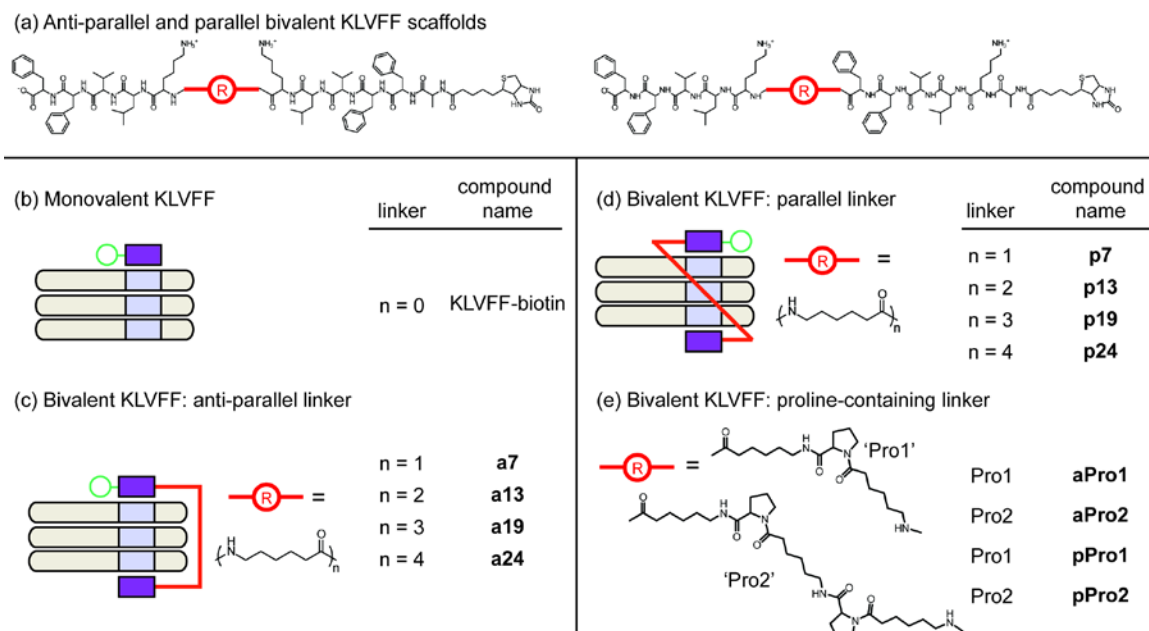
Figure 4.3 Collection of KLVFF-based probes. Purple regions represent 'KLVFF' on Aβ, and the green circle demarcates a biotin tag. Linkers are shown in red. (a) General chemical structure of bivalent KLVFF ligands. The second KLVFF motif was added such that the linker 'R' has a predicted orientation either anti-parallel (left) or 'parallel' (right) to the Aβ molecule. (b) The monovalent control ligand *KLVFF-biotin*, where no linker is present, thus, n = 0. (c, d) Two KLVFF motifs are joined by a linker 'R' consisting of one to four (n = 1 - 4) aminohexanoic acid molecules. The second KLVFF motif was added such that the linker 'R' has a predicted orientation either (c) anti-parallel or (d) 'parallel' (diagonal) to the Aβ molecule. Compounds are named according to their approximate extended linker length and their linker orientation (*e.g.* **a7** has a linker that is 7 Å with anti-parallel orientation). (e) Proline residues were added to the linker region to reduce flexibility. Either one (Pro1) or two (Pro2) prolines were placed between aminohexanoic acids, and both anti-parallel and parallel linker orientations were synthesized. Thus, **aPro1** has one proline residue and the linker has an anti-parallel orientation.

derivatives consisted of between one to four aminohexanoic (Ahx) acid molecules, resulting in extended linkers that ranged in length from roughly 7 – 24 Å. Thus, based on our proposed model and MD simulations, we predicted that these linker lengths should be sufficient to span the distance of an Aβ dimer, trimer, and tetramer. These compounds were named according to the orientation of the linker relative to the Aβ molecule and the approximate length of the extended linker (*e.g.* **a7** has a linker that is anti-parallel with an estimated length of ~ 7 Å) (Figure 4.3c) [41].

In addition, we sought to decrease linker flexibility to perhaps reduce the entropy required for binding by the second KLVFF motif. Toward this goal, we generated four probes containing proline residues embedded within the Ahx linker region (**aPro1**, **aPro2**, **pPro1**, **pPro2**) (Figure 4.3e). Introduction of the proline residues were intended to reduce the number of rotatable bonds, thus decreasing the amount of sampled chemical space. These were constructed in both anti-parallel and parallel versions and they contained either one (Pro1) or two (Pro2) proline residues. Linker length was limited to 13 – 24 Å, which were found to be ideal with the 'a' and 'p' series (see below). We found that all 12 probes were soluble and non-aggregating in aqueous solution at low concentrations (below 10 µM), and, at these concentrations, did not interfere with Aβ aggregation as measured by thioflavin T fluorescence (data not shown).

4.2.3 PICUP crosslinking of Aβ (1-40)

To test binding of these probes, we employed an established, UV cross-linking approach to produce Aβ samples containing a mixture of small oligomers [42]. Photo-induced cross-linking of unmodified proteins (PICUP) is often applied to amyloid systems to stabilize transient aggregates. Briefly, 25 µM Aβ (1-40) was cross-linked with a Ru(II) catalyst (tris(2,2'-bipyridyl)dichlororuthenium(II) hexahydrate and excess catalyst was removed using resin [43]. The resulting "ladder" of three various amounts of Aβ (0.4, 0.8, 2.0 µg) was separated by native-gel electrophoresis. By silver staining, we observed approximately equal levels of monomer, dimer, and trimer, along with lesser quantities of tetramer and pentamer (Figure 4.4a, silver stain). Following transfer to nitrocellulose, we probed this ladder further with a pan-Aβ antibody (6E10), and found the most intense binding to dimer, trimer, and tetramer, with reduced binding to monomer and pentamer (Figure 4.4a, 6E10). Together, these observations suggested

that our PICUP experiments were working as predicted and yielding qualitatively equal distributions of the small oligomers.

4.2.4 Western blot evaluation of crosslinked Aβ (1-40)

We next explored the binding of the bivalent KLVFF probes to LMW Aβ. Our strategy entailed incubating the nitrocellulose membrane with a solution containing the biotinylated-probe, washing and then identifying the bound material using streptravidin coupled to horseradish peroxidase (HRP). In order to optimize binding and wash steps, we varied probe concentration (1-20 μM), streptavidin-HRP concentration (1-10 μg/mL), blocking conditions (0-3% BSA), and the number (1-10) and duration (1-10 minutes) of wash steps. We determined that no initial blocking step was required, but that including 0.5-1% BSA with the 2 μM probe incubation (one hour) is ideal. Ten washes (5 minutes) were necessary to remove non-specific probe binding, followed by incubation with 1 μg/mL streptavidin-HRP (20 minutes) and ten additional washes. We found that not including these extensive wash steps resulted in unacceptably high background.

Under these conditions, we observed no binding by the **KLVFF-biotin** control (Figure 4.4a), a result consistent with its weak affinity [29]. Similarly, the KLVFF-based probes with relatively short linkers, **a7** and **a13**, also had weak binding, with a faint band at the molecular weight of an Aβ trimer (Figure 4.4a, b). However, the compounds with longer linkers, **a19** and **a24**, interacted strongly with the trimer and tetramer regions, with some binding to the dimers and pentamers (Figure 4.4a). These findings are consistent with the measurements obtained by MD simulations (Figure 4.2c), and the dependence upon linker length is clearly demonstrated upon quantification of each band (Figure 4.4b). The relatively poor binding to the Aβ dimers might suggest that it is not as ordered as the other structures, a concept that is consistent with recent

MD and NMR studies [18, 25]. Importantly, Aβ monomer was not recognized by any of the ligands at these concentrations, supporting an important role for multivalent interactions.

Interestingly, we observed partially similar binding patterns with the parallel series. Trimer and tetramer were, again, predominantly recognized, while dimer and pentamer showed reduced binding, and no binding to monomer was observed (Figure 4.4a, c). Analogous to the anti-parallel series, the probe with the longest linker, **p24**, displayed the best binding. In contrast to the anti-parallel ligands, however, the 'p' series showed little dependence upon linker length, as **p7** and **p13** clearly recognized trimer and tetramer. These data suggest an alternative binding mechanism relative to the anti-parallel series. One possibility is that the binding mode for this series relies on intramolecular contacts of the second KLVFF motif within the Aβ oligomer, thus creating new requirements for linker distance.

Finally, we found that the proline-containing ligands displayed enhanced selectivity for trimer and tetramer relative to the previous eight ligands. Recognition of dimer and pentamer was nearly absent, and no binding to monomer was observed (Figure 4.4a, d). Indeed, trimer comprised 56% and 63% of the total binding by **aPro2** and **pPro2**, respectively. In contrast, these values range from 36-40% in **a24** and **p24**. These findings are consistent with increasing the rigidity of the linker region, as this may reduce the entropy required for the binding of the second KLVFF motif to Aβ. Each of the proline-containing derivatives showed similar recognition patterns, with **aPro2** binding slightly more material than the others (Figure 4.4d). However, similar to the previous findings, 30 second exposures revealed that **pPro1** and **pPro2** bound monomer, while no such bands were seen with the **aPro** ligands, suggesting perhaps divergent binding mechanisms. Interestingly, **aPro1**, which contains only two aminohexanoic acid linkers

separated by one proline residue (Figure 4.3e), has an extended linker length only slightly longer than **a13** (~ 13 Å), which shows no binding to LMW Aβ under these conditions. In contrast, **aPro1** recognized both trimer and tetramer, suggesting an important role for reducing the flexibility of the linker region to facilitate binding of the second KLVFF motif.
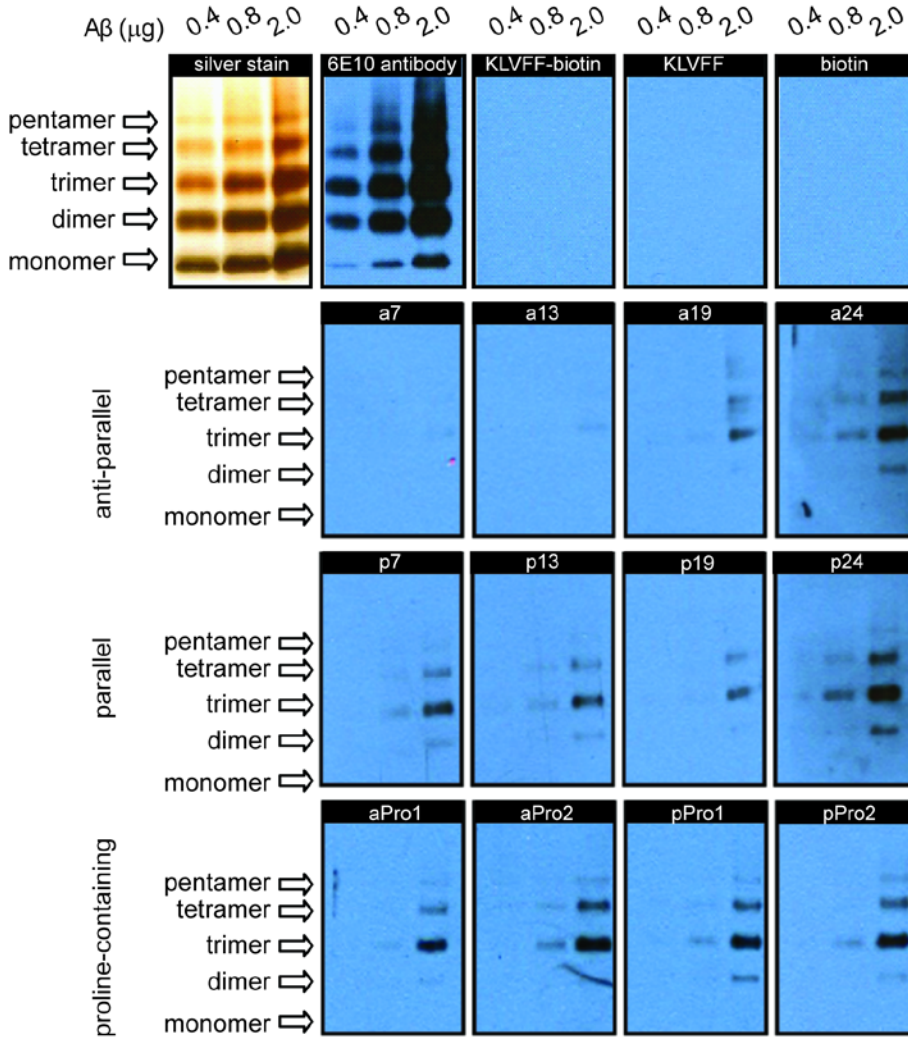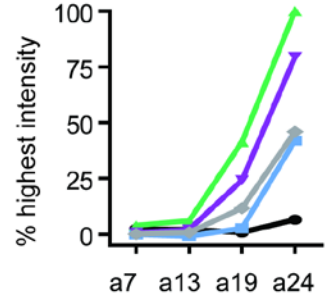
Figure 4.4 KLVFF-based probes selectively bind Aβ trimers and tetramers. (a) Binding properties of bivalent probes. Aβ (1-40) was crosslinked as described, separated using 10-20% tris-tricine electrophoresis, and transferred to nitrocellulose. Silver stain and probing with the pan Aβ-antibody 6E10 were used to visualize the total Aβ in each sample. Compounds (2 μM) were incubated with the membranes, which were then washed and imaged with streptavidin-HRP. Quantification of each Aβ band for the (b) anti-parallel, (c) parallel, and (d) proline-containing series. Results were quantified as the percent band intensity relative to the most intense band within each series (**a24** trimer, **p24** trimer, and **aPro2** trimer). Results are representative of two to four replicates.

4.2.5 Western blot evaluation of Aβ (1-42)

Based upon the results using crosslinked Aβ samples, we wanted to further test binding in more complex mixtures. Towards that goal, we probed aged samples of non-crosslinked Aβ (1-42) with bivalent KLVFF. Samples prepared by this method are known to contain a mixture of monomer (4.5 kDa), poorly resolved trimers and tetramers (~12 to 18 kDa) and higher order oligomers (~40 to 200 kDa) [44]. Using these samples, we found that the monovalent KLVFF-biotin control did not recognize any of the bands. Next, we chose to probe with **a24** and **aPro2** because these ligands displayed a combination of the highest selectivity with the greatest binding intensity against Aβ (1-40). Similar to our results with Aβ (1-40), **a24** and **aPro2** remained bound to the region corresponding to trimer and tetramer, suggesting that selectivity is maintained (Figure 4.5a).

In order to compare the recognition of monomer, trimer/tetramer, and high-molecular weight (HMW) material, we quantified the relative intensity of each of these regions (Figure 4.5b). As expected, silver staining and 6E10 binding showed that monomer, trimer/tetramer, and HMW species are recognized almost equally. In contrast, **a24**, and to a greater extent, **aPro2**, predominantly bound trimer and tetramer. Specifically, trimer/tetramer binding comprised 47% and 71% of the total amount of Aβ recognized by **a24** and **aPro2**, respectively. Minimal binding to monomer and HMW material further emphasized the selectivity of these probes for early structures in the Aβ aggregation pathway.

(a) Ligands **a24** and **aPro2** recognize Aβ trimers and tetramers in mixed samples
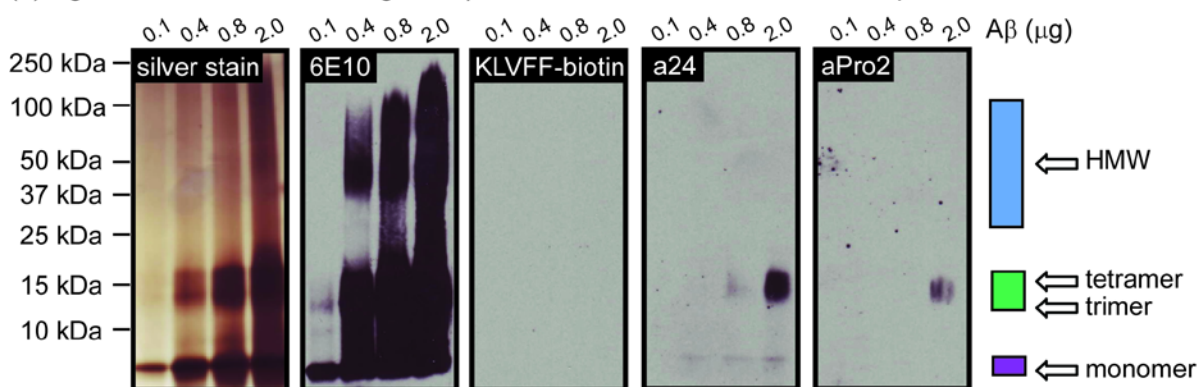
(b) Quantification of three regions reveals predominant recognition of trimer/tetramer
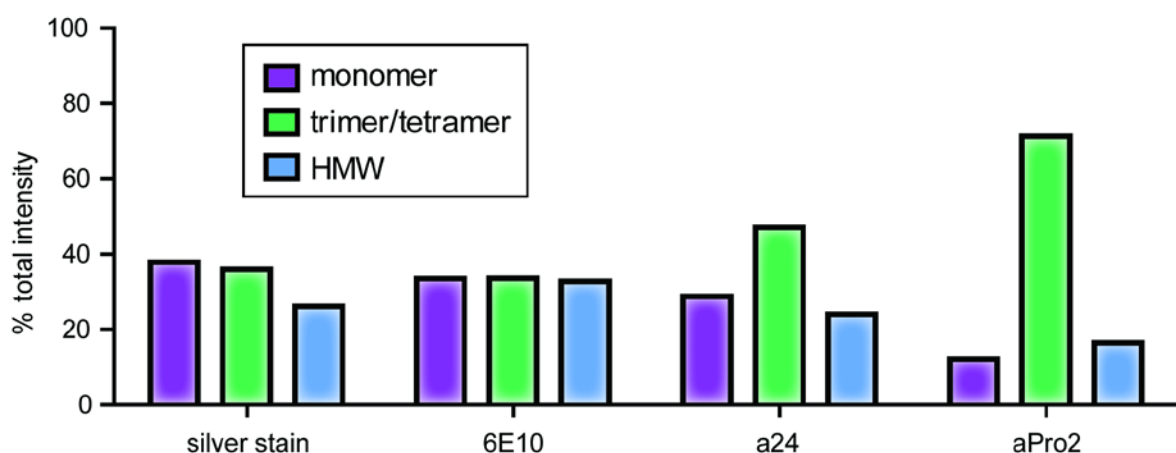
Figure 4.5 KLVFF-based ligands selectively recognize trimers and tetramers in mixed Aβ (1-42) samples. (a) Aβ (1-42) was separated and probed as described in Figure 4.4. Silver stain and probing with the anti-Aβ antibody 6E10 shows a mixture of monomer, trimer, tetramer, and high-molecular weight species. Previous studies confirm the absence of dimer, and a 'smear' of trimer/tetramer with un-crosslinked Aβ (1-42).The control compound **KLVFF-biotin** showed no binding, while **a24** and **aPro2** predominantly bound trimer and tetramer within this mixture. The outline (far right) represents the areas quantified for monomer (purple), trimer/tetramer (green) and high-molecular weight (HMW) species. (b) The intensity of each region was quantified (2.0 μg lane), and the total intensity was determined. Using this summation, the percent total intensity for each region was calculated.Silver stain and 6E10 show approximately equal recognition of monomer, trimer/tetramer, and HMW Aβ. In contrast, **a24** and **aPro2** predominantly bind the trimer/tetramer region. The trimer/tetramer band bound by **aPro2** represents71% of the total bound material.

4.2.6 Testing recognition of LMW Aβ in human CSF

Next, we wanted to evaluate binding in human cerebrospinal fluid (CSF), which provides a more

challenging environment than aqueous buffers in which to retain avidity and selectivity.

However, Aβ levels, although varied, are often less than (10 ng/mL) [45-47] in normal human

CSF, and based on our results against purified Aβ, we predicted that we may not detect these low levels of native Aβ. Thus, to determine if these probes could still bind Aβ in this milieu, we added 1 μg of cross-linked Aβ (1-40) to CSF samples from non-AD patients (6 μg of total protein) and characterized the resulting "spiked" mixture by silver stain, 6E10 antibody, **a24** and **aPro2**. Silver stain and 6E10 analysis revealed that the Aβ (1-40) LMW pattern was not altered when added to CSF (Figure 4.6a). We found that **a24** and **aPro2** recognized several unrelated bands within the CSF sample; however, this off-target reactivity was largely restricted to proteins > 50 kDa. Thus, we were still able to visualize binding to Aβ trimers and tetramers (Figure 4.6a). Similar findings were obtained using Aβ (1-42). In order to survey the repeatability of this finding, we performed five individual replicates with **a24** against both Aβ (1-40) and Aβ (1-42) (Figure 4.6b). Trimer and tetramer bands were quantified together, and we found that recognition of these species was identical in the absence and presence of CSF. Together, these results suggest that the multivalent probes can exploit unique inter-KLVFF distances to
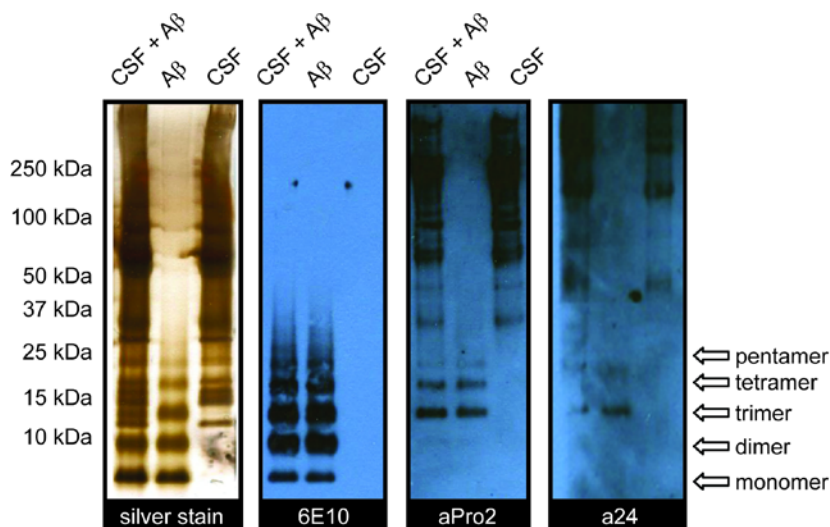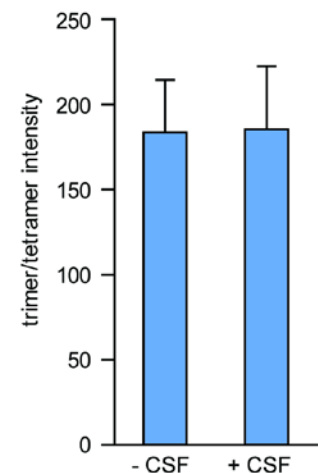
Figure 4.6 **a24** and **aPro2** selectively recognize trimers and tetramers in human cerebrospinal fluid (CSF). (a) Cross-linked Aβ (1-40) was added to human CSF and probed with **a24** and **aPro2**, which both retain selectivity for only trimer and tetramer in this biological context. Similar results were found for Aβ (1-42). (b) The trimer/tetramer reactivity with **a24** was quantified with and without CSF over five independent replicates. These data have been compiled across three separate preparations of **a24** and include reactivity against Aβ (1-40) and Aβ (1-42).

distinguish between otherwise closely related Aβ structures. Based on these findings, we anticipate that derivatives of **a24** and **aPro2** with further improvements in affinity and selectivity, may be promising probes for detecting the appearance of the earliest Aβ aggregates.

4.2.7 Affinity studies of KLVFF derivatives for Aβ

In order to further characterize the binding interactions between KLVFF and Aβ, we used surface plasmon resonance (SPR) and ELISA platforms to explore affinity. For SPR, LMW Aβ (1-42) was immobilized (350-550 immobilization response units (RUs)). We first confirmed that **KLVFF** has a weak affinity for Aβ ($K_{d (app)}$ = 1.4 mM) (Table 4.1). Due to non-specific interactions of biotin with the ethanolamine surface, we were unable to measure the binding of biotinylated **KLVFF** and **a24**. Thus, we synthesized an **a24** derivative lacking the alanine-biotin tag (**a24***), and, as expected, we found that **a24*** displayed over a 23-fold increase in affinity ($K_{d (app)}$ = 60 μM) relative to **KLVFF**. To confirm that the biotinylated versions showed similar binding patterns, we employed a competition ELISA approach in where **biotin**, **KLVFF-biotin**, or **a24** competed with an **a24**-coated surface for binding to Aβ. We found that **biotin** and **KLVFF-biotin** did not compete with **a24** for binding (K_i > 500 μM) (Table 4.1). Analogous to our SPR results, we found that **a24** (K_i = 48 μM) binds with similar affinity as **a24*** to LMW Aβ (1-42).

Table 4.1 Comparison of KLVFF ligands binding to LMW Aβ (1-42) by two methods

compound	ELISA K_i (μM)	SPR $K_{d (app)}$ (μM)
biotin	> 500	not tested
KLVFF-biotin	> 500	not tested
KLVFF	not tested	1400 ± 108
a24*	not tested	60 ± 13
a24	48 ± 1.1	not tested

* not biotinylated

In order to further optimize our probes for use in biological mixtures, we aimed to increase the affinity and reduce non-specific binding. Specifically, we predicted that binding to native levels of Aβ might require at least nanomolar affinity. Toward this goal, we first explored the impact of modifying the KLVFF recognition element. For instance, as detailed in Chapter 1, Cairo *et al*.

found that the addition of charged residues (Lys, Arg, or Glu) to KLVFF improved both the affinity (40 – 80 μM) and the ability to modulate Aβ aggregation [29]. We, in turn, sought to incorporate this finding into our bivalent derivatives by synthesizing KLVFFKK (**A**) and KLVFFKKKK (**B**) (Figure 4.7a). Interestingly, however, we discovered that the affinities of **A** (1.1 mM) and **B** (0.6 mM) were not significantly higher than **KLVFF** (1.4 mM). To explain this, we realized that the previous studies used Aβ (10-35) fibrils as a target, while we employed LMW Aβ (1-42), suggesting that the binding site might be different between these two amyloids. Still, we developed a bivalent ligand that incorporates these residues in place of the original KLVFF (**C**). However, we found that **C** ($K_{d\ (app)}$ = 0.6 mM) had an identical binding affinity to its monovalent counterpart **B** (Figure 4.7a, b). Thus, we concluded that this strategy was not a productive way of readily increasing affinity. Ideas for future studies are presented in Chapter 5.

To make one more attempt to increase affinity, we turned to the native sequence of Aβ surrounding the KLVFF motif (Figure 4.7c). Specifically, we proposed that incorporating these adjacent residues may increase self-recognition. Indeed, previous studies have demonstrated that adding the native amino acids that are N-terminal to KLVFF (*e.g. QKLVFF, HQKLVFF*, and *HHQKLVFF*) resulted in peptides with high affinity for Aβ [16]. Thus, we synthesized a collection of six KLVFF derivatives (**D** through **I**) with additional amino acids on either end (Figure 4.7d). We also included in this library two derivatives that have been implicated in inhibiting Aβ aggregation (**J** and **K**) [48-50]. Using SPR, we screened each peptide at 400 μM for differences in association relative to **KLVFF**. Interestingly, we found that the addition of two to three (Ala-Glu or Ala-Glu-Asp) residues on the C-terminal end of KLVFF resulted in

(a) Lysine-based derivatives of KLVFF

peptide	sequence	K_d (mM)
	KLVFF	1.4 ± 0.1
A	KLVFFKK	1.1 ± 0.3
B	KLVFFKKKK	0.6 ± 1.9
a24	FFVLK (Ahx)₄ KLVFF	0.06 ± 0.01
C	FFVLK (Ahx)₄ KLVFFKKKK	0.6 ± 0.05

(b) Lysine addition impacts effects of bivalency
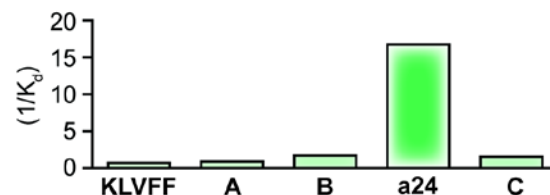
(c) Aβ (13-23) HHQ-KLVFF-AED

(d) Sequence-based KLVFF derivatives

peptide	sequence	ΔRU (400 μM)
	KLVFF	< 15
D	KLVFFA	< 15
E	KLVFFAE	184.3 ± 33.4
F	KLVFFAED	194.8 ± 37.9
G	QKLVFF	< 15
H	HQKLVFF	< 15
I	HHQKLVFF	< 15
J	LPFFD	< 15
K	RGKLVFFGR	40.0 ± 2.2

(e) ΔRU correlates with ThT reactivity
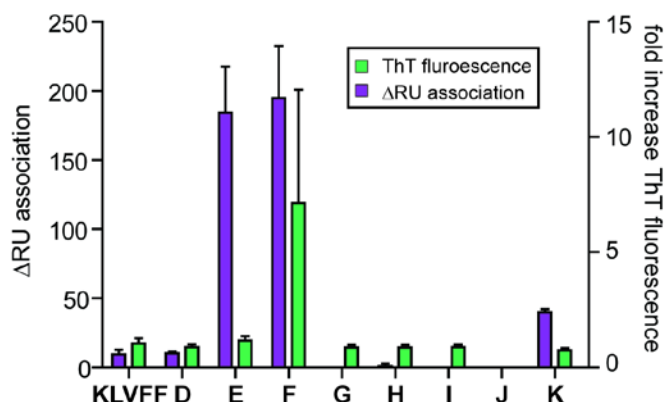
Figure 4.7 Modifying the monovalent KLVFF recognition element. (a) A series of lysine-based KLVFF derivatives were evaluated for their binding affinity ($K_{d\ (app)}$) to LMW Aβ (1-42) using surface plasmon resonance (SPR). The addition of four lysines to KLVFF (**B**) increased the affinity over 2-fold. However, bivalency had no further effect on binding affinity (**C**) relative to the monovalent recogntion element (**B**). (b) The inverse ($1/K_d$) plotted as a function of peptide reveals the high affinity of **a24** relative to the bivalent ligand **C**. The only difference between these peptides is the addition of four lysine residues. These data suggest that the binding sites for KLVFF and KLVFFKKKK are distinct. Together, these indicate that KLVFF is sensitive to minor additions, and that modifying the KLVFF sequence may not be useful toward increasing the affinity of bivalent KLVFF for Aβ. (c) The residues surrounding the KLVFF sequence in Aβ, represented by Aβ (13-23). This sequence was used to design the derivatives listed in (d) (**D** through **I**). We predicted that adding these residues might increase the self-recognition propensity of KLVFF for Aβ. Peptides **J** and **K** are peptides previously shown to interact with Aβ. SPR was used to screen the association of **D** through **K** at 400 μM. We found that only **E**, **F**, and **K** showed greater association with Aβ relative to **KLVFF**. (e) ThT fluorescence was used to survey the aggregation properties of **D** through **K**. From these studies, we found that **E** and **F** aggregate either immediately (**F**), or upon incubation (**E**) (data not shown).Thus, the nearly 20-fold increase in association by SPR is likely due to binding of an aggregate of **E** and **F**. In contrast, **K** did not aggregate, and showed approximately a 4-fold greater association than **KLVFF** to Aβ.

nearly a 20-fold increase in association compared to **KLVFF** (Figure 4.7d). This promising result, however, led us to determine whether these peptides may be aggregating, as was suggested in previous studies [51], resulting in a higher apparent association. Indeed, thioflavin T fluorescence revealed that immediately upon suspension in buffer, peptide **F** self-assembled (Figure 4.7e). Although **E** did not immediately aggregate, its ThT fluorescence increased at later time points (data not shown). Thus, we suspect that the increased association by SPR observed

with **E** and **F** might be due to aggregation rather than an increased affinity of these peptides for Aβ. In contrast, **K** showed over a 2-fold higher association than **KLVFF**, but no ThT fluorescence above background, suggesting that **K** may be a promising candidate for bivalency.

4.2.8 aPro2 labels amyloid-β pathology in APPswe/PS1 transgenic mouse tissue

Based upon the selectivity observed by **aPro2** in the presence of CSF, we proposed that our probes may have utility in staining amyloid in diseased brain tissue. This hypothesis is based on our observations that the binding affinity of aPro2 is similar to that of congo red (CR) (K_d = 40 μM) [29], one of the most commonly used histopathological markers of Aβ deposition. Further, several groups have had success in probing amyloid in tissue using biotinylated peptides [52, 53]. For instance, Heng *et al.* visualized aggregated foci (AF) of the huntingtin protein in diseased brain tissue using a polyglutamine peptide tagged with biotin [52]. Thus, background binding of biotin did not preclude staining of amyloid *ex vivo*. Based on these observations, we sought to compare the staining patterns of the LMW-specific probes described in this Chapter, specifically **aPro2**, with non-specific chemical probes such as CR and thioflavin S (ThS) in mouse and human AD tissue.

We first evaluated Aβ pathology in frozen brain slices from AD transgenic mice containing two mutations; one in the amyloid precursor protein (APP) and the other in presenilin 1 (PS1) (APPswe/PS1ΔE9) [54, 55]. After six months, these mice develop age-dependent Aβ plaque pathology that correlates with cognitive decline [56]. CR and ThS staining of tissue obtained at 13 months of age confirmed Aβ deposition in the cerebellum, hippocampus, and cerebral cortex (Figure 4.8a). Preliminary studies with **aPro2** suggest that it specifically labels Aβ lesions in this tissue as well (Figure 4.8a). Significantly less staining was observed in tissue obtained from an

age-matched wild-type mouse (data not shown). These initial findings indicate that **aPro2** labels deposits within the same brain regions as those visualized with ThS and CR. Additional co-staining experiments with **aPro2** and ThS will discern whether identical deposits are visualized by these chemical probes, and may highlight any differences in morphology. Next, we performed an initial evaluation of labeling in human AD hippocampal tissue. Bielschowsky silver staining, CR, and ThS highlight $A\beta$ and tau deposits in this tissue (Figure 4.8b). Thus far, we have not observed staining of $A\beta$ deposits in human tissue with **aPro2**; however, we propose that optimized
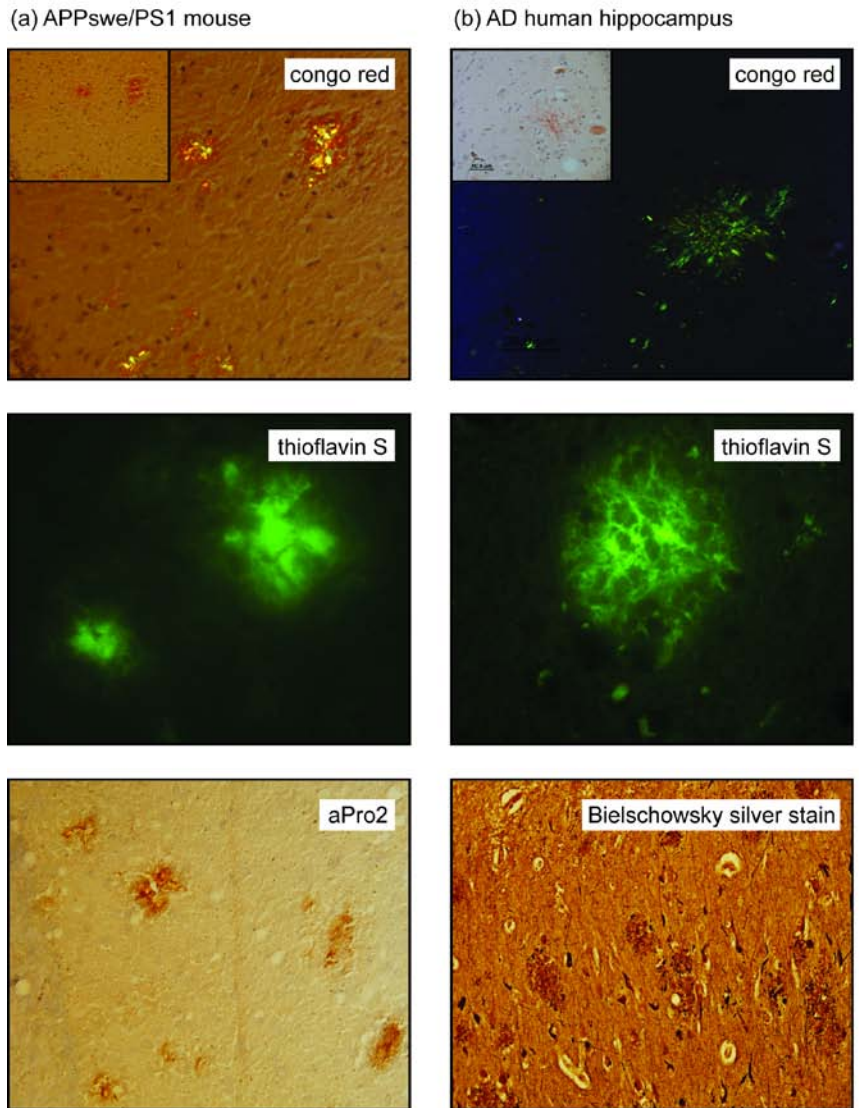
Figure 4.8 **aPro2** labels $A\beta$ pathology in diseased mouse tissue (a) Frozen brain tissue sections from 13-month old double transgenic APPswe/PS1 mice stained with congo red, thioflavin S, and **aPro2**. Deposits were primarily observed in the hippocampus, cerebral cortex, and cerebellum. Importantly, no staining was observed in an age-matched wild-type control. Congo red image under polarized light, inset: brightfield. (b) Paraffin-fixed human hippocampal tissue from AD patients shows $A\beta$ plaques and tau NFTs by silver stain, and $A\beta$ deposits visualized with congo red and thioflavin S. Further optimization of amplificiation procedures may reveal staining of human $A\beta$ deposition with **aPro2**.

amplification procedures, perhaps in conjunction with antigen retrieval on the fixed tissue may aid in staining with this probe. Further evaluation of the morphology of the $A\beta$ lesions in both the diseased mouse and human tissue with our collection of LMW-specific markers may provide

insight into the composition and localization of these deposits. Mention time course experiment.

4.3 Discussion

By using a portion of the amyloid-β peptide sequence involved in self-recognition, we developed the first selective probes for LMW Aβ. We employed multivalency and molecular modeling to synthesize bivalent KLVFF derivatives with increased binding avidity and selectivity for LMW Aβ, specifically trimers and tetramers. Importantly, based on the observations that Aβ aggregates display an exposed KLVFF at each 'end,' we designed the linker region of these molecules such that binding to larger oligomers and fibrils was precluded. Furthermore, no binding to monomer was observed, suggesting that bivalency plays a pivotal role in recognition.

Interestingly, as reviewed in Chapter 1, Ma and Nussinov used MD simulations to evaluate the different orientations of that KLVFF might access within Aβ (Figure 1.10). Two distinct orientations were explored; one in where KLVFF binds its identical residues on the neighboring strand (Figure 4.9a), and another in which the strands alternate (*e.g.* only one of the phenylalanine residues binding its homologous side-chain on another strand) (Figure 4.9b). Interestingly, they concluded that the latter orientation lends the structure more stability, but that both orientations are possible. Although crystallographic data suggests that KLVFF binds distinctly to its homologous residues on neighboring strands in fibrils [27], it is not surprising that LMW Aβ may access different orientations, as these species have been shown to be much more dynamic than stable fibrils [18, 20, 21]. Thus, the possibility for two distinct peptide orientations presents the possibility of at least four binding modes by our two classes of bivalent ligands (anti-parallel and parallel). In fact, this model suggests that, since trimer is

predominantly recognized, that bivalent KLVFF may not recognize the difference between identical and alternating strands (Figure 4.9c, d). In contrast, however, since no significant length dependence was observed with the parallel collection (**p7** through **p24**), perhaps the 'a' and 'p' series recognize distinct orientations. This hypothesis might be addressed through competition of parallel and anti-parallel ligands in order to observe whether they recognize the same or distinct populations of Aβ trimers.
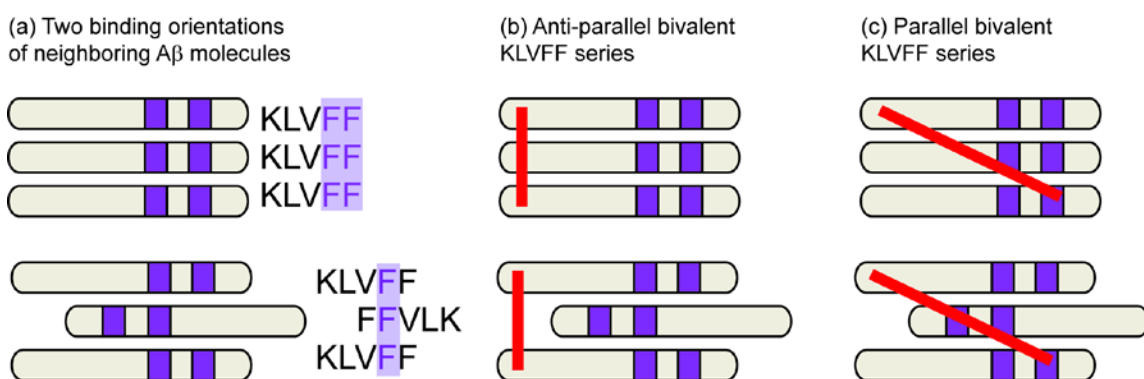
Figure 4.9 KLVFF may access two binding modes within Aβ (a) Using MD simulations, Ma and Nussinov suggested that KLVFF may be oriented in two ways relative to its neighboring strand. (Top) KLVFF binds its identical residues on the next strand; (Bottom) KLVFF only contacts one identical residue (phenylalanine) because strands alternate. While both orientations are possible energetically, the bottom model was shown to be more stable. (b, c) The potential existence of two binding orientations presents four binding modes for bivalent KLVFF molecules. The presence of multiple possible binding modes may explain why the 'a' series shows linker length dependence, while the 'p' series does not display these trends.

Importantly, we observed that two of our ligands, **a24** and **aPro2**, retain selectivity for trimers and tetramers in a complex biological background of human CSF (Figure 4.6). Therefore, in contrast to the indole-based tools discussed in Chapter 3, our KLVFF ligands are not limited to interactions with purified amyloid systems. However, the detection limit with the Western blot platform precludes recognition of native levels of Aβ in CSF. Specifically, we cannot visualize less than 16 μg/mL with bivalent KLVFF, and, in contrast, levels of Aβ within CSF are at least 10-fold lower than this value. Despite this current limitation, it is pertinent to continue exploring platforms and scaffolds with increased sensitivity (discussed in Chapter 5). Many studies suggest

that Aβ levels within CSF are dramatically altered in AD patients relative to healthy controls. However, the correlation between disease progression and Aβ levels in the CSF remains unclear. Moreover, changes in the amounts of different Aβ morphologies has yet to be explored, namely due to a lack of conformation-specific reporters. Thus, these ligands could be useful for probing changes in the levels of early oligomers in CSF or blood, and correlating these findings with pathology in the brain and overall disease progression. Similarly, they might be used as solid-phase affinity reagents for capturing small oligomers from solutions. For any of these potential applications, the affinity and selectivity should be optimized.

One approach by which the utility of these ligands might be increased is through improving their affinity for Aβ. Toward this goal, we attempted to develop derivatives with increased binding affinity for Aβ. However, we discovered that modification of the recognition element may not be a useful strategy for driving affinity. For instance, we improved the affinity over 2-fold by adding four lysine residues to KLVFF, but this increase in affinity did not translate into better bivalent compounds. We propose that this lack of improvement is likely due to a change in the binding orientation or the binding site of KLVFFK$_4$ relative to KLVFF. In addition, we found that extending the KLVFF sequence (*e.g.* KLVFFAED) can produce motifs that are capable of self-recognition, but that they are prone to aggregation. In this regard, KLVFF is perhaps the most ideal monovalent recognition element, as it retains recognition to Aβ, but itself does not form sufficiently strong contacts to aggregate. Thus, other regions of the molecule, such as the linker, may be a more ideal target for improving binding affinity. For example, the linker region of the current molecules primarily contains uncharged carbon chains. However, it is likely that charged, not hydrophobic, side chains are exposed on the surface of the Aβ molecule, and incorporating charged or polar groups within the linker may increase the association of this region with Aβ.

Further, replacing one of the KLVFF binding motifs with an alternative Aβ ligand might yield higher affinity ligands. We showed in Chapter 2 that Congo Red and curcumin bind LMW preparations of Aβ with low micromolar affinity (15 - 35 μM). Therefore, a promising approach may be to generate hetero-bivalent ligands containing KLVFF and a second scaffold with higher affinity. These and other scaffolds are further explored in Chapter 5.

Finally, we have performed preliminary studies of Aβ deposition in diseased tissue using the bivalent KLVFF probe **aPro2**. In mouse tissue obtained at 13 months of age, we found that **aPro2** specifically labels Aβ deposits in the hippocampus, cortex, and cerebellum. Cognitive decline and heavy plaque deposition in this transgenic model emerges at approximately 6 months, and behavioral deficits worsen with age [56]. However, it is unclear whether early Aβ oligomers are present in mice younger than 6 months, and how these levels change throughout lifespan is unknown. We propose that **aPro2** may recognize LMW Aβ in transgenic animals at various ages, and this approach may complement existing non-selective Aβ probes.

4.4 Experimental Procedures

4.4.1 Materials

Aβ (1-40) was obtained from Anaspec (San Jose, CA) and Aβ (1-42) from EZBiolab (Westfield, IN). Fmoc-protected amino acids, biotin, and Wang resin were purchased from Anaspec. Unless otherwise noted, all solvents were purchased from Fisher. DIC and HOBt were purchased from Fluka (Milwaukee, WI) and GenScript (Piscataway, NJ), respectively. Microwave-assisted peptide synthesis was performed on a Biotage Initiator EXP using the times and temperatures described. All NMR data were collected and analyzed on a Varian 600 MHz system using VnmrJ™ version 2.2 revision C. Mass spectrometry data were obtained on a Micromass LCT time-of-flight mass

spectrometer in the ES+ mode. Cerebrospinal fluid was collected by the University of Michigan Hospitals. Samples were pooled from six non-coded donors. An IRB notification (HUM00033486) of "not regulated" status was received on 9/2/2009. Human brain tissue. Mouse brain tissue. Microscope.

4.4.2 Molecular dynamics simulations

The AMBER 10 [57] package was used to perform the unrestrained all-atom Molecular Dynamics (MD) simulations. Coordinates of Aβ (16-42)-fibril were obtained from PDB [58] (PDB: 2BEG [27]), and the first frame of the NMR ensembles was used in the system construction. Because the N-termini of Aβ (16-42)-fibril are unresolved, an acetyl capping group was added to each Aβ (16-42)-fibril chain. The synthetic KLVFF-based ligand was constructed and placed on the Aβ chains using Molecular Operating System (MOE) [59] and PyMOL [60, 61]. The initial placement of the KLVFF-based ligand was guided by the position of the KLVFF in the adjacent monomer. Parameters for the linker and biotin groups were generated using AM1-BCC charges and the ANTECHAMBER module of AMBER [62], while the protein was parameterized using the FF99SB force field [63]. Counter ions were added to neutralize both the dimer (3 Na^+) and trimer (5 Na^+) systems. Boxes of 3931 and 3986 TIP4P water were used to solvate the systems, respectively.

Following assembly of the bound ligand-Aβ system, MD simulations were run in the NPT ensemble and the SHAKE algorithm [64] was used to constrain all bonds to hydrogen atoms. A 1-fs time step was used along with a 10 Å cut-off for non-bonded interactions and particle mesh Ewald for long-distance electrostatics. For both systems, hydrogen atoms were first minimized, followed by the side chains and then all atoms. The system were then equilibrated by gradually heating the water molecules from 10 to 310 K over 50 ps, followed by water equilibrium for 100

ps at 310 K with protein restrained. This was followed by a full-system heating from 10 to 310 K over 30 ps and a full system equilibration with unrestrained protein for 200 ps. The production phase was run for 4 ns at 310 K. To measure the distance between the two Aβ peptide "ends" over the MD trajectory, the distance between the carbonyl carbons of Lys7 was generated using PTRAJ module of AMBER. To estimate this distance in the tetramer complex, we have added the difference between the medians of the dimer and trimer simulation (approximately 4.8 Å) to the median of the trimer simulation (19.3 Å).

4.4.3 Aβ preparation and PICUP crosslinking

Aβ (1-40) and Aβ (1-42) were prepared as previously described [40]. Briefly, 1 mg was suspended in hexafluoroisopropanol (Fluka), aliquoted, dried down to a film under nitrogen, and stored at -30 °C. Immediately prior to the start of an experiment, 0.1 mg was suspended in PBS pH 7.2 (140 mM NaCl, 2.7 mM KCl, 10 mM Na_2HPO_4, 1.8 mM KH_2PO_4) containing 1% DMSO to a final concentration of 25 μM, vortexed for 15 seconds and sonicated for 30 seconds. Aβ (1-42) was then used immediately after sonication. Aβ (1-40) was cross-linked as described [42]. Briefly, ammonium persulfate (1 mM) and Tris(2,2′-bipyridyl)dichlororuthenium(II) hexahydrate (Ru(II)) (50 μM) were added to Aβ (final concentration 22.5 μM). The mixture was mixed by pipetting and exposed to UV light for 1 second. Excess Ru(II) was then removed using ~ 5 mg Isolute SI-Thiol (EC) resin (Biotage) per 200 μL Aβ mixture until the solution was no longer yellow. The sample was then gently centrifuged (5,000 rpm) for 30 seconds to pellet the resin, and the supernatant (22.5 μM Aβ) was used in the gel electrophoresis experiments.

4.4.4 Native gel-electrophoresis, silver staining, and Western blot with 6E10

Varying amounts (0.4 – 2.0 μg) of crosslinked Aβ (1-40) or non-crosslinked (1-42) were separated by native gel gradient electrophoresis (10-20% tric-tricine, Invitrogen, Carlsbad, CA) using non-denaturing, non-reducing loading buffer (300 mM tris-HCl, 8% glycerol, 0.01% bromophenol blue). Gels were either stained using the ProteoSilver Silver Stain Kit (Sigma) according to the manufacturer's protocol, or transferred (1 hour, 180 milliamps, 4 °C) to 0.2 μm Protran nitrocellulose (Whatman). The membrane was blocked with 3% BSA in TBS-T (140 mM sodium chloride, 25 mM tris, 0.1% Tween-20) for 90 minutes at room temperature. The membrane was washed (3 X 5 minutes) with TBS-T and incubated overnight in 1:2000 6E10 (Covance, Dedham, MA) containing 3% BSA in TBS-T at 4 °C. The membrane was then washed again (3 X 5 minutes), incubated for one hour with HRP-conjugated goat anti-mouse IgG (Abcam, Cambridge, MA) in TBS-T, washed (3 X 5 minutes) and developed using the Western Lightning Plus-ECL kit according to the manufacturer's protocol (PerkinElmer, Waltham, MA).

4.4.5 Western blot with biotinylated KLVFF peptides

Native gel-electrophoresis with Aβ (1-40) and Aβ (1-42) and transfer to nitrocellulose were performed as described. Ponceau staining was performed to ensure proper transfer to the membrane. Membranes were then spatially separated in order to probe the samples with individual peptides. The membrane was placed in a petri dish (100 mm X 15 mm) and 10 mL of 2 μM KLVFF peptide (0.5% BSA in TBS-T) was added. Note that the peptide and BSA were mixed immediately prior to the start of the experiment. The membrane was incubated with the peptide for 1 hour followed by TBS-T washes (10 X 5 minutes each), and incubation with 1 μg/mL streptavidin-HRP (Pierce, Rockfod, IL) for 20 minutes. Following a final TBS-T wash step (12 X 5 minutes each), the membrane was developed using the Western Lightning Plus-ECL kit according to the manufacturer's protocol (PerkinElmer, Waltham, MA). Each step was

performed on a rocker at room temperature. All blots were exposed for 3, 10, 30 and 60 seconds. Bands were quantified using Image J software following two treatments; the background was first automatically subtracted and the image was inverted. Quantifications were expressed as described in the text and figure legends.

4.4.6 Peptide synthesis and characterization

Microwave-assisted solid-phase Fmoc-peptide synthesis was performed generally as described [65, 66]. Briefly, for each peptide, 1 eq of Wang resin (1mmol/g) was activated with 6 eq each of DIC and HOBt for 30 minutes stirring in DMF at room temperature, after which 0.6 eq DMAP and 10 eq Fmoc-Phe were added. The reaction mixture was then irradiated for 60 minutes at 60 °C (pre-stirring 30 seconds). The coupling efficiency was measured by filtering and washing (DMF, methanol, and DCM) 1-2 mg of resin, to which 3 mL of 20% piperidine in DMF was added in a quartz cuvette. The absorbance at 290 nm (A_{290}) was then measured after a 5 minute incubation and inverting the cuvette several times. The percentage of coupled resin was then calculated using the following equation: % coupled = $[(A_{290})/(1.65*\text{mass resin in mg})]*100\%$. The coupling efficiency for each peptide was > 70%. The resin was then washed with DMF, methanol, and DCM. The Fmoc group was then removed (20% piperidine in DMF) by irradiating the mixture for 3 minutes at 60 °C, and then resin was again washed as described.

The peptides were subsequently built using 3 eq of each Fmoc-protected amino acid, and 5 eq each of DIC and HOBt. The reagents were combined in DMF and, after 5 minutes of stirring, were irradiated for 8-15 minutes at 60 °C, depending upon the amino acid. Coupling efficiency was evaluated using a standard Kaiser test. The resin was washed and the Fmoc group was

removed as already described. These steps were also followed for the addition of biotin on the N-terminus of each peptide, except for Fmoc deprotection.

Following the addition of biotin, the peptides were cleaved from resin in 20-30% TFA in DCM, stirring at room temperature for 45 minutes. The resin was then filtered and washed with DCM. For the bivalent peptides, the biotinylated product was then precipitated from the resulting filtrate by H_2O addition, filtered, and dried under vacuum. For monovalent KLVFF derivatives, the cleaved filtrate was precipitated immediately in cold diethyl ether and filtered. Yields for each peptide are listed below. All HPLC runs were performed on a Beckman-Coulter HPLC system measuring at 254nm with a Waters Spherisorb 10μm ODS2 4.6X250mm analytical column at a flow rate of 1 mL/min (acetonitrile:water gradient containing 0.1% trifluoroacetic acid). Only the monovalent control and 'a' series were re-run on the HPLC under analytical conditions to obtain purity percentage values.

HO-Phe-Phe-Val-Leu-Lys-Ala-biotin (**KLVFF-biotin**): ^{1}H NMR (600 MHz, DMSO) δ 8.24 (d, J = 7.8 Hz, 1H), 8.06 (d, J = 7.1 Hz, 1H), 7.99 (t, J = 7.6 Hz, 2H), 7.96 (d, J = 8.2 Hz, 1H), 7.78 (s, 3H), 7.69 (d, J = 9.0 Hz, 1H), 7.32 – 7.17 (m, 10H), 6.48 (s, 1H), 6.45 (s, 1H), 4.59 (td, J = 9.0, 4.5 Hz, 1H), 4.49 (td, J = 8.1, 5.6 Hz, 1H), 4.38 – 4.31 (m, 2H), 4.31 – 4.24 (m, 2H), 4.15 (ddd, J = 15.8, 8.3, 5.7 Hz, 2H), 3.17 – 3.06 (m, 2H), 2.98 (ddd, J = 22.3, 14.0, 6.3 Hz, 2H), 2.86 (dd, J = 12.5, 5.1 Hz, 1H), 2.78 (t, J = 11.6 Hz, 3H), 2.62 (d, J = 12.4 32Hz, 1H), 2.15 (t, J = 7.3 Hz, 2H), 1.90 (td, J = 13.6, 6.8 Hz, 1H), 1.71 – 1.62 (m, 2H), 1.61 – 1.49 (m, 8H), 1.44 (dd, J = 23.7, 9.0 Hz, 1H), 1.33 (dd, J = 11.3, 7.2 Hz, 4H), 1.22 (d, J = 7.1 Hz, 3H), 0.88 (d, J = 6.6 Hz, 3H), 0.83 (d, J = 6.5 Hz, 3H), 0.74 (d, J = 6.7 Hz, 6H). ^{13}C NMR (600 MHz, DMSO) δ 172.58, 172.49, 172.18, 171.56, 171.24, 170.87, 170.40, 162.80, 158.55, 158.33, 158.11, 157.89, 143.02, 137.58, 137.29, 129.06, 128.17, 127.95, 126.43,

126.15, 117.56, 115.59, 60.99, 59.26, 57.45, 55.35, 53.37, 52.10, 50.98, 48.24, 40.49, 38.72, 37.55, 36.75, 34.82, 31.21, 30.69, 28.06, 27.98, 26.57, 25.18, 24.09, 23.10, 22.11, 21.57, 19.14, 17.91, 17.90. M/Z expected for $C_{48}H_{72}N_9O_9S^+$ 950.5; observed M + H 950.3 (100%). Purity 92.4%.

HPLC chromatogram:

Retention time (min)	Area	% Area
24.53	693389	4.2
26.42	15267340	92.4
29.58	565001	3.4

HO-Phe-Phe-Val-Leu-Lys-Ahx-Lys-Leu-Val-Phe-Phe-Ala-biotin (**a7**): ^{1}H NMR (600 MHz, DMSO) δ 8.26 (d, J = 7.5 Hz, 1H), 8.14 (s, 1H), 8.07 − 7.92 (m, 6H), 7.86 (d, J = 28.8 Hz, 3H), 7.74 (s, 6H), 7.67 (d, J = 9.3 Hz, 1H), 7.48 − 7.06 (m, 20H), 6.79 (d, J = 38.5 Hz, 1H), 6.43 (d, J = 21.7 Hz, 1H), 4.65 (s, 1H), 4.60 (s, 1H), 4.49 (d, J = 5.5 Hz, 2H), 4.34 (s, 3H), 4.29 (s, 2H), 4.23 (s, 3H), 4.15 (d, J = 6.9 Hz, 2H), 3.38 (d, J = 12.8 Hz, 1H), 3.07 (dd, J = 20.6, 15.3 Hz, 5H), 3.00 − 2.90 (m, 3H), 2.85 (dd, J = 22.2, 10.0 Hz, 2H), 2.81 − 2.71 (m, 6H), 2.61 (d, J = 12.2 Hz, 1H), 2.19 − 2.06 (m, 4H), 2.00 (dd, J = 13.9, 7.3 Hz, 1H), 1.90 (dd, J = 13.6, 6.7 Hz, 1H), 1.80 − 1.71 (m, 1H), 1.64 (s, 4H), 1.57 − 1.45 (m, 13H), 1.40 (s, 4H), 1.33 − 1.21 (m, 7H), 1.16 (s, 1H), 1.13 − 1.11 (m, 1H), 0.88 (ddd, J = 33.7, 22.8, 6.5 Hz, 18H), 0.75 (t, J = 5.9 Hz, 6H). ^{13}C NMR (600 MHz, DMSO) δ 172.56, 172.11, 172.07, 171.55, 170.91, 170.85, 170.80, 170.72, 170.69, 170.39, 162.73, 158.06, 157.84, 143.02, 137.54, 137.26, 129.17, 129.13, 129.05, 128.15, 128.00, 127.92, 126.40, 126.13, 117.91, 115.93, 60.92, 59.19, 58.54, 57.72, 57.35, 55.67, 55.27, 53.64, 53.33, 52.69, 52.23, 51.95, 51.07, 50.95, 48.07, 40.46, 38.70, 38.36, 37.55, 36.72, 35.08, 31.53, 31.34, 30.73, 30.55, 28.80, 27.99, 27.94, 26.62, 26.59, 26.00, 24.99, 24.13, 24.06, 23.07, 23.04, 22.21, 22.17, 21.59, 21.54, 19.13, 18.21, 17.87, 17.83. M/Z expected for $C_{89}H_{134}N_{16}O_{15}S^{2+}$: (Z = 1) 1698.99, (Z =2) 850.0; observed M + H 1697.9 (1%), M + H/2 849.4 (100%). Purity 90.9%.

HPLC chromatogram:

Retention time (min)	Area	% Area
49.22	1038265	9.0
58.82	10522303	90.9
63.33	10734	0.1

HO-Phe-Phe-Val-Leu-Lys-Ahx-Ahx-Lys-Leu-Val-Phe-Phe-Ala-biotin (**a13**): ^{1}H NMR (600 MHz, DMSO) δ 8.24 (d, *J* = 7.7 Hz, 1H), 8.13 (d, *J* = 7.8 Hz, 1H), 8.07 − 7.94 (m, 5H), 7.86 (dd, *J* = 23.2, 7.5 Hz, 3H), 7.77 (s, 8H), 7.69 − 7.62 (m, 1H), 7.32 − 7.12 (m, 20H), 6.46 (s, 2H), 4.69 − 4.44 (m, 5H), 4.37 − 4.26 (m, 4H), 4.22 (dd, *J* = 16.3, 9.0 Hz, 3H), 4.17 − 4.10 (m, 2H), 3.13 − 2.91 (m, 10H), 2.88 − 2.82 (m, 2H), 2.81 − 2.72 (m, 6H), 2.61 (d, *J* = 12.4 Hz, 1H), 2.15 − 2.09 (m, 3H), 2.06 (t, *J* = 7.4 Hz, 2H), 2.00 (dd, *J* = 13.5, 6.9 Hz, 1H), 1.90 (dd, *J* = 13.6, 6.8 Hz, 1H), 1.68 − 1.59 (m, 4H), 1.50 (s, 16H), 1.43 − 1.37 (m, 6H), 1.35 − 1.20 (m, 11H), 1.12 (d, *J* = 7.0 Hz, 2H), 0.93 − 0.82 (m, 18H), 0.74 (t, *J* = 5.6 Hz, 6H). ^{13}C NMR (600 MHz, DMSO) δ 172.57, 172.13, 171.99, 171.79, 171.56, 170.94, 170.86, 170.79, 170.72, 170.43, 162.77, 158.35, 158.12, 143.01, 137.55, 137.27, 129.20, 129.15, 129.06, 128.16, 128.00, 127.92, 126.42, 126.14, 117.46, 115.49, 60.95, 59.22, 57.73, 57.40, 55.29, 53.62, 53.35, 52.26, 52.00, 51.10, 50.95, 48.12, 40.47, 38.72, 38.69, 38.39, 38.33, 37.55, 37.27, 36.75, 35.35, 35.11, 34.83, 31.59, 31.37, 30.73, 30.58, 29.00, 28.79, 28.03, 27.94, 26.61, 26.12, 26.05, 25.05, 24.15, 24.08, 23.07, 23.03, 22.23, 22.17, 21.60, 21.56, 19.14, 18.20, 17.89, 17.87. M/Z expected for $C_{95}H_{145}N_{17}O_{16}S^{2+}$: (Z = 1) 1812.08, (Z =2) 906.0; observed M + H 1811.9 (1%), M + H/2 906.4 (100%). Purity 95.4%.

HPLC chromatogram:

Retention time (min)	Area	% Area
32.35	2155200	4.6
34.9	45102305	95.4

HO-Phe-Phe-Val-Leu-Lys-Ahx-Ahx-Axh-Lys-Leu-Val-Phe-Phe-Ala-biotin (**a19**): ^{1}H NMR (400 MHz, DMSO) δ 8.27 − 8.02 (m, 6H), 8.01 − 7.93 (m, 2H), 7.83 (ddd, *J* = 29.4, 12.1, 6.7 Hz, 10H), 7.62 (d,

J = 9.5 Hz, 1H), 7.35 − 7.10 (m, 20H), 6.45 (d, *J* = 15.0 Hz, 2H), 4.69 − 4.61 (m, 1H), 4.58 (dd, *J* = 13.4, 9.2 Hz, 1H), 4.51 − 4.44 (m, 1H), 4.40 − 4.29 (m, 3H), 4.29 − 4.18 (m, 4H), 4.18 − 4.05 (m, 3H), 3.15 − 2.90 (m, 12H), 2.89 − 2.81 (m, 2H), 2.75 (dd, *J* = 17.9, 10.4 Hz, 6H), 2.61 (d, *J* = 12.4 Hz, 1H), 2.18 − 2.09 (m, 4H), 2.02 (dt, *J* = 13.7, 7.7 Hz, 6H), 1.62 (dd, *J* = 13.9, 7.0 Hz, 5H), 1.58 − 1.44 (m, 19H), 1.40 (dt, *J* = 14.6, 7.2 Hz, 8H), 1.34 − 1.15 (m, 12H), 1.12 (d, *J* = 7.1 Hz, 2H), 0.88 (ddd, *J* = 19.0, 14.8, 6.4 Hz, 18H), 0.71 (dt, *J* = 23.5, 11.9 Hz, 6H). ^{13}C NMR (600 MHz, DMSO) δ 172.63, 172.11, 171.97, 171.79, 171.77, 171.55, 170.91, 170.78, 170.72, 170.69, 170.47, 162.74, 157.95, 157.74, 143.00, 137.56, 137.46, 129.18, 129.14, 128.96, 127.99, 127.91, 126.23, 126.16, 118.36, 116.34, 60.93, 59.20, 57.69, 55.28, 53.65, 53.59, 52.25, 51.09, 48.06, 40.45, 40.05, 38.67, 38.30, 37.28, 36.67, 35.35, 35.09, 3963.4.82, 31.56, 30.73, 30.55, 28.98, 28.78, 28.01, 27.93, 26.60, 26.14, 26.04, 25.06, 25.04, 24.14, 23.12, 23.05, 22.15, 21.54, 21.37, 19.15, 19.04, 18.20, 17.85. M/Z expected for $C_{101}H_{156}N_{18}O_{17}S^{2+}$: (Z = 1) 1925.16, (Z =2) 963.2; observed M + H 1924.9 (1%), M + H/2 962.9 (100%). Purity 92.7%.

HPLC chromatogram:

Retention time (min)	Area	% Area
33.12	720021	4.9
34.9	13626546	92.7
39.4	360138	2.4

HO-Phe-Phe-Val-Leu-Lys-Ahx-Ahx-Ahx-Ahx-Lys-Leu-Val-Phe-Phe-Ala-biotin (**a24**): ^{1}H NMR (600 MHz, DMSO) δ 8.39 (d, *J* = 8.5 Hz, 1H), 8.12 (d, *J* = 8.0 Hz, 1H), 8.06 − 8.00 (m, 1H), 7.96 (d, *J* = 8.9 Hz, 3H), 7.88 − 7.80 (m, 3H), 7.76 (t, *J* = 5.4 Hz, 3H), 7.66 (s, 8H), 7.33 − 7.12 (m, 20H), 6.43 (d, *J* = 20.9 Hz, 2H), 4.62 (d, *J* = 32.8 Hz, 2H), 4.48 (s, 2H), 4.33 (d, *J* = 5.6 Hz, 3H), 4.28 (d, *J* = 6.3 Hz, 1H), 4.25 − 4.18 (m, 3H), 4.14 (s, 2H), 3.11 (d, *J* = 10.3 Hz, 2H), 3.03 (dd, *J* = 12.9, 6.7 Hz, 10H), 2.96 (s, 2H), 2.85 (dd, *J* = 21.3, 9.1 Hz, 3H), 2.77 (s, 6H), 2.65 (s, 1H), 2.61 (d, *J* = 12.5 Hz, 1H), 2.58 (s, 1H), 2.13 (d, *J* = 7.5 Hz, 3H), 2.06 (t, *J* = 7.5 Hz, 6H), 2.00 (s, 1H), 1.90 (d, *J* = 6.6 Hz, 1H), 1.64 (s, 4H),

1.49 (dd, J = 14.7, 7.4 Hz, 20H), 1.40 (dd, J = 14.6, 7.3 Hz, 10H), 1.31 (s, 5H), 1.27 − 1.20 (m, 9H), 1.12 (d, J = 7.1 Hz, 2H), 0.94 − 0.82 (m, 18H), 0.78 − 0.70 (m, 6H). ^{13}C NMR (600 MHz, DMSO) δ 172.75, 172.11, 171.79, 171.76, 171.54, 170.89, 170.68, 170.55, 170.32, 162.73, 157.63, 142.98, 137.34, 129.19, 128.13, 127.91, 126.19, 63.72, 60.93, 59.12, 57.70, 55.25, 53.27, 52.19, 51.09, 40.42, 38.30, 35.36, 35.10, 31.55, 28.98, 28.79, 28.01, 26.61, 26.14, 26.06, 25.06, 24.13, 24.06, 23.05, 22.16, 19.14, 18.19, 17.92, 17.83. M/Z expected for $C_{107}H_{167}N_{19}O_{18}S^{2+}$: (Z = 1) 2038.3, (Z =2) 1019.1; observed M + H 2036.2 (1%), M + H/2 1019.5 (68%). Purity 93.1%.

HPLC chromatogram:

Retention time (min)	Area	% Area
33.3	16047611	93.1
36.4	326682	1.9
38.9	854220	5

HO-Phe-Phe-Val-Leu-Lys-Ahx-Ahx-Ahx-Ahx-Lys-Leu-Val-Phe-Phe-NH$_2$ (**a24***): M/Z expected for $C_{94}H_{148}N_{16}O_{15}S^{2+}$: (Z = 1) 1741.0, (Z =2) 871, (Z = 3) 581.0; observed M + H/2 870.5 (13%), M + H/3 580.7 (90%), M − 2H 1739.0 (12%). Purity 91.1%.

HO-Phe-Phe-Val-Leu-Lys-Ahx-Phe-Phe-Val-Leu-Lys-Ala-biotin (**p7**): M/Z expected for $C_{89}H_{134}N_{16}O_{15}S^{2+}$: (Z = 1) 1698.99, (Z =2) 850.0; observed M + H 1697.9 (1%), M + H/2 849.4 (100%).

HO-Phe-Phe-Val-Leu-Lys-Ahx-Ahx-Phe-Phe-Val-Leu-Lys-Ala-biotin (**p13**): M/Z expected for $C_{95}H_{145}N_{17}O_{16}S^{2+}$: (Z = 1) 1812.08, (Z =2) 906.0; observed M + H 1811.9 (1%), M + H/2 906.4 (100%).

HO-Phe-Phe-Val-Leu-Lys-Ahx-Ahx-Ahx-Phe-Phe-Val-Leu-Lys-Ala-biotin (**p19**): M/Z expected for

$C_{101}H_{156}N_{18}O_{17}S^{2+}$: (Z = 1) 1925.16, (Z =2) 963.2; observed M + H 1924.9 (1%), M + H/2 962.9

(100%).

HO-Phe-Phe-Val-Leu-Lys-Ahx-Ahx-Ahx-Ahx-Phe-Phe-Val-Leu-Lys-Ala-biotin (**p24**): M/Z expected

for $C_{107}H_{167}N_{19}O_{18}S^{2+}$: (Z = 1) 2038.3, (Z =2) 1019.1; observed M + H 2036.2 (1%), M + H/2 1019.5

(68%).

HO-Phe-Phe-Val-Leu-Lys-Ahx-Pro-Ahx-Lys-Leu-Val-Phe-Phe-Ala-biotin (**aPro1**): M/Z expected for

$C_{100}H_{152}N_{18}O_{17}S^{2+}$: (Z = 1) 1910, (Z =2) 850.0; observed M + H 1697.9 (1%), M + H/2 849.4 (100%).

HO-Phe-Phe-Val-Leu-Lys-Ahx-Pro-Ahx-Pro-Ahx-Lys-Leu-Val-Phe-Phe-Ala-biotin   (**aPro2**):   M/Z

expected for $C_{111}H_{170}N_{20}O_{19}S^{2+}$: (Z = 1) 2120, (Z =2) 850.0; observed M + H 1697.9 (1%), M + H/2

849.4 (100%).

HO-Phe-Phe-Val-Leu-Lys-Ahx-Pro-Ahx-Phe-Phe-Val-Leu-Lys-Ala-biotin (**pPro1**): M/Z expected for

$C_{100}H_{152}N_{18}O_{17}S^{2+}$: (Z = 1) 1910, (Z =2) 850.0; observed M + H 1697.9 (1%), M + H/2 849.4 (100%).

HO-Phe-Phe-Val-Leu-Lys-Ahx-Pro-Ahx-Pro-Ahx-Phe-Phe-Val-Leu-Lys-Ala-biotin   (**pPro2**):   M/Z

expected for $C_{111}H_{170}N_{20}O_{19}S^{2+}$: (Z = 1) 2120, (Z =2) 850.0; observed M + H 1697.9 (1%), M + H/2

849.4 (100%).

HO-Lys-Leu-Val-Phe-Phe-NH$_2$ (**KLVFF**): M/Z expected for $C_{35}H_{22}N_6O_6$: (Z = 1) 652.8; observed M +

H 653.4 (100%). Purity 98.4%.

HO-Lys-Leu-Val-Phe-Phe-Lys-Lys-NH$_2$ (**A**) M/Z expected for C$_{47}$H$_{76}$N$_{10}$O$_8$: (Z = 1) 909.2, (Z = 2) 454.6; observed M 909.6 (1%), M + H/2 455.3 (70%), M − H 908.6 (10%). Purity 98.2%.

HO-Lys-Leu-Val-Phe-Phe-Lys-Lys-Lys-Lys-NH$_2$ (**B**): M/Z expected for C$_{59}$H$_{100}$N$_{14}$O$_{10}$: (Z = 1) 1165.5, (Z = 2) 582.8, (Z = 3) 388.5; observed M + H/2 583.4 (40%), M + H/3 389.6 (28%), M − 2H 1163.8 (5%). Purity 95%.

HO-Phe-Phe-Val-Leu-Lys-Ahx-Ahx-Ahx-Ahx-Lys-Leu-Val-Phe-Phe-Lys-Lys-Lys-Lys-NH$_2$ (**C**) M/Z expected for C$_{118}$H$_{200}$N$_{24}$O$_{19}$: (Z = 1) 2259, (Z = 2) 1129.5, (Z = 3) 753, (Z = 4) 564.8, (Z = 5) 451.8; observed M +H/2 1129.5 (1%), M + H/3 752.2 (10%), M + H/4 564.0 (90%), M + H/5 451.6 90%), M − 8H 2251.2 (1%). Purity 95.3%.

HO-Lys-Leu-Val-Phe-Phe-Ala-NH$_2$ (**D**): M/Z expected for C$_{38}$H$_{57}$N$_7$O$_7$: (Z = 1) 723.9; observed M 724.2 (100%).

HO-Lys-Leu-Val-Phe-Phe-Ala-Glu-NH$_2$ (**E**): M/Z expected for C$_{43}$H$_{64}$N$_8$O$_{10}$: (Z = 1) 853.0; observed M 853.1 (80%), M + H 854.1 (20%), M − 2H 851.3 (100%).

HO-Lys-Leu-Val-Phe-Phe-Ala-Glu-Asp-NH$_2$ (**F**): M/Z expected for C$_{47}$H$_{69}$N$_9$O$_{13}$: (Z = 1) 968.1; observed M 968.1 (30%), M + H 969.1 (10%), M − 2H 966.4 (75%).

HO-Gln-Lys-Leu-Val-Phe-Phe-NH$_2$ (**G**): M/Z expected for C$_{40}$H$_{60}$N$_8$O$_8$: (Z = 1) 781.0; observed M 781.2 (90%), M + H 782.2 (20%).

HO-His-Gln-Lys-Leu-Val-Phe-Phe-NH$_2$ (**H**): M/Z expected for C$_{46}$H$_{67}$N$_{11}$O$_9$: (Z = 1) 918.1, (Z =2) 459.1; observed M 918.3 (85%), M + H 919.3 (30%), M + H/2 459.7 (100%).

HO-His-His-Gln-Leu-Val-Phe-Phe-NH$_2$ (**I**): M/Z expected for C$_{52}$H$_{74}$N$_{14}$O$_{10}$: (Z = 1) 1055.2, (Z =2) 527.6; observed M 1055.3 (40%), M + H 1056.3 (13%), M + H/2 528.2 (100%).

HO-Leu-Pro-Phe-Phe-Asp-NH$_2$ (**J**): M/Z expected for C$_{33}$H$_{43}$N$_5$O$_8$: (Z = 1) 637.7; observed M + H 637.9 (100%).

HO-Arg-Gly-Lys-Leu-Val-Phe-Phe-Gly-Arg-NH$_2$ (**K**): M/Z expected for C$_{51}$H$_{82}$N$_{16}$O$_{10}$: (Z = 1) 1079.3, (Z =2) 539.7; observed M 1079.3 (1%), M + H 1080.3 (1%), M + H/2 540.2 (100%), M+H/3 360.5 (12%).

4.4.7 Surface Plasmon Resonance (SPR)

LMW 25 μM Aβ (1-42) was immobilized on an activated CM5 chip as described in Chapter 2. Immobilization resulted in at least 350 response units, and a lane capped with 250 mM ethanolamine served as a negative control for binding. Dilutions of **a24*** (6-200 μM) were prepared in HEPES-buffer saline (HBS) from a 5 mM stock (4% DMSO) immediately prior to being injected over the chip surface. **KLVFF**, **A**, and **B** (100 mM stocks) were prepared and injected similarly (0.003-4 mM), as was peptide **C** (3-200 μM). Data was fit thermodynamically as described in Chapter 2 to obtain an apparent K$_d$. For peptides **D** through **K**, 400 μM samples were prepared in HBS from 10 mM stocks (4% DMSO). The ΔRU of association was taken 5 seconds prior to the end of the injection, and non-specific binding to the ethanolamine lane was

subtracted. Association values from two separate injects were averaged, and the error is expressed as the standard deviation.

4.4.8 Enzyme-linked immunosorbent assay (ELISA)

In order to determine the binding affinity of **biotin**, **KLVFF-biotin**, and **a24**, a competition ELISA approach was used. Reacti-bind streptavidin-coated black 96-well plates (Pierce, Rockford, IL) were first rinsed twice with 200 μL wash buffer (tris-buffered saline, 0.1% BSA, 0.05% Tween-20), followed by immobilization of **a24** (100 μL/well, 1 μM) for one hour. During this incubation, Aβ (1-42) was prepared as described in 4.4.2 and diluted to 5 μM in PBS. Dilutions of **biotin**, **KLVFF-biotin**, and **a24** (5-300 μM) were then prepared. Immediately prior to plating, 50 μL of 5 μM Aβ (1-42) was added to 100 μL ligand, and the total mixture (150 μL) was mixed gently by pipetting in each well. The plate was incubated for one hour, after which 100 μL 6E10 (1:1000) was added for one hour, followed by another hour incubation with goat anti-mouse-HRP (1:10,000). All reagents were suspended in wash buffer except for Aβ. Incubations were performed on a rocker at room temperature, and between each step all wells were washed (2 X 5 minutes) with 200 μL wash buffer. Bound Aβ was quantified using the 3,3',5,5''-tetramethylbenzidine (TMB) substrate kit (Cell Signaling, Boston, MA) according to the manufacturers' protocols, and all samples were performed in triplicate. Error represents the standard deviation between the triplicates. Immediately prior to development, the solution in each well was transferred to a clear, 96-well plate, after which the absorbance was read at 450 nm. The addition of Aβ in the absence of competing ligand was treated as the total bound Aβ, and the percent bound in the presence of competitor was calculated. The resulting sigmoidal dose-response curves were fit by Graphpad prism software using non-linear regression curve fitting.

4.4.9 Thioflavin T fluorescence

To determine the extent of aggregation of the KLVFF derivatives **D** through **K**, the peptides were diluted to 200 μM in PBS from a 10 mM DMSO stock. ThT was prepared, administered, and developed according to the protocols in Chapter 3.

4.4.10 Histochemical (CR, aPro2) and fluorescence (ThS) tissue staining

APPswe/PS1ΔE9 double transgenic mice were obtained from Jackson Laboratories. Mice were sacrificed at 13 months of age, and brains were flash-frozen in isopentane, after which 16 μM sections were mounted on glass slides by Cryostat. Slides were frozen at -80 °C until immediately prior to staining. Human brain tissue slices were chemically fixed in paraffin, and all sections were de-paraffinized and hydradated prior to staining using the following protocol: 2 X 5 minutes xylenes, 2 X 3 minutes 100% ethanol, 3 minutes 95% ethanol, 3 minutes 70% ethanol, and 2 X 5 minutes water. Frozen mouse tissue sections were used immediately after equilibrating to room temperature. All slides were then stained with the nuclear-specific dye hematoxylin (Electron Microscopy Sciences, Hatfield, PA) for 1 minute, followed a 2 minute water wash and a water rinse. Bielschowsky silver staining was performed by Dr. Andrew Lieberman. ABC Elite and Immpact DAB kits were purchased from Vector Labs (Burlingame, CA). All slides were visualized using a Nikon Eclipse 80i microscope at 10, 60, or 100X or an Olympus BX-51 microscope under brightfield or polarized light at 20 or 40X.

Congo red: Solution A = 170 mM NaCl in 80% aqueous ethanol, 1% NaOH; Solution B = Solution A + 3 mM Congo Red. All solutions are filtered, and NaOH is added immediately prior to use. For human tissue, slides were hydrated and stained with hematoxylin, followed by a 20 minute

incubation in solution A. Slides were immediately transferred to solution B for 20 additional minutes, rinsed briefly in 2 exchanges of 100% ethanol, cleared 3 times in xylenes and mounted using Permount. The same protocol was used for mouse tissue except that slides were only stained with solution B (3 minutes).

Thioflavin S: For both human and mouse tissue, following hydration and hematoxylin staining, slides were incubated in filtered, 0.5% (w/v) thioflavin S in 1:1 ethanol:water for 8 minutes and protected from light. Slides were subsequently washed using the following protocol: 1 minute 80% ethanol, 2 minutes 80% ethanol, 1 minute 95% ethanol, and 10 seconds 100% ethanol. Slides were dehydrated using an aqueous ethanol gradient, cleared twice in xylenes, and mounted using Permount. Images were visualized under a FITC filter (excitation 460-500 nm).

aPro2 staining: Previously published methods were used for staining mouse tissue with biotinylated **aPro2** [52]. Briefly, after hematoxylin staining, sections were washed in PBS (2 X 10 minutes) and PBS-T (0.4% Triton-X 100; 1 X 10 minutes, 1 X 30 minutes, 1 X 10 minutes). Slides were then incubated overnight in 2.5 μM **aPro2** in 12 mL PBS-T, washed with PBS-T (4 X 15 minutes), and incubated in ABC Elite reagent (according to the manufacturer's protocols) for one hour. Following washes with PBS-T (2 X 15 minutes) and TI buffer (0.05M tris, 0.05 M imidazole, pH 7.4; 2 X 15 minutes), the signal was amplified using 20 μM biotinylated tyramine and 30% hydrogen peroxide in TI buffer (1:10,000) for 15 minutes. Slides were washed again with TI buffer (2 X 15 minutes) and PBS-T (2 X 15 minutes), incubated a second time in ABC Elite reagent for one hour, and washed a final time in PBS-T (2 X 15 minutes) and TI buffer (1 X 15 minutes). HRP was visualized using the Immpact DAB kit (5 minutes) according to the

manufacturer's protocol, and slides were dehydrated to ethanol and cleared in xylenes. All steps

were performed at room temperature on an orbital shaker (35 rpm).

KLVFF-biotin

a7

176

a13

a19

a24

KLVFF-biotin

a7

a19

a24

17.83
17.92
18.19
19.14
22.16
23.05
24.06
24.13
25.06
26.06
26.14
26.61
28.01
28.79
28.98
31.55
35.10
35.36
38.30
40.42
51.09
52.19
53.27
55.25
57.70
59.12
60.93
63.72
126.19
127.91
128.13
129.19
137.34
142.98
157.63
162.73
170.32
170.55
170.68
170.89
171.54
171.76
171.79
172.11
172.75

f1 (ppm)
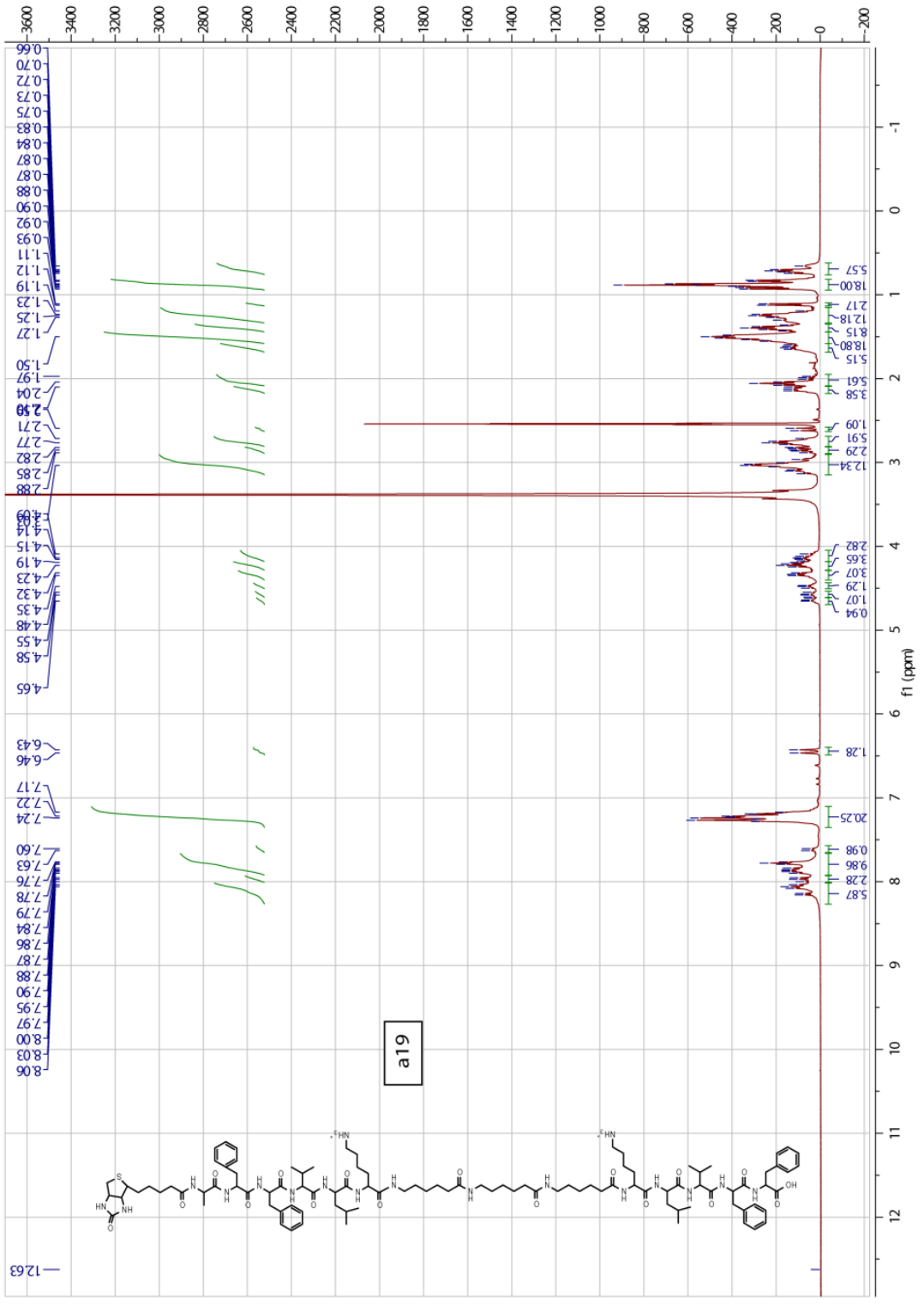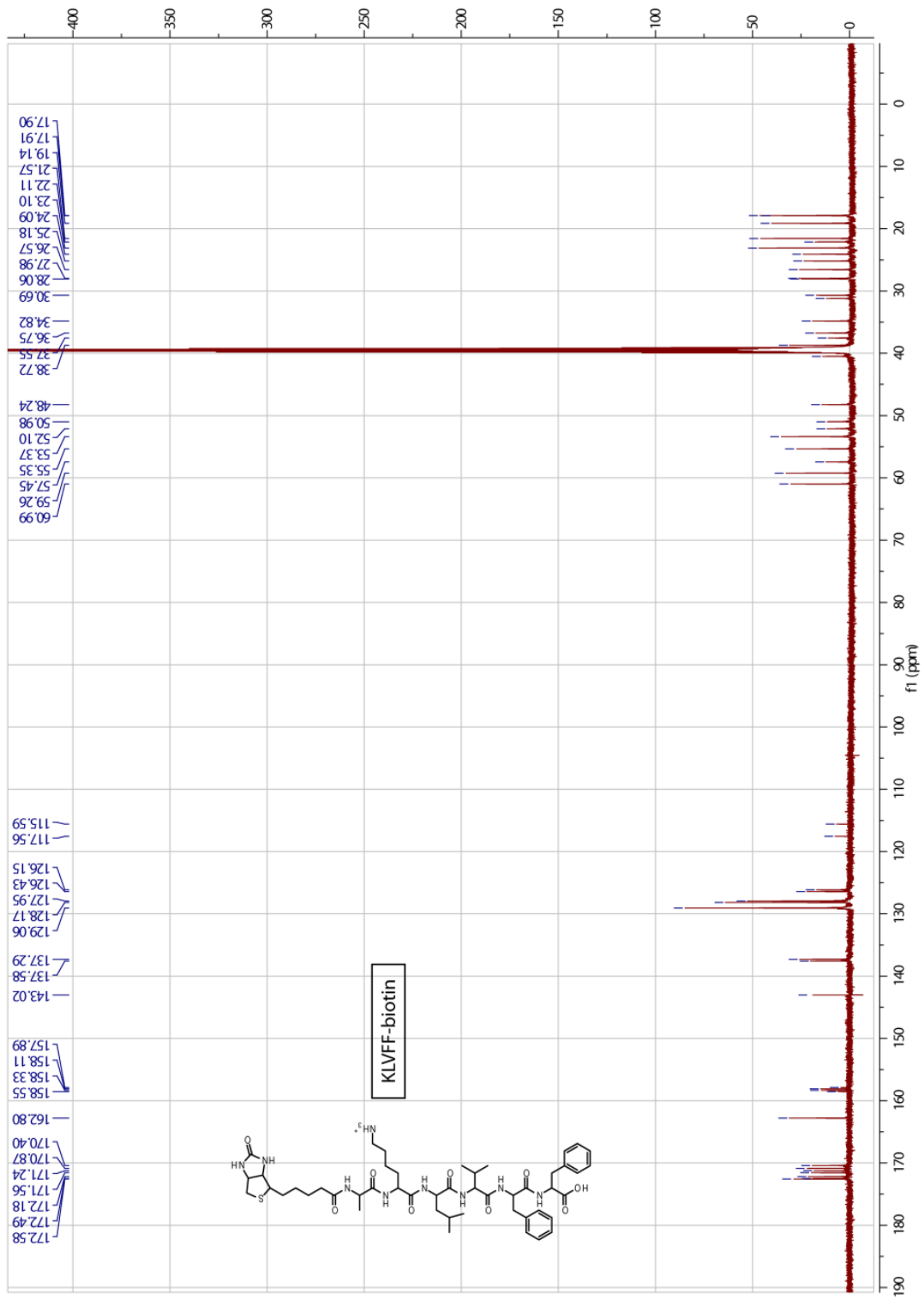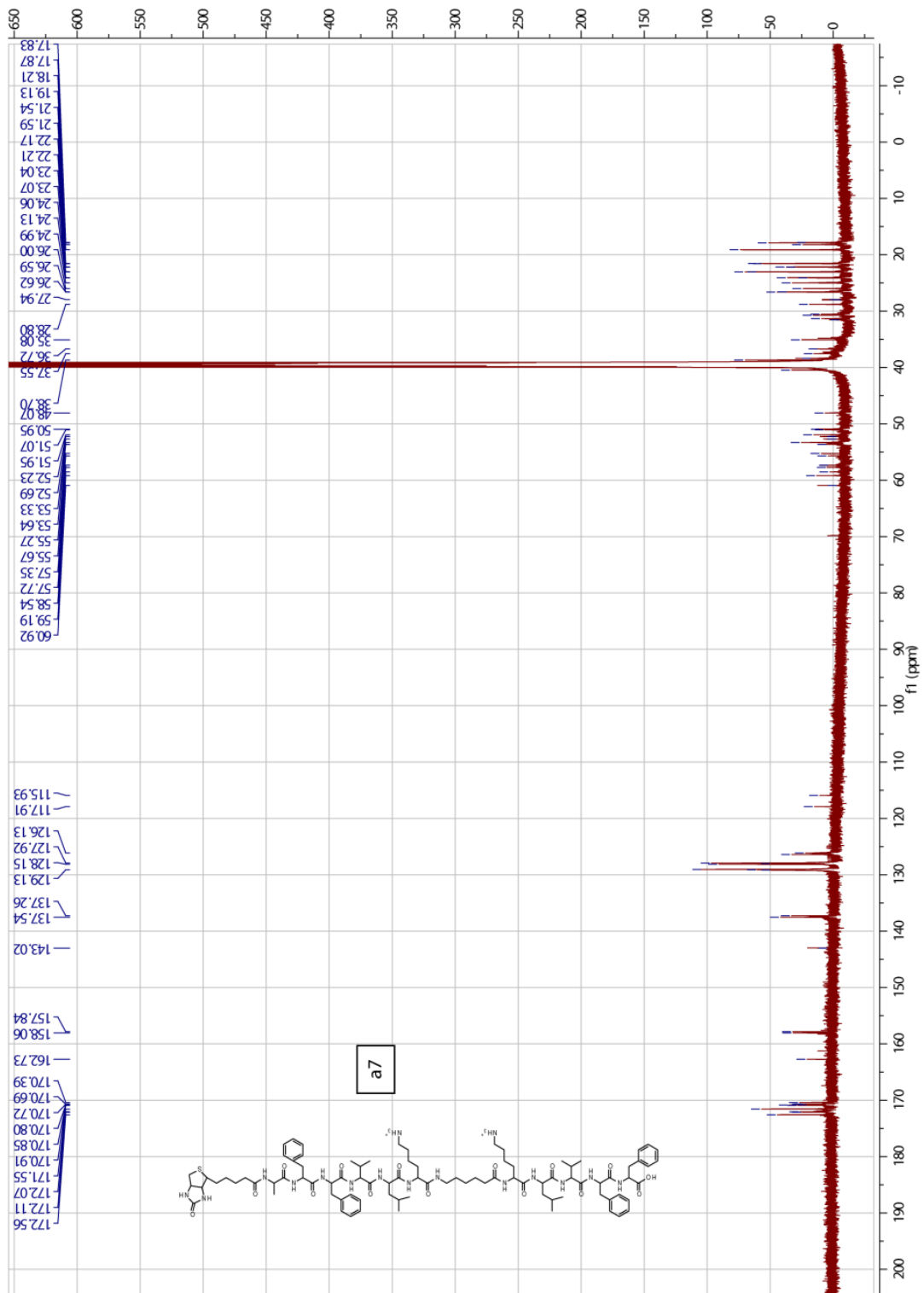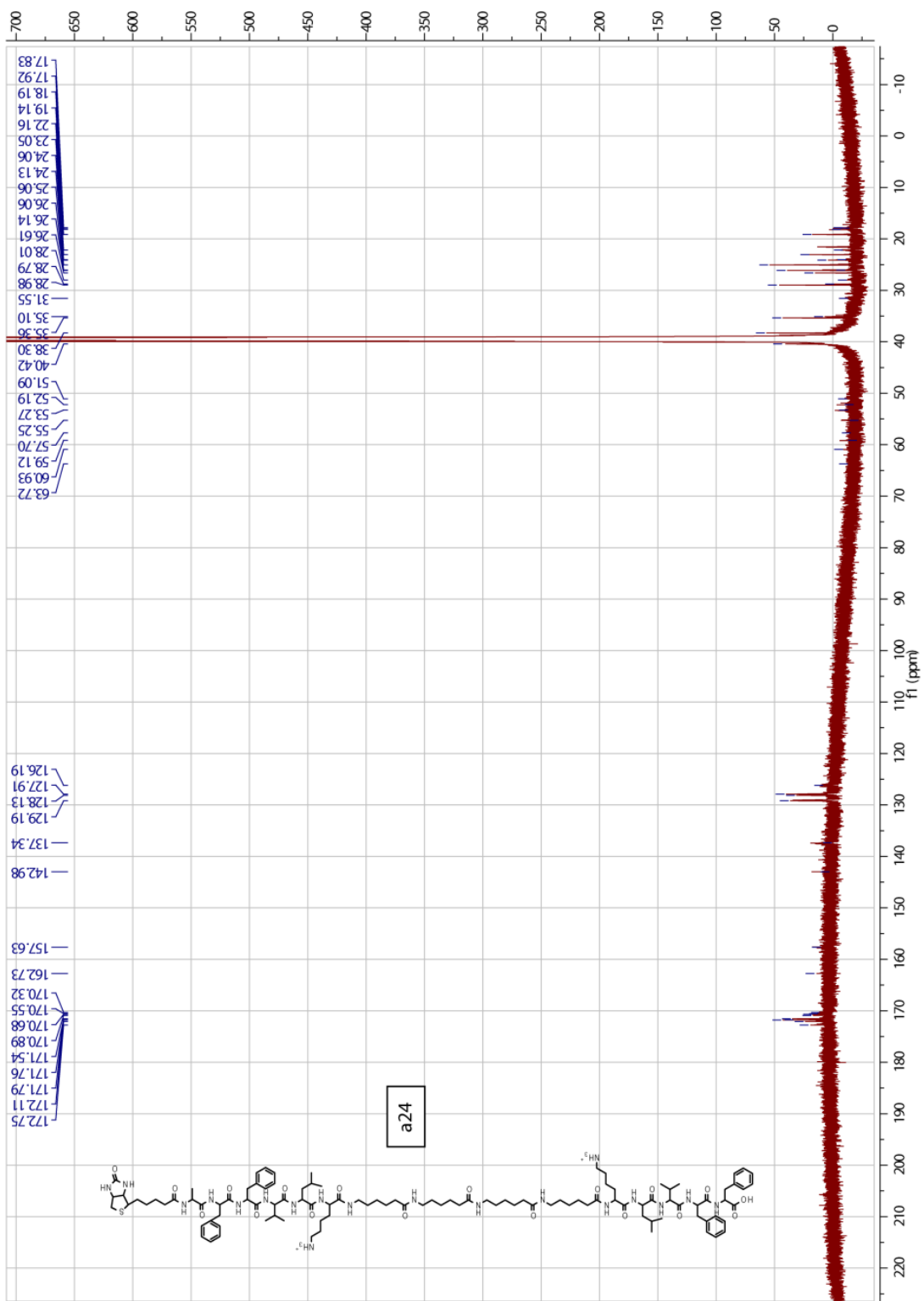
Notes

This work has been partially published as "Chemical probes That Selectively Recognize the Earliest Aβ Oligomers in Complex Mixtures." **2010** Journal of the American Chemical Society. *132*; 17655-57.

4.6 References

[1]   Hung LW, Ciccotosto GD, Giannakis E, Tew DJ, Perez K, Masters CL, et al. Amyloid-beta peptide (Abeta) neurotoxicity is modulated by the rate of peptide aggregation: Abeta dimers and trimers correlate with neurotoxicity. J Neurosci. 2008 Nov 12;28(46):11950-8.
[2]   Klyubin I, Betts V, Welzel AT, Blennow K, Zetterberg H, Wallin A, et al. Amyloid beta protein dimer-containing human CSF disrupts synaptic plasticity: prevention by systemic passive immunization. J Neurosci. 2008 Apr 16;28(16):4231-7.
[3]   Leon WC, Canneva F, Partridge V, Allard S, Ferretti MT, DeWilde A, et al. A novel transgenic rat model with a full Alzheimer's-like amyloid pathology displays pre-plaque intracellular amyloid-beta-associated cognitive impairment. J Alzheimers Dis. 2010;20(1):113-26.
[4]   Ono K, Condron MM, Teplow DB. Structure-neurotoxicity relationships of amyloid beta-protein oligomers. Proceedings of the National Academy of Sciences of the United States of America. 2009 Sep 1;106(35):14745-50.
[5]   Shankar GM, Bloodgood BL, Townsend M, Walsh DM, Selkoe DJ, Sabatini BL. Natural oligomers of the Alzheimer amyloid-beta protein induce reversible synapse loss by modulating an NMDA-type glutamate receptor-dependent signaling pathway. J Neurosci. 2007 Mar 14;27(11):2866-75.
[6]   Shankar GM, Li S, Mehta TH, Garcia-Munoz A, Shepardson NE, Smith I, et al. Amyloid-beta protein dimers isolated directly from Alzheimer's brains impair synaptic plasticity and memory. Nature medicine. 2008 Aug;14(8):837-42.

[7]   Townsend M, Shankar GM, Mehta T, Walsh DM, Selkoe DJ. Effects of secreted oligomers of amyloid beta-protein on hippocampal synaptic plasticity: a potent role for trimers. The Journal of physiology. 2006 Apr 15;572(Pt 2):477-92.

[8]   O'Nuallain B, Freir DB, Nicoll AJ, Risse E, Ferguson N, Herron CE, et al. Amyloid beta-protein dimers rapidly form stable synaptotoxic protofibrils. J Neurosci. 2010 Oct 27;30(43):14411-9.

[9]   Aguzzi A, O'Connor T. Protein aggregation diseases: pathogenicity and therapeutic perspectives. Nature reviews. 2010 Mar;9(3):237-48.

[10]   Roychaudhuri R, Yang M, Hoshi MM, Teplow DB. Amyloid beta-protein assembly and Alzheimer disease. The Journal of biological chemistry. 2009 Feb 20;284(8):4749-53.

[11]   Esler WP, Stimson ER, Ghilardi JR, Lu YA, Felix AM, Vinters HV, et al. Point substitution in the central hydrophobic cluster of a human beta-amyloid congener disrupts peptide folding and abolishes plaque competence. Biochemistry. 1996 Nov 5;35(44):13914-21.

[12]   Ahmed M, Davis J, Aucoin D, Sato T, Ahuja S, Aimoto S, et al. Structural conversion of neurotoxic amyloid-beta(1-42) oligomers to fibrils. Nature structural & molecular biology. 2010 May;17(5):561-7.

[13]   Bieschke J, Siegel SJ, Fu Y, Kelly JW. Alzheimer's Abeta peptides containing an isostructural backbone mutation afford distinct aggregate morphologies but analogous cytotoxicity. Evidence for a common low-abundance toxic structure(s)? Biochemistry. 2008 Jan 8;47(1):50-9.

[14]   Chini MG, Scrima M, D'Ursi AM, Bifulco G. Fibril aggregation inhibitory activity of the beta-sheet breaker peptides: a molecular docking approach. J Pept Sci. 2009 Mar;15(3):229-34.

[15]   Hilbich C, Kisters-Woike B, Reed J, Masters CL, Beyreuther K. Substitutions of hydrophobic amino acids reduce the amyloidogenicity of Alzheimer's disease beta A4 peptides. Journal of molecular biology. 1992 Nov 20;228(2):460-73.

[16]   Tjernberg LO, Naslund J, Lindqvist F, Johansson J, Karlstrom AR, Thyberg J, et al. Arrest of beta-amyloid fibril formation by a pentapeptide ligand. The Journal of biological chemistry. 1996 Apr 12;271(15):8545-8.

[17]   Wood SJ, Wetzel R, Martin JD, Hurle MR. Prolines and amyloidogenicity in fragments of the Alzheimer's peptide beta/A4. Biochemistry. 1995 Jan 24;34(3):724-30.

[18]   Yu L, Edalji R, Harlan JE, Holzman TF, Lopez AP, Labkovsky B, et al. Structural characterization of a soluble amyloid beta-peptide oligomer. Biochemistry. 2009 Mar 10;48(9):1870-7.

[19]   Watanabe K, Segawa T, Nakamura K, Kodaka M, Konakahara T, Okuno H. Identification of the molecular interaction site of amyloid beta peptide by using a fluorescence assay. J Pept Res. 2001 Oct;58(4):342-6.

[20]   Qi W, Zhang A, Patel D, Lee S, Harrington JL, Zhao L, et al. Simultaneous monitoring of peptide aggregate distributions, structure, and kinetics using amide hydrogen exchange: application to Abeta(1-40) fibrillogenesis. Biotechnology and bioengineering. 2008 Aug 15;100(6):1214-27.

[21]   Zhang A, Qi W, Good TA, Fernandez EJ. Structural differences between Abeta(1-40) intermediate oligomers and fibrils elucidated by proteolytic fragmentation and hydrogen/deuterium exchange. Biophysical journal. 2009 Feb;96(3):1091-104.

[22]   Antzutkin ON, Balbach JJ, Leapman RD, Rizzo NW, Reed J, Tycko R. Multiple quantum solid-state NMR indicates a parallel, not antiparallel, organization of beta-sheets in Alzheimer's beta-amyloid fibrils. Proceedings of the National Academy of Sciences of the United States of America. 2000 Nov 21;97(24):13045-50.

[23]   Costa PR, Kocisko DA, Sun BQ, Lansbury PT, Griffin RG. Determination of Peptide Amide Configuration in a Model Amyloid Fibril by Solid-State NMR. Journal of the American Chemical Society. 1997;119:10487-93.

[24]   Hetenyi C, Kortvelyesi T, Penke B. Mapping of possible binding sequences of two beta-sheet breaker peptides on beta amyloid peptide of Alzheimer's disease. Bioorganic & medicinal chemistry. 2002 May;10(5):1587-93.

[25]   Horn AH, Sticht H. Amyloid-beta42 oligomer structures from fibrils: a systematic molecular dynamics study. The journal of physical chemistry. 2010 Feb 18;114(6):2219-26.

[26]   Hwang W, Zhang S, Kamm RD, Karplus M. Kinetic control of dimer structure formation in amyloid fibrillogenesis. Proceedings of the National Academy of Sciences of the United States of America. 2004 Aug 31;101(35):12916-21.

[27]   Luhrs T, Ritter C, Adrian M, Riek-Loher D, Bohrmann B, Dobeli H, et al. 3D structure of Alzheimer's amyloid-beta(1-42) fibrils. Proceedings of the National Academy of Sciences of the United States of America. 2005 Nov 29;102(48):17342-7.

[28]   Wallace JA, Shen JK. Probing the strand orientation and registry alignment in the propagation of amyloid fibrils. Biochemistry. 2010 Jun 29;49(25):5290-8.

[29]   Cairo CW, Strzelec A, Murphy RM, Kiessling LL. Affinity-based inhibition of beta-amyloid toxicity. Biochemistry. 2002 Jul 9;41(27):8620-9.

[30]   Chafekar SM, Malda H, Merkx M, Meijer EW, Viertl D, Lashuel HA, et al. Branched KLVFF tetramers strongly potentiate inhibition of beta-amyloid aggregation. Chembiochem. 2007 Oct 15;8(15):1857-64.

[31]   Lowe TL, Strzelec A, Kiessling LL, Murphy RM. Structure-function relationships for inhibitors of beta-amyloid toxicity containing the recognition sequence KLVFF. Biochemistry. 2001 Jul 3;40(26):7882-9.

[32]   Watanabe K, Nakamura K, Akikusa S, Okada T, Kodaka M, Konakahara T, et al. Inhibitors of fibril formation and cytotoxicity of beta-amyloid peptide composed of KLVFF recognition element and flexible hydrophilic disrupting element. Biochemical and biophysical research communications. 2002 Jan 11;290(1):121-4.

[33]   Zhang G, Leibowitz MJ, Sinko PJ, Stein S. Multiple-peptide conjugates for binding beta-amyloid plaques of Alzheimer's disease. Bioconjugate chemistry. 2003 Jan-Feb;14(1):86-92.

[34]   Kiessling LL, Gestwicki JE, Strong LE. Synthetic multivalent ligands as probes of signal transduction. Angewandte Chemie (International ed. 2006 Apr 3;45(15):2348-68.

[35]   Byeon SR, Jin YJ, Lim SJ, Lee JH, Yoo KH, Shin KJ, et al. Ferulic acid and benzothiazole dimer derivatives with high binding affinity to beta-amyloid fibrils. Bioorganic & medicinal chemistry letters. 2007 Jul 15;17(14):4022-5.

[36]   Dolphin GT, Chierici S, Ouberai M, Dumy P, Garcia J. A multimeric quinacrine conjugate as a potential inhibitor of Alzheimer's beta-amyloid fibril formation. Chembiochem. 2008 Apr 14;9(6):952-63.

[37]   Kim Y, Lee JH, Ryu J, Kim DJ. Multivalent & multifunctional ligands to beta-amyloid. Current pharmaceutical design. 2009;15(6):637-58.

[38]   Suemoto T, Okamura N, Shiomitsu T, Suzuki M, Shimadzu H, Akatsu H, et al. In vivo labeling of amyloid with BF-108. Neuroscience research. 2004 Jan;48(1):65-74.

[39]   Qin L, Vastl J, Gao J. Highly sensitive amyloid detection enabled by thioflavin T dimers. Molecular bioSystems. 2010 Oct 1;6(10):1791-5.

[40]   Reinke AA, Gestwicki JE. Structure-activity relationships of amyloid beta-aggregation inhibitors based on curcumin: influence of linker length and flexibility. Chemical biology & drug design. 2007 Sep;70(3):206-15.

[41]   Thomas LL, Christakis TJ, Jorgensen WL. Conformation of alkanes in the gas phase and pure liquids. The journal of physical chemistry. 2006 Oct 26;110(42):21198-204.

[42]   Bitan G, Teplow DB. Rapid photochemical cross-linking--a new tool for studies of metastable, amyloidogenic protein assemblies. Accounts of chemical research. 2004 Jun;37(6):357-64.

[43]   Marinec PS, Evans CG, Gibbons GS, Tarnowski MA, Overbeek DL, Gestwicki JE. Synthesis of orthogonally reactive FK506 derivatives via olefin cross metathesis. Bioorganic & medicinal chemistry. 2009 Aug 15;17(16):5763-8.

[44]   Cerf E, Sarroukh R, Tamamizu-Kato S, Breydo L, Derclaye S, Dufrene YF, et al. Antiparallel beta-sheet: a signature structure of the oligomeric amyloid beta-peptide. The Biochemical journal. 2009 Aug 1;421(3):415-23.

[45]   Bateman RJ, Wen G, Morris JC, Holtzman DM. Fluctuations of CSF amyloid-beta levels: implications for a diagnostic and therapeutic biomarker. Neurology. 2007 Feb 27;68(9):666-9.

[46]   Bibl M, Mollenhauer B, Esselmann H, Lewczuk P, Klafki HW, Sparbier K, et al. CSF amyloid-beta-peptides in Alzheimer's disease, dementia with Lewy bodies and Parkinson's disease dementia. Brain. 2006 May;129(Pt 5):1177-87.

[47]   Sunderland T, Linker G, Mirza N, Putnam KT, Friedman DL, Kimmel LH, et al. Decreased beta-amyloid1-42 and increased tau levels in cerebrospinal fluid of patients with Alzheimer disease. Jama. 2003 Apr 23-30;289(16):2094-103.

[48]   Matharu B, El-Agnaf O, Razvi A, Austen BM. Development of retro-inverso peptides as anti-aggregation drugs for beta-amyloid in Alzheimer's disease. Peptides. 2010 Oct;31(10):1866-72.

[49]   Soto C, Sigurdsson EM, Morelli L, Kumar RA, Castano EM, Frangione B. Beta-sheet breaker peptides inhibit fibrillogenesis in a rat brain model of amyloidosis: implications for Alzheimer's therapy. Nature medicine. 1998 Jul;4(7):822-6.

[50]   Taylor M, Moore S, Mayes J, Parkin E, Beeg M, Canovi M, et al. Development of a proteolytically stable retro-inverso peptide inhibitor of beta-amyloid oligomerization as a potential novel treatment for Alzheimer's disease. Biochemistry. 2010 Apr 20;49(15):3261-72.

[51]   Tjernberg LO, Callaway DJ, Tjernberg A, Hahne S, Lilliehook C, Terenius L, et al. A molecular model of Alzheimer amyloid beta-peptide fibril formation. The Journal of biological chemistry. 1999 Apr 30;274(18):12619-25.

[52]   Heng MY, Duong DK, Albin RL, Tallaksen-Greene SJ, Hunter JM, Lesort MJ, et al. Early autophagic response in a novel knock-in model of Huntington disease. Human molecular genetics. 2010 Oct 1;19(19):3702-20.

[53]   Osmand AP, Berthelier V, Wetzel R. Imaging polyglutamine deposits in brain tissue. Methods in enzymology. 2006;412:106-22.

[54]   Jankowsky JL, Slunt HH, Ratovitski T, Jenkins NA, Copeland NG, Borchelt DR. Co-expression of multiple transgenes in mouse CNS: a comparison of strategies. Biomolecular engineering. 2001 Jun;17(6):157-65.

[55]   Saluja I, Paulson H, Gupta A, Turner RS. X11alpha haploinsufficiency enhances Abeta amyloid deposition in Alzheimer's disease transgenic mice. Neurobiology of disease. 2009 Oct;36(1):162-8.

[56]   Filali M, Lalonde R. Age-related cognitive decline and nesting behavior in an APPswe/PS1 bigenic model of Alzheimer's disease. Brain research. 2009 Oct 6;1292:93-9.

[57]   Case DA, Darden TA, Cheatham III TE, Simmerling CL, Wang J, Duke RE, et al. AMBER 10. University of California, San Francisco 2008.

[58]   Berman HM, Westbrook J, Feng Z, Gilliland G, Bhat TN, Weissig H, et al. The Protein Data Bank. Nucleic acids research. 2000 Jan 1;28(1):235-42.

[59]   MOE: Molecular Operating Environment (v2008). Chemical Computing Group, Inc. 1255 University St. Suite 1600, Montreal, Quebec, Canada H3B 3X3 2008.

[60]   Jakalian A, Bush BL, Jack DB, Bayly CI. Fast, efficient generation of high-quality atomic charges. AM1-BCC model: I. Method. J Comput Chem. 2000;21:132-46.

[61]   DeLano WL. The Pymol Molecular Graphics System. Palo Alto, CA: DeLano Scientific 2002.

[62]   Wang JM, Wang W, Kollman PA, Case CA. Automatic atom type and bond type perception in molecular mechanical calculations J Mol Graph Model. 2006(25):247-60.

[63]   Hornak V, Abel R, Okur A, Strockbine B, Roitberg A, Simmerling C. Comparison of multiple Amber force fields and development of improved protein backbone parameters. Proteins. 2006 Nov 15;65(3):712-25.

[64]   Ryckaert JP, Ciccotti G, Berendsen HJC. Numerical-integration of Cartesian equations of motion of a system with constraints - Molecular-dynamics of N-Alkenes. J Comp Phys. 1977;23:327-41.

[65]   Bacsa B, Kappe CO. Rapid solid-phase synthesis of a calmodulin-binding peptide using controlled microwave irradiation. Nature protocols. 2007;2(9):2222-7.

[66]   Wisen S, Androsavich J, Evans CG, Chang L, Gestwicki JE. Chemical modulators of heat shock protein 70 (Hsp70) by sequential, microwave-accelerated reactions on solid phase. Bioorganic & medicinal chemistry letters. 2008 Jan 1;18(1):60-5.

Chapter 5

Conclusions and future directions: multiple generations of amyloid probes

5.1 Abstract

The data presented in the previous chapters has revealed that small molecules are capable of distinguishing between distinct conformations of amyloids. If the well-known amyloid ligands, thioflavin T and Congo Red, may be classified as first-generation probes, then, together, the ligands described in the previous Chapters begin to define the second generation of amyloid probes. However, as discussed in Chapters 3 and 4, these probes remain somewhat limited in their applications. For example, TROL fluorescence is still sensitive to non-amyloidogenic proteins, and bivalent KLVFF derivatives bind high-molecular weight proteins in human CSF and are not sufficiently sensitive to detect native Aβ levels. This Chapter discusses the potential future directions that may improve these probes. In addition, we also outline how rational design can be used to assemble peptide-based probes that bind other (*e.g* non-Aβ) amyloids. Collectively, we propose that third-generation ligands, with improved affinity and selectivity for amyloids, can be generated using some of the principles described here.

5.2 Conclusions: Second generation amyloid probes selectively detect Aβ conformations

The last decade of research on amyloid-β has yielded a plethora of evidence for distinct quaternary structures. The overall aim of this thesis was to generate chemical probes that could distinguish between these structures. As described in Chapter 1, first-generation probes, such as ThT, curcumin and Congo Red, only differentiate between monomeric and aggregated Aβ (Figure 5.1). In Chapter 2, we explored the binding site for curcumin using a series of synthetic analogs. One of our goals was to reveal features of the binding site as a step towards building more selective derivatives. We found that the most striking design feature was the length and rigidity of these molecules. However, we also found that none of these ligands were able to distinguish between distinct forms of Aβ, suggesting that curcumin is not a promising scaffold for development of conformation-specific probes.

Thus, to develop an alternative approach towards second-generation Aβ probes, we turned to a non-biased screening method. In Chapter 3, we described a fluorescence-based screen in which we examined a diverse collection of amyloid ligands. We found that the fluorescence of several indole-based compounds was altered in the presence of pre-fibrils, but was unchanged upon fibril addition. In order to optimize this effect for assay development, we performed a secondary screen of a focused collection of indoles. Using a lead compound from this screen, tryptophanol (TROL), we developed an inexpensive spectroscopic assay for monitoring pre-fibril levels. Because we based the conditions for this assay on previously well-established methods, the TROL assay can be employed side-by-side with ThT to follow the self-assembly process. Further, we demonstrated that TROL can be used to observe pre-fibril depletion in solutions of several amyloidogenic proteins. Prior to this thesis work, it was unknown whether small molecules had

the ability to differentiate between aggregated Aβ species. Thus, indoles represent the first class

of second-generation probes capable of this activity (Figure 5.1).
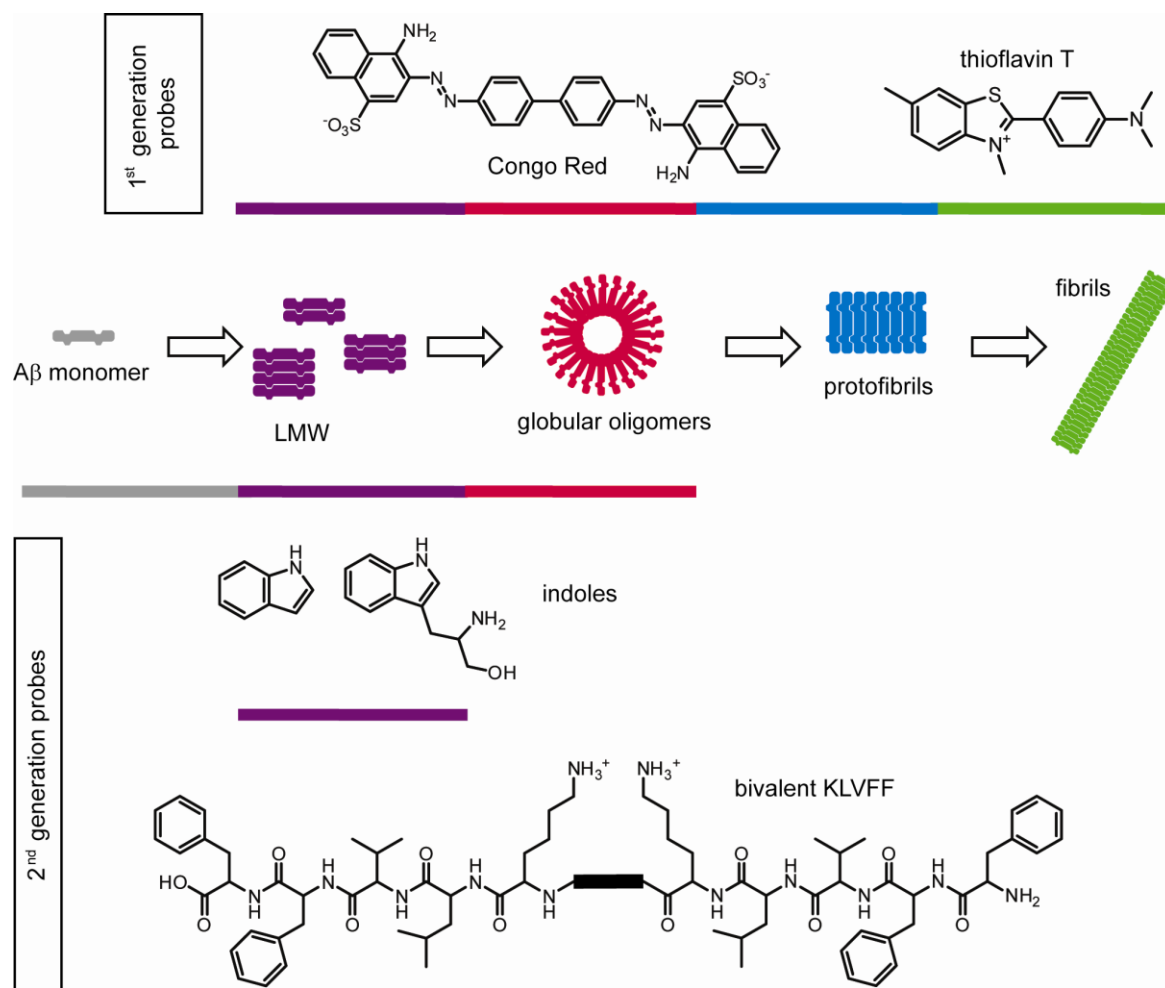
Figure 5.1 First and second generation Aβ probes. Congo Red and thioflavin T represent two of the major classes of first-generation Aβ probes. These probes distinguish between the broadest classification of structures, monomeric and aggregated. This thesis describes two classes of second-generation probes, or probes that differentiate between conformations of aggregated Aβ. Indoles distinguish between pre-fibrillar (monomer, low-molecular weight, oligomers) and fibrillar amyloids. Bivalent KLVFF specifically binds LMW Aβ in complex biological mixtures.

We discuss in Chapter 3 that indole-based scaffolds cannot be used in biological mixtures, but

instead are ideal for purified amyloid systems. Thus, as detailed in Chapter 4, we rationally

designed probes to target low-molecular weight (LMW) structures. We synthesized a 5-residue

portion of the Aβ peptide, KLVFF, which is known to bind its homologous residues at the ends of

Aβ aggregates. We proposed that bivalent versions of KLVFF might have increased selectivity and avidity for Aβ. Using Western blotting to evaluate binding, we found that several bivalent ligands indeed selectively detect Aβ trimers and tetramers. Furthermore, we observed no significant recognition of monomeric or fibrillar Aβ. As mentioned, we sought to use these ligands to detect Aβ in complex biological mixtures, and found that our ligands retained selectivity for trimers and tetramers in human cerebrospinal fluid (CSF). Thus, these bivalent ligands represent an additional set of second-generation Aβ probes (Figure 5.1). Here, in Chapter 5, we discuss potential improvements to generate third-generation probes, with higher affinity and selectivity.

5.3 Future directions

5.3.1 Applying the TROL assay to investigate roles of pre-fibrils

As discussed in Chapter 1, first generation probes such as ThT have been used for decades to elucidate the mechanisms and kinetics of amyloid aggregation. For instance, the three distinct phases of amyloid formation (lag phase, nucleated growth, equilibrium) were in part elucidated using ThT fluorescence, as were the effects of seeding on monomer acquisition [1]. Further, the distinct kinetics of Aβ (1-40) versus (1-42) aggregation were explored by applying first-generation probes [2], along with effects that mutations have on Aβ aggregation [3]. Using TROL side-by-side with the first-generation probe ThT, we learned that Aβ pre-fibrils remain in solution following equilibration of the ThT signal [4]. Thus, Aβ aggregation is more dynamic than observed with ThT alone. We propose that TROL could be useful in many similar applications to those described above to 're-define' the kinetics of amyloid aggregation.

Several mutations exist within the Aβ fragment of amyloid precursor protein (APP), many of which cause enhanced cleavage of APP, and, in turn, increased Aβ accumulation. Further, the majority of mutations correlate with early onset familial AD. *In vitro*, these mutated peptides also show different self-assembly kinetics when evaluated by ThT [5]. For example, mutations at E22 (E22K, E22Q, E22G) as well as D23N, show faster rates of aggregation, while self-assembly of A21G is slower than wild-type (WT). However, it is not known whether these mutations influence accumulation of pre-fibrils. Interestingly, despite faster rates of aggregation, mutants at E22 and D23 are more toxic than WT [6], while A21G, which aggregates slower, is less toxic. Thus, ThT reactivity does not correlate with toxicity. Further, structural studies have revealed that mutations at E22 enhance the stability of the oligomeric form [7], and a rare mutant E22Δ found in Japanese pedigrees displays enhanced oligomerization and no fibril formation [8]. We propose that the relationships between aggregation, pre-fibril formation and toxicity might be clarified using TROL.

5.3.2 Determining the indole binding site(s)

As discussed in Chapter 3, we began trying to identify the binding site of indoles through truncation and mutagenesis studies [4, 9]. Unfortunately, we were limited by the fact that most modifications to Aβ impact aggregation [10]. However, advances in structural techniques may allow for more detailed characterization of the indole binding site. For example, crystallization of peptide self-assembly mimics (PSAMs), whose fundamental structures mirror those of amyloids, have been performed in complex with ThT [11]. These structural studies have yielded information on the requirements that define a ThT binding site, as we described in Chapter 1. Thus, PSAMs may be a useful tool for studying indoles. Further, recent biochemical and solid-state NMR data have revealed that nearly homogenous populations of globular oligomers can

be generated [12, 13]. With further advances, NMR and hydrogen-deuterium exchange (HDX) techniques may be useful in determining which portions of Aβ define the indole binding site.

The purpose of determining the indole-binding site is two-fold. First, by characterizing this site, we may be able to learn more about the differences in small molecules accessibility, and therefore structure, between oligomers and other conformations. Second, once information is gained on the binding site, it may help guide the design of derivatives with improved specificity. One major goal of those studies would be to reduce binding to

(a) Known Aβ ligands with sites for further chemical modification

BSB

Rosmarinic acid

6A10

2C9

pipurmin

TZDM
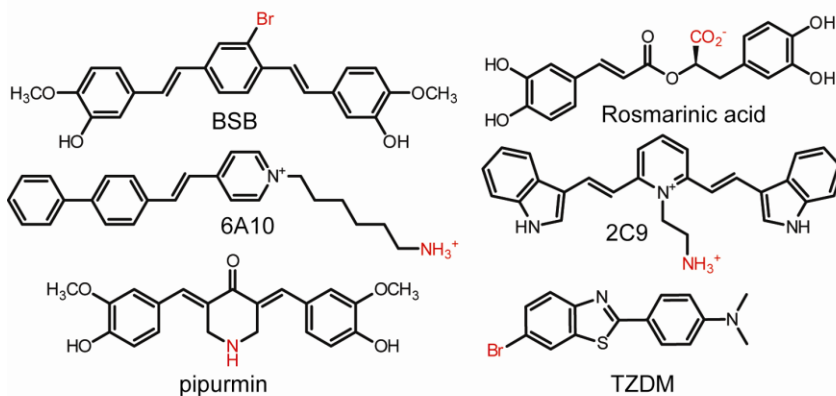
(b) Hetero-multivalent Aβ probes; accessing multiple binding modes

linker region

K_d = 1.4 mM

K_d = 15 μM

KLVFF (parallel)

curcumin-like ligand (anti-parallel)

heterobivalent ligand
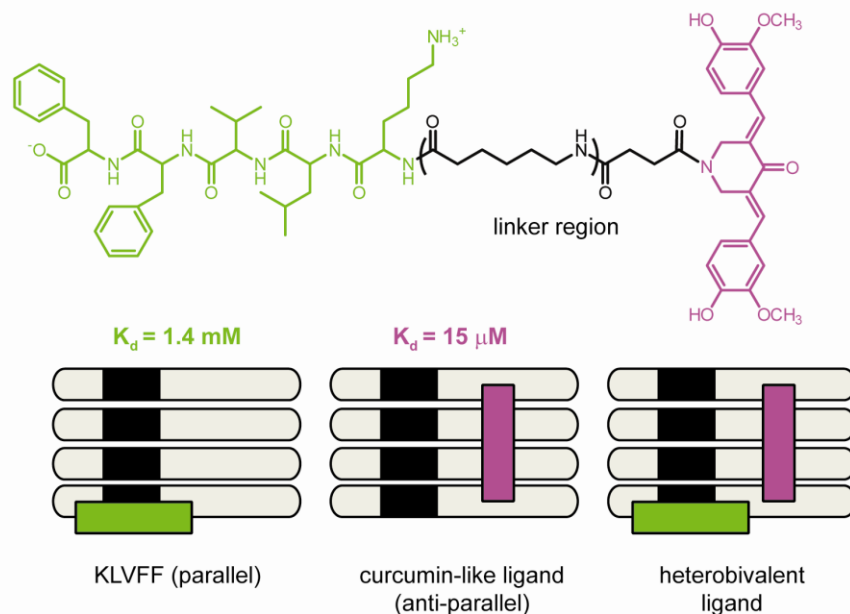
Figure 5.2 New scaffolds for Aβ recognition elements and exploring heterovalent combinations. (a) Chemical structures of known amyloid ligands. On each scaffold, reactive sites (red) for further chemical modification are shown. This is an important feature not present in classic amyloid probes such as curcumin and thioflavin T. (b) By replacing one KLVFF recognition element with an Aβ ligand (pipurmin), having a 100-fold higher binding affinity, the overall affinity of these ligands for Aβ may be improved. Further, new selectivity patterns may emerge by accessing distinct (parallel and anti-parallel) binding modes.

non-amyloids.

5.3.3 Modification of recognition elements and architecture of multivalent ligands

In Chapter 4, we began studies to increase the affinity of the KLVFF ligands for Aβ, with the aim of increasing the sensitivity of these probes in biological mixtures. However, simple additions and modifications to the KLVFF sequence were unsuccessful. Instead, the affinity of these ligands may be improved by other methods. For example, alternative scaffolds might be built by replacing one of the KLVFF motifs for a congo red-like ligand, such as BSB [14] (Figure 5.2a). Importantly, BSB can be modified at the central benzyl ring without damaging binding to amyloids. Thus, this position could be used for linker attachment. Alternatively, other amyloid ligands could be used, such as rosmarinic acid (IC$_{50}$ = 12 μM), 6A10 and 2C9 [15, 16], pipurmin (IC$_{50}$ =26 μM), or ThT analogs [17-20]. One of these ligands may be useful in driving affinity of KLVFF-based ligands for Aβ. For instance, KLVFF has a weak binding affinity (K$_d$ = 1.4 mM) [21], and the affinity of our best bivalent version was mid-micromolar (K$_d$ = 60 μM; Chapter 4). However, if the affinity of one probe, or "recognition element (RE)", alone is 100-fold greater than KLVFF, a hetero-bivalent conjugate may have greater affinity than two KLVFF elements together. For instance, by linking curcumin analogs to KLVFF, the affinity of these heterobivalent ligands may be increased dramatically (Figure 5.2b). As described in Chapter 1, there is a modest amount of information on the curcumin binding site. Thus, exploration and variation of linker length and identity would likely be required in order to retain selectivity for LMW Aβ.

An additional way in which affinity may be gained is by altering the architecture of the KLVFF ligands. This includes features such as valency, density, size, shape, flexibility, branching, and orientation of the RE [22]. We have developed preliminary synthetic routes of simple bivalent and trivalent cores, while some additional cores are commercially available (Figure 5.3a). These cores represent only a small subset of the diversity that is available for RE conjugation. Importantly, the core mediates the amount of synthetic control over RE additions. For instance, two distinct REs can be added to the non-equivalent sites on 2-(2,5-dichlorophenyl)ethanamine, while the sites on benzene 1,3,5-tricarbonyl trichloride are identical, making it more difficult to introduce distinct Res (Figure 5.3a).

Other classical ways to synthesize multivalent scaffolds with higher selectivity and avidity are through altering

(a) Synthetic and commercially-available cores for RE conjugation
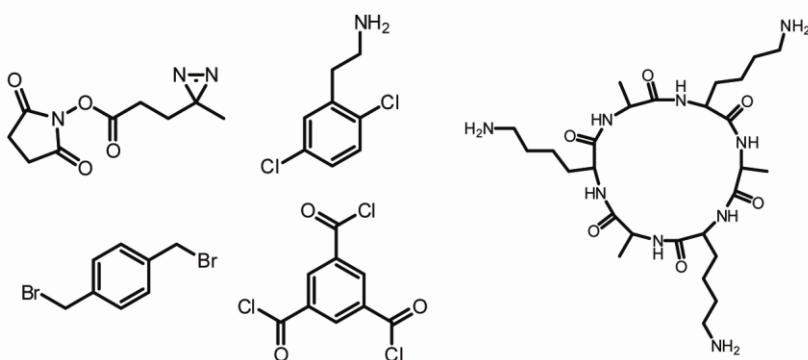
(b) Varying number of total REs: valency

(c) Varying density

(d) Varying architecture: branching, size, shape, and flexibility
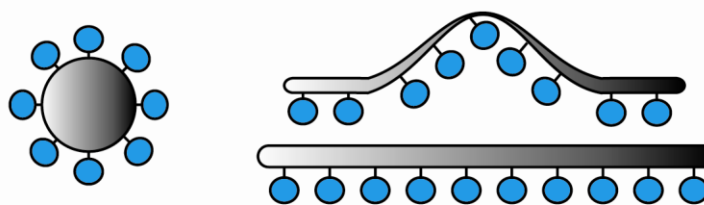
Figure 5.3 Exploring different architectures of multivalent ligands
A limitation of our bivalent KLVFF collection is affinity and sensitivity. This may be remedied by (a) exploring different cores for KLVFF conjugation, and varying (b) valency and (c) density of KLVFF. (d) Altering the architecture, or overall presentation of the KLVFF recognition element, is a traditional way of exploring options for multivalent conjugation and driving affinity.

presentation of the RE on the core. Two ways to accomplish this is by varying the valency and density of the RE (Figures 5.3b, c). This has been done using cyclic peptide scaffolds in order to have tight control over the number of reactive binding sites, which has been demonstrated with KLVFF as the RE [23]. Finally, the overall architecture of the ligand can be altered by using different sources for conjugation, including solid-phase beads, dendrimers, and flexible and rigid linear polymers (Figure 5.3d). A large amount of literature is devoted to the synthetic routes for developing such polymers, many of which can be end-labeled for evaluating ligand-protein interactions [24-26]. Generation of new multivalent ligands with amyloid-binding REs, including KLVFF, may address our aims of driving affinity. Further, these approaches will likely aid in development of third-generation probes, as the repetitive structure of multivalent architectures mirrors that of amyloids.

5.3.4 Multivalent ligands as probes for small molecule binding sites on amyloids

As we mentioned in Chapter 1, multivalency will likely prove useful in probing the nature of small molecule binding sites on amyloids. Specifically, ThT binds at three distinct sites; two high-density sites (BS1, BS2) anti-parallel to the β-sheet and a less populated site (BS3) at the end of amyloids, parallel to the β-sheet (Figure 5.4a) [27]. Similarly, congo red accesses two non-equivalent sites. The predominant site (BS2) is located anti-parallel to the β-sheet and is shared

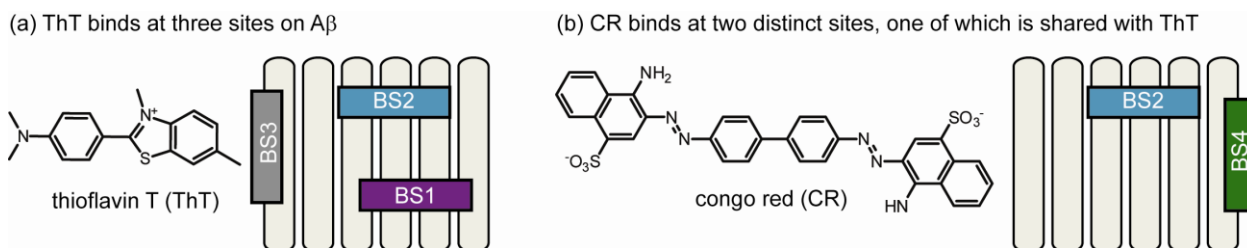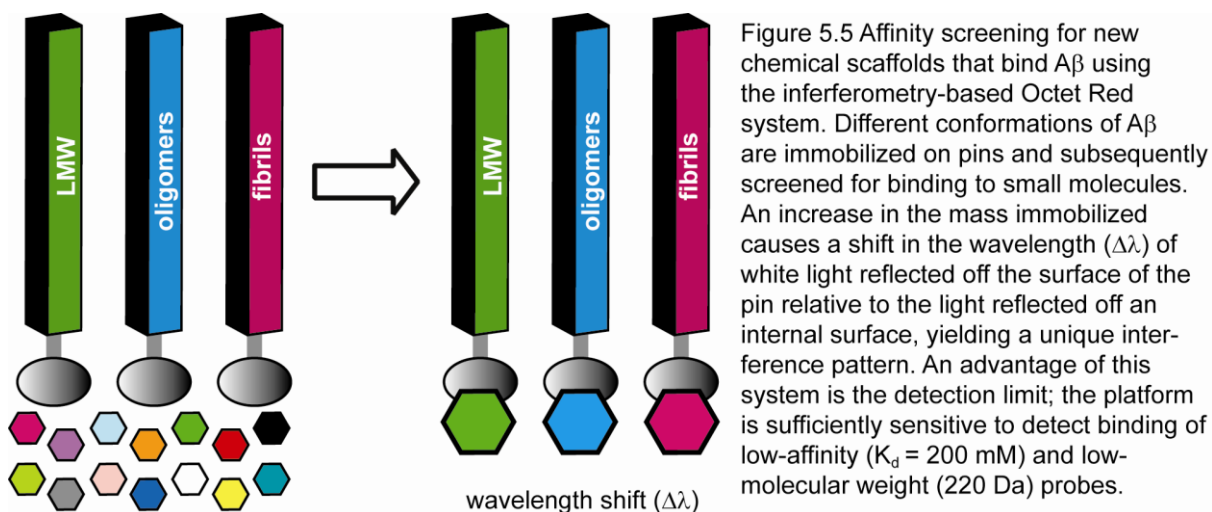Figure 5.4 Probing the proximity of small molecule binding sites on amyloids. As described in Chapter 1, ThT (a) and congo red (b) each bind at multiple sites on amyloids. However, the location of these four non-equivalent sites relative to one another remains unclear. We predict that the proximity of these sites may be probed using multivalent versions of these ligands with different linker lengths and flexibilities.

by ThT, while the less populated site (BS4) is parallel to the β-sheet (Figure 5.4b) [28]. Despite

our knowledge of stoichiometry and local binding site structure, the relative proximity of these

binding sites is unknown. Chemical "mapping" with bivalent small molecules may permit insights

into this question. Many bivalent versions of ThT and CR have already been synthesized [23, 29-

33]. However, the effects of varying linker length and flexibility have not been explored. These

data may shed light on the relationship between these binding sites, and, in turn, offer a

structural landscape of small molecule binding sites on amyloids.

5.3.5 Finding new scaffolds using novel screening platforms

An additional approach that may yield novel high affinity amyloid ligands is further small

molecule screening. In Chapter 2, we described using surface plasmon resonance (SPR) to

directly determine the binding affinity of CR for different Aβ conformations. The advantage of

using SPR with amyloids is that fibrils, oligomers, and LMW Aβ are spatially separated and

unable to proceed through the fibrillization or re-arrangement processes. However, as described

in Chapter 2, we encountered a signal-to-noise issue using SPR; namely, we could not observe

binding of molecules under ~500 Da. Thus, other binding platforms with increased sensitivity

Figure 5.5 Affinity screening for new chemical scaffolds that bind Aβ using the inferferometry-based Octet Red system. Different conformations of Aβ are immobilized on pins and subsequently screened for binding to small molecules. An increase in the mass immobilized causes a shift in the wavelength (Δλ) of white light reflected off the surface of the pin relative to the light reflected off an internal surface, yielding a unique interference pattern. An advantage of this system is the detection limit; the platform is sufficiently sensitive to detect binding of low-affinity (K_d = 200 mM) and low-molecular weight (220 Da) probes.

that also incorporate the advantages of SPR may be useful in identifying novel chemical scaffolds that are specific for Aβ conformations. One such technology is based on optical inferferometry. Following immobilization of an analyte on a pin surface, the surface is brought into contact with the second analyte (*e.g.* protein, small molecule). The increase in mass induces a shift in the reflected white light. As with SPR, this change in wavelength ($\Delta\lambda$) can be correlated to the amount of mass on the surface. Thus, this technique may be useful for Aβ; distinct conformations are prepared and immobilized on pins (Figure 5.5). As envisioned, these pins, each loaded with a specific Aβ morphology, are then exposed to diverse chemical libraries, and an Aβ-small molecule interaction can be detected.

5.3.6 New methods for evaluating amyloid-probe interactions in complex mixtures

The limitations of the Aβ-binding Western blot platform were detailed in Chapter 4. Briefly, even with our highest affinity ligands, this platform does not allow visualization of native levels of Aβ in primary tissues,
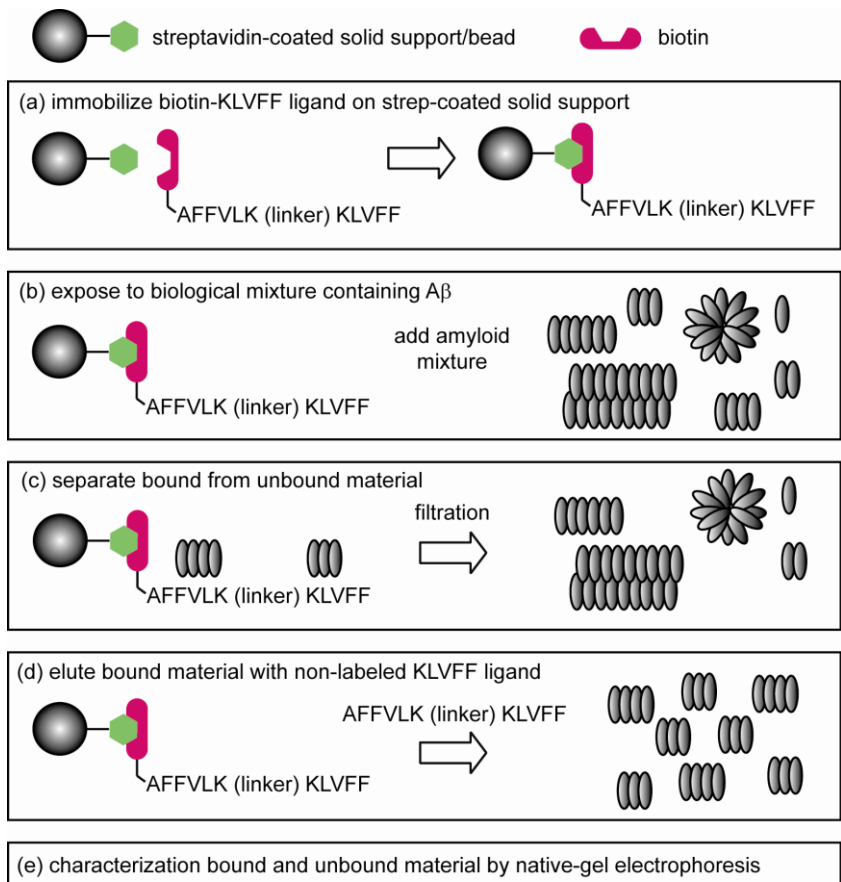
Figure 5.6 Binding Aβ in complex mixtures using solid-phase capture. (a) Biotinylated, bivalent KLVFF is immobilized on streptavidin-conjugated resin. (b) A mixture (*e.g.* CSF) that includes Aβ is added to the resin and incubated. (c) The material bound to the resin is separated from unbound material through filtration or centrifugation of the resin, after which the bound material is eluted using a non-biotinylated KLVFF ligand (d). Both bound and unbound material may then be characterized through electrophoresis and Western blotting.

such as blood or CSF. One solution to this problem is to increase the sensitivity and yield of the detection method. A possibility is to probe KLVFF-Aβ interactions using an 'in-gel' format, in which the probe is pre-added to the Aβ mixture. Native conditions may allow bound structures to remain intact throughout electrophoresis, and these interactions may be visualized using streptavidin-HRP.

Another approach would be to use solid-phase-based pre-concentration of Aβ using a KLVFF-conjugated resin (Figure 5.6a). As envisioned, amyloid-containing mixtures would be exposed to resin (Figure 5.6b), and bound material is separated using filtration (Figure 5.6c). Finally, bound material is eluted using non-tagged ligands, (Figure 5.6d, e). We began using this type of technology, and found one of the only difficulties was non-specific binding of Aβ. These issues could likely be remedied with further experimental optimization.

5.3.7 Using peptide-based approaches with other amyloid systems

The concept of using a segment of an amyloid-forming protein in order to construct a probe is not limited to Aβ. This approach is also observed with polyglutamine (polyQ)-containing proteins, such as the huntingtin (Htt) protein [34], ataxin-3 [35] and the androgen receptor [36]. Aggregation and toxicity of these proteins is dependent upon the length of its polyQ expansion, and there is evidence of distinct Htt structures [37]. Similar to Aβ and AD, it is unclear what roles various conformations play in disease. Like the HCR in Aβ, the polyQ region is required for aggregation, and is thought to nucleate through self-recognition. Thus, it follows that a peptide composed of glutamine residues recognizes polyQ-containing aggregates. Indeed, several groups have described a 34-mer peptide containing 30 glutamine residues that binds aggregated foci (AF) composed of Htt in brain tissue [34, 38]. Also similar to Aβ and KLVFF, it may be

possible to design these ligands such that they specifically recognize different assemblies of Htt

and other polyQ-containing proteins. We have made preliminary efforts toward this goal by

developing peptides composed of varying lengths of polyQ stretches (*e.g.* 5, 10, or 20 glutamine

residues). We anticipate that by varying the size of the polyQ stretch, as well as the valency of

this peptide, we may develop ligands that specifically interact with various types of polyQ-

containing amyloids.

The potential for developing peptide ligands based on the sequence of an amyloid-prone

protein is also presented in many other amyloid proteins, including insulin, IAPP, α-synuclein,

prion, and tau [39]. Segments of each of these proteins have been shown to be required for

aggregation through self-recognition, and thus present the potential for designing peptides with

specific binding to these proteins. An example is the well-characterized sequence VQIVYK (306-
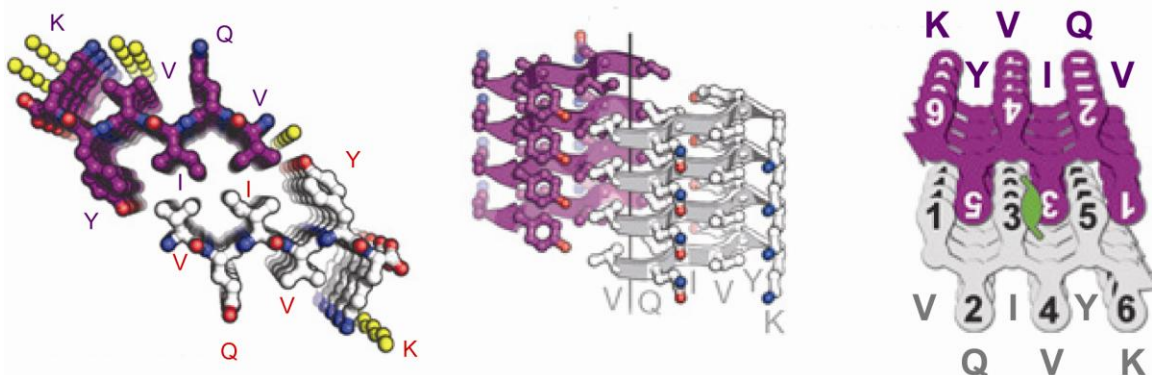
Figure 5.7 A region of the tau protein, [VQIVYK (306-311)] that is required for aggregation aligns through self-recognition. Thus, it may be targeted for probe development. This 6-mer region is necessary and sufficient for tau aggregation. It is thought to align through recognition of homologous side-chains on neighboring molecules, much vlike KLVFF within the hydrophobic core region of Aβ. Figures adapted from Sawaya *et al.* (2007) Nature. We propose that this region, and similar peptide regions in other amyloid proteins, will provide a useful starting point for generating conformation-specific probes in each of these sytems.

311) in the microtubule binding protein tau (Figure 5.7). Tau becomes hyperphosphorylated and

subsequently self-assembles to form neurofibrillary tangles (NFTs) [40]. NFTs correlate with

neurodegeneration in a plethora of disorders, such AD and the frontotemporal dementias [40].

And, similar to Aβ, tau forms distinct quaternary structures, including toxic oligomers [41, 42]. Like KLVFF in Aβ, VQIVYK (also known as PHF6) has been shown to be to be necessary and sufficient for aggregation [43-45], and is thought to mediate assembly through self-recognition. Thus, VQIVYK may be a novel scaffold for developing conformation-specific probes to target tau. These data present the opportunity to broaden the definition of third-generation probes to include many amyloid systems.

5.4 Concluding remarks

The observations presented in this thesis collectively reveal, for the first time, that small molecules are capable of differentiating between distinct Aβ structures. This realization could have important implications for Alzheimer's disease, as well as other neurodegenerative diseases. Specifically, the chemical scaffolds developed here can be used as a foundation for the development of third-generation Aβ probes. Ideally, these future probes, with higher affinity and sensitivity, will help reveal the roles of Aβ conformers in disease, and allow for earlier detection of Alzheimer's disease.

As partially described in these future directions, we predicted one avenue of this project to be an in-depth exploration of multivalent architectures in the development of Aβ probes. In fact, this began as my intended rotation project four years ago. Instead, we immediately gained an appreciation for the way that curcumin and related scaffolds interact with Aβ. These preliminary studies allowed me to utilize synthetic chemistry in order to further explore the SAR surrounding these small molecules. I am likely a better scientist for being given the opportunity to broaden my skill-set in a way I had not predicted.

From these early studies, we also realized that finding compounds that bind differently to

distinct Aβ conformations was also not going to be as simple as we had predicted; we thought

we had the appropriate recognition elements (*i.e*. curcumin), and that we could immediately

explore multivalency. However, we soon discovered that a more basic question was emerging –

could small molecules even distinguish between conformations? We had to find scaffolds that

responded differently (*e.g*. binding, fluorescence) to various Aβ morphologies. Through

literature reading and correspondence at conferences, we learned that others believed this to

be a critical question as well. In this regard, we contributed to the field by answering this

question in several different ways. And, these answers, we envision, will have a lasting impact as

the next generations of probes emerge. I look forward to seeing the next steps taken in this

project. A detailed look at multivalent scaffolding of Aβ recognition elements (both those

discovered here and those found in future studies) will allow for continued exploration of the

relationship(s) between amyloid structure and function.

5.5 References

[1]   Paravastu AK, Qahwash I, Leapman RD, Meredith SC, Tycko R. Seeded growth of beta-amyloid fibrils from Alzheimer's brain-derived fibrils produces a distinct fibril structure. Proceedings of the National Academy of Sciences of the United States of America. 2009 May 5;106(18):7443-8.
[2]   Hasegawa K, Yamaguchi I, Omata S, Gejyo F, Naiki H. Interaction between A beta(1-42) and A beta(1-40) in Alzheimer's beta-amyloid fibril formation in vitro. Biochemistry. 1999 Nov 23;38(47):15514-21.
[3]   Walsh DM, Hartley DM, Condron MM, Selkoe DJ, Teplow DB. In vitro studies of amyloid beta-protein fibril assembly and toxicity provide clues to the aetiology of Flemish variant (Ala692-->Gly) Alzheimer's disease. The Biochemical journal. 2001 May 1;355(Pt 3):869-77.
[4]   Reinke AA, Abulwerdi GA, Gestwicki JE. Quantifying prefibrillar amyloids in vitro by using a "thioflavin-like" spectroscopic method. Chembiochem. 2010 Sep 3;11(13):1889-95.
[5]   Betts V, Leissring MA, Dolios G, Wang R, Selkoe DJ, Walsh DM. Aggregation and catabolism of disease-associated intra-Abeta mutations: reduced proteolysis of AbetaA21G by neprilysin. Neurobiology of disease. 2008 Sep;31(3):442-50.
[6]   Murakami K, Irie K, Morimoto A, Ohigashi H, Shindo M, Nagao M, et al. Synthesis, aggregation, neurotoxicity, and secondary structure of various A beta 1-42 mutants of familial

Alzheimer's disease at positions 21-23. Biochemical and biophysical research communications. 2002 May 31;294(1):5-10.

[7]   Kassler K, Horn AH, Sticht H. Effect of pathogenic mutations on the structure and dynamics of Alzheimer's A beta 42-amyloid oligomers. Journal of molecular modeling. 2010 May;16(5):1011-20.

[8]   Tomiyama T, Nagata T, Shimada H, Teraoka R, Fukushima A, Kanemitsu H, et al. A new amyloid beta variant favoring oligomerization in Alzheimer's-type dementia. Annals of neurology. 2008 Mar;63(3):377-87.

[9]   Reinke AA, Seh HY, Gestwicki JE. A chemical screening approach reveals that indole fluorescence is quenched by pre-fibrillar but not fibrillar amyloid-beta. Bioorganic & medicinal chemistry letters. 2009 Sep 1;19(17):4952-7.

[10]   Williams AD, Shivaprasad S, Wetzel R. Alanine scanning mutagenesis of Abeta(1-40) amyloid fibril stability. Journal of molecular biology. 2006 Apr 7;357(4):1283-94.

[11]   Biancalana M, Makabe K, Koide A, Koide S. Molecular mechanism of thioflavin-T binding to the surface of beta-rich peptide self-assemblies. Journal of molecular biology. 2009 Jan 30;385(4):1052-63.

[12]   Chimon S, Shaibat MA, Jones CR, Calero DC, Aizezi B, Ishii Y. Evidence of fibril-like beta-sheet structures in a neurotoxic amyloid intermediate of Alzheimer's beta-amyloid. Nature structural & molecular biology. 2007 Dec 2.

[13]   Stine WB, Jr., Dahlgren KN, Krafft GA, LaDu MJ. In vitro characterization of conditions for amyloid-beta peptide oligomerization and fibrillogenesis. The Journal of biological chemistry. 2003 Mar 28;278(13):11612-22.

[14]   Schmidt ML, Schuck T, Sheridan S, Kung MP, Kung H, Zhuang ZP, et al. The fluorescent Congo red derivative, (trans, trans)-1-bromo-2,5-bis-(3-hydroxycarbonyl-4-hydroxy)styrylbenzene (BSB), labels diverse beta-pleated sheet structures in postmortem human neurodegenerative disease brains. The American journal of pathology. 2001 Sep;159(3):937-43.

[15]   Li Q, Lee JS, Ha C, Park CB, Yang G, Gan WB, et al. Solid-phase synthesis of styryl dyes and their application as amyloid sensors. Angewandte Chemie (International ed. 2004 Nov 26;43(46):6331-5.

[16]   Li Q, Min J, Ahn YH, Namm J, Kim EM, Lui R, et al. Styryl-based compounds as potential in vivo imaging agents for beta-amyloid plaques. Chembiochem. 2007 Sep 24;8(14):1679-87.

[17]   Wang Y, Mathis CA, Huang GF, Debnath ML, Holt DP, Shao L, et al. Effects of lipophilicity on the affinity and nonspecific binding of iodinated benzothiazole derivatives. J Mol Neurosci. 2003;20(3):255-60.

[18]   Kung MP, Hou C, Zhuang ZP, Zhang B, Skovronsky D, Trojanowski JQ, et al. IMPY: an improved thioflavin-T derivative for in vivo labeling of beta-amyloid plaques. Brain research. 2002 Nov 29;956(2):202-10.

[19]   Zhuang ZP, Kung MP, Hou C, Plossl K, Skovronsky D, Gur TL, et al. IBOX(2-(4'-dimethylaminophenyl)-6-iodobenzoxazole): a ligand for imaging amyloid plaques in the brain. Nuclear medicine and biology. 2001 Nov;28(8):887-94.

[20]   Zhuang ZP, Kung MP, Hou C, Skovronsky DM, Gur TL, Plossl K, et al. Radioiodinated styrylbenzenes and thioflavins as probes for amyloid aggregates. Journal of medicinal chemistry. 2001 Jun 7;44(12):1905-14.

[21]   Cairo CW, Strzelec A, Murphy RM, Kiessling LL. Affinity-based inhibition of beta-amyloid toxicity. Biochemistry. 2002 Jul 9;41(27):8620-9.

[22]   Kiessling LL, Gestwicki JE, Strong LE. Synthetic multivalent ligands as probes of signal transduction. Angewandte Chemie (International ed. 2006 Apr 3;45(15):2348-68.

[23]   Zhang G, Leibowitz MJ, Sinko PJ, Stein S. Multiple-peptide conjugates for binding beta-amyloid plaques of Alzheimer's disease. Bioconjugate chemistry. 2003 Jan-Feb;14(1):86-92.

[24]   Gordon EJ, Gestwicki JE, Strong LE, Kiessling LL. Synthesis of end-labeled multivalent ligands for exploring cell-surface-receptor-ligand interactions. Chemistry & biology. 2000 Jan;7(1):9-16.

[25]   Owen RM, Gestwicki JE, Young T, Kiessling LL. Synthesis and applications of end-labeled neoglycopolymers. Organic letters. 2002 Jul 11;4(14):2293-6.

[26]   Pontrello JK, Allen MJ, Underbakke ES, Kiessling LL. Solid-phase synthesis of polymers using the ring-opening metathesis polymerization. Journal of the American Chemical Society. 2005 Oct 26;127(42):14536-7.

[27]   Lockhart A, Ye L, Judd DB, Merritt AT, Lowe PN, Morgenstern JL, et al. Evidence for the presence of three distinct binding sites for the thioflavin T class of Alzheimer's disease PET imaging agents on beta-amyloid peptide fibrils. The Journal of biological chemistry. 2005 Mar 4;280(9):7677-84.

[28]   Ye L, Morgenstern JL, Gee AD, Hong G, Brown J, Lockhart A. Delineation of positron emission tomography imaging agent binding sites on beta-amyloid peptide fibrils. The Journal of biological chemistry. 2005 Jun 24;280(25):23599-604.

[29]   Chafekar SM, Malda H, Merkx M, Meijer EW, Viertl D, Lashuel HA, et al. Branched KLVFF tetramers strongly potentiate inhibition of beta-amyloid aggregation. Chembiochem. 2007 Oct 15;8(15):1857-64.

[30]   Lenhart JA, Ling X, Gandhi R, Guo TL, Gerk PM, Brunzell DH, et al. "Clicked" bivalent ligands containing curcumin and cholesterol as multifunctional abeta oligomerization inhibitors: design, synthesis, and biological characterization. Journal of medicinal chemistry. 2010 Aug 26;53(16):6198-209.

[31]   Qin L, Vastl J, Gao J. Highly sensitive amyloid detection enabled by thioflavin T dimers. Molecular bioSystems. 2010 Oct 1;6(10):1791-5.

[32]   Shi W, Dolai S, Rizk S, Hussain A, Tariq H, Averick S, et al. Synthesis of monofunctional curcumin derivatives, clicked curcumin dimer, and a PAMAM dendrimer curcumin conjugate for therapeutic applications. Organic letters. 2007 Dec 20;9(26):5461-4.

[33]   Reinke AA, Ung PM, Quintero JJ, Carlson HA, Gestwicki JE. Chemical probes that selectively recognize the earliest Abeta oligomers in complex mixtures. Journal of the American Chemical Society. 2010 Dec 22;132(50):17655-7.

[34]   Heng MY, Duong DK, Albin RL, Tallaksen-Greene SJ, Hunter JM, Lesort MJ, et al. Early autophagic response in a novel knock-in model of Huntington disease. Human molecular genetics. 2010 Oct 1;19(19):3702-20.

[35]   Ellisdon AM, Pearce MC, Bottomley SP. Mechanisms of ataxin-3 misfolding and fibril formation: kinetic analysis of a disease-associated polyglutamine protein. Journal of molecular biology. 2007 Apr 27;368(2):595-605.

[36]   Monks DA, Johansen JA, Mo K, Rao P, Eagleson B, Yu Z, et al. Overexpression of wild-type androgen receptor in muscle recapitulates polyglutamine disease. Proceedings of the National Academy of Sciences of the United States of America. 2007 Nov 13;104(46):18259-64.

[37]   Lotz GP, Legleiter J, Aron R, Mitchell EJ, Huang SY, Ng C, et al. Hsp70 and Hsp40 functionally interact with soluble mutant huntingtin oligomers in a classic ATP-dependent reaction cycle. The Journal of biological chemistry. 2010 Dec 3;285(49):38183-93.

[38]   Osmand AP, Berthelier V, Wetzel R. Imaging polyglutamine deposits in brain tissue. Methods in enzymology. 2006;412:106-22.

[39]   Sawaya MR, Sambashivan S, Nelson R, Ivanova MI, Sievers SA, Apostol MI, et al. Atomic structures of amyloid cross-beta spines reveal varied steric zippers. Nature. 2007 May 24;447(7143):453-7.

[40]   Ballatore C, Lee VM, Trojanowski JQ. Tau-mediated neurodegeneration in Alzheimer's disease and related disorders. Nature reviews. 2007 Sep;8(9):663-72.

[41]   Kayed R. Anti-tau oligomers passive vaccination for the treatment of Alzheimer's disease. Human vaccines. 2010 Nov 1;6(11):47-51.

[42]   Lasagna-Reeves CA, Castillo-Carranza DL, Guerrero-Muoz MJ, Jackson GR, Kayed R. Preparation and characterization of neurotoxic tau oligomers. Biochemistry. 2010 Nov 30;49(47):10039-41.

[43]   Rojas Quijano FA, Morrow D, Wise BM, Brancia FL, Goux WJ. Prediction of nucleating sequences from amyloidogenic propensities of tau-related peptides. Biochemistry. 2006 Apr 11;45(14):4638-52.

[44]   Vaden TD, Gowers SA, de Boer TS, Steill JD, Oomens J, Snoek LC. Conformational preferences of an amyloidogenic peptide: IR spectroscopy of Ac-VQIVYK-NHMe. Journal of the American Chemical Society. 2008 Nov 5;130(44):14640-50.

[45]   Li W, Lee VM. Characterization of two VQIXXK motifs for tau fibrillization in vitro. Biochemistry. 2006 Dec 26;45(51):15692-701.